Beta secretase inhibition in aging pancreatic beta cells:

A possible role for Rooibos

By: Yonela Ntamo

Student no: 201159667

A dissertation submitted in fulfilment of the requirement for the degree of Doctor of Philosophy in Biochemistry at the Faculty of Science and Agriculture, Department of Biochemistry and Microbiology, University of Zululand

Supervisor: Dr Nireshni Chellan

Co-supervisors: Prof Abidemi Paul Kappo and Prof Christo John Frederick Muller

April 2020

DECLARATION

I,……..., hereby declare that the work on which this thesis is based is my original work (except where acknowledgements indicate otherwise), and that neither the whole work or part of it has been, is being, or is to be submitted for another degree in this or any other university.

I empower the University of Zululand to reproduce for the purpose of research either the whole or any portion of the contents in any manner whatsoever.

Signature: _____ Date: _____

Yonela Ntamo (201159667)

ABSTRACT

In type 2 diabetes (T2D), hyperglycemia induces pancreatic β-cell glucotoxicity, characterised by β-cell functional mass decline. T2D patients are thus both insulin resistance and insulin deficient. In addition, to changes in insulin production and secretion, the hormone amylin is also dysregulated. Amylin is a pancreatic β-cell peptide hormone with a key role in glucose homeostasis and is co-secreted with insulin. Beta-secretase (BACE)-regulated cleavage of pre-amylin results in the aggregation and deposition of toxic amyloid plaques, characteristic of long-term diabetic patient pancreata. Thus, BACE inhibition is a promising therapeutic target in managing the progression of T2D. Research has shown that unfermented Rooibos has numerous health promoting benefits, including anti-inflammatory, anti-oxidative and anti-diabetic effects. This extract is unique for containing relatively high levels of aspalathin, a glycosyl dihydrochalcone with robust anti-oxidant properties and ameliorative effects against several metabolic complications. In this study, we aimed to assess the effects of chronic glucotoxicity in a novel 3D β-cell spheroid model and the potential therapeutic effects of GRT™ and BACE inhibition, thereof. Additionally, we determined the effect of BACE inhibition and GRT™ in the pancreata of aged C57BLKS *db/db* mice.

The *in vitro* toxicity model was established using INS-1 β-cell spheroids created using the 3D BioArray Matrix (BAM) culture system, based on T2D-associated glucotoxicity. Spheroids were exposed to the following conditions: Normal glucose control (NG-11 mM glucose), high glucose (glucotoxicity) control (HG-33 mM glucose), high glucose with GRT™ (HG-GRT™) and high glucose with BACE inhibitor LY2886721 (HG-BACE). Spheroids ultra-structural features were assessed using transmission electron microscope (TEM) and toluidine blue stain (TB). Spheroid viability and survival were assessed by measuring cellular ATP content, glucose utilization and size profiling. Functional parameters (i.e. glucose stimulated insulin & amylin secretion) and pro-inflammatory cytokines were assessed. The *in vitro* findings were validated *in vivo* using lean non-diabetic *db*+ and obese diabetic *db/db* mice. There were three phases : 10, 16 and 32 weeks treatment, divided into five treatment groups (n=8 per group): Control (vehicle equivalent/day), pioglitazone (15 mg/kg/day), BACE inhibitor (30 μM/kg/day), GRT™-1(74 mg/kg/day) and GRT™-2 (740 mg/kg/day). Physiological parameters, glucose metabolism and pancreatic islet morphology were assessed by

measuring body weight and food intake; performing an oral glucose tolerance test, measuring serum insulin, C-peptide and amylin levels; and immunohistochemical labelling of pancreata with insulin and glucagon.

In the spheroids, glucotoxicity (HG) significantly reduced cellular ATP content (73.63% ± 2.13 vs 100.0% ± 0.36; p< 0.001), while GRT™ ameliorated this effect (82.49% ± 1.07 vs 73.63% ± 2.13; p<0.05). Increased insulin secretion after glucose stimulation was observed in the NG compared to basal glucose levels (41.08 ng/mL ± 5.23 vs 22.6 ng/mL ± 3.49; p=0.001) and this effect was negated in the HG group; this was restored in the HG-GRT™ group (30.8 ng/mL ± 2.49 vs 17.9 ng/mL ± 2.54; p=0.05). HG and HG-BACE groups increased amylin secretion following glucose stimulation (41.7 pg/mL ± 7.18 vs 20.3 pg/mL ± 4.39; p=0.01; 43.9 pg/mL ± 5.38 vs 21.5 pg/mL ± 3.57; p=0.007). HG increased TNF-α compared to the NG group (2.4 pg/mL ± 0.24 vs 1.1 pg/mL ± 0.23; p= 0.001), while HG-BACE group had significantly lower TNF-α levels compared to HG group (2.4 pg/mL ± 0.24 vs 0.67 pg/mL ± 0.15; p< 0.0001). Additionally, after 2 weeks of treatment, HG-GRT™ reduced TNF-α levels (1.6 pg/mL ± 0.16 vs 2.6 pg/mL ± 0.33; p= 0.02). Interestingly, HG-BACE had a short-lived inhibitory effect as TNF-α levels increased after 2 weeks (2.4 pg/mL ± 0.24 vs 0.9 pg/mL ± 0.20; p= 0.0001). *In vivo*, changes were associated with normal animal aging in the *db*+ mice. In *db/db* mice, BACE inhibitor and GRT™-1 (phase I) improved glucose tolerance without concomitant BW gain (2412 ± 121.0; p=0.01 and 2293 ± 105.6, p= 0.02 vs 2970 ± 95.62, respectively), had higher HOMA-β and improved islet architecture of older animals (phase II). Pioglitazone significantly improved glucose tolerance (1884 ± 296.0 vs 3238 ± 260.5; p= 0.004), had lower HOMA-IR in phase II. Amylin levels were significantly reduced in phase II compared to phase I in all treatment groups (p<0.001). In phase I, GRT™-2 effectively improved glucose tolerance, whereas GRT™-2 remained ineffective. Additionally, GRT™-2 tended to have lower HOMA-IR and HOMA-β compared to GRT™-1.

In conclusion, glucose tolerance was improved by BACE inhibition and GRT™ by regulating both insulin resistance and β-cell survival and function in both an *in vitro* and *in vivo* model. Thus, both treatments have the potential to supplement current anti-diabetic therapy.

.

ACKNOWLEDGEMENTS

I would like to express my sincere gratitude to the following people, whose contributions have made it possible to complete my PhD degree:

Dr Nireshni Chellan, my supervisor, for the support, personal guidance, motivation and sharing your pearls of wisdoms throughout the project. Thank you for dedicating time to help me become the researcher I am today. It was an honour to be your student; and without your help, I would not have made it this far.

Prof Christo Muller, my co-supervisor, for taking your time to offer your scientific input and technical support. Thank you for simple believing in me and for encouraging, guiding and always giving your valuable input during this study.

Prof Abidemi, my co-supervisor, thank you for your scientific input and support throughout this study.

Prof Johan Louw, for granting me with the opportunity to conduct my PhD research at the Biomedical Research and Innovation Platform (BRIP), (SAMRC).

To National Research Foundation Thuthuka funding (Grant UID 106951) and Ernst & Ethel Eriksen funding, thank you for financial support.

Dr Ebrahim Samodien, for all your support, motivation, and scientific input. Thank you for extending your knowledge and for your willingness to help even when your schedule was busy.

Dr Thabi Martin and Research Development and Capacity development unit of the South African Medical Research Council, for financial support during this study.

A special thank you also goes to Ms Charna Chapman, Mr Desmond Linden and Ms Ruzayda Van Aarde for technical assistance.

Thank you Dr Sthandiwe Mazibuko, Dr Phiwa Dludla and Dr Kwazi Gabuza for your technical support and offering words of encouragement.

To my mother, N.C Ntamo & Siblings (Pam, Noxy and Siphiwo), thank your constant encouragement, support and prayers throughout this study. Thank you for believing in me and supporting me with my life choices. I am blessed to have you in my life.

To my best friends, Nokulunga “Luh” Hlengwa and Charity “Dr sweet pie” Masilela, words cannot explain how grateful I am to have you in my life. You are my family away from family. Thank you for your motivation, for sharing my cries, my excitement and for always being there to say, “It will be okay”.

To BRIP students, thank you for always being available to offer help whenever needed and for all the words of encouragement.

To God almighty, for I am nothing without you.

This dissertation is dedicated to parents:

Nomawethu and Solomzi Ntamo

TABLE OF CONTENTS

LIST OF FIGURES

LIST OF TABLES

Chapter 2: Literature review

Chapter 3: Methods and Materials

Chapter 4: Results

Chapter 8: Appendix

ABBREVIATIONS

2D	Two-dimensional
3D	Three-dimensional
AD	Alzheimer's disease
AKT	Protein kinase B
AMPK	5' AMP-activated protein kinase
ANOVA	One-way analysis of variance
APP	Amyloid precursor protein
Asp	Aspalathin
ATCC	American Type Culture Collection
ATP	Adenosine triphosphate
AUC	Area under the curve
Aβ	Amyloid-beta
BACE	Beta-site amyloid precursor protein cleaving enzyme
BAM	BioArray Matrix driver
BCA	Bicinchoninic acid
Bcl-2	B-cell lymphoma 2
BrdU	5-bromo-2'-deoxyuridine
BSA	Bovine serum albumin
BSA	Bovine serum albumin
Ca^{2+}	Calcium
cAMP	Cyclic adenosine monophosphate
CAT	Catalase
CO_2	Carbon dioxide
COX2	Cyclooxygenase 2
CRP	C-reactive protein
Db+	Lean non-diabetic mice
Db/db	Obese diabetic mice
DCF	Dichlorofluoroscein
DMSO	Dimethyl sulfoxide
DNA	Deoxyribonucleic acid

DPBS	Dulbecco’s phosphate buffered saline
ECL	Enhanced chemiluminescence
ELISA	Enzyme-linked immunosorbent assay
ER	Endoplasmic reticulum
ERK	Extracellular signal-regulated kinases
EtOH	Ethanol
FA	Fatty acids
fa/fa	Zucker obese rat
FAS	First apoptosis signal receptor gene
FBG	Fasting blood glucose
FBS	Fetal bovine serum
FFA	Free fatty acids
FRET	Fluorescence resonance energy transfer
GLUT-2/4	Glucose transporter 2/4
GRT™	Aspalathin rich, unfermented Rooibos extract
GSH-Px	Glutathione peroxide
GSIS	Glucose stimulated insulin secretion
GSK3 α/β	Glycogen synthase kinase-3 alpha/beta
HCl	Hydrochloric acid
HEPES	4-(2-hydroxyethyl)-1-piperazineethanesulfonic acid
HG	High glucose
HG-BACE	High glucose supplemented with BACE
HG-GRT™	High glucose supplemented with GRT™
HOMA-IR	Homeostatic model of assessment of insulin resistance
HOMA- β	Homeostatic model of assessment of β-cell function
hIAPP	Human islet amyloid polypeptide
HIT	Hamster pancreatic beta cells
HRP	Horseradish peroxidase
Hz	Hertz

IAPP	Islet amyloid polypeptide
IDF	International Diabetes Federation
IFN-γ	Interferon-gamma
IFN-τ	Interferon-tau
Ig	Immunoglobulin
IGF-1	Insulin growth factor-1
IL-1β/2/610	Interleukin 1 beta/6/10
INS-1	Rat insulinoma pancreatic beta cells
IR	Insulin resistance
IRS	Insulin receptor substrates
JNK	C-Jun terminal kinases
K+	Potassium
KRBH	Krebs-Ringer bicarbonate-HEPES buffer
MAPK	Mitogen-activated protein kinases
Mg2+	Magnesium
MIN	Transgenic C57BL/6 mouse insulinoma cells
mRNA	Messenger ribonucleic acid
NF-κB	Nuclear factor kappa-B
NG	Normal optimal glucose
NLRP3	NBD, LRR and PYD domains-containing protein 3
OGTT	Oral glucose tolerance test
PC 1/2/3	Pro-protein convertase 1/2/3
PDX-1	Pancreatic and duodenal homeobox 1
PI3K/AKT	Phosphatidylinositol 3-kinase AKT
PKC	Protein kinase C
PMSF	Phenylmethane sulfonyl fluoride
PMSF	Phenylmethylsulfonyl fluoride
PPAR-γ	Peroxisome proliferator-activated receptor-gamma
PVDF	Polyvinylidene difluoride

RC/DC	Reducing agent compatible and detergent compatible
RIN	Rat insulinoma cells
ROS	Reactive oxygen species
RPMI- 1640	Rosewell park memorial institute media-1640 media
SB	Sample buffer
SDS-PAGE	Sodium dodecyl sulphate polyacrylamide gel electrophoresis
SDS-PAGE	SDS-polyacrylamide gel electrophoresis
SEM	Standard error of mean
SOD	Superoxide dismutase
T2D	Type 2 diabetes
TB	Toluidine blue stain
TBS	Tris-buffered saline
TBST	Tris-buffered saline with tween
TBST-20	Tris-buffered saline containing Tween-20
TEM	Transmission electron microscopy
TMB	3,3′,5,5′-tetramethylbenzidine
TMEM27	Transmembrane protein 27
TNF-α	Tumor necrosis factor-alpha
UPR	Unfolded protein response

UNITS OF MEASUREMENTS	
°C	Degree Celsius
Em	Emission
Ex	Excitation
FL-1/4	Fluorescence green (1) / red (4)
g	Gram
Hz	Hertz
kDa	Kilodalton
Kg	Kilogram
L	Litre
mg	Milligram
mL	Millilitre
mM	Millimolar
mm	Millimetre
MW	Molecular weight
ng	Nanogram
nm	Nanometre
pg	Picogram
pH	Potential of hydrogen
pmol	Picomole
RLU	Relative light units
SS	Soluble solids
V	Volts
x g	Gravity
µg	Microgram
µL	Microliter
µM	Micromolar

OUTPUTS

Conference presentations

Yonela Ntamo, Nireshni Chellan, Abidemi MP Kappo, Johan Louw, and Christo JF Muller. Metabolic profiling of 3D INS-1 Spheroids. Early Career young scientist convention, Cape Town, 12-13 October 2017.

Yonela Ntamo, Nireshni Chellan, Abidemi MP Kappo, Johan Louw, and Christo JF Muller. Protection of pancreatic Beta cells under diabetic conditions by Aspalathus linearis (Rooibos). Biomedical research and innovation platform, Annual Symposium, Cape Town, 16 October 2017.

Yonela Ntamo, Nireshni Chellan, Abidemi MP Kappo, Johan Louw, and Christo JF Muller. The Role of Beta Secretase (BACE) in Aging Pancreatic Beta cells: A Potential Role for Rooibos. Early Career young scientist convention, Cape Town, 16-17 October 2018.

Yonela Ntamo, Nireshni Chellan, Abidemi MP Kappo, Johan Louw, and Christo JF Muller. Long-term effects of Beta Secretase Inhibitor and Rooibos in *db/db* mice. Biomedical research and innovation platform, Annual Symposium, Cape Town, 25 October 2018.

Yonela Ntamo, Nireshni Chellan, Abidemi MP Kappo, Johan Louw, and Christo JF Muller. The amelioration of chronic glucotoxicity in pancreatic beta cell spheroids by an aspalathin rich Rooibos extract (GRT™). 4th Annual Joint HDI-SAMRC Research Conference, Shaka's Rock, Durban, 25 – 27 July 2019.

Yonela Ntamo, Nireshni Chellan, Abidemi MP Kappo, Johan Louw, and Christo JF Muller. The effect of Beta Secretase Inhibitor and Rooibos treatment on C57BLKS db/db mice. 13th Annual Early Career young scientist convention, Cape Town, 09-11th October 2019.

Yonela Ntamo, Nireshni Chellan, Abidemi MP Kappo, Johan Louw, and Christo JF Muller. The amelioration of chronic glucotoxicity in pancreatic beta cell spheroids by an aspalathin rich Rooibos extract (GRT™). Biomedical research and innovation platform, Annual Symposium, Cape Town, 21 October 2019.

Article Title: Popular three-dimensional models: Advantages for cancer, Alzheimer's, and cardiovascular diseases (2020). Tissue and Cell Journal. 65

By: **Yonela Ntamo**; Ebrahim Samodien; Christo. J.F. Muller; Johan Louw, Nireshni Chellan

CHAPTER ONE

Introduction

Introduction

Type 2 diabetes (T2D) is characterised by hyperglycaemia as a result of insulin resistance and consequent pancreatic β-cell dysfunction and failure. Initially the β-cells can compensate for the additional insulin demand, but eventually progression of the disease results in β-cell failure (Donath *et al*., 2005; Prentki, 2006; Wiederkehr and Wollheim, 2008; Cowie *et al*., 2009; Donath, 2014; Esterházy *et al*., 2011). In diabetics, persistent hyperglycemia induces pancreatic islets inflammatory responses, which results to increases in pro-inflammatory cytokines synthesis, thus contributing to apoptosis, β-cell function impairment and loss of functional β-cell mass, a notion known as glucotoxicity (Cernea and Dobreanu, 2013). Aging is a common risk factor for the development of metabolic diseases including T2D with the prevalence peaking from 60-74 years (Gunasekaran and Gannon, 2011; Iozzo *et al*., 1999; Cowie *et al*., 2009).

Aging is commonly associated with an increase in visceral fat mass, glucose intolerance, inflammation, insulin resistance, insulin secretory defects, hyperglycemia and dyslipidemia (De Tata, 2014; Jackson, 1990; Saini, 2010). With insulin resistance and long-term hyperinsulinemia, hyperamylinemia occurs, as amylin is a pancreatic β-cell hormone that is co-stored and co-secreted with insulin (Westermark *et al*., 1986; Clark *et al*., 1989; Cao *et al*., 2013; Potter *et al*., 2015). Abnormalities in amylin folding, secretion, and function aggravates β-cell dysfunction (Clark *et al*., 1996a, 1996b; Kahn *et al*., 1999a), as the increase in amylin secretion is associated with aggregation of amyloid plaques which disrupt pancreatic islet structure and function, a characteristic feature of T2D (Vassar, 1999; Westermark et al., 2011).

Enzymatic cleavage of amylin by β-site amyloidogenic-cleaving enzyme (BACE) forms part of the cycling of amylin (Esterházy *et al*., 2011; Alcarraz-Vizán *et al*., 2017). Literature has reported on two secretases; BACE1, which is expressed in the brain and known to contribute to the development of Alzheimer's disease (AD) and dementia (Vassar, 1999; Abedini and Schmidt, 2013; Cao *et al*., 2013; Potter *et al*., 2015, 2010); while BACE2 is mainly expressed in the pancreas with several physiological functions (Vassar, 2004; Casas *et al*., 2010; Esterházy *et al*., 2011). Beta-site amyloidogenic-

cleaving enzyme 2 is known to cleave the pro-proliferative type I transmembrane protein 27 (TMEM27), a protein with an important role in pancreatic β-cell functional physiology, β-cell proliferation and insulin signalling (Esterházy *et al*., 2011; Visa *et al*., 2015; Alcarraz-Vizán *et al*., 2017). Although TMEM27 plays a beneficial role in β-cells, its cleavage by BACE2 has been implicated to increase the deposition of toxic amyloid plaques and thus BACE inhibition represents a therapeutic target (Casas *et al*., 2010; Esterházy *et al*., 2011; Cao *et al*., 2013; Alcarraz-Vizán *et al*., 2017).

It is therefore important to explore the mechanisms behind inhibition of BACE as a pharmaceutical target, particularly in glucotoxicity induced aged pancreatic β-cells, a condition β-cells are exposed to in T2D.

Plant polyphenols, such as flavonoids, have been reported to reduce β-peptide levels via modulation of secretase-mediated amyloid polypeptide processing (Fluhrer *et al*., 2002; Cox *et al*., 2015). In this study, the impact of BACE inhibition and aspalathin-rich Rooibos extract (GRT™) treatment were investigated. An *in vitro* 3D β-cell spheroid model was established to experimentally assess the effects of a chemical-based BACE inhibitor and plant-derived unfermented aspalathin-rich Rooibos extract containing 12-14% aspalathin. An obese, diabetic *db/db* mouse model was used to determine the *in vivo* effect.

CHAPTER TWO

Literature review

2. Aging and lifestyle diseases

Aging refers to the changes that occur during an organism's lifespan, which vastly differ in rate from organism to organism (Kirkwood, 2005). In humans, aging increases the risk of lifestyle diseases including inflammation, impaired glucose tolerance, hypertension, high glucose, excess fat around the waist and high cholesterol etc. (DeFronzo, 1981; Kirkwood, 2005; Ritz and Berrut, 2005; Chung *et al*., 2008; Monteiro and Azevedo, 2010; Gunasekaran and Gannon, 2011; Esser *et al*., 2014). These sequentially increase the prevalence for development of metabolic diseases such as cardiovascular diseases (CVDs), stroke, insulin resistance (IR) and obesity, likely due to sedentary lifestyles and adoption of unhealthy eating habits (Scheen, 2003). Additionally, aging has been reported to be an important risk factor for type 2 diabetes (T2D) development (Christensen *et al*., 2009), with the prevalence known to increases with age and peaks from 60-74 years of age (De Tata, 2014; Gunasekaran and Gannon, 2011).

2.1. Aging and T2D

Normal aging is associated with a progressive wear in many endocrine functions, becoming a liability for serious disturbances in metabolic homeostasis (De Tata, 2014; Vitale *et al*., 2013). In fact, glucose tolerance impairments are documented as a well-known feature of aging in both animal and human studies (Jackson, 1990; Saini, 2010; De Tata, 2014). Type 2 diabetes is a metabolic disorder characterized by the inability of cells to respond adequately to insulin, thereby leading to beta-cell (β-cell) dysfunction and chronic hyperglycemia (Figure 1) (Ferrannini *et al*., 2010; Inzucchi *et al*., 2012; Noriega-Cisneros *et al*., 2012). The prevalence of T2D is increasing drastically with 2040 global projection estimated at about 439 million adults, with sub-Saharan Africa having 18.8 million adults with T2D by 2040 (Cho *et al*., 2018; Shaw *et al*., 2010). However, although T2D is commonly seen in older adults, it is increasingly seen in children, adolescents and younger adults due to the increasing prevalence of obesity, physical inactivity and poor unhealthy diets (Cho *et al*., 2018; da Rocha Fernandes *et al*., 2016; De Tata, 2014). In South Africa, T2D is the seventh most common cause of death and the leading cause of cardiovascular diseases, disabilities and premature death (Bradshaw *et al*., 2007; Mayosi *et al*., 2009; Nojilana *et al*., 2016) placing an enormous burden on South Africa's health

resources and subsequently affecting the country's socio-economic development (American Diabetes Association, 2019; da Rocha Fernandes *et al*., 2016). T2D can be managed effectively by a healthy lifestyle which includes the adoption of healthy non-sedentary living, reducing overweight and the combination with medication (Tuomilehto *et al*., 2001; Clark *et al*., 2004; Snel *et al*., 2012).

Elderly people, mainly those over the age of 60 years, are known to be susceptible to T2D. In 2008, 15% of the elderly population worldwide were reported to be diabetic, and this figure is estimated that it would have increased to approximately 26% by 2026 (Kowal *et al*., 2012; De Tata, 2014). It is well documented that aging is considered as a risk factor for T2D, in a manner that is associated with defective insulin secretion, glucose response and insulin clearance failure (Chung *et al*., 2008; Esposito and Giugliano, 2004; Esser *et al*., 2014; Monteiro and Azevedo, 2010; Valko *et al*., 2007). Additionally, a theory suggesting that IR increases with age is related to several well-known age-related changes, including increased adiposity, increased accumulation of lipid metabolites in the liver and muscle, mitochondrial dysfunctions, hormonal changes, increased oxidative stress and inflammation (Barzilai *et al*., 2012; Bunprajun *et al*., 2013; De Tata, 2014; Kim *et al*., 2007; Salameh *et al*., 2016).

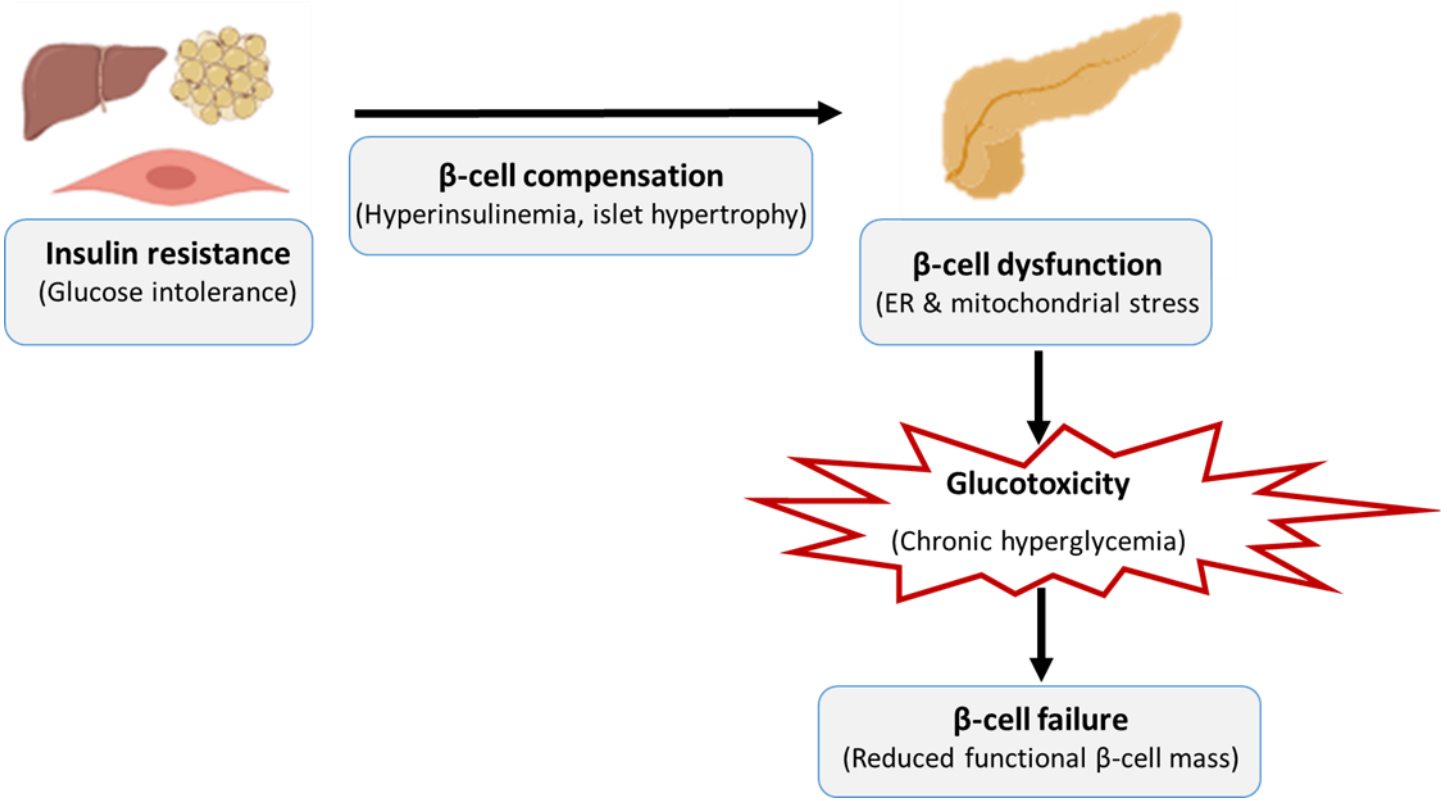

Figure 1: Diagrammatic representation of the progression of T2D with aging. The initial stages of IR in liver, adipose and muscle tissues are characterized by glucose intolerance and hyperinsulinemia, without increases in fasting plasma glucose. Pancreatic β-cells compensate for increased insulin demand during IR by increasing their functional mass. Prolonged hyperglycemia as a result of dysfunctional β-cells, causes glucotoxicity, and along with destructive amyloid plaque deposition, ultimately results in reduced functional β-cell mass and T2D.

2.1.1. Insulin action and insulin signaling

While IR is central to the development of T2D, IR alone does not lead to T2D in the absence of a β-cell defect associated with abnormal insulin secretion. Beta cell-dysfunction is known to play a key role in T2D pathogenesis (Christensen and Gannon, 2019; Gastaldelli *et al*., 2004; Maassen *et al*., 2007). Pancreatic β-cells produce, store and secrete the hormone insulin to maintain glucose homeostasis (Weiss, 2009). Insulin is a β-cell peptide hormone composed of approximately 51 amino acids with a crucial role in the metabolism of not only carbohydrates but also lipids and proteins. In adipose tissue, insulin is liable for the suppression of lipolysis to promote fat storage, an antilipolytic effect mediated through the inhibition of hormone-sensitive lipase (Mayer *et al*., 2007; Meijssen *et al*., 2001; Weiss, 2009). In the liver, the hormone promotes lipogenesis and glycogen storage (Maassen *et al*., 2007; Snel *et al*., 2012) while in the muscle, it is responsible for glucose uptake and storage in the form of glycogen (Dimitriadis *et al*., 2011). Additionally, in both the liver and skeletal muscle, insulin is responsible for decreasing the rate of glycogen breakdown (Saltiel and Kahn, 2001; Zierath *et al*., 2000). The major regulator of insulin secretion is glucose together with other known secretagogues such as potassium chloride (KCL), tolbutamide and arginine (Donath *et al*., 2005; Maedler *et al*., 2002). Elevated blood glucose concentrations initiate insulin signaling by insulin receptors located in insulin sensitive tissues (skeletal muscle, liver and adipose), where insulin binds to its specific receptors and initiates glucose uptake, utilization and storage (Bhattacharya *et al*., 2014; Chang *et al*., 2004; DeFronzo, 1981; Saltiel and Kahn, 2001; Snel *et al*., 2012).

The insulin signaling pathway includes at least four insulin receptor substrate proteins (IRS-1/2/3/4), with IRS-1 and IRS-2 known to be closely linked to the actions of insulin and β-cell function (Chang *et al*., 2004; Greenberg and McDaniel, 2002; Kulkarni *et al*., 1999; Michael *et al*., 2000; Pessin and Saltiel, 2000). Knockout of IRS-2 and IRS-1 has been shown to cause IR, β-cell dysfunction and hyperinsulinemia, supporting that a signaling balance between IRS-1 and IRS-2 is necessary for normal β-cell function (Burks and White, 2001; Kahn, 1998). In essence, the phosphorylation of IRS activates

phosphatidylinositol 3-kinase-protein kinase B (PI3K/AKT) and mitogen-activated protein kinase (MAPK) pathways (D'Cruz *et al*., 2012). The PI3K/AKT pathway is activated downstream to insulin receptor and is involved in insulin's action on glucose uptake and gluconeogenesis suppression (D'Cruz *et al*., 2012). The MAPK pathway interacts with the PI3K/AKT pathway for cellular growth regulation and differentiation and is related to gene expression (D'Cruz *et al*., 2012; Schultze *et al*., 2012). The family of MAPKs, such as extracellular signal-regulated kinases (ERK1/2), c-Jun terminal kinases (JNK) and p38, are activated by cellular stressors e.g. free fatty acids (FFAs), interleukin 1-beta (IL-1-β), interleukin-6 (IL-6) and tumor necrosis factor-alpha (TNF-α) (Huang *et al*., 2009).

2.1.2. Insulin resistance

Insulin resistance (IR) is defined as the failure of insulin to facilitate glucose and lipid metabolism (Gual *et al*., 2005; Kahn *et al*., 2006; Muoio and Newgard, 2008). This leads to impaired fasting glucose (IFG), impaired glucose tolerance (IGT) and, subsequently hyperglycemia (Kim and Choi, 2010; Muoio and Newgard, 2008). Insulin resistance is associated with hyperinsulinemia resulting from the β-cell compensation mechanism which ultimately leads to the loss of β-cell function and T2D (Gual *et al*., 2005; Kahn *et al*., 2006; Muoio and Newgard, 2008). Beta-cell compensation promotes the deterioration of β-cell function, leading to β-cell exhaustion which, later causes β-cell death (Ferrannini *et al*., 2010; Talchai *et al*., 2012). Additionally, IR is associated with unfolded protein response known to upregulate genes involved in post-translational modification, mitochondrial stress and alleviation of endoplasmic reticulum (ER) stress (Bravo *et al*., 2013; Bravo *et al*., 2013; Hotamisligil and Erbay, 2008; Salvadó *et al*., 2015). Endoplasmic reticulum (ER) stress triggers the production and release of inflammatory cytokines, which in turn disrupt insulin signaling and induce chronic inflammation (Bailey-Bucktrout *et al*., 2013; Hasnain *et al*., 2012; Kawasaki *et al*., 2012; Zhang and Kaufman, 2008). Noteworthy, chronic inflammation is a pervasive feature of aging tissues and several age-related diseases e.g. T2D.

2.1.3. Pancreatic β-cell dysfunction and failure

Pancreatic β-cell dysfunction is central to the development of T2D (Bollheimer *et al*., 1998; Gastaldelli *et al*., 2004; Saltiel, 2012). There are five described β-cell dysfunction stages initially proposed by Weir and Bonner-Weir., (2004) in the progression to diabetes (as summarized in Figure 2). Stage one, known as the compensatory stage, is characterized by elevated insulin secretion to maintain normoglycemia in the face of IR, resulting from either of the following: obesity, physical inactivity or genetic predisposition (Figure 2) (Weir *et al*., 2001; Weir and Bonner-Weir, 2004). Increased insulin secretion results from increased β-cell mass, known to be regulated through a balance of β-cell birth (by β-cell replication and islet neogenesis) and β-cell death (by apoptosis or necrosis) (Assmann *et al*., 2009; Weir and Bonner-Weir, 2013). Literature has reported that β-cell apoptosis is the main cause of β-cell death (Augstein et al., 1998; Eizirik and Mandrup-Poulsen, 2001; Lally *et al*., 2001; Renehan *et al*., 2001; Yu and Chung, 2006). During this stage, increased β-cell mass is attributed to hyperplasia and hypertrophy (Weir and Bonner-Weir, 2013).

Stage two is known as stable adaptation where β-cells adapt to increased glucose levels (approximately 5.1-6.5 mmol/L), and is characterized by IFG as β-cells can no longer compensate (Figure 2) (Weir *et al*., 2001; Genuth, 2003; Weir and Bonner-Weir, 2004 Tripathy *et al*., 2019). In this stage, the loss of glucose stimulated insulin secretion (GSIS) occurs and is marked by changes in β-cell phenotype, caused by dysregulations in gene and protein expression of glucose-6-phosphatase, fructose-1,6-bisphosphatase, lactate dehydrogenase, and hexokinase as observed from diabetic ZDF rats (Bollheimer et al., 1998; Iizuka *et al*., 2000; Weir and Bonner-Weir, 2013, 2004). Furthermore, β-cell hypertrophy in the islets is known to occur (Weir and Bonner-Weir, 2004).

The third stage, known as unsteady early decompensation, is characterized by elevation in non-fasting glucose and fasting glucose levels, due to critical β-cell mass decline and/or increase in IR (Weir and Bonner-Weir, 2004). Thus, insulin secretion aberrations and dedifferentiation occur, even in the absence of a diabetes diagnosis. Processes involved in this stage include mild decompensation and decreased gene expression of glucose transporters and transcription factors, such as glucose transporter 2 (GLUT-2),

glucokinase, pyruvate carboxylase, pancreas duodenum homeobox-1 (PDX-1), V-maf musculoaponeurotic fibrosarcoma oncogene homologue A (MafA), hepatic nuclear factors (HNFs), NK6 Homeobox 1 (Nkx6.1) and paired box protein-6 (Pax6) (Iizuka *et al*., 2000; Gastaldelli *et al*., 2004; Weir and Bonner-Weir, 2004).

Stage four is stable decompensation categorized by severe hyperglycemia, loss of glucose and non-glucose secretagogues-induced insulin secretion. Also there is reduced β-cell mass, degranulation and increased expression of glucose-stress and oxidative-stress genes, inflammatory genes (explained in section 2.1.5), followed by the early onset of T2D (Figure 2) (Gastaldelli *et al*., 2004; Weir *et al*., 2001; Weir and Bonner-Weir, 2004; Lundberg *et al*., 2018).

Finally, the severe decompensatory state manifests (stage five), where profound and complete β-cell failure persists, with marked manifestation of a complete diabetic disease state where hyperglycemia, hyperinsulinemia, increased amylin, inflammation, apoptosis, amyloid deposits, complete degranulation and loss of functional β-cell mass occur (Figure 2) (Weir *et al*., 2001; Abdul-Ghani *et al*., 2006; Weir and Bonner-Weir, 2004; Genuth and Kahn, 2008). Increases in amylin (islet amyloid polypeptide) results in amyloid plaque formation, recently implicated as a contributing factor to β-cell dysfunction especially in relation to T2D (Hull *et al*., 2003; Weir and Bonner-Weir, 2013; Courtade *et al*., 2017).

Beta-cell dysfunction is a critical determinant for T2D development, however the interplay with IR remains highly complex. However, it is known that the onset of hyperglycemia has the ability to trigger both β-cell dysfunction and IR (Chen *et al*., 2016). Genome-wide association studies (GWAS) has conducted a lot of research to identify the genes that are associated β-cell dysfunction. To date more than 40 genes are known to increase the risk for T2D (Ashcroft and Rorsman, 2012; Esser *et al*., 2014).

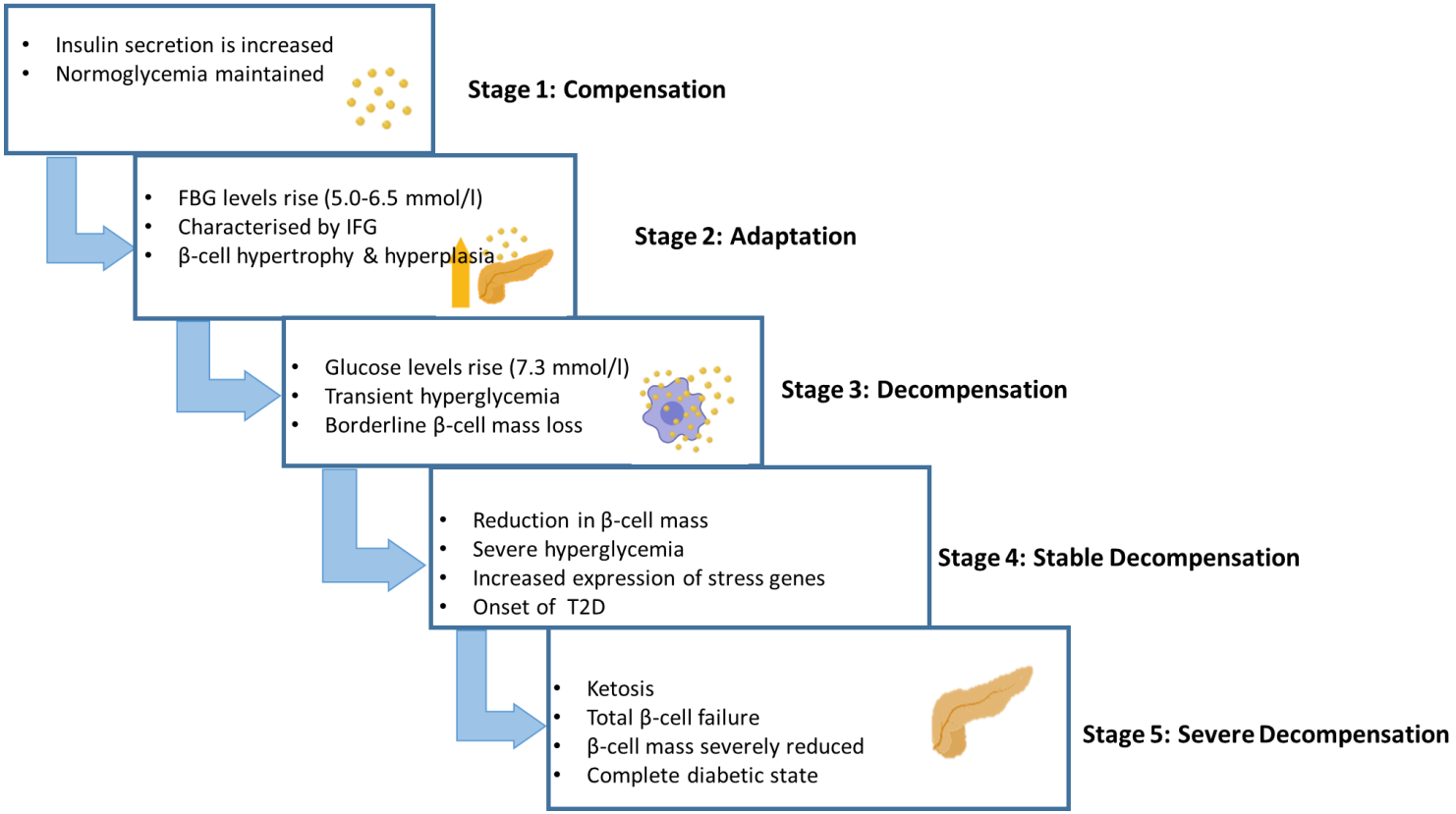

Figure 2:Schematic representation of the stages of β-cell dysfunction (Modified from Weir and Bonner-Weir., 2004).

2.1.4. The implications of Inflammation in β-cell dysfunction and failure

Inflammation is a major contributor to IR and is linked to increased adiposity and chronic elevations in blood glucose (Savage *et al* ., 2005; Wellen and Hotamisligil, 2005; Garg *et al*., 2012; Esser *et al*., 2014; Sandovici *et al*., 2016). Although inflammation primarily induces protective mechanisms vital for the well-being of an organism, chronic hyperstimulation of inflammatory responses has proven to be detrimental (Maedler et al., 2002).

Over stimulation of pro-inflammatory pathways drives pancreatic β-cell inflammation (Pradhan, 2001). Inflammatory markers such as tumor necrosis factor-alpha (TNF-α), C-reactive protein (CRP) and interleukins (IL-1β and IL-6) are positively correlated with IR (Pradhan, 2001; Vozarova *et al*., 2002 Ford, 2003). Interleukin-1-β is the most studied cytokine released by monocytes and resides in macrophages where pancreatic β-cells themselves are perceived to be a source of IL-1β in islets (Meier *et al*., 2014; Westwell-Roper *et al*., 2014; Li *et al*., 2017;). Signaling of IL-1β is mediated through IL-1 receptor type 1 (IL-1R1), which is abundant in β-cells and associated with β-cell sensitivity to IL-1β action (Garlanda et al., 2013). It is known that, increased glucose levels together with amyloid formation contribute to elevated IL-1β levels (Lundberg, 2000; Maedler *et al*., 2002; Park *et al*., 2012; Garlanda *et al*., 2013; Li *et al*., 2017). On the other hand, TNF-α induces IR by inhibiting IRS-1 signaling, causing a decrease in hepatic and skeletal muscle insulin stimulated glucose uptake and β-cell death (Beg and Baltimore, 1996; Hotamisligil *et al*., 1996; Van Antwerp *et al*., 1996; Hotamisligil and Erbay, 2008; Blaser *et al*., 2016) and also stimulates the activation of other pro-inflammatory cytokines such as IL-6 (Wang *et al*., 2017; Kwon and Pessin, 2018). Unlike TNF-α and IL-1β, literature has shown that IL-6 exerts both pro-inflammatory and anti-inflammatory effects by protecting pancreatic β-cells from pro-inflammatory cytokine-induced cell death and functional impairment *in vitro* and *in vivo* (Xing *et al*., 1998; Starkie *et al*., 2003; Steensberg *et al*., 2003; Choi *et al*., 2004; Kamimura *et al*., 2004).

2.1.5. Glucotoxicity

Glucose is important for the normal functioning of β-cells, as these cells have an ability to respond to glucose challenges due to adequate expression of several genes such as preproinsulin, GLUT-2, glucokinase (GCK), etc. (Bensellam *et al*., 2012). In contrast, when glucose is available in excess, as in the case of chronic hyperglycemia, it becomes paradoxically deleterious to pancreatic β-cell function and survival (Bensellam *et al*., 2012). Chronic hyperglycemia induces the loss of β-cell differentiation and increases the rate of β-cell apoptosis, along with increased expression of genes under-expressed in normal β-cells, leading to glucotoxicity (Augstein *et al*., 1998; Butler *et al*., 2007; Friedrichsen *et al*., 2006; Shi *et al*., 2011). Glucotoxicity is defined as the deleterious effects of prolonged supraphysiological glucose levels which causes a malicious cycle of progressive β-cell functional decline, β-cell loss and irreversible β-cell damage (Robertson *et al*., 2004, 2003; Hou *et al*., 2008; Zini *et al*., 2009). The latter contributes to progressive worsening of glucose intolerance and T2D patients (Buchanan, 2003; Weir *et al*., 2009). In β-cell function, chronic hyperglycemia effects include glucose desensitization, β-cell exhaustion and thus, glucotoxicity (Zini *et al*., 2009). Glucose desensitization is a rapid, reversible β-cell exocytotic mechanism occurring as a result of short exposure to elevated glucose. These elevated glucose levels reduce insulin secretion, where insulin secretion is not completely cut off but rather inhibited (Kilpatrick and Robertson, 1998; Poitout and Robertson, 2002; Robertson *et al*., 2007, 2004; Alnahdi *et al*., 2019), while β-cell exhaustion is the complete depletion of the freely releasable intracellular insulin pool after prolonged glucose/ other secretagogues exposure (Paolisso *et al*., 1995; Kilpatrick and Robertson, 1998; Maedler *et al*., 2002; Seino *et al*., 2011). A clear distinction between glucose desensitization, β-cell exhaustion and glucose toxicity has been described by many researchers (Sako and Grill, 1990; Buchanan, 2003; Robertson *et al*., 2007; Kahn *et al*., 2014). Glucotoxicity is categorized into early and final stage glucose toxicity, each marked by a decline in β-cell functional mass and dysregulations in glucose induced genes (Kahn, 1998; Burcelin *et al*., 2003). Mechanisms underlying β-cell glucotoxicity have been described by many and these include: β-cell overstimulation prompted by either IR, IGT, hyperglycemia and / or prolonged high glucose stimulation (Gadot et al., 1995; Ling *et al*., 2003), resulting to impaired GSIS as

a consequence of defects in insulin biosynthesis (Gadot *et al*., 1995; Paolisso *et al*., 1995; Ling *et al*., 2003). Furthermore, a link between oxidative stress and glucotoxicity exists since β-cells express low levels of principal antioxidant enzymes: superoxide dismutase (SOD), glutathione peroxidase (GPX) and catalase (CAT) (Tonooka *et al*., 2007; Modak *et al*., 2009). Various *in vitro* and *in vivo* models have shown that antioxidants protect β-cells against the deleterious effects of high glucose levels, by improving insulin secretion and regulating insulin gene expression (Banday *et al*., 2005; Houstis *et al*., 2006; Blouet *et al*., 2007),and enhancing β-cell survival (Kaneto *et al*., 2005a, 2005b; Robertson *et al*., 2003). In addition, endoplasmic reticulum (ER) plays a pivotal role in a number of biological activities, but a dysfunction in ER result in ER stress (Novials *et al*., 2014) through exaggerated activation of unfolded protein response (UPR), subsequently causing β-cell apoptosis (Scheuner and Kaufman, 2008; Oslowski and Urano, 2010). β-cells are sensitive to ER stress due to their high rate of proinsulin biosynthesis. Therefore, glucotoxicity can be identified by the expression of early high glucose-induced stress genes including heme-oxygenase 1 (Hmox1) and metallothionein 1a (Mt1a) (Jonas *et al*., 2003; Pascal *et al*., 2010; Bensellam *et al*., 2012), a decrease in expression of glucose-dependent network of genes and transcription factors such as glucose transporter-2 (GLUT-2), pre-proinsulin, pancreas duodenum homeobox-1 (PDX-1), V-maf musculoaponeurotic fibrosarcoma oncogene homologue A (MafA), and neurogenic differentiation 1 (NeuroD1) (Bensellam *et al*., 2012) and an increase in β-cell dedifferentiation (Matsuoka *et al*., 1997; Poitout and Robertson, 2002; Robertson *et al*., 2003; Bensellam *et al*., 2012).

2.1.6. The role of amylin and beta secretase

Islet amyloid polypeptide (IAPP) is a major component protein of islet amyloid plaques which have been found in more than 80% of T2D patients (Westermark *et al*., 2011; Cao *et al*., 2013). Hyaline lesions of the pancreas, later identified as amyloid were first described approximately 100 years ago (Cao *et al*., 2013; Opie, 1901). Initially the deposits were presumed to be composed of both insulin/pro-insulin and insulin fragments (Clark *et al*., 1989). However, in 1987 it was shown that the major protein component of

islet amyloid is a 37-residue pancreatic hormone known as amylin (Westermark *et al*., 1986; Cao *et al*., 2013; Stridsberg *et al*., 1993).

2.1.6.1. Amylin secretion and function

Amylin is synthesized as an 89-residue pre-prohormone (Sanke *et al.*, 1988), followed by the removal of a 22-residue signal peptide by TMEM27. This leads to a 67-residue pre-IAPP which is enzymatically cleaved by pro-protein convertase-1/3 (PC1/3), PC2 in the Golgi apparatus forming a 37-residue mature hormone (Badman *et al.,* 1996; Higham *et al*., 2000; Marzban *et al*., 2006). Amylin is stored with insulin in the β-cell secretory granules and is co-secreted with insulin at a ratio of 1:100 in response to β-cell stimulation by glucose / other similar secretagogues (Westermark *et al*., 1987; Clark *et al*., 1989; Stridsberg *et al*., 1993; Cao *et al*., 2013; Zhang *et al*., 2016). Amylin inhibits glucose release from the liver through a reduction of glucagon secretion and delays gastric emptying, subsequently improving postprandial glucose and insulin secretion (Gedulin *et al*., 2006; Young, 2005; Paulsson *et al*., 2014). Known functions of amylin are highlighted in Table 1.

Table 1: Roles of Amylin as studied in various experimental models documented thus far

Model used	Associated with T2D	Role of amylin	Reference
***In vitro* rat hepatocytes**	Insulin resistance	High concentrations of amylin impair glucose utilization	(Leighton and Cooper, 1988; Rafacho *et al.*, 2014)
Rat pancreatic islets	Insulin resistance in skeletal muscle	Amylin impair insulin secretion	(Ohsawa *et al*., 1989)
Rat pancreas	Inhibition of insulin response	Amylin controls insulin secretion	(Stridsberg *et al*., 1993; Rafacho *et al.*, 2014)
Neonatal rat islet cultures		IAPP-LI is released by non-diabetic neonatal rat islet thus is a normal β-cell product	*(Kahn et al., 1990; Lukinius et al*., 1996)
Pancreas from h-IAPP transgenic mouse	β-cell dysfunction Insulin resistance Impaired fasting glucose	Amyloid plaques species elicit β-cell dysfunction and apoptosis	(Kayed, 2003; Li and Hölscher, 2007; Courtade *et al*., 2017)
Diabetic macaques	Impaired glucose tolerance Impaired fasting glucose	Amylin increases with reduction in insulin secretion and increase in glucose intolerance	(Leighton and Cooper, 1988; Westermark *et al*., 2011)

2.1.6.2. Amyloid plaque formation

Amyloid deposits formed from polymerized amylin progressively accumulate in the islets of T2D patients (Courtade *et al*., 2017). While, accumulation of amyloid deposits does not cause the onset of hyperglycemia in T2D, they are greatly associated with islet cell destruction and diminished islet function as the disease advances (Novials *et al*., 2014; Potter *et al*., 2015; Courtade *et al*., 2017). The causal factors for the first formation of amyloid plaques is unknown but continued hyperinsulinemia and elevated amylin secretion due to IR and or nutrient over-stimulation, promotes binding of amyloid to preformed plaques and the extension of amyloid deposits (Clark *et al*., 1989, 2004; Kayed, 2003). Additionally, enzymatic processing of amylin carried out by β-secretase (BACE) enzyme has been implicated in amyloid formation (Courtade *et al*., 2017). Because amylin exists unfolded in its monomeric state, any abnormalities in folding contribute to amyloid formation and aggregation, which disrupts islet and amylin function leading to islet amyloidosis, β-cell dysfunction and subsequent T2D development (Kahn *et al*., 1990; Clark *et al*., 2004; Cao et al., 2013; Novials *et al*., 2014; Courtade *et al*., 2017). Amylin aggregation is hypothesized to play an important role in β-cell loss in T2D as well as T1D transplanted pancreatic islets (Westermark *et al*., 2011). Thus, strategies that prevent amyloid formation can prolong graft survival and/or existing islets in T2D patients subsequently preventing β-cell loss (Westermark *et al*., 2011; Courtade *et al*., 2017).

2.1.6.3. Beta-secretase and amyloid plaque formation

BACE 1 is a 501-amino acid-long glycosylated type I transmembrane endoprotease with an important role in myelin sheaths formation in peripheral nerve cells and plays a role in the aggregation of amyloid following cleavage of amyloid protein precursor (Sinha *et al*., 1999; Vassar, 2004; Hampel *et al*., 2010; Willem *et al*., 2015). This protease contains two active site aspartate residues located extracellularly and may function as a dimer. BACE1 has earned its popularity as the major enzyme involved in cellular pathways that result in AD pathogenesis, dementia and impaired cognitive-related diseases (Vassar, 1999; Casas *et al*., 2010). Recent studies have strongly hypothesized that BACE1 has a role in T2D by regulating amyloid plaque deposition (Shen *et al*., 2018), since in theory, BACE inhibitors may slow and/or stop AD development and T2D by preventing the build-up and formation of amyloid plaques (Vassar, 2004; Hampel *et al*., 2010; Esterházy *et al*., 2011).

BACE2 is a closely related homolog of BACE1 known to cleave the variant of Alzheimer's amyloid precursor protein. Unlike its homolog, known to be highly expressed in neurons, BACE2 is minimally expressed in the central nervous system and highly expressed in peripheral tissues including the pancreas where it has a physiological role (Bennett *et al*., 2000). Although BACE2 can cleave amyloid at β-sites, it is more commonly associated with cleavage in sites of α-secretase (Farzan *et al*., 2000; Fluhrer *et al*., 2002; Alcarraz-Vizán *et al*., 2017). BACE2 suppression has been reported to promote β-cell survival and function in a T2D model overexpressing human islet amyloid polypeptide (hIAPP) (Alcarraz-Vizán *et al*., 2017).

2.2. Conventional antidiabetic drugs

The primary line of T2D treatment involves the use of oral anti-diabetic therapeutics in combination with recommendations of increased physical activity and healthy eating habits. These therapeutics have proven to be effective either alone and/or in combination with lifestyle changes to manage the disease (Ferriolli *et al*., 2014).

Biguanides, such as metformin, which is the most commonly used drug for T2D treatment, are the first line of T2D drugs. Metformin actively decreases hepatic gluconeogenesis and glycogenolysis in T2D patients (Viollet *et al*., 2012; Woo *et al*., 2014; Wu *et al*., 2014).

Metformin also improves insulin secretion, subsequently positively affecting glucose uptake in skeletal muscles (Jiang *et al*., 2014). More so, it activates AMP-activated protein kinase (AMPK), which is important for the expression of genes related to hepatic gluconeogenesis and therefore improving glucose tolerance (Kim *et al*., 2012).

Sulfonylureas, such as glimepiride have a mode of action involving stimulation of insulin secretion through inhibition of potassium influx via ATP dependent potassium channels in pancreatic β-cells (Miyazaki *et al*., 2002).

Alpha glycosidase inhibitors inhibit α-glucosidase enzymes to delay the absorption of sugars in the gut (van de Laar, 2008). These are anti-hyperglycemic drugs that enhance the action of G-protein-coupled bile acid receptor-1 (TGR5), resulting in increased secretion of glucagon-like peptide-1 (GLP-1) and hepatic glycogenolysis inhibition, thus improving insulin sensitivity (Handelsman, 2011; Nwose and Jones, 2013).

Thiazolidinediones (TZDs) are commonly renowned as insulin sensitizers acting through the activation of peroxisome proliferator-activated receptor-γ (PPAR-γ) which promotes the uptake of fatty acids in adipose tissues (Quinn *et al*., 2008). In pancreatic β-cells, they improve function by increasing insulin sensitivity and reducing lipid accumulation in the pancreas (Kawasaki *et al*., 2005).

Dipeptidyl peptidase-4 (DPP-4) inhibitors are the last anti-diabetic drug class that are used in the management of T2D (Pratley and Salsali, 2007; Baetta and Corsini, 2011). These drugs promote normal glucose secretion while preserving the structure and the integrity of β-cells via blocking DPP-4 enzyme action (Pratley and Salsali, 2007).

Although current anti-diabetic drugs are effective, their use is hindered by their ability to treat the disease state due to patient compliance issues, the lack of systemic efficacy and adverse side effects (Ku *et al*., 2015). Some major side effects associated with these drugs include gastrointestinal discomfort (metformin & glucagon-like peptide-1 agonists), hypoglycemia and weight gain (sulfonylureas); bladder cancer risk, edema, heart failure and weight gain (pioglitazone) (McClean *et al*., 2010; Hampp *et al*., 2014; Lewis *et al*., 2015). More so, these therapeutics do not directly protect β-cells from pathophysiological factors they experience in T2D. Therefore, traditional plant-based products are being

studied for their beneficial properties (Ekor, 2014; Waisundara and Hoon, 2015). In addition, plant polyphenols such as flavonoids have been reported to reduce β-peptide levels through secretase-mediated amyloid polypeptide modulation (Baptista *et al*., 2014; Cox *et al*., 2015). Therefore, it becomes crucial to explore the effect of Rooibos in a glucotoxic aged β-cell model and an obese diabetic model with particular focus on BACE inhibition.

2.2.1. Rooibos-based potential therapeutic

Aspalathus linearis (*A. linearis*), commonly known as Rooibos, is a South African indigenous plant found in the Cederberg area of Western Cape province (Joubert *et al* ., 2008). The beneficial effects of Rooibos are well reported and are attributed to its phenolic composition, specifically the dihydrochalcone C-glucoside, aspalathin (Figure 44, Appendix I). The activities of Rooibos include the following: anti-oxidant (Joubert and de Beer, 2011; Sanderson *et al*., 2014; Monsees and Opuwari, 2017), cancer modulating (Joubert and de Beer, 2011; Marnewick *et al*., 2005; Canda *et al*., 2014; Johnson *et al*., 2016), hepatoprotective (Beltrán-Debón et al., 2011), *in vitro* and *in vivo* evidence of anti-obesity (Beltrán-Debón *et al*., 2011; Muller *et al*., 2012; Ajuwon *et al*., 2013; Sanderson *et al*., 2014), anti-inflammatory (Ajuwon et al., 2013), anti-mutagenic (Canda et al., 2014), anti-lipogenic (Beltrán-Debón et al., 2011; Sanderson et al., 2014), anti-diabetic (Muller *et al*., 2012; Ajuwon *et al*., 2013; Mazibuko *et al*., 2013) and hypoglycemic effects (Kawano *et al*., 2009; Beltrán-Debón *et al*., 2011; Kamakura *et al*., 2015). In particular, Aspalathin, have been shown to increase the bioactivity of the plant (Joubert and de Beer, 2011, Kawano *et al*., 2009, Muller *et al*., 2012, Son *et al*., 2013). Additionally, Aspalathin has been proven to have several activities such as, glucose lowering (Muller *et al*., 2012; Snijman *et al*., 2009), ameliorated palmitate insulin-resistance (Mazibuko *et al*., 2013; Son *et al*., 2013), anti-oxidant (Snijman *et al*., 2009) and anticoagulant (Ku *et al*., 2015a). Of particular interest in this study are the anti-inflammatory and glucose lowering effects of Rooibos. Rooibos lowered TNF-α, IL-6 and NF-κB (nuclear factor kappa-light-chain-enhancer of activated B cells) responses in models of diabetic vascular inflammation (Ku *et al*., 2015).

2.3. Laboratory based models in diabetes research

Cell culture has been employed for over a decade to answer research questions in various fields (Figliolini *et al*., 2014; Zanoni *et al*., 2016). However, one limitation for the use of primary human β-cells in biochemical and molecular research is the availability of pancreatic tissue as well as cellular and hormonal heterogeneity from donors (Shahjalal et al., 2018). Technical challenges known to be limiting factors include the isolation, purification and maintenance of the isolated tissues from donors. *In vitro* cell culture and *in vivo* animal models are available, and these are discussed below. These models allow researchers to investigate cell biology, tissue morphology, mechanisms of diseases, drug actions and interactions and protein production to answer basic and advanced research questions (Barré-Sinoussi and Montagutelli, 2015).

2.3.1. *In vitro* pancreatic β-cell models

Cell cultures studies *in vitro* provide an opportunity for the assessment of physiological and pathophysiological processes prior to translating the findings to *in vivo* models. Furthermore, cell lines allow researchers to study treatment effects under different conditions potentiating the discovery of new therapeutics (Macdonald, 1990; Skelin, 2010). Immortalized cell lines represent cell populations with an ability to continuously undergo division, not limited by the “Hayflick” limit initially proposed by Leonard Hayflick. These cells, therefore, are employed in numerous *in vitro* research (Shay and Wright, 2000). Because the majority of immortalized cell lines used are of tumourogenic origin, they may have genetic mutations, altered chromosomal content and protein expressions, and thus modified metabolic profiles (Macdonald, 1990). Over time, these changes may indicate that cell lines are indeed not without disadvantages, thus highlighting the need for the use of animal models to validate *in vitro* findings. There are various β-cell lines that are used in research, however none of them entirely mimics human β-cell physiology. However they are still valuable in investigating molecular mechanisms underlying β-cell function and dysfunction (Skelin, 2010). Insulin-secreting cell lines popularly employed in β-cell studies are rat insulinoma cells (RIN), hamster pancreatic β-cells (HIT), transgenic C57BL/6 mouse insulinoma cells (MIN), beta-tumor cells (βTC) and rat insulinoma cells

(INS-1). Each cell line presents with both advantages and disadvantages as detailed in Table 2.

Table 2: Commonly used *in vitro* β-cell lines and their advantages.

Cell line	Origin	Species	Advantage	Disadvantage	References
RIN	Insulinoma	Rat	Responsive to normal range of glucose levels	Abnormal properties of glucose transport and/or phosphorylation and exhibit abnormal glucose sensitivity. Insulin level decreases with induced passages.	(Gazdar *et al*., 1980; Praz *et al*., 1983)
HIT	Insulinoma	Hamster	Expresses membrane bound granules	Has a low insulin content Not all HIT subclones respond to glucose stimulation	(Santerre *et al*., 1981).
MIN	Insulinoma	Mouse	Contains a mixture of endocrine cells; Express glucokinase and GLUT-2	Treatment with nicotinamide activates response to glucose; loss of glucose-induced insulin secretion as passage goes high	(Miyazaki *et al*., 1990; Ishihara *et al*., 1993)
βTC	Hyperplastic islets	Mouse	expresses GLUT-2 and glucokinase	Increased hexokinase activity. Glucose stimulation response lost with increased passage	(Efrat *et al*., 1988; Liang *et al*., 1996; Efrat, 2004)
INS-1	Insulinoma	Rat	Responsiveness to glucose within physiological range; high insulin content	Mercaptoethanol required in the culture media	(Asfari *et al*., 1992)

2.3.2. Three-dimensional (3D) culture

Traditional two-dimensional (2D) culturing systems have been widely employed as models for *in vitro* studies. However, efficiency of these models is questionable due to the species specificity and the lack of adequate representation of *in vivo* state (Baharvand *et al.*, 2006; Huh *et al*., 2011). Cell structure behaviour, and functional preservation is vital in ensuring that the responses observed represent responses in the mammalian body. Furthermore, by using a single cell line, heterogenous cell-to-cell interaction is absent, which influences other cellular mechanisms and cell functions. The latter may explain why some pancreatic β-cell lines present with impaired secretory properties and are unable to respond to glucose under normal physiological conditions (Skelin, 2010).

As such, over the years researchers have been drawn to the use of three dimensional (3D) culturing systems as an alternative to *in vitro* models that can be more closely translated into *in vivo* models due to physiological relevance which vastly improves prediction made by cell-based assays (Sabra and Vermette, 2013). Cells grown in a 3D culturing systems have proven to be more physiologically relevant with improvements in several biological mechanisms such as high fidelity, viability, morphology, proliferation, differentiation, response to drugs, gene expression and long term maintenance, the latter being important in relation to aging (Levenberg *et al*., 2003; Haycock, 2011; Ravi *et al*., 2015; Jacobi *et al*., 2017). Three dimensional cultures create an artificial environment in which biological cell lines are permitted to grow in fabricated devices creating 3D structures that mimic tissue and/or organ microarchitecture, thus resulting in physiological characteristics closer to that seen *in vivo* (Chang and Hughes-Fulford, 2009; Fey and Wrzesinski, 2012; Gauvin *et al*., 2012; Fennema *et al*., 2013; Jacobi *et al*., 2017). Recently, improved methodologies capable of producing 3D models of tumors, C3A spheroids and other cell lines have been reported (Choi *et al*., 2015; D'Avanzo *et al*., 2015; Kim *et al*., 2015; Jacobi *et al*., 2017). These methodologies include extracellular matrix-based 3D system, 3D matrix scaffold as single cells or aggregates, clinostatic 3D BioArray Matrix (BAM) system, and organ on chip technology.

One of the most important advantages of 3D culturing systems is their ability to allow for uninterrupted culture of cell-derived spheroids for longer periods than conventional

cultures would permit, therefore allowing a model that is representative of aging. Spheroids tend to grow in constant contact without the requirement of regular passaging which tends to be straining and usually subjects cells to stressful conditions such as shear force (Fey and Wrzesinski, 2012; Wrzesinski and Fey, 2013). Other advantages of 3D culture over 2D culturing include the following: a low-turbulence, low-shear force, preserved morphology and way of divisions, expression of genes and biochemistry of cells as *in vivo* (Powers et al., 2002; Ravi *et al*., 2015; Wrzesinski and Fey, 2015). Although, 3D cultures offer some crucial benefits, there are drawbacks into their use including: more expensive, time-consuming, labor intensive, repeatability and variable access to oxygen and nutrients (Frieboes *et al*., 2006; Breslin and O'Driscoll, 2013; Krishnamurthy and Nör, 2013; Wrzesinski and Fey, 2015).

2.4. *In vivo* models of T2D

Rodent animal models have been widely used to conduct T2D research (Samuels *et al* ., 2015) with the leptin deficient *ob/ob* mice, Zucker diabetic fatty rats, JCR: LA-CP rats and leptin receptor deficient obese Lepr *db/db* mice being models extensively used (Samuels *et al* ., 2015). Genetically modified animal models of T2D are mostly used in T2D research because they spontaneously develop diabetes, thus researchers do not need to use time consuming feeding processes to induce diabetes in these animals (Islam and Wilson, 2012; Ernst *et al* ., 2013; Samuels *et al* ., 2015). Moreover, such animals allow researchers to perform experiments much faster than they can in humans, since rodents are known to age and metabolize more rapidly (Srinivasan, 2007).

2.4.1. Homozygous obese diabetic *db/db* mice

The homozygous Lepr *db/db* mouse model is spontaneously obese and develops IR and T2D (Srinivasan and Ramarao, 2007). This mouse model carries a deleterious point mutation in the leptin receptor gene resulting in hyperphagia, hyperglycemia, hyperinsulinemia and obesity (Kobayashi *et al*., 2000; Dalbøge *et al*., 2013; Ernst *et al*., 2013; Wang *et al*., 2014; Burke *et al*., 2017). The model represents a phenotype like that observed in patients with T2D (Kawano *et al*., 2009; Ernst *et al*., 2013; Zheng *et al*., 2015). Leptin is a hormone that is secreted by adipose tissue with a role in appetite and energy homeostasis regulation (Friedman and Halaas, 1998; Patton and DeGolier, 2010; Wang

et al., 2014). When leptin binds to leptin receptor, a signaling pathway is initiated, so the loss or disruption of the leptin signaling as in the case of *db/db* mice, induces several physiological abnormalities such as a disturbance in the hypothalamus (Wang *et al*., 2014). Both insulin and leptin have receptors located in the hypothalamus and literature has shown that leptin inhibits insulin secretion by activation of PI3K-dependent phosphodiesterase 3B (PDE3B) and by decreased cAMP levels (Belgardt *et al*., 2010; Wang *et al*., 2014) Disturbances in leptin signaling cause progressive metabolic deterioration including hyperphagia, glucose intolerance, hyperglycemia, hyperinsulinemia, obesity and T2D (Chen *et al*., 1996; Ritchie *et al*., 2008; Kawano *et al*., 2009; King, 2012; Dalbøge *et al*., 2013; Wang *et al*., 2014). The use of the *db/db* mouse model allows for the screening of non-toxic compounds without the worry of side effects associated with chemical diabetes inducers e.g. alloxan and streptozotocin (STZ) (King, 2012). Moreover, the use of this *in vivo* animal model is useful in representing the complexity and heterogeneous conditions that are associated with obesity including IR, dyslipidemia and T2D (Srinivasan and Ramarao, 2007). Be that as it may, *db/db* mice have a short life span, making it difficult to investigate the long-term complications of T2D and increased leptin plasmatic level, and this is related to other physiological processes like immune response modulation, reproduction, and oncogenesis (Wang *et al*., 2014). More so, leptin signaling is greatly linked with diabetes in rodents but has been reported less critical in humans (Veniant and LeBel, 2003).

2.5. Hypothesis

We hypothesized that the protective effects of Rooibos on pancreatic β-cells involves the modulation of BACE activity, thereby protecting pancreatic β-cells against IAPP-induced toxicity associated with aging and T2D. Furthermore, we hypothesized that a correlation exists between circulating BACE and BACE expression in the pancreata of *db/db* mice.

2.6. Aim of the study

The aim of this study is to determine the effect of Rooibos extract (GRT™) on pancreatic β-cell survival *in vitro* and *in vivo*, with a special focus on BACE modulatory properties related to β-cell aging.

2.7. Objectives

In order to address the aim of the study, we have assessed the role of BACE activity as a therapeutic target in aging pancreatic β-cells using two experimental models with specific objectives enlisted below:

2.7.1. *In vitro* model

- Establishing long-term INS-1 β-cell spheroids using a clinostatic BAM 3D culture system to confirm the role of BACE in pancreatic β-cell aging.
- Determine if an aspalathin-enriched, unfermented Rooibos extract (GRT™), inhibits BACE activity.
- Assess viability and function of the INS-1 pancreatic β-cell spheroids.
- Determine the molecular mechanisms underlying the effects of BACE and aging β-cells.

2.7.2. *In vivo* model

- Assess the effect of GRT™ on pancreatic β-cell survival in *db/db* mice, with a focus on BACE modulatory properties.
- Evaluate molecular mechanisms and morphology through analysis of pancreata.

CHAPTER THREE

Materials and Methods

3.1. Research design

To address the aim of the study, an extensive *in vitro* component was designed in a laboratory environment that mimics aged pancreatic β-cell pathophysiology (Figure 3). For this model, a rat insulinoma pancreatic β-cell line INS-1 was cultured in RPMI-1640 media containing 10% FBS in a clinostatic three dimensional (3D) BAM culture system previously described by Fey *et al*., 2013. This was used to develop a long-term functional 3D pancreatic β-cell spheroid culture model. 3D culture was used since the spheroids are known to physiologically more closely resemble *in vivo* tissues and cells. 3D cultures allow for long-term culture without disruptive sub-culture, a characteristic feature that is lacking in the traditionally used two-dimensional culturing systems. Additionally, it allows for chronic treatment of spheroids. Subsequently, glucotoxic conditions were induced by high glucose (HG-33 mM glucose) where two of the HG groups were treated simultaneously as follows: high glucose treated with an aspalathin-rich unfermented Rooibos extract (HG-GRT™), the highest concentration of 1000 µg/mL with inhibitory effect determined during the non-cell based assay and with BACE inhibitor LY2886721 (HG-BACE), used at a concentration of 39 µM. Media containing optimal physiological glucose levels were used as a normal control (NG-11 mM glucose). Treatment was administered for 16 days during which cell survival and viability was assessed using the following assays and techniques: Light microscopy (LM), transmission electron microscopy (TEM), cellular ATP content, size profiling and glucose utilization. Functional parameters were assessed, using insulin and amylin secretion in response to glucose stimulation as well as the secretion of pro-inflammatory cytokines following short and long-term glucotoxicity induction. Furthermore, the expression of proteins of interest relating to β-cell function and survival was assessed by Western blotting. To further supplement our findings, a non-cell-based assay was used to kinetically assess the BACE inhibitory activity of GRT™ in a purified BACE enzyme assay.

To substantiate our 3D *in vitro* findings, six-week-old C57BLKS obese diabetic Lepr *db/db* mice and their lean non-diabetic *db*+ littermates were treated with GRT™ and BACE inhibition to assess amelioration of hyperglycemic induced changes in the pancreas (Figure 9). These mice were randomized into three experimental phases: Phase I (10 weeks treatment : with 40 *db*+ and 40 *db/db* mice); Phase II (16 weeks treatment: with 40 *db*+ and 40 *db/db* mice) and Phase III (32 weeks treatment: with 40 *db*+ mice only). For each phase, the mice were divided into five treatment groups (n = 8) as follows: Normal control (untreated), pioglitazone 15 mg/kg/day; BACE Inhibitor 30 μM/kg/day; GRT™-1 74 mg/kg/day and GRT™-2 740 mg/kg/day. The two concentrations of GRT™ used such as GRT™-2 (740 mg/kg/day) was calculated based on the translated 60 mg/kg/day dose and a 10 x lower dose, GRT™-1 (74 mg/kg/day) calculated and adjusted for mice using FDA approved formula for animal to human dose translation (Reagan-Shaw et al., 2008). All treatments were administered by mixing with ground rodent food. Body weight, fasting blood glucose and food intake were monitored over the course of the treatment phases. An oral glucose tolerance test (OGTT) was performed a week prior to respective terminations in each phase. Pancreata and blood were collected for post-mortem analysis.

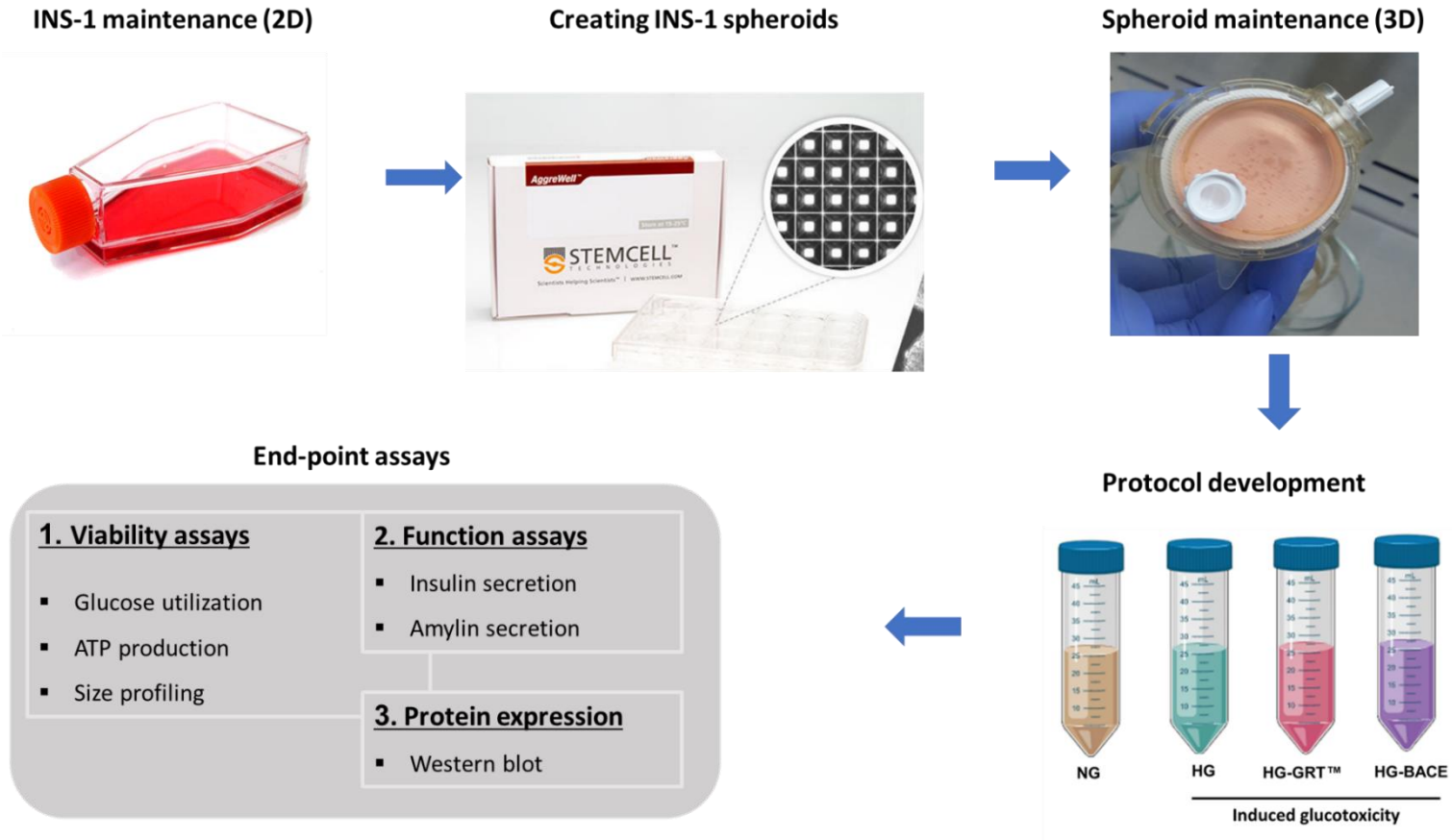

Figure 3: *In vitro* experimental design overview. Pancreatic beta INS-1 cells were cultured and grown into 3D β-cell spheroids under standard culture conditions (section 3.3.4.) and seeded into an AggreWell™ 400Ex plate to form cell aggregates (section 3.3.6 - 3.3.7.). Thereafter, were assayed for viability (section 3.4.1), functionality (section 3.4.3 - 3.4.6.) and protein expression (3.4.5.) following exposure to normal glucose (NG), high glucose (HG) and subsequent treatment with GRT™ (HG-GRT™) and a beta secretase inhibitor (HG-BACE) for 16 days. (ATP – adenosine triphosphate).

3.2. Source of extract, cell line and animal model

The green Rooibos extract (GRT™) used was from Afriplex (Pty) Ltd and this standardised extract was selected based on its high aspalathin content. Rat insulinoma derived INS-1 pancreatic β-cells used in this study were a kind gift from Professor Luc Bouwens, Vrije Universtiteit, Brussels, Belgium. Mice were sourced from Jackson Laboratories Pvt Ltd. and housed at the Primate Unit and Delft Animal Centre (PUDAC) of the South African Medical Research Council. Suppliers and catalogue numbers of consumables, reagents, kits and equipment's used in this study are detailed in Appendix A-E.

3.3. *In vitro* experiments

3.3.1. Cell culture

All experiments were performed under standard tissue culture conditions unless otherwise specified. These included the use of sterile incubators at standard culture conditions (37 °C temperature with 5% carbon dioxide and humidified air). A sterile biological safety cabinet and 70% ethanol were used to maintain sterility. As recommended by American Type Culture Collection (ATCC), INS-1 cells are cultured in RPMI medium which contains 11 mM glucose (Appendix for medium composition) and as such regarded as the optimal physiological glucose concentration for culturing this cell line.

3.3.2. Thawing of INS-1 cells

INS-1 cells were removed from liquid nitrogen storage and thawed by placing in a 37 °C circulating water bath for 1 minute until there was just a small piece of ice left in the vial in a circulating water bath. After sterilizing the outside of the vial with 70% ethanol, the cell suspension, originally frozen at 2.0 x 10^6 cells per mL of DMSO/complete growth media (RPMI-1640 containing 10% fetal bovine serum (FBS), was carefully transferred into 10 mL prewarmed (37 °C) complete growth media in a biological safety cabinet, followed by centrifugation at 800 × *g* for 5 minutes. Thereafter, the supernatant was aseptically decanted without disturbing the pellet and the pellet resuspended in 6 mL prewarmed (37 °C) complete growth media and transferred into a 75 cm^2 flask containing 12 mL complete growth media. The cell suspension was gently pipetting up and down several times and then incubated at standard culture

conditions. For this study sub-culturing of cells was limited to 10 passages (between passages 19 and 29), in order to prevent phenotypic drift.

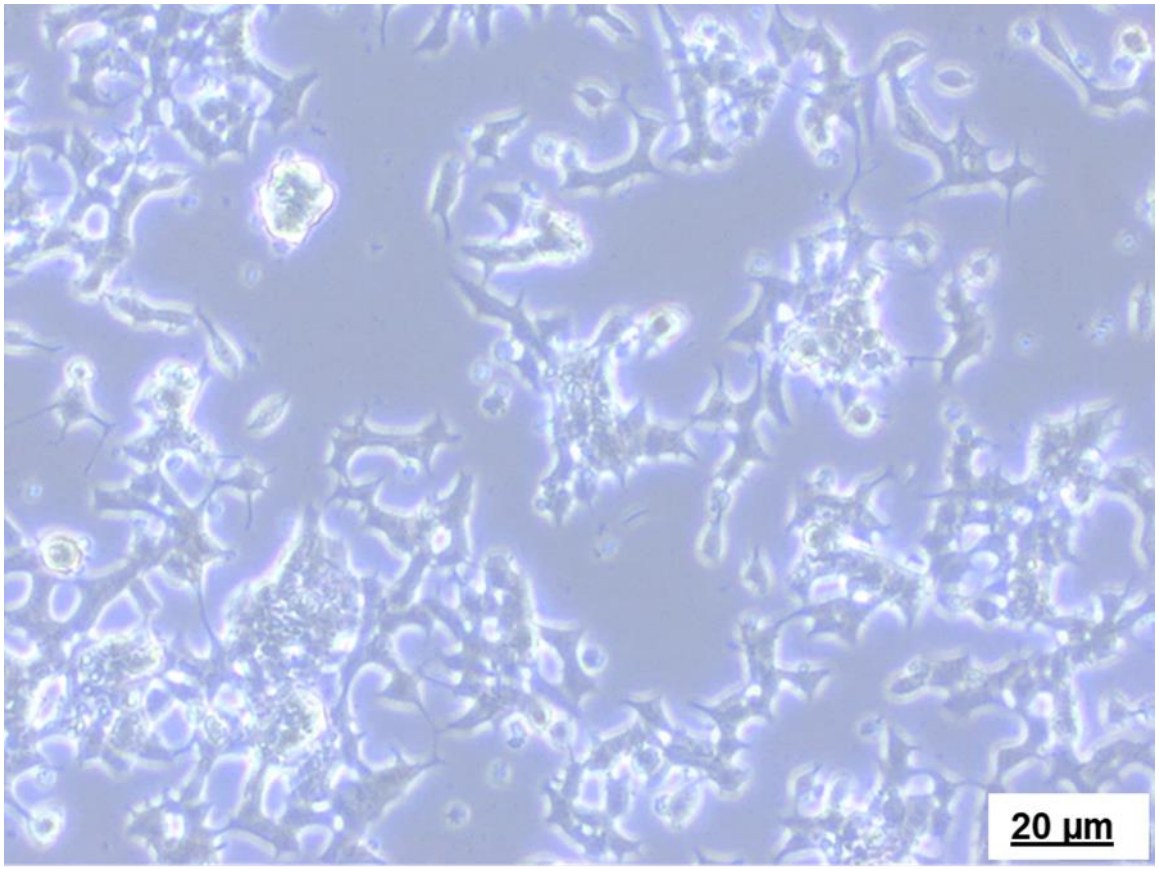

Figure 4: INS-1 cell cluster in culture. INS-1 pancreatic β-cells were grown in complete growth media at 37 °C in humidified air containing 5% CO_2 where media was refreshed every 2-3 days. The cell growth was monitored daily by observing under a microscope and the cells passaged when their confluency was greater than 75%.

3.3.3. Counting cells

A 20 µL sample of cell suspension was stained 1:1 with 0.4% trypan blue in Dulbecco's phosphate buffered saline (DPBS) and cells counted on a hemocytometer (Figure 5). Briefly, approximately 10 µL of the trypan blue/cell suspension was pipetted under the coverslip of the hemocytometer and counted using an inverted light microscope (10 x magnification) in four of the 1 mm^2 grid chambers (Figure 5). The average of the four counts (N) was used to determine the number of cells per mL in the diluted sample (D). The following formula was used:

A. $$\text{Cells/mL} = \frac{\text{Average count per mm}^2\ (1.1\ \text{cell suspension and trypan blue solution})}{\text{Volume counted (1x1x0.1mm= 0.1µL)}}$$

B.

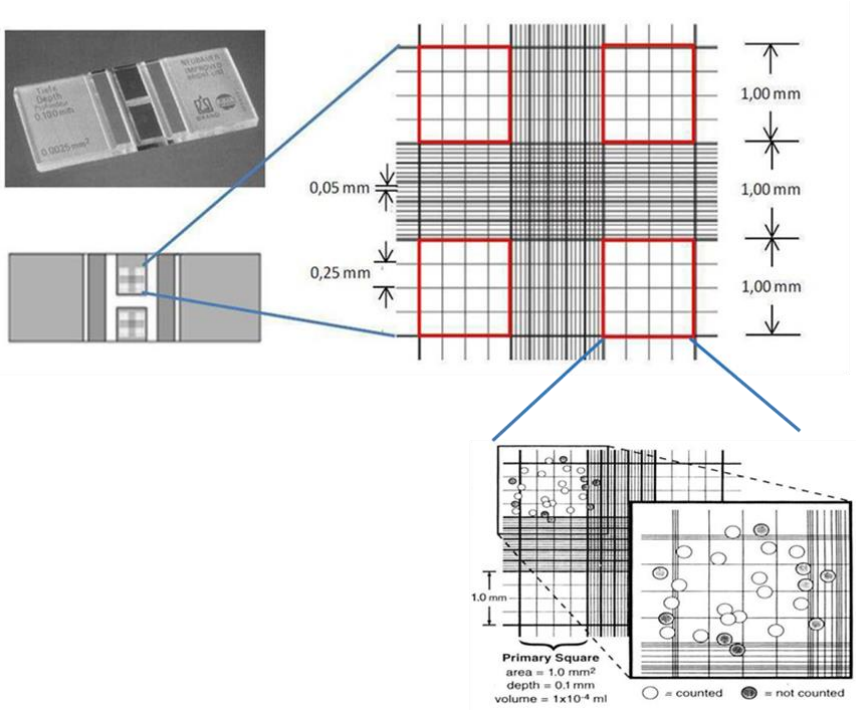

Figure 5: Schematic illustration of a hemocytometer chamber and a 1 mm^2 grid within the chamber (Julien Olivet., 2015). Equation for calculating cell viability (A); blocks (1.0 x 1.0 mm) counted on a haemocytometer to calculate the cell number and relative viability of the cells (B).

3.3.4. Sub-culturing of cells

INS-1 cells were seeded in 75 cm^2 culture flasks at a density of 8 $x10^5$ cells per culture flask to a total volume of 18 mL in pre-warmed (37°C) complete growth media. Cells were then incubated at 37 °C in 5% CO_2 and humidified air for three days until they were approximately 75-80% confluent. Media was refreshed every 2-3 days. When cells were approximately 75-80% confluent, cells were scraped using cell scrapers until the majority of cells were detached from the flask. An inverted light microscope was used to confirm detachment of the cells from the 75 cm^2 culture flask. Thereafter, the single cell suspension (as observed under a light microscope) was then transferred into a 50 mL centrifuge tube and the tube was centrifuged at 800 × *g* for 5 minutes. After centrifugation, the supernatant was discarded by aspiration and the pellet re-suspended with prewarmed (37 °C) complete media. The cells were counted (section 3.3.3.) and the density recorded. Cells were routinely seeded at 1:3 - 1:5 split ratio.

3.3.5. Setting up bioreactors

Bioreactors were assembled as follows: bioreactors were removed from the sterile packaging inside the biological safety cabinet to maintain sterility. The bioreactor cell culture chamber was filled with 9 mL pre-warmed (37 °C) DPBS via the apical port and the humidity chamber was filled with 40 mL of cell culture grade sterile water filled via the apical-back port (Figure 6). Following this, the apical growth chamber port area was cleaned with 70% ethanol (300 µL) in order to avoid contamination. The bioreactors were firmly attached onto the rotors of the BAM system, fitted in an incubator at 37°C and CO_2 set at 5%. The bioreactors were set to rotate at 13 rpm speed.

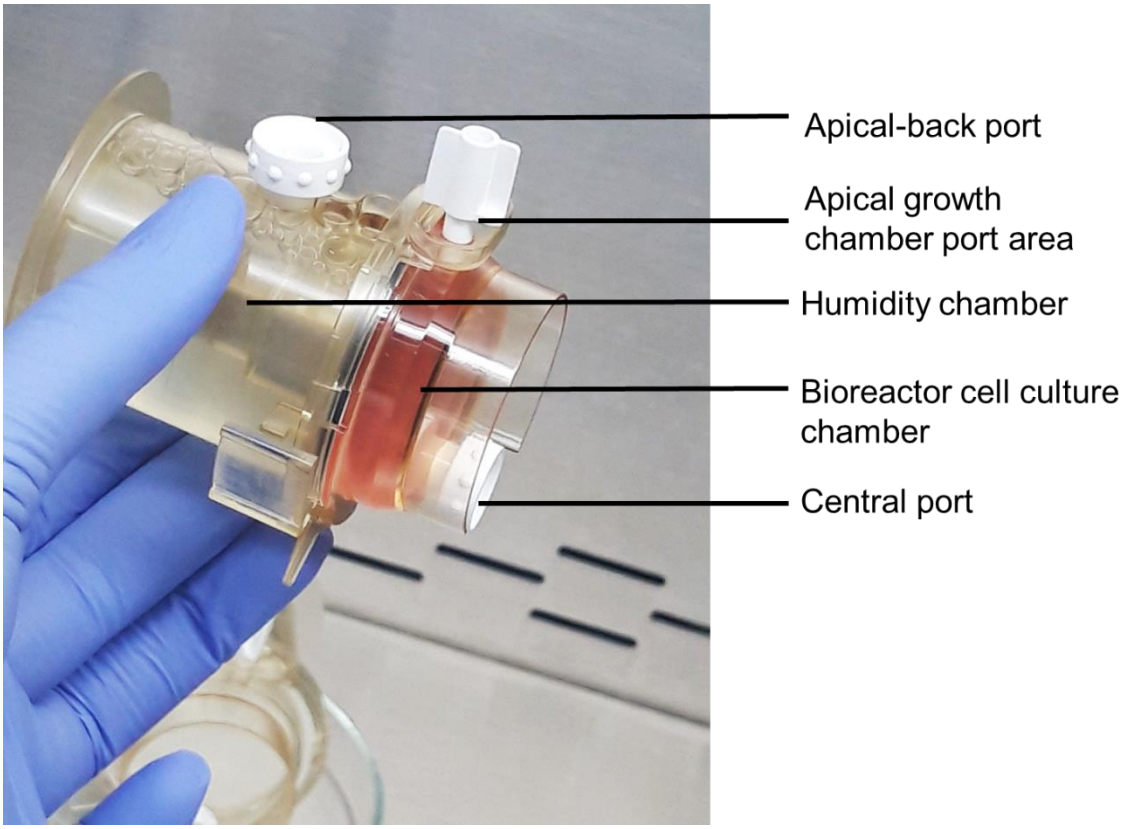

Figure 6: Bioreactor culture vessel used to grow the spheroids. The apical growth chamber port area is an opening for media and or DPBS change and is sealed by a plastic plug, the central port is used for sampling and transferring of spheroids, while the humidity chamber was filled with 40 mL water to maintain humidity. The bioreactor cell growth chamber contains the spheroids in complete growth media.

3.3.6. Seeding of cells into an AggreWell™ plate

INS-1 cells were seeded into an AggreWell™ 400Ex plate. This plate contains 400 µm microwells that provides a simple method of generating large numbers of uniform cell aggregates. These cell aggregates serve as seeding aggregates for β-cell spheroids. As a preparation step, 500 µL of complete media was added into the wells of an AggreWell™ 400Ex plate followed by centrifugation at 2182 x *g* for 9 minutes at room temperature to equilibrate the plate. INS-1 cells were seeded into the plate at a density of 7.2 x 10^6 cells/mL and a volume of 500 µL per well. After seeding, the plate was centrifuged at 100 x *g* for 3 minutes at room temperature to allow cells to be evenly distributed and settle into the micro wells of the plate. The organization of the cells in the micro wells of the plate was observed under a light microscope to confirm even distribution. Following this, 1000 µL of complete growth media was used to top up the wells in a gentle manner, without disturbing the cells. The AggreWell™ 400Ex plate was then incubated under standard conditions for 20-24 hours.

3.3.7. Transferring spheroids into a bioreactor

Following an overnight incubation, and confirmation of uniform cell aggregate formation under a light microscope, the cell aggregates were transferred into the bioreactors. A disposable sterile Pasteur pipette was used to gently dislodge the spheroids from the micro wells of the AggreWell™ 400Ex plate by pipetting, taking care not to make bubbles in the media. The dislodging process was observed under a light microscope. Once approximately 50% of the spheroids were dislodged, they were added to pre-warmed (37 °C) 3 mL complete growth media in a 35 mm x 10 mm petri dish. The process of dislodging was repeated until approximately 90% of the spheroids were retrieved. The petri dish was swirled gently to aggregate the spheroids into the center of the dish and the spheroids were transferred using the central port into the bioreactor culture vessel (Figure 6). Complete growth media was used to top up the bioreactor cell growth chamber to 10 mL until the vessel was full and small media bubbles were displaced. The apical port area was cleaned with 70% ethanol (~300 µL) to sterilize and prevent contamination. The bioreactors were incubated (37 °C in humidified air containing 5% CO_2) as described in section 3.3.5. Pre-warmed (37 °C) heating blocks were used to regulate the temperature during transfer of the newly formed spheroids from the AggreWell™ 400Ex plate to the BAM bioreactors.

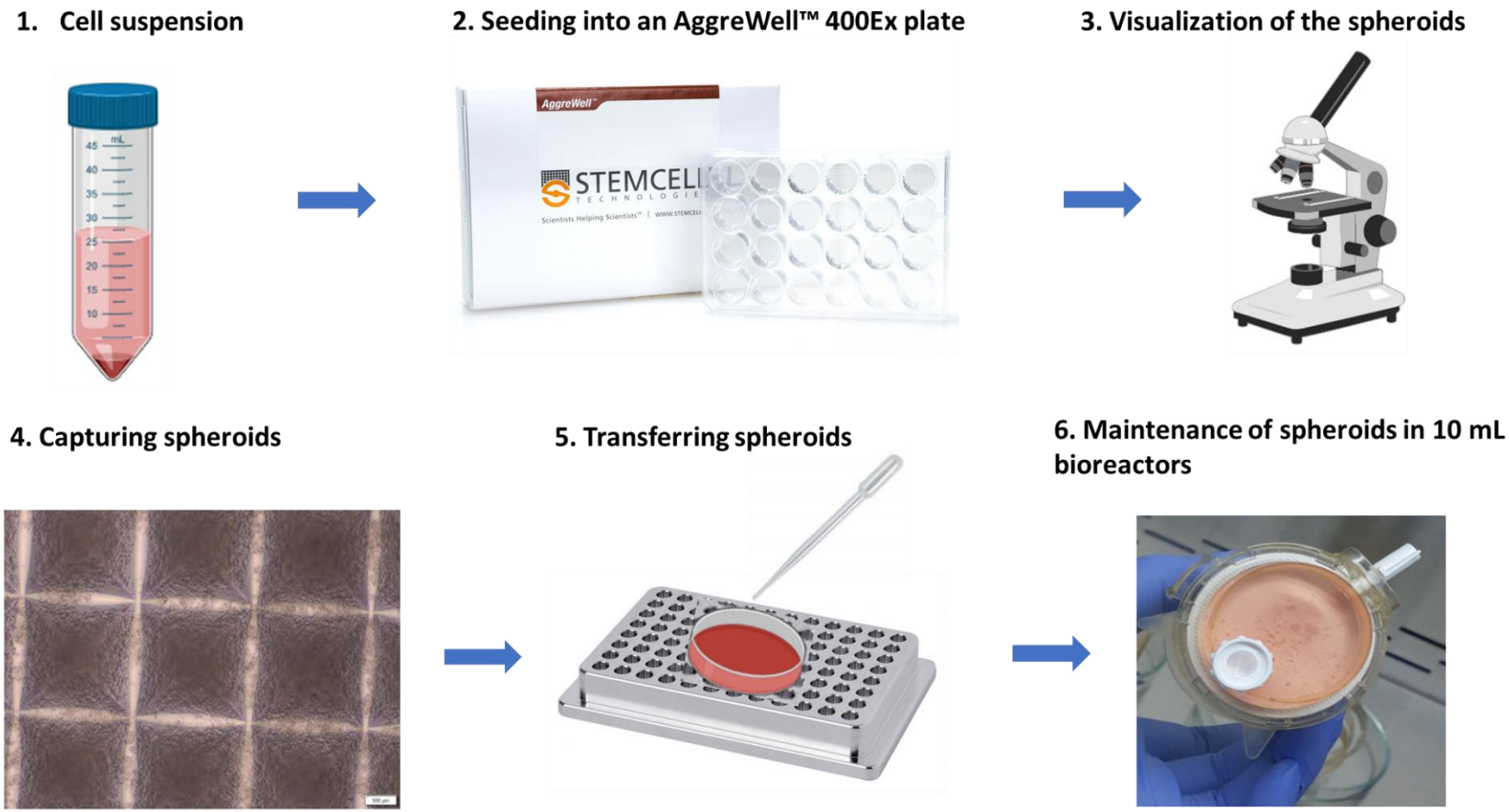

Figure 7: Illustration showing the steps involved in the creation of 3D β-cell spheroids. INS-1 cells were seeded in an AggreWell™ 400Ex plate with approximately 1200 micro wells to encourage the formation of 3D β-cell spheroids. The plate was incubated overnight at standard tissue culture conditions and the formation of cell aggregates was visualized using a light microscope, before being dislodged from the AggreWell™ 400Ex plate and seeding in 10 mL bioreactors.

3.3.8. Electron microscopy (method modified after Kay *et al*., 1967)

Fourteen-day old, untreated spheroids were sampled for transmission electron microscopy. Spheroids were fixed in 2.5% glutaraldehyde in 0.1 M phosphate buffer pH 7.4 at 4 °C for 4-6 hours and cut into small blocks of no more than 1-2 mm thickness. Following fixation, the tissue was rinsed in phosphate buffer to remove unbound glutaraldehyde. The tissue was post-fixed with 1.5% osmium tetroxide in Palade's buffer pH 7.4 for one hour and then rinsed with two changes distilled water to remove excess unbound osmium. Tissue was processed further in a Leica EM tissue processor through 2% uranyl acetate in 70% ethyl alcohol and ascending concentrations of ethyl alcohol (70% for 5 minutes, 2 x 96% for 5 minutes each, 3 × 100% for 10, 15 and 20 minutes respectively). Following dehydration, the tissue was impregnated initially with a 50/50 mixture of Spurr's resin (NSA × 13 mL, ERL 4206 × 5 mL, DER × 3 mL and DMAE× 0.2 mL) and 100% ethyl alcohol followed by two changes of clean Spurr's resin. Resin impregnated tissue was embedded into resin filled gelatin capsules and the blocks allowed to polymerize overnight at 60°C. The tips of the capsules were trimmed with a Reichert TM60 block trimmer to expose the embedded tissue. Semi-thin sections (1 m) were cut on a Leica EM UC7 ultra-microtome with a glass knife fitted with a water trough. Sections were removed from the trough and placed on a drop of water and the sections allowed to dry on a hot plate. Once the drop of water had evaporated and the sections adhered to the slide, the resin was then removed from the sections with sodium methoxide. Sodium methoxide was prepared by reacting 1% metal sodium in absolute methanol. The slides were washed in tap water, to remove the sodium methoxide and stained with warm 1% toluidine blue in 1% sodium tetraborate for 1 minute. Slides were washed in distilled water, blotted on filter paper and dried on a hot plate. Dry sections were mounted with DPX and studied under the light microscope. The area of interest was identified light microscopically and matched with the corresponding area in the resin block. The resin block was retrimmed into a small (max 2 ×1 mm) trapezium shape containing the area of interest by a Reichert TM60 block trimmer fitted with a diamond tip trimming blade. Thin gold ribbon sections, thickness 90 - 120 nm, were cut on the Leica EM UC7 using the heat feeding mechanism and a glass knife fitted with a water trough. A ribbon of sections were then picked up from the water bath, onto a G200 copper grid and

allowed to dry on a filter paper. The sections were then stained for 5 minutes with 2% acetyl acetate in 50% ethyl alcohol, rinsed in clean 50% ethyl alcohol and double stained with Reynold's lead citrate (Kay *et al*., 1967) for a further 5 minutes. Reynold's lead citrate was prepared by mixing lead nitrate (1.33 g) with sodium citrate (1.76 g) in distilled water (30 mL). After thorough mixing the solution was allowed to react for at least one hour for the lead nitrate to convert to lead citrate. Lead citrate was dissolved with 1 N sodium hydroxide (8 mL) and distilled water added to a final volume of 50 mL. After staining the grids were washed in two changes of distilled water and replaced onto a filter paper in a closed Petri dish. Once the grids had dried the sections were viewed in a JEOL JEM-1011 transmission electron microscope operated at 75 kV.

3.3.9. Treatment of the spheroids

Fourteen days following seeding into the AggreWell™ 400Ex plate, glucotoxic conditions were induced by high glucose (HG-33 mM glucose), where two of the HG groups were treated simultaneously as follows: high glucose treated with GRT™ (HG-GRT™) and high glucose treated with BACE inhibitor LY2886721 (HG-BACE). Complete growth media containing normal physiological glucose levels were used as a normal control (NG-11 mM glucose). Treatment was conducted for 16 days and followed by experimental assays described.

3.4. Experimental assays

3.4.1. ATP Assay for viability determination

The viability of the 3D pancreatic β-cell spheroids was measured based on their ability to produce ATP using CellTiter-Glo® Luminescent Cell Viability Assay kit following the manufacturer's instructions. For this, approximately 10 spheroids were sampled from the bioreactor into a 2 mL centrifuge tube. A total volume of 100 µL of the ATP reaction mixture was added to each 2 mL tube with 10 spheroids, followed by gently mixing of the spheroids by pipetting up and down to lyse them to create a spheroid / ATP. This suspension was incubated for 8 minutes at room temperature protected from light by covering with foil. The spheroids / ATP suspension was then plated (20 µL per well) into a 96 well plate. The plate was incubated for an additional 2 minutes at room

temperature while covered with foil. The quantification of ATP levels was conducted by luminometric measurement using the SpectraMax i3 multimode plate reader.

3.4.2. Bradford assay

The Bradford assay is a spectroscopic method extensively used to determine total protein concentration. It is based on the absorbance shift of Coomassie brilliant blue G-250, which changes color to blue when it comes into contact with proteins. The binding of the protein to the dye stabilizes the blue form of the dye allowing for measurement of protein concentration. The ionic form of the dye (blue) has an absorbance maximum at 590 nm (Bradford, 1976). Firstly, the standard was prepared by serially diluting bovine serum albumin (BSA) in lysis buffer at the following concentrations 0.125, 0.25, 0.5, 0.75, 1, 1.5, and 2 mg. Thereafter, 5 µL of the sample of the cell homogenate or BSA standards were added to wells of a 96-well plate in duplicate, followed by addition of 200 µL of the Bradford reagent. Plates were incubated in the dark while covered with aluminium foil for 10 minutes at room temperature. After incubation, the absorbance was measured at 570 nm on a plate reader. Protein content values used were extrapolated from the standard curve generated. The protein content was then used to normalize the ATP viability results.

3.4.3. Glucose stimulated insulin secretion (GSIS)

The response of the β-cell spheroids in different conditions to glucose stimulation was used to assess the function of the spheroids. On the day of the experiment, 10 spheroids were sampled and collected from the NG, HG, HG-GRT™ and HG-BACE treatment bioreactors and transferred into new bioreactors respectively. Following this transfer, the spheroids were washed with basal glucose media (2.6 mM) for 30 minutes while rotating at 13.0 rpm at standard culture conditions. This was then followed by removal of the basal media (~90%) by a sterilized glass Pasteur pipette without disturbing the spheroids. The spheroids were further treated with basal glucose treatment for 90 minutes while rotating at 18.0 rpm. Ninety minutes post treatment, the media was collected and stored at -20 °C. This was then followed by treating the spheroids further with a stimulatory glucose treatment (16.7 mM) for an additional period of 90 minutes after which, the spheroids and media were collected and stored at -20 °C.

3.4.4. Insulin ELISA

An ultra-sensitive insulin ELISA kit was used to quantify the insulin secreted by the pancreatic β INS-1 spheroids. The media samples collected during GSIS were brought to room temperature alongside the insulin standards provided in the kit and the pre-coated Mouse insulin ELISA plate. As per the instructions in the protocol, the GSIS samples and the kit standards were loaded into the Mouse insulin ELISA plate. Bound insulin was detected using biotinylated polyclonal antibody, horseradish peroxidase and 3, 3', 5, 5'-tetramethylbenzidine substrate detection by measuring the absorbance of the bound substrates at 450 and 630 nm using the SpectraMax i3 multimode plate reader. The relative insulin concentrations in each sample were extrapolated from the standard curve generated. The insulin concentrations used for the standard curve were 1.0, 2.0, 4.0, 8.0, 16.0, 32.0 and 64.0 ng/mL.

3.4.5. Amylin ELISA

Islet amyloid polypeptide (IAPP) commonly known as amylin levels in the GSIS samples frozen at -20 °C were quantified using a Rat amylin ELISA kit. Strictly following the instructions from manufacturers, samples and kit standards were loaded into the pre-coated Rat amylin ELISA microplate and incubated for 2 hours. Bound amylin was detected as described in subsection 3.4.4. The relative amylin concentrations in each sample were extrapolated from the standard curve generated. The amylin concentrations used for the standard curve were 0, 62.5, 125, 250, 500, 1000 and 4000 pg/mL.

3.4.6. TNF-alpha ELISA

Levels of TNF- α in the media collected at 1 week and 2-weeks of glucotoxicity were quantified using a TNF- α ELISA kit. Strictly following manufacturer's instructions, the microplate was pre-coated overnight with TNF- α capture antibody. Bound TNF- α, was detected as described in subsection 3.4.4. The relative TNF- α concentrations in each sample were extrapolated from the standard curve generated. The TNF- α concentrations used for the standard curve were 0, 31.25, 62.5, 125, 250, 500, 1000 and 2000 pg/mL.

3.4.7. Interleukins ELISA

Quantification of IL-6 and IL-10 in the samples from week 1 and week 2 of glucotoxicity was performed using interleukin IL-6 and IL-10 ELISA kit. Strictly following instructions from manufacturers, the microplate was pre-coated with the respective capture antibodies (IL-6 and IL-10) overnight. Bound IL-6 and IL-10 was detected as described in subsection 3.4.4. The relative IL-6 and IL-10 concentrations in each sample was extrapolated from the standard curve generated. The IL-6 and IL-10 concentrations used for the standard curve were 0, 15.625, 31.25, 62.5, 125, 250, 500 and 1000 pg/mL.

3.5. Western blot analysis

Western blot analysis was used to determine the effects of the different treatment on selected proteins known to be involved in β-cell function and apoptosis using a method modified from Mahmood and Yang (2012).

3.5.1. INS-1 pancreatic β-cell spheroids collection

Following exposure of the 3D β-cell spheroids to the different treatments as previously explained (section 3.3.8), 10 spheroids were collected into 2 mL Eppendorf tube and snap frozen with liquid nitrogen and stored at -80 °C. The spheroids were then resuspended in ~75 µL of commercial cell lysis buffer. The spheroid / suspension was mechanically lysed using a tissue lyser by adding a steel ball to each tube and homogenising at 25 Hertz for 60 seconds, with 1 minute rest intervals on ice (homogenizing of the samples was repeatedly done for a minimum of 5 times). Following this, the spheroid lysate was centrifuged at 15 000 rpm at 4 °C for 15 minutes and the supernatant transferred into a clean 2 mL Eppendorf tube. Sample protein concentration was quantified using a reducing agent compatible and detergent compatible (RC/DC) protein concentration determination kit, based on the method described by Lowry (1951). Approximately 5 µL of each BSA standard and/ or spheroid sample was transferred into a clean 96 well assay plate, followed by addition of 25 µL of Reagents A[I] and 200 µL of reagent B to each well. The plate was covered with foil and incubated for 10 minutes at room temperature. The plate was agitated for 10 seconds before measuring absorbance at 630 nm using a SpectraMax i3 multimode plate reader. Relative protein concentration of the samples was determined by extrapolating the values from the BSA standard curve that was generated.

3.5.2. Protein separation by gel electrophoresis

Protein samples were diluted and mixed with a 2 times sample buffer (1:1) and then placed on a heating block and heated at 95 °C for 5 minutes in order to denature the proteins. Following this, samples were centrifuged briefly and placed on ice. Samples at a concentration of 30 µg were pipetted into a 10% SDS-polyacrylamide gel electrophoresis (SDS-PAGE) precast gel. A molecular weight marker (Precision Plus Western C Standard) was loaded in the first lane in order to monitor the electrophoretic separation through the gel (PageRuler marker). The gel was run for a minimum of 45 minutes at 150 V in a mini protein tetra cell tank (Trans-Blot Cell) filled with running buffer.

3.5.3. Transfer of the protein from gel to membrane

Following protein separation by SDS-PAGE (Trans-Blot Cell), proteins were transferred into a polyvinylidene difluoride (PVDF) membrane. Briefly, the 7 cm x 9 cm PVDF membrane was pre-wet by shaking gently in 100% methanol for 5 minutes prior to being submerged in transfer buffer for 5 minutes. Meanwhile, transfer fibre pads were equilibrated in transfer buffer for 20 minutes. After equilibration, a ‘transfer sandwich' was prepared as illustrated in Figure 8**.** To facilitate protein transfer to the membrane, the sandwich was placed into a semi-dry transfer machine and transfer of proteins was carried out at 160 V at 4 °C for 10 minutes.

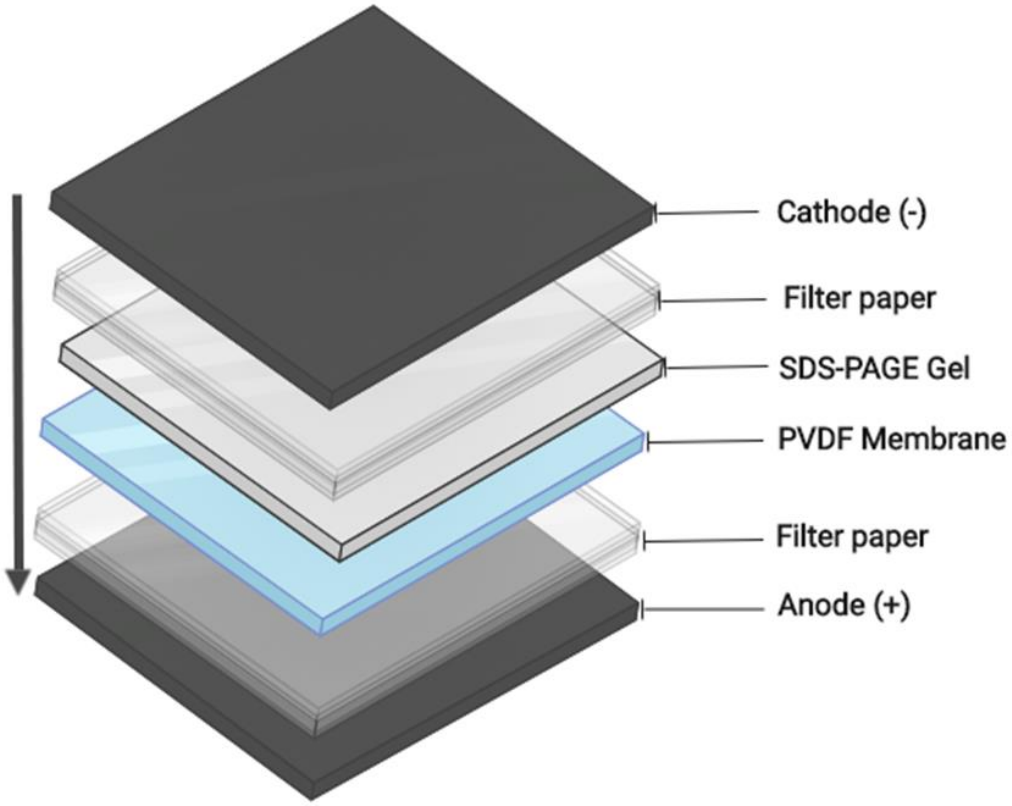

Figure 8: Schematic representation of a transfer sandwich used to transfer proteins from a gel to the PVDF membrane. A 'transfer sandwich' was assembled in the following order from cathode (negative side) to anode (positive side), fibre pad, PVDF membrane, SDS-PAGE gel, filter paper and lastly fibre pad in a support grid. The assembled transfer sandwich was then placed in an into a semi-dry transfer machine for protein transfer.

3.5.4. Ponceau S stain

Ponceau S stain is a sodium salt of thiazo dye used for rapid reversible detection of proteins transferred on a PVDF membrane. The transfer of proteins from the gel to the PVDF membrane was confirmed by Ponceau S staining immediately after the transfer process with gentle agitation on an orbital shaker for 5 minutes. After confirming that the protein bands were clearly visible, the membrane was de-stained by washing the membrane with 1 x Tris-buffered saline containing Tween-20 (TBST-20).

3.5.5. Blocking and labelling with primary and secondary antibodies

After removal of Ponceau S stain, the PVDF membrane containing the proteins of interest were blocked for non-specific antibody binding in 1 x Tris-buffered saline containing Tween-20 (TBST-20) in 5% (w/v) non-fat milk powder for 2 hours with gentle agitation on an orbital shaker at 2.5 rpm at room temperature. Thereafter, the membrane was labelled with the relevant primary antibody made up in TBST-20 overnight at 4 °C. The following day the membrane was washed 3 times for 10 minutes with 1× TBST-20 at room temperature on an orbital shaker, before incubation with the respective horseradish peroxidase (HRP) (1:2000) conjugated secondary antibody (anti-rabbit/ anti-mouse HRP) in 2.5% non-fat milk powder dissolved in 1× TBST-20 at room temperature for 90 minutes. After this period, the membrane blots were again washed for 10 minutes in 3 times with 1× TBST-20 and detected as detailed in the next section.

Table 3: List of primary and secondary antibodies and dilution used for Western blot analysis

Primary antibody	Monoclonal/ Polyclonal	Size (kDa)	Dilution	Secondary antibody (1:2000)
Anti-Amylin	Monoclonal	± 10	1:500	Anti-Mouse
Anti-LC3A/B	Monoclonal	± 17	1:500	Anti-rabbit
Anti-TMEM27	Monoclonal	± 27	1:500	Anti-rabbit
Anti-p38	Monoclonal	± 41	1:500	Anti-rabbit
Anti-pdx-1	Monoclonal	± 42	1:1000	Anti-rabbit
Anti-ERK	Monoclonal	± 45	1:1000	Anti-rabbit
Anti-BACE	Polyclonal	± 56	1:500	Anti-rabbit
Anti-Glut 2	Monoclonal	± 57	1:500	Anti-rabbit
Anti-phospho-AKT	Monoclonal	± 60	1:500	Anti-rabbit
Anti-Insulin receptor	Monoclonal	± 95	1:500	Anti-rabbit
Anti-Ki67	Monoclonal	± 359	1:500	Anti-rabbit

3.5.6. ChemiDoc detection

Detection of the labelled proteins was visualized using a chemiluminescent kit. The membrane was incubated for 5 minutes with enhanced chemiluminescent substrate (ECL) in a 1:1 ratio in the dark, followed by imaging of the membrane on the Chemi Doc MP imager. Image Lab Software was used to analyse images.

3.5.7. Housekeeping protein detection

Detected proteins were normalized to the housekeeping protein, β-tubulin, in order to determine the relative expression of the specific protein. To detect the housekeeping protein (i.e. β-tubulin), the respective membranes were stripped of the previously detected proteins by immersing the membrane in stripping buffer for 8 minutes with gentle agitation followed by 2 washes with DPBS and 1x TBS wash. The membrane was blocked with TBST-20 containing 5% non-fat milk powder for 2 hours and incubated with β-tubulin antibody diluted 1:500 overnight. Following overnight incubation, β-tubulin labelling was detected as described in subsection 3.5.6.

3.6. Non-cell-based assay of Purified BACE enzyme

Beta secretase inhibition profiling of GRT™ was assessed using fluorescence resonance energy transfer (FRET) in a purified enzyme assay. The assay is based on the FRET method which measures the fraction and/or efficiency, of transferred energy from a donor (fluorophore) to an acceptor (chromophore) (Jares-Erijman and Jovin, 2003). Thus, by attaching fluorophores, referred to as probes, to known sites within the BACE molecule, the efficiency of energy transfer can be measured. In this assay, the fluorescence signal becomes enhanced when BACE cleaves the substrate. The BACE inhibition activity of various concentrations of GRT™ was investigated following 2 hours incubation with the enzymes at room temperature. Following this, the fluorescent signal was quantified at Ex320 nm / Em405 nm on a SpectraMax i3 multimode plate reader. BACE inhibition GRT™ was compared to a known BACE inhibitor, N - (3 - ((4aS, 7aS) - 2 - amino - 4a, 5, 7, 7a - tetrahydro - 4H - furo [3, 4-d] [1, 3] thiazine - 7a - yl) - 4 - fluorophenyl) - 5 - fluoropicolinamide (LY2886721). This inhibitor is a potent and selective BACE inhibitor with an IC_{50} of 20 nM for recombinant hBACE. Fluorescence values read were

extrapolated from the standard curve (100, 200, 300, and 500 pmol). Concentrations of GRT™ and LY2886721 are represented in the Table 4. The concentrations of GRT™ used are based on concentrations that have been used in other cell models, while BACE concentrations are literature review based.

Table 4: Concentrations of Afriplex GRT™ used for the non-cell based BACE inhibition assay.

Treatment concentrations	GRT™ (µg/mL)	LY2886721 (µM)
	0.01	0.0039
	1.0	0.039
	10.0	0.39
	100	3.9
	1000	39

3.7. *In vivo* experiments

An *in vivo* model of type 2 diabetes (T2D) (C57BLKS obese diabetic Lepr *db/db* male mouse) and their *db*+ lean littermates (control) were used in this study. This *in vivo* component was divided into three treatment phases commencing from 6 weeks of age and based on the duration of treatment as depicted (Figure 6). Phase I (10 weeks treatment) and Phase II (16 weeks treatment) comprised of both obese diabetic Lepr *db/db* mice and lean, non-diabetic *db*+ mice, while Phase III (32 weeks treatment) comprised of only lean, non-diabetic *db*+ mice. Obese diabetic Lepr *db/db* mice were not used in Phase III of the study due to their advanced diabetic condition (Sataranatarajan *et al*., 2016). Within each phase, mice were further sub-grouped into five treatment groups with each group starting off with a total of eight mice (n=8) as denoted below (Table 5).

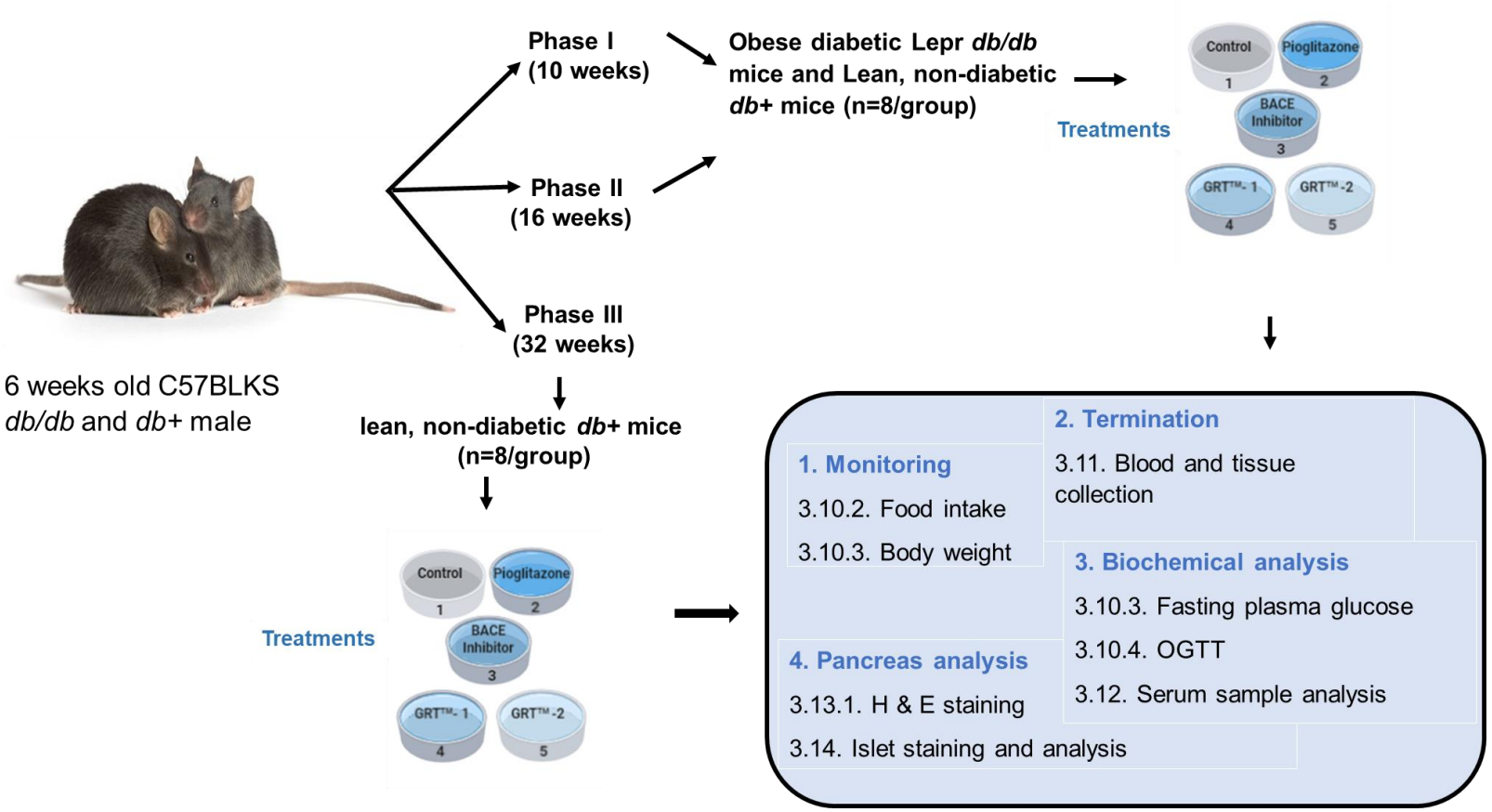

Figure 9: *In vivo* experimental design overview. Male obese Lepr *db/db* mice and lean *db*+ (control) mice were randomized into three study phases. Within the phases, mice were grouped into 5 treatment groups as follows: Normal control (ground rodent food), Pioglitazone 15 mg/kg/day; BACE Inhibitor 30 µM/kg/day; GRT™-1 74 mg/kg/day and GRT™-2 740 mg/kg/day for both the lean groups and obese groups. The mice were treated for 10, 16 and 32 weeks respectively for each phase, after which food intake, bodyweight and metabolic parameters were assessed. (OGTT: Oral glucose tolerance test, H&E: Haematoxylin and eosin)

3.7.1. Ethical clearance

All procedures in this study were performed in accordance with the ethical code of conduct, principles and guidelines as outlined by the South African Medical Research Council "Guidelines on Ethics for Medical Research Council". In addition, Ethical approval for this study was granted by the Ethics Committee for Research on Animal (ECRA) at the South African Medical Research Council, Tygerberg, Cape Town (ECRA approval number (Ref 05/17) and the University of Zululand Research Ethics Committee (UZREC) and the Faculty Research Ethics Committees (FRECs) (UZREC/FRECS: UZREC 1711110-030 PDG 2017/207) (Appendix H).

3.7.2. Animal observations

Two hundred six-week old mice were obtained from and housed at South African Medical Research Councils' PUDAC Unit under standard environment conditions (12 hour light/dark cycle at 22 ± 2 °C). The mice were randomised into groups (Table 5). Routine health observations were performed and recorded on daily basis during all study phases as recommended by the guidelines of the South African Medical Research Council Ethics for Medical Research: use of animals in research and training. Daily observations included any visible signs of changes in skin and fur condition, eyes, teeth and mucous secretions and excretions. More so, behaviours such as shivering, pilorection, breathing rate, changes in posture, response to handling were noted on daily basis. Additionally, the presence of clonic or tonic movements, excessive or lack of grooming, severe dehydration and excessive weight loss or any other bizarre behaviour was monitored. Food and water consumption were monitored throughout the study phases. In accordance to the ethical guidelines for rodent handling, any atypical behaviours in the animals that was not anticipated as part of disease progression resulted in the exclusion of the respective animal from the study. Some of the animals in some treatment groups exhibited some atypical behaviours and thus not all groups were n = 8 at the end of the affected phase.

3.7.3. C57BLKS *db/db* mouse housing

Diabetic C57BLKS *db/db* and *db*+ male mice were bred and housed at the South African Medical Research Councils' PUDAC Unit. Mice were housed (cage size 461 cm x 165 cm x 174 cm) from weaning period and acclimatized until 6 week old. The

mice were supplied with fresh water, as well as food (standard rodent pellets) *ad libitum*. The cages were provided with autoclaved bedding material (CobTech) and cleaned according to the PUDAC SOP (Rodent Section, updated version from 2014). Forty (40) six week-old male obese diabetic *db/db* and forty (40) lean male *db*+ mice were randomly selected and assigned into five groups. The mice were housed as two mice per cage where they had free access to food (ground rodent food) and water. From 6 weeks of age, mice received their respective treatments added into their ground food according to their respective treatment phases (Table 5). The dose of the extract, GRT™-2 (740 mg/kg/day) is based on the translated 60 mg/kg/day dose and a 10 x lower dose (GRT™-1, 74 mg/kg/day) calculated and adjusted for mice using FDA approved formula for animal to human dose translation (Reagan-Shaw *et al*., 2008). While Pioglitazone is based on studies by Patel *et al*., 2016, BACE inhibitor concentration is literature based. Prior to the beginning of the study, all selected mice were weighed and fasted in order to record their baseline body weights and fasting plasma glucose levels. Food intake was monitored three times a week whereas fasting glucose levels and body weights were monitored weekly.

Table 5: Treatment groups for the three study phases and their corresponding daily doses of treatments, n=8.

	Lean non-diabetic *db+*		Obese diabetic *db/db*		Treatment groups
Phase I	Vehicle control		Vehicle control		Ground rodent food
	Pioglitazone		Pioglitazone		15 mg/kg/day
	BACE inhibitor (AZD3293)		BACE inhibitor (AZD3293)		30 µM/kg/day
	GRT™ -1		GRT™ -1		74 mg/kg/day
	GRT™ -2		GRT™ -2		740 mg/kg/day
Phase II	Vehicle control		Vehicle control		Ground rodent food
	Pioglitazone		Pioglitazone		15 mg/kg/day
	BACE inhibitor (AZD3293)		BACE inhibitor (AZD3293)		30 µM/kg/day
	GRT™ -1		GRT™ -1		74 mg/kg/day
	GRT™ -2		GRT™ -2		740 mg/kg/day
Phase III	Vehicle control				Ground rodent food
	Pioglitazone				15 mg/kg/day
	BACE inhibitor (AZD3293)				30 µM/kg/day
	GRT™ -1				74 mg/kg/day
	GRT™ -2				740 mg/kg/day

3.8. C57BLKS *db/db* mice maintenance

3.8.1. Preparation of treatments

Food was prepared weekly, and the daily dose of each treatment was calculated and adjusted weekly according to the average body weights in each treatment group. The amount of food allocated to each cage was adjusted accordingly to the average food consumed. The treatments (Pioglitazone; BACE Inhibitor; GRT™-1 and GRT™-2 Table 5) were mixed into the ground rodent food. Obese and lean controls received only ground rodent food. Food that remained was stored at room temperature under desiccation.

3.8.2. Food intake monitoring

To determine daily food intake, food was weighed before it was given to the mice. The remaining food was weighed and recorded the next day before new food could be given to the mice per cage. Daily food intake was calculated by subtracting the remaining food from the initial food given to the mice per cage. Food was given in cups and placed on a cup holder to minimize food spills and ensure that mice had access to food spill.

3.8.3. Body weight monitoring

Mice were weighed weekly throughout the study to assess the efficacy of the treatments on body weight and to determine total body weight gain. Body weight gain was calculated by subtracting the baseline body weight from the final body weight of each mice.

3.8.4. Fasting plasma glucose concentration monitoring

Fasting plasma glucose levels were measured weekly after an overnight (16 hour) fasting period. Blood was collected by pricking the tail of the mice with a needle. Thereafter, the sample was loaded onto a glucose strip inserted into a glucometer (Johnson & Johnson). Values obtained from the glucometer were recorded and the average glucose concentration of each group was calculated.

3.8.5. Oral glucose tolerance test (OGTT)

Oral glucose tolerance tests were conducted on the day prior to the respective terminations with slight modifications from the protocol described by Mazibuko (2014). Mice were fasted overnight (16 hour) and fasting plasma glucose concentrations were measured as described in section 3.10.3. Following this, treatments were administered to the mice by oral gavage. Treatments were freshly prepared by dissolving the daily dose of all extracts and control agents in distilled water (dH_2O). Obese and lean control groups received dH_2O without treatments. An hour after administering treatments, the mice received 2 g/kg of glucose bolus via oral gavage. Blood glucose concentrations were measured at the following time intervals: 15, 30, 60 and 120 minutes. An area under the curve was calculated to indicate the level of glucose tolerance of the mice.

3.9. Blood and tissue collection

Mice were anaesthetized at the end of the study phases (Phase I, Phase II and Phase III) respectively by inhaling 2% fluothane. A mid-line abdominal incision was made, and blood was collected from the abdominal vena cava and transferred into serum separating tube (SST) which was stored on ice and kept at 4 °C. This blood was not used to determine fasting blood glucose levels as it is known to give abnormally high glucose values. Serum samples were prepared by centrifuging the blood collected at 14000 rpm for 15 minutes at 4 °C. Serum samples were analysed for biochemical measurements as described below: The Pancreas of each mouse was harvested and fixed in 10% buffered formalin for immunohistochemically analysis.

3.10. Serum samples analysis

3.10.1. Fasting plasma insulin determination

Serum insulin levels were quantified using an Ultra-sensitive Mouse Insulin ELISA kit from Crystal Chem. The samples were loaded onto the antibody pre-coated microplate ELISA plate with the insulin standards provided in the kit according to the protocol instructions. Samples were allowed to bind to the anti-insulin antibody in the pre-coated plate for 2 hours. Unbound material was removed by washing five times. Bound insulin was detected as described in subsection 3.4.4. The relative insulin concentrations in each sample were extrapolated from the standard curve generated. The insulin concentrations used for the standard curve were 1.0, 2.0, 4.0, 8.0, 16.0, 32.0 and 64.0 ng/mL.

3.10.2. Homeostatic model calculations

Homeostatic Model Assessment of beta cell function (HOMA-β) and Homeostatic Model Assessment of Insulin Resistance (HOMA-IR) were calculated using the formulas below, where fasting insulin quantified in section 3.12.1. and fasting blood glucose measured described in section 3.10.4. were extrapolated below.

$$1.\ \text{HOMA-}\beta = 20 \times (\frac{Insulin}{Glucose}) - 3{,}5$$

$$2.\ HOMA\text{-}IR = \frac{(Insulin \times\ Glucose)}{22{,}5}$$

3.10.3. Serum C-peptide determination

C-peptide levels were quantified using Mouse C-peptide ELISA kit from Crystal Chem. Strictly following the instructions in the protocol, serum samples, and kit standards were loaded into the plate and allowed to bind to the rabbit anti-C-peptide antibody coated in the microplate for 1 hour. Unbound material was removed by washing six times. Bound C-peptide was detected as described in subsection 3.4.4. The relative C-peptide concentrations in each sample was extrapolated from the standard curve generated. The C-peptide concentrations used for the standard curve were 1.0, 2.0, 4.0, 8.0, 16.0, 32.0 and 64.0 ng/mL.

3.10.4. Serum amylin determination

Islet amyloid polypeptide (IAPP) commonly known as amylin levels in the serum samples were quantified using an amylin ELISA kit. Strictly following the instructions from manufacturers, serum samples, and kit standards were loaded into the Rat amylin ELISA plate and incubated for 2 hours. Bound amylin was detected as described in subsection 3.4.4. The relative amylin concentrations in each sample were extrapolated from the standard curve generated. The amylin concentrations used for the standard curve were 0, 62.5, 125, 250, 500, 1000 and 4000 pg/mL.

3.11. Histological tissue processing

Pancreata fixed in 10% buffered formalin overnight, were processed in an automated tissue processer, using a predetermined processing schedule through ascending concentrations of ethanol (70% for 1.5 hours, 2 x 96% for 1 hour each and 3x 100% for 1 hour each) and three hourly changes of xylene. Thereafter, tissues were impregnated with molten paraffin wax (2 changes of 2 hours) and the tissue embedded into histology cassettes. Tissue sections of approximately 5 µm were cut from the cassettes on a rotary microtome. The sections were floated onto a water bath set at ± 40 °C and thereafter attached to aminopropyltriethoxysilane (APES) coated glass slides. Slides were incubated at 65 °C for 30 minutes to facilitate adherence of the tissue sections to the slides.

3.11.1. Pancreatic islet staining and analysis

For assessing pancreatic islet morphology and function, immunocytochemistry using insulin and glucagon antibodies were performed on sections of the pancreas. Images of the pancreatic islets were digitally captured by Nikon microscope and analysed using Image J software.

3.11.2. Insulin and glucagon double labelling

To assess islet phenotypic morphology, an immunolabelling method modified from Louw et al. (1997) was used in this study. Dewaxed and hydrated pancreas sections were incubated in 3% hydrogen peroxide (H_2O_2) to block endogenous peroxidase. To block non-specific binding, sections were incubated in 1:20 dilution of normal goat serum. The slides were blotted and primary antibody, 100 µL polyclonal anti-glucagon (1:50), was applied to the slides at room temperature (±25 ºC) for 30 minutes. The slides were washed with 0.05M TBS buffer, and the area around the sections was dried. The tissue was incubated with biotinylated rabbit anti-IgG for a further 30 minutes. The slides were washed again and thereafter incubated with Vectastain® Avidin biotin complex for 1 hour to detect biotin molecules. After washing, liquid 3'3-diaminobenzidine (DAB) substrate chromogen solution was added to slides for five minutes. During the DAB staining, the progress was viewed under a standard light microscope to prevent overstaining. The slides were washed with distilled water followed by a 0.05 M TBS washing step to conclude anti-glucagon labelling. For insulin labelling the sections were again blocked, using normal horse serum, after which a 1:5000 dilution monoclonal anti-insulin antibody was added and the slides were incubated overnight (20-24 hours) in a refrigerator at 4 ºC. Following incubation, the slides were brought to room temperature and the EnvisionTM G/2 double stain system rabbit/mouse kit was used according to manufacturer's instructions to complete the anti-insulin antibody labelling.

3.12. Statistical analysis

Statistical analyses were performed using GraphPad Prism 5.0 Software (GraphPad Software Inc., La Jolla, USA) for generating graphs and for statistical analysis thereof; statistics such as mean values, standard deviations, and standard errors with a 95% confidence interval were calculated. Additionally, Grubbs test was used to identify and remove outliers from data sets. One-way Analysis of Variance (ANOVA) with a Tukey *post hoc* test was conducted if $p < 0.05$. Two-way ANOVA's were conducted, where applicable, in the *in vivo* study. Significant differences between groups (i.e. $p < 0.05$) were determined by student T-test. A Pearson's correlation was used for correlation analyses, where relevant. P-values < 0.05 were considered statistically significant. Data is expressed as mean ± standard error of the mean (SEM).

For the *in vitro* component of the study, all experiments were performed with three independent experiments, with at least three technical repeats each. The analysis of Western blots was performed using ImageLab software. For the *in vivo* component, one experiment was conducted with eight animals per experimental group.

CHAPTER FOUR

Results

4.1. In vitro results

The initial step of the project was the development and characterization of INS-1 derived pancreatic β-cell spheroids, to assess the feasibility of generating functional β-cell spheroids using the BAM 3D clinostat system, as previously described for C3A liver spheroids by Fey and Wrzesinski., 2013. Measurements of ATP content and size profiling were conducted as part of optimization and characterization. Transmission electron microscopy was used to investigate the ultra-structural features of these spheroids.

Once the model was established, glucotoxicity was experimentally induced in the spheroids by supplementing RPMI 1640 media which normally contains 11 mM glucose to a final concentration of 33 mM (HG-33 mM). The spheroids were subjected to the following treatment conditions: Optimal glucose control (NG; 11 mM glucose), high glucose (HG; 33 mM glucose), high glucose supplemented with an aspalathin-rich green Rooibos extract GRT™ (HG-GRT™) and high glucose supplemented with BACE inhibitor LY2886721 (HG-BACE) and treated for 2 weeks.

Subsequently the effects of supplemented treatments (GRT™ and BACE inhibitor) to ameliorate glucotoxicity were examined by assessing cell viability using an ATP assay, spheroid size profiling and glucose utilization. More so, the effects of the treatments on the function of the spheroids was assessed by performing a glucose stimulated insulin secretion (GSIS) and amylin (IAPP) secretion assays. Additionally, the effect of the treatments on pro-inflammatory cytokine production and the expression of proteins relating to spheroid function and/or morphology were assessed.

4.1.1. BACE Inhibition

Beta secretase inhibition activity of GRT™ was assessed in a non-cell-based assay. The BACE inhibition assay indicates a concentration dependent response following 2 hours of incubation with a known BACE inhibitor (LY2886721). After 2 hours, the two highest concentrations of the known inhibitor; 3.9 and 39 µM significantly reduced activity of BACE compared to the lowest concentration (0.0039 µM) (71.9% ± 6.44; p=0.0010; 23.5% ± 5.88 p<0.001 vs 103.6% ± 0.73, respectively). Moreover, the highest GRT™ concentration (1000 µg/mL) significantly reduced BACE activity (83.4% ± 3.40, p<0.001 vs 102.2% ± 1.75) (Figure 10). GRT™ did not have any massive effect on BACE inhibition.

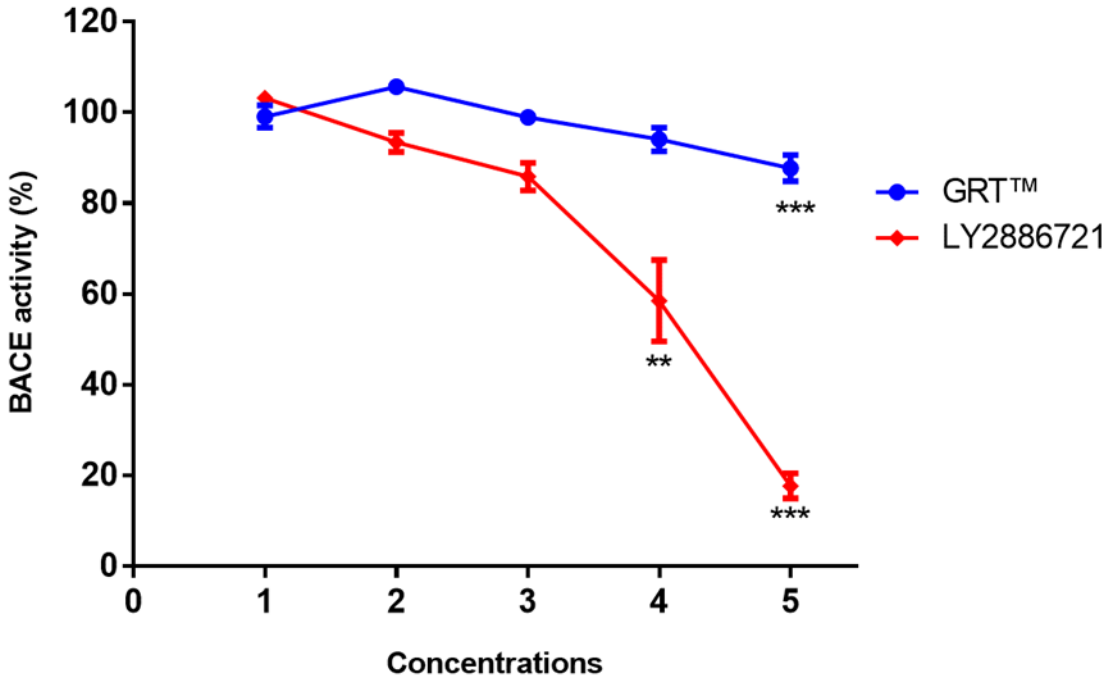

Figure 10: BACE inhibition profile of GRT™. BACE inhibition activity of GRT™ was compared to a known inhibitor (LY2886721) using a purified BACE enzyme assay. Concentrations: LY2886721 (µM): 1=0.0039. 2=0.039. 3=0.39. 4=3.9. 5=39; GRT™ (µg/mL): 1=1; 2=10; 3=100; 4=500; 5=1000.

Data is presented as the mean (± SEM) of three independent experiments (n=3), relative to that specific treatment's lowest concentration used; One-way ANOVA and Student T-test; ##=p<0.05. ###=p<0.001 vs. control of LY2886721; ***=p<0.001 vs. control of GRT™.

4.1.2. Characterization of the β-cell spheroids

A method for establishing long-term culture of β-cell spheroids was adopted from Fey and Wrzesinski., 2013. Briefly, INS-1 cell aggregates were formed in AggreWell™ 400Ex plates (Figure 11B). A visual volume and/or fullness of about 80 - 95 % per microwell was accepted and those spheroids were transferred into bioreactors to form β-cell spheroids. The spheroids were established and maintained using the BAM 3D clinostat system. The rotation speed of the bioreactors was adjusted to spheroid size and morphology to achieve microgravitational conditions that allow spheroids to remain suspended at fixed positions in the media (Wrzesinski, 2009).

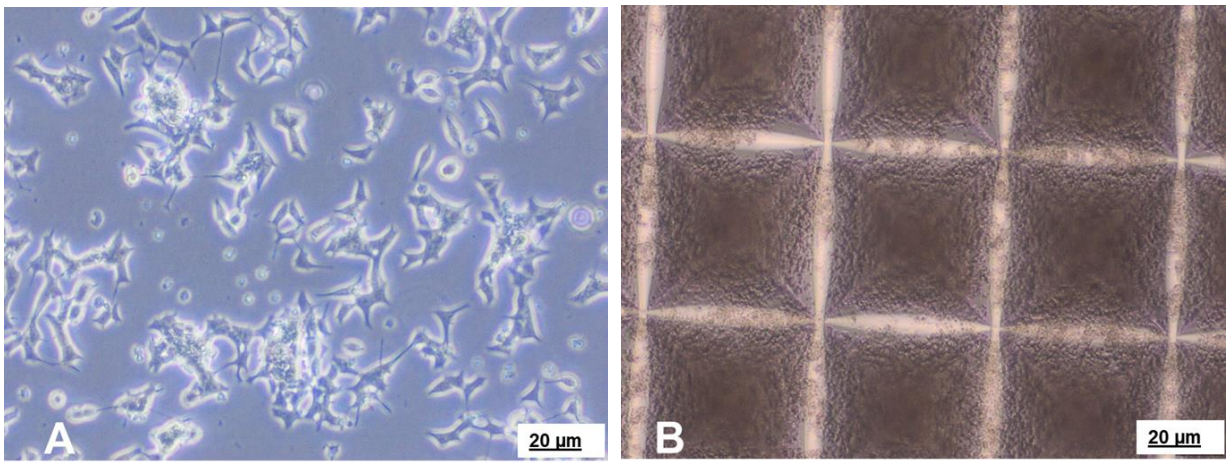

Figure 11: Representative images of INS-1 cells in conventional culture and in a AggreWell™ 400Ex plate. INS-1 cells at 75 % confluency cultured in a 75 cm^2 culture flask (A) after 3 days of incubation at standard culture conditions (10X magnification). The formation of INS-1 clusters (10X magnification) following seeding and centrifugation into an AggreWell™ 400Ex plate (B). INS-1 β-cells and clusters were grown at standard culture conditions (37 °C in 5% CO_2 and humidified air)

4.1.3. ATP content of the β-cell spheroids

The ATP content of the developed spheroids (day 1 to day 14) was determined as an indicator of viability, cell growth and to confirm the validity of the model. The ATP content of the spheroids increased proportionally to the number of days in culture representing metabolically active spheroids. From day 10, the ATP content of the spheroids stabilised and reached an equilibrium plateau.

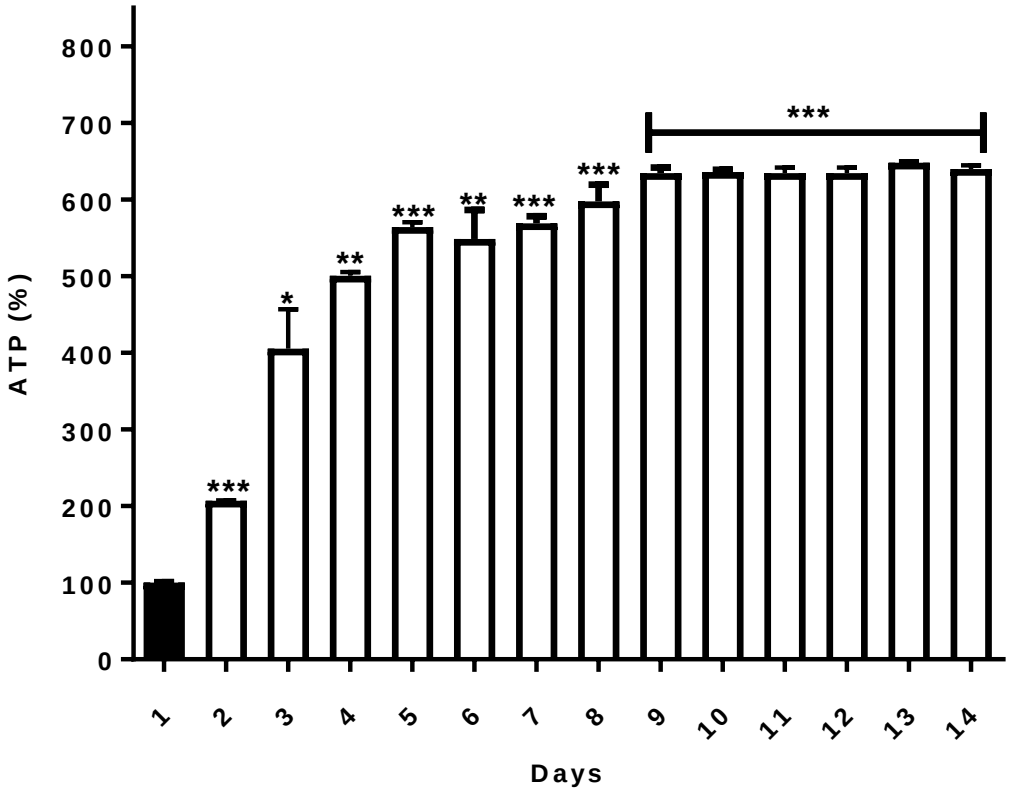

Figure 12: ATP content of INS-1 spheroids. The total ATP content was assessed in untreated spheroids grown for up to 14 days using ATP assay. In each assay average relative light units (RLU) from triplicates (3 independent experiments) was normalized to proteins of the spheroids and set to 100%.

Data expressed as mean ± SEM, Student-T test was used to conduct analysis; ***= $p<0.0001$ vs day 1.

4.1.4. Spheroid size profile

The spheroids sizes were profiled and measured by image analysis using an inverted light microscope to monitor their growth as an indicator of viability (Figure 13). The measured time points were as follows: day 1, representing the day spheroids were dislodged from the AggreWell™ plate and transferred into the bioreactors, and days 4, 10 and 14 after transfer into the bioreactors. The sizes of the spheroids determined by total area measurements increased proportionally to the number of days in culture (Figure 13).

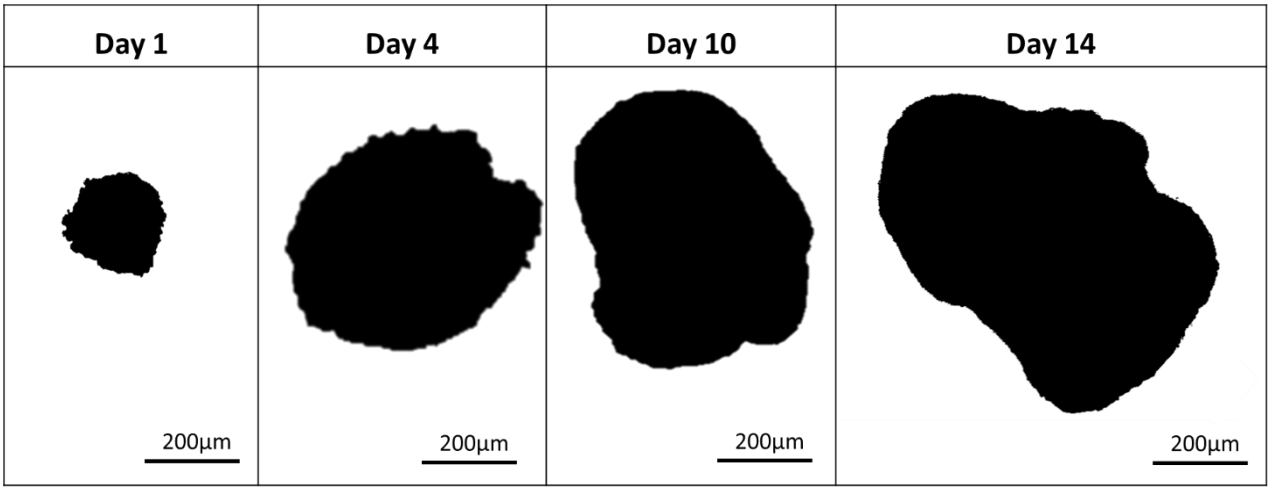

Figure 13: Size profile of INS-1 spheroids. The total area of the spheroids showing an increase in sizes proportional to the number of days in culture (day 1 to 14). Scale bars: 200 µm.

4.1.5. Morphology of the spheroids in semi-thin toluidine blue (TB) sections

Semi-thin resin sections stained with TB revealed the morphological features of β-cell spheroids. Light microscopy clearly revealed a mantel of viable cells. A clear distinction between viable cells and dead cells was observed. The outer mantel of viable cells was of a similar thickness surrounding the spheroid (Figure 14).

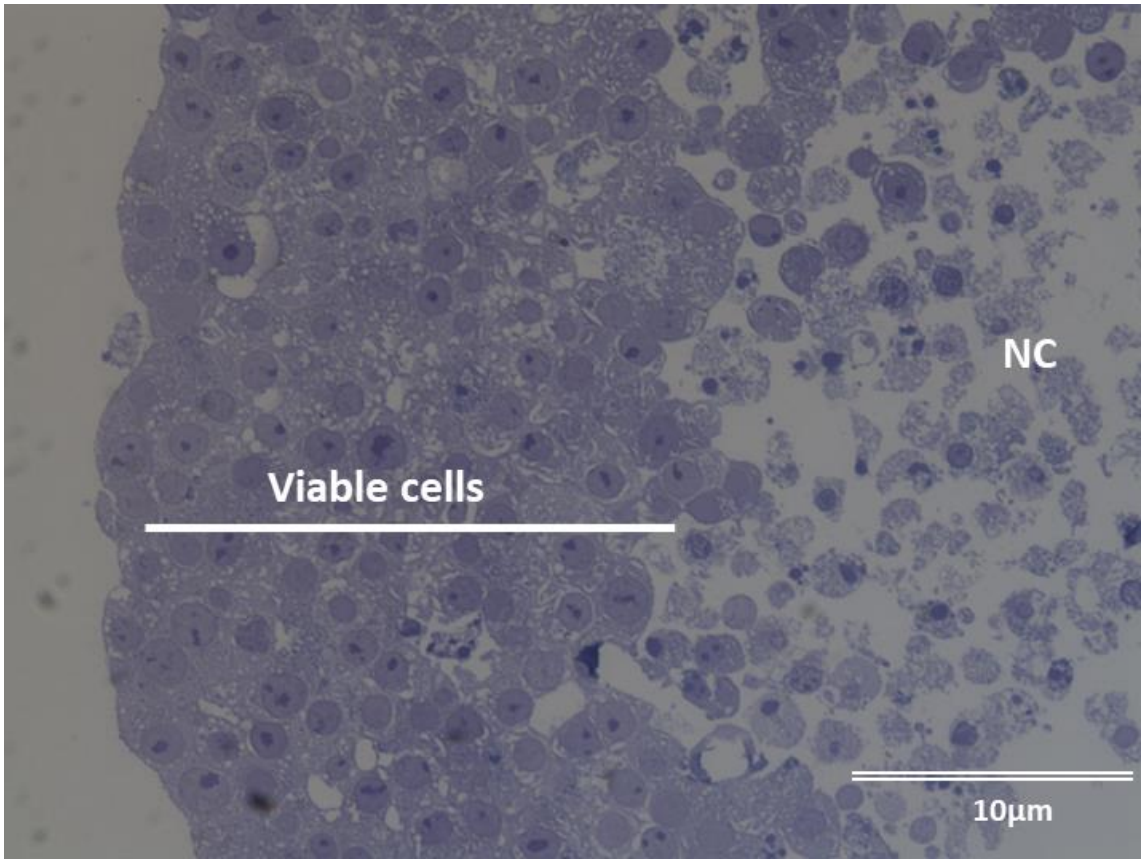

Figure 14: Histological images of toluidine blue INS-1 spheroid sections. Semi-thin TB sections revealing morphological features of β-cell spheroids. These morphological features include a central necrotic core (NC), outer mantel of viable cells with euchromatic nuclei prominent nucleoli. A clear delineation between the viable cell mantel and the apoptotic/necrotic core is apparent. Additionally, within the outer mantel, the outer layer of cells on the surface of the spheroid appeared to have less vacuoles than the cells deeper within the spheroid. Section captured using a 40 x objective.

4.1.6. Ultra-structural examination of spheroids by TEM

Transmission electron microscopy (TEM) was used to assess the cellular changes on a structural level, demonstrating ultrastructural features of the β-cell spheroids (Figure 15). Notably, the spheroids expressed ultra-structural features synonymous with pancreatic β-cells as evident in the electron micrographs (Figure 15).

The insulin-like secretory β granules were visible (Figure 16). Ultrastructural features including the presence of rough endoplasmic reticulum (RER), Golgi apparatus, nuclei, nucleoli and mitochondria were confirmed (Figure 16).

Mitotic cells were occasionally observed, confirming cell turn-over within the outer mantel (Figure 15 & Figure 16). The central core of the spheroids presented with an area of dead cells at different stages of apoptosis and cellular debris (Figure 18).

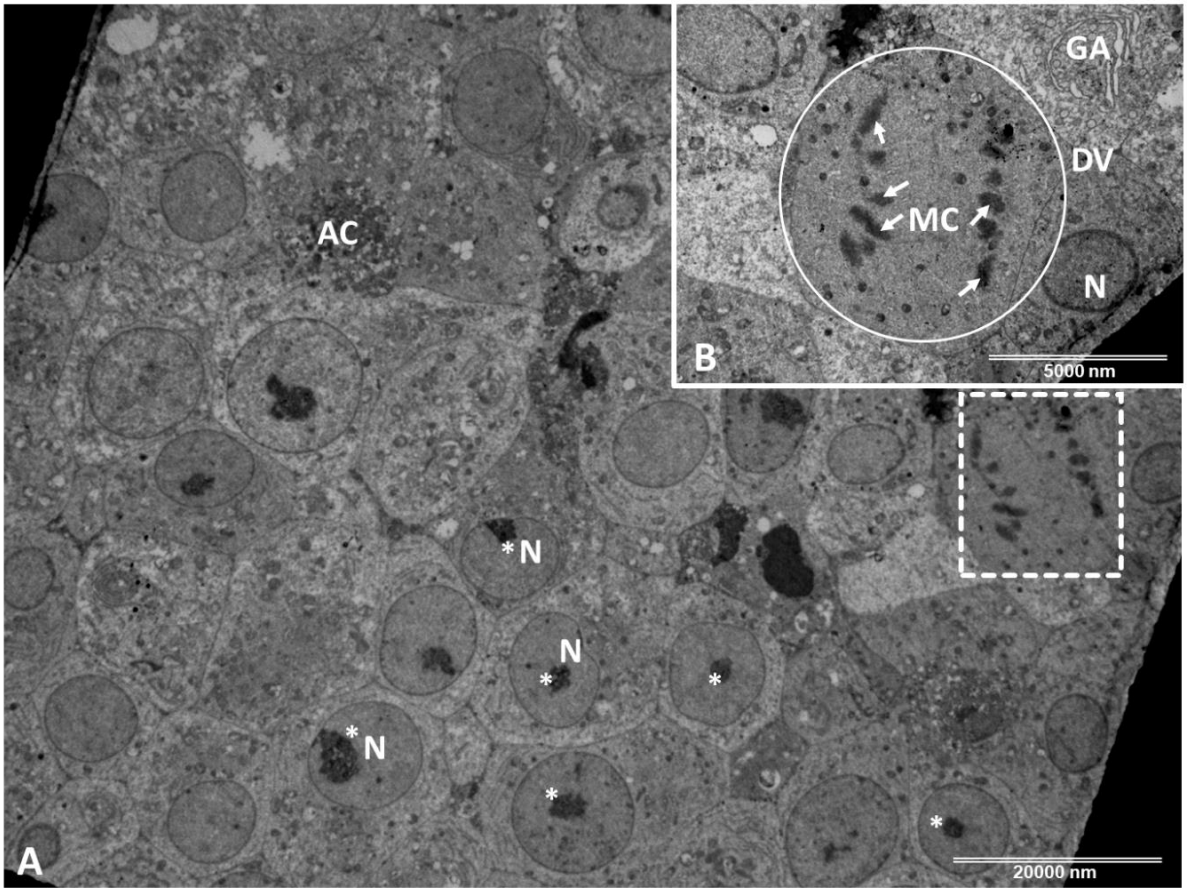

Figure 15: Transmission electron micrograph of INS-1 spheroids showing characteristics features synonymous to pancreatic β-cells. The EM shows the typical presence of neuroendocrine cell demonstrating some characteristic ultrastructural features synonymous with pancreatic β-cells. These features include euchromatic nuclei with prominent nucleoli, RER and Golgi apparatus indicative of active protein synthesis (A). The presence of some apoptotic cells and a mitotic cell (insert) confirms active cellular turnover (B). The chromosomes are evident in the dividing cell (anaphase).

N= Nucleus, * = Nucleolus, White Arrows = Chromosome cell, Circle DV = dividing cell, GA = Golgi apparatus. Scale bars = 5000 nm and 20000 nm.

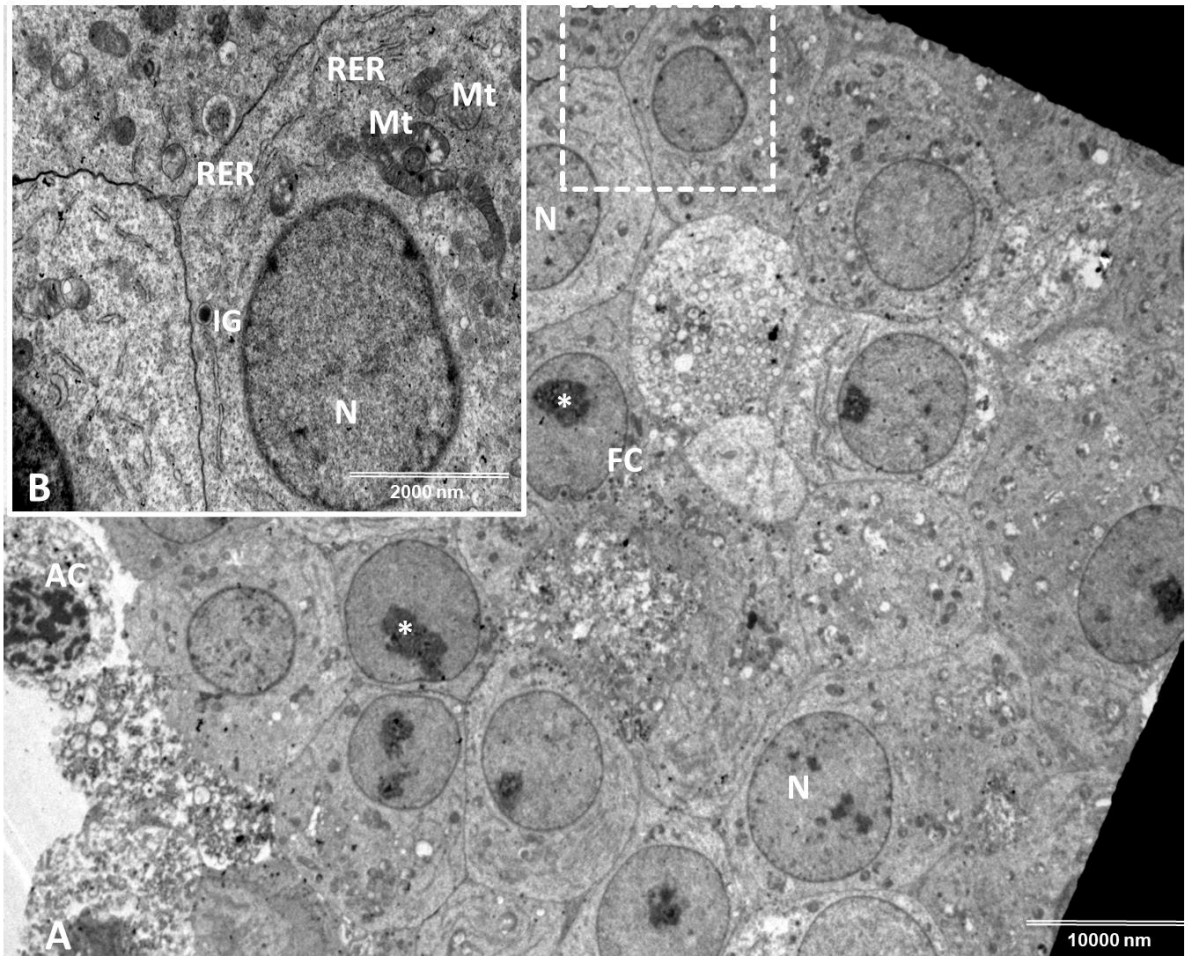

Figure 16: Transmission electron micrograph of INS-1 spheroids. Electron micrograph showing functional neuroendocrine cell with insulin-like secretory β granules i.e. membrane-bound granules of approximately 300 nm in dimeter with an electron-dense central crystalloid core surrounded by electron-lucent area (A). The insert shows an enlarged area demonstrating mitochondria, RER and insulin granules (B).

FC = Functional β-cells containing many insulin-like secretory β granules, (*) = Nucleolus, N= Nucleus, AC = Apoptotic cell, RER = Rough endoplasmic reticulum, Mt = Mitochondria (Mt), IG = Insulin-like secretory β granules. Scale bar = 10000 nm and 2000 nm (Insert).

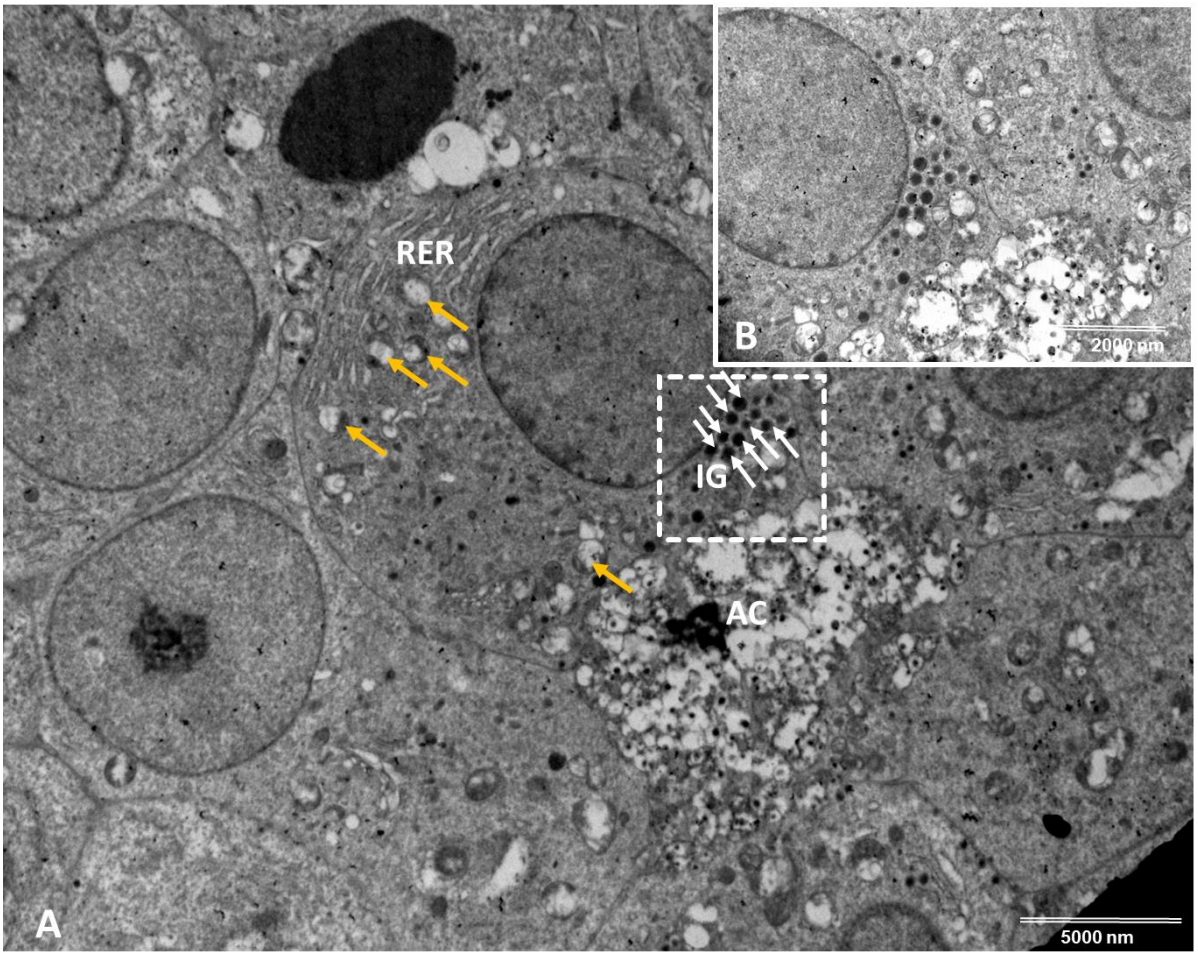

Figure 17: Transmission electron micrograph of INS-1 spheroids showing β-cell characteristics. Electron micrograph confirming the presence of characteristic insulin-like β granules and the presence of an early apoptotic cell located next to the live cells (A). The insert micrograph showing an active cell with numerous insulin-like secretory β granules. The presence of blebbing mitochondria is indicative of ischemic cellular stress (B).

Orange arrows = blebbing mitochondria, AC = Apoptotic cell, RER = Rough endoplasmic reticulum, white arrows IG = Insulin secretory β granules. Scale bar = 5000 nm and 2000 nm (Insert).

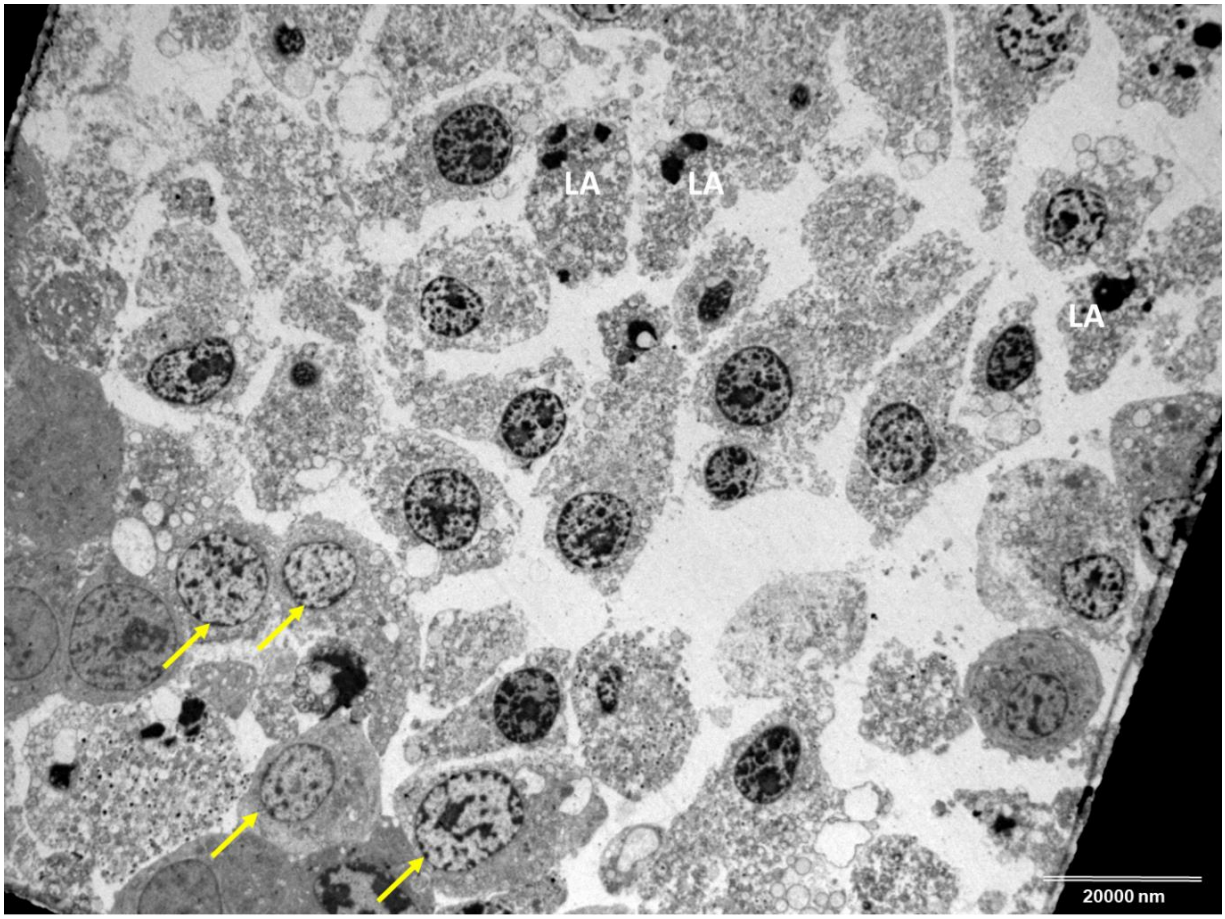

Figure 18: Transmission electron micrograph of apoptotic region in INS-1 spheroids. Ultrastructural features of the central portion of the spheroids demonstrates an area of apoptotic cells in various stages of apoptosis, indicative of an area of ischemia and nutrient deficiency**.**

LA = Late apoptosis, Arrows = Early apoptosis. Scale bar = 20000 nm.

4.1.7. Experimental induction of glucotoxicity in the spheroids

We induced *in vitro* glucotoxicity by supplementing glucose to RPMI-1640 media which, originally contained 11 mM glucose, to a total concentration of 33 mM glucose (HG). In addition, two treatment conditions, plant-based (HG-GRT™) and chemical based (HG-BACE) were used to assess their effect in ameliorating glucotoxic conditions on the novel spheroid model. RPMI-1640 media was used as the normal control (NG: 11 mM glucose). The following: week 1 and week 2 are used to denote treatment periods, while day 14 represents the day when treatment was started.

4.1.7.1. Improved size profiles in glucotoxic spheroids

The spheroids size profiles from day 1 to day 14 were determined as previously described in (subsection 4.1.3). Glucotoxicity was induced at day 14 and thereafter, the effect of HG and subsequent treatments (GRT™ and BACE) on spheroid sizes was measured (Figure 19). The time points when the spheroids total areas were measured were: Day 14 (before treatment), and 1 and 2 weeks (after glucotoxicity induction and treatment).

At day 14, spheroid sizes were comparable to each other (Figure 20). After 1 week of glucotoxicity induction, a significant decrease in spheroid size was observed in the HG group compared to the NG (7185 μm^2 ± 100 vs 25030 μm^2 ± 500; p <0.0001). Interestingly, HG-GRT™ and HG-BACE improved the sizes of the spheroids compared to the HG group (13308 μm^2 ± 1500; p= 0.001; 10812 μm^2 ± 250; p= 0.04 vs 7185 μm^2 ± 100; respectively).

After 2-weeks of glucotoxicity induction, spheroids in the HG group seemed to have recovered from the “shocking deleterious” effect of high glucose shown by an increase in spheroid size compared to week 1 (22658 μm^2 ± 350 vs 7185 μm^2 ± 100) (Figure 20). A similar effect was observed in the HG-GRT™ and HG-BACE (24992 μm^2 ± 500 vs 13308 μm^2 ± 1500) and (23593 μm^2 ± 497.5 vs 10812 μm^2 ± 250) (Figure 20).

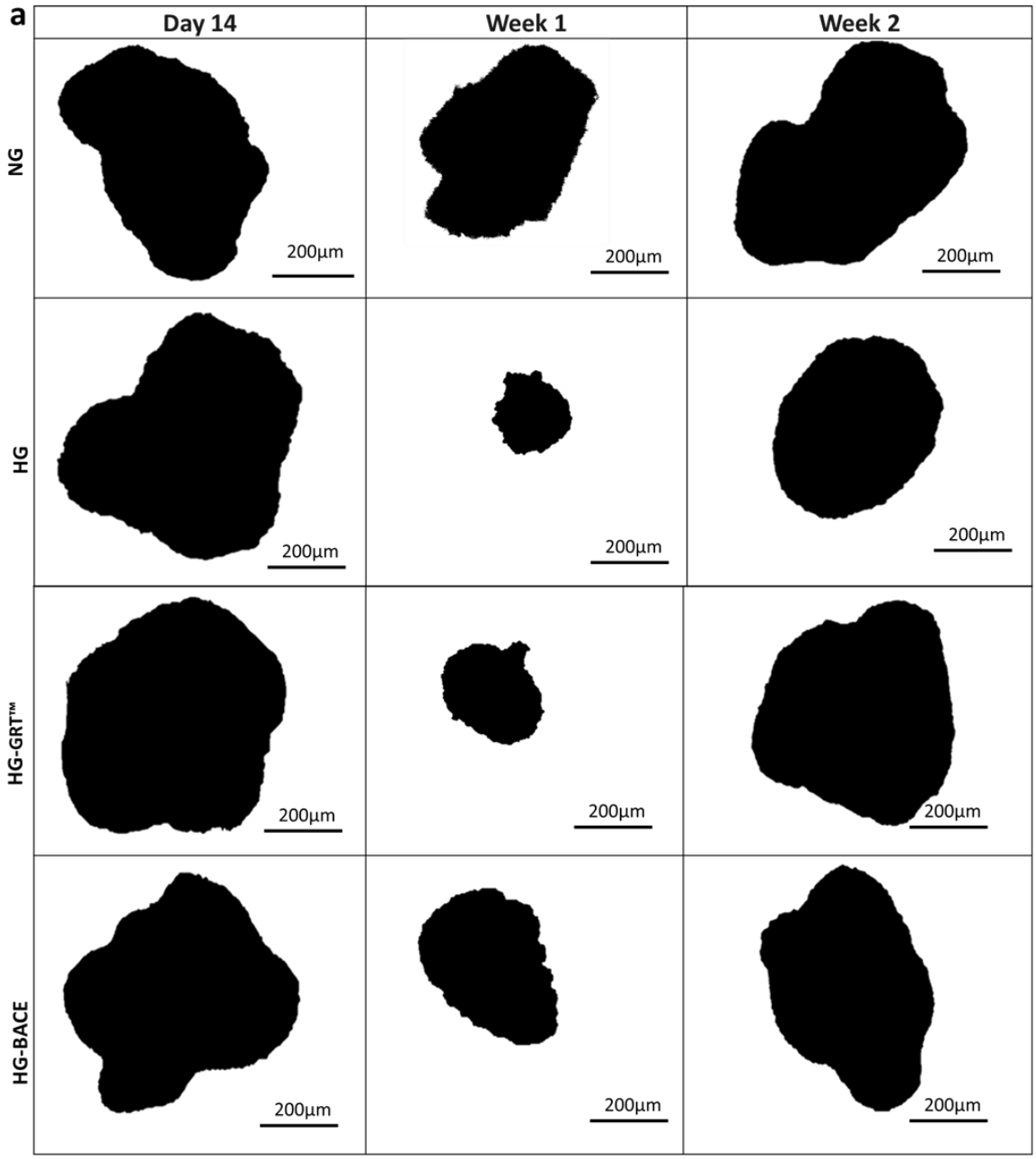

Figure 19: Size profile of INS-1 spheroids. The effect of glucotoxicity and treatments on the spheroids is represented from week 1 and week 2. Day 14 represents the day of the start of the treatment where spheroid sizes were comparable in all groups. One week after inducing glucotoxicity, the size of the HG treated spheroids was drastically reduced compared to NG group, with GRT™ and BACE treatments improving the size of the spheroids compared to HG group. After 2-weeks, the spheroid sizes improved, although in the HG treated spheroids remained smaller compared to the NG group while the GRT™ and BACE treatments were larger than HG group. Scale bars: 200 µm (Day 14, Week 1 and Week 2).

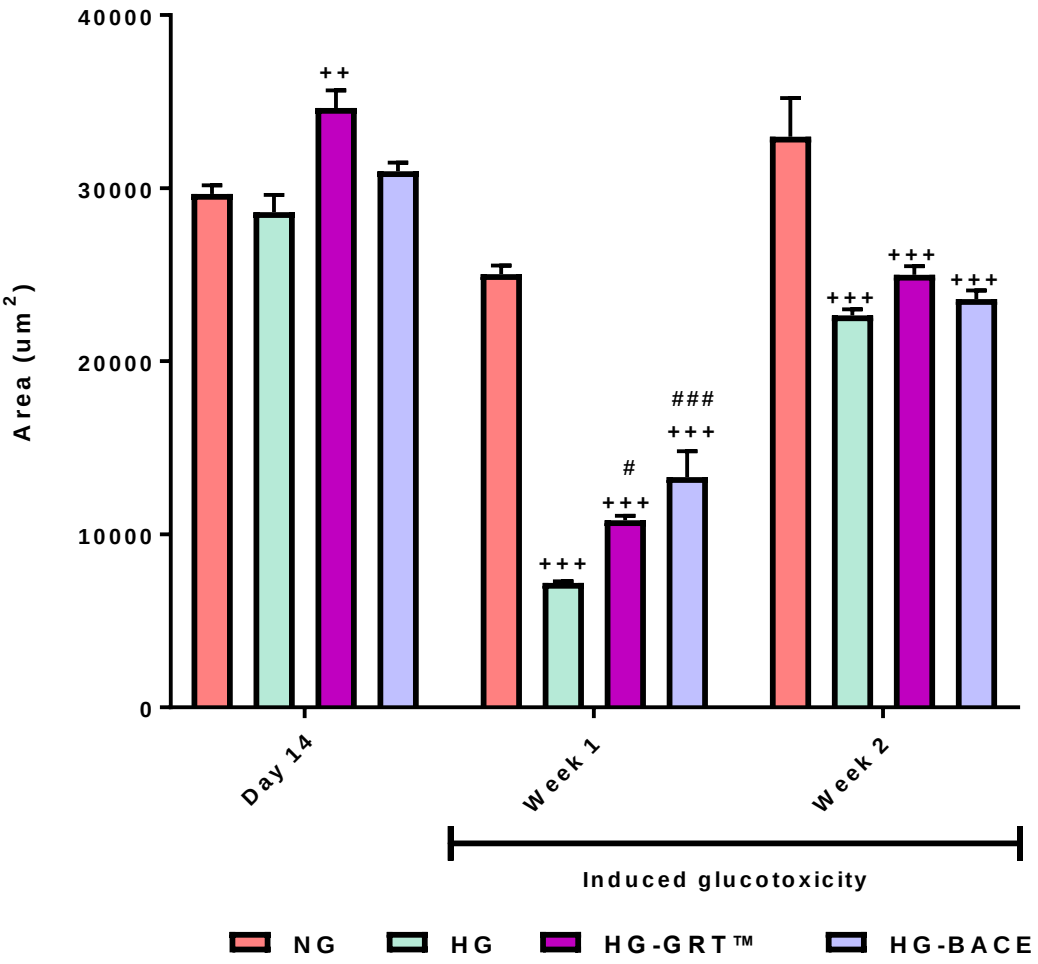

Figure 20: Average INS-1 spheroid sizes. Area of the spheroids before the start of the treatment (Day 14), and one week and two weeks after inducing glucotoxicity.

Data presented as the mean ± SEM of three independent experiments (n=3). Two-way ANOVA (Sidak's multiple comparisons test); followed by a Student-T test where appropriate; # = p<0.05; ### = p<0.0001 vs HG at the specific time point, ++ = p<0.001; +++ =p<0.0001 vs. NG group at the specific time point.

4.1.7.2. The amelioration of high glucose-induced toxicity

The ATP production as a measure of the spheroid's viability and cell growth in spheroids experimentally exposed to glucotoxicity were assessed. Overall, the ATP production of the spheroids grown in NG- 11 mM significantly increased proportionally over time in culture (Figure 21).

In the HG treated group, there was a reduction in cellular ATP production when compared to the NG (73.63% ± 2.13 vs 100.0% ± 0.36; $p< 0.001$) week 1 after inducing glucotoxicity (Figure 21). Meanwhile, HG-GRT™ group significantly improved the viability of the spheroids when compared to the HG group (82.49% ± 1.07 vs 73.63% ± 2.13; $p<0.05$), while HG-BACE had a non-statistically significant increase of ATP (Figure 21).

After two weeks of inducing glucotoxicity, significant reductions in cellular ATP content were observed in the HG, HG-GRT™ and HG-BACE groups compared to the NG (58.07% ± 0.51, 75.5% ± 1.91, and 73.3% ± 1.89 vs 100.0% ± 0.49; $p<0.0001$). Interestingly, although reduced spheroid ATP content was observed in both HG-GRT™ and HG-BACE, compared to NG group, both groups had a higher spheroid ATP content than the HG group (75.5% ± 1.91, and 73.3% ± 1.89, respectively vs 58.07% ± 0.51; $p<0.001$) (Figure 21).

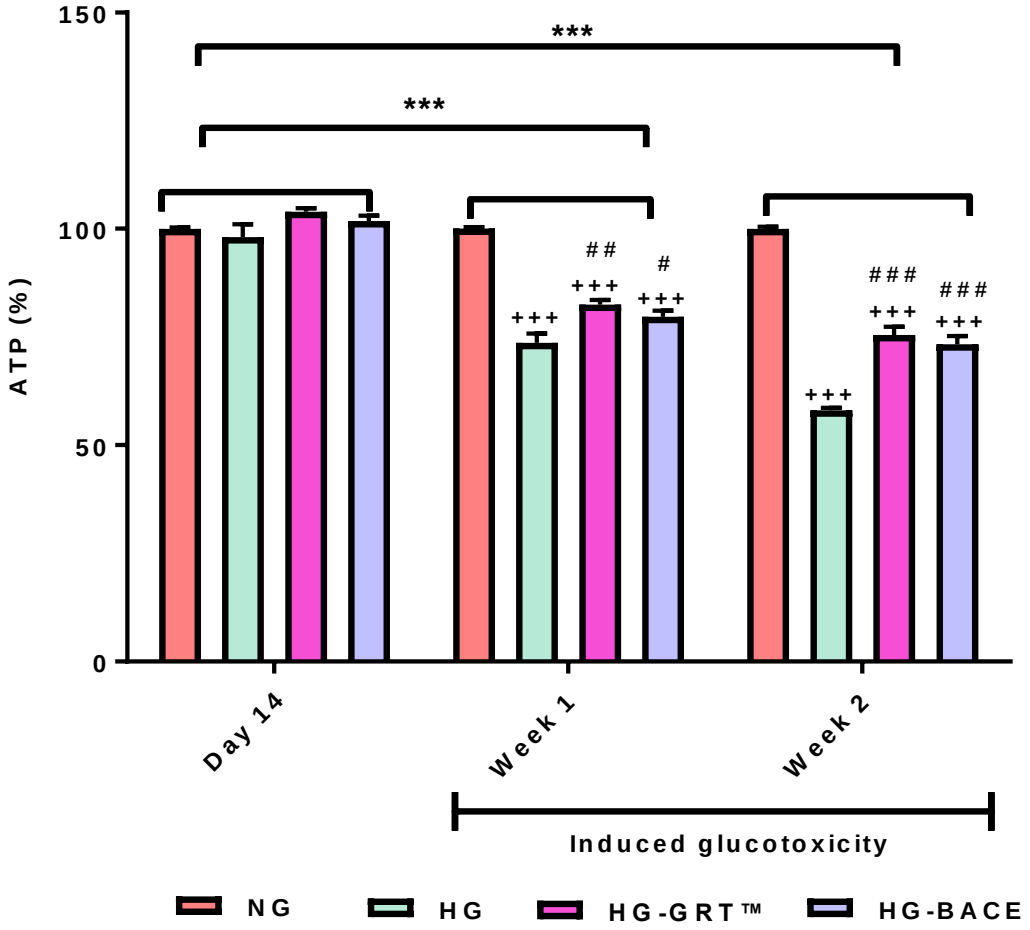

Figure 21: ATP content profile. The effect of glucotoxicity and treatments on INS-1 spheroids viability following exposure for two weeks was assessed. Cell viability was quantified by using ATP luminescence assay and normalised to protein.

Data presented as the mean ± SEM of three independent experiments (n=3). Two-way ANOVA (Sidak's multiple comparisons test); followed by a Student T-test where appropriate; *** =p<0.0001 vs. NG from day 14; # = p<0.05; ## =p<0.001; ### p< 0.0001 vs HG at the specific time point, +++ =p<0.0001 vs. day at the specific time point.

4.1.7.3. Glucose utilization profiling

Despite the effects observed on size profiling and ATP production, the glucose utilization profile of the spheroids was comparable throughout the study (Figure 22).

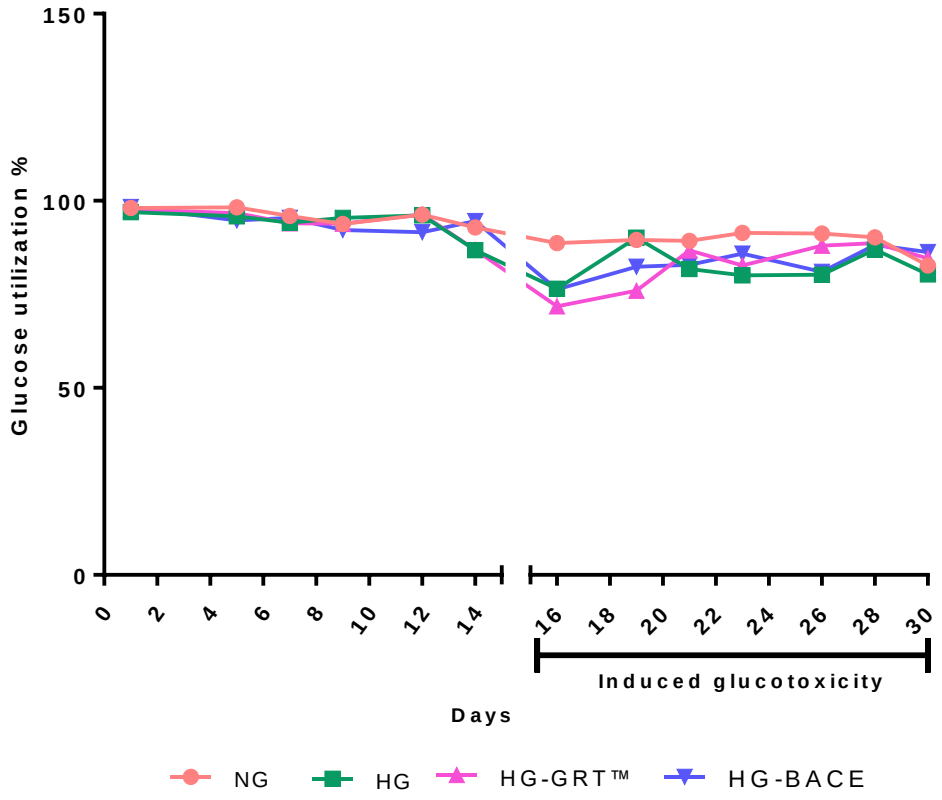

Figure 22: Glucose utilisation profile of INS-1 spheroids. Glucose utilization was monitored throughout the culturing of the spheroids under the following conditions: normal glucose levels (NG), glucotoxicity (HG) and during treatments: HG-GRT™ and HG-BACE. Glucose utilization was comparable in all the groups throughout the study. Glucose concentration was measured in mmol/L when growth media was refreshed and calculated as a percentage relative to the freshly added media at 100%.

Data is presented as the mean ± SEM of three independent experiments (n=3).

4.1.8. Function of the spheroids

Spheroids function was assessed by performing a glucose stimulated insulin secretion (GSIS) assay. Insulin secretion and concomitant amylin secretion from basal (2.8 mM) and stimulated (16.7 mM) glucose concentrations were determined.

4.1.8.1. Glucose Stimulated Insulin Secretion in the spheroids

In the NG group insulin secretion was increased at stimulated glucose levels compared to basal levels (41.08 ng/mL ± 5.23 vs 22.6 ng/mL ± 3.49; p=0.001), while no statistical significance was observed in the HG group. Similarly, stimulated glucose levels enhanced insulin secretion in the HG-GRT™ group compared to basal levels (30.8 ng/mL ± 2.49 vs 17.9 ng/mL ± 2.54; p=0.05) (Figure 23).

In the HG and HG-BACE group, significant increases in basal insulin secretion was observed compared to the NG group (48.8 ng/mL ± 2.39 ng/mL; p=0.0001 and 37.77 ng/mL ± 4.87; p= 0.02 vs 22.6 ng/mL ± 3.49; respectively) (Figure 23). Interestingly, HG-GRT™ blunted the glucotoxic effects compared to the HG group (17.9 ng/mL ± 2.54 vs 48.8 ng/mL ± 2.39 ng/mL; p< 0.0001). HG-BACE induced a trend towards reducing insulin secretion (37.8 ng/mL ± 4.87 vs 48.8 ng/mL ± 2.39 ng/mL; p=0.07) (Figure 23).

4.1.8.2. Intracellular Amylin Secretion in the spheroids stimulated with glucose

Glucose stimulation had no effect on amylin secretion in the NG group. However, in the HG and the HG-BACE groups, significant increase in amylin secretion was observed following glucose stimulation (41.7 pg/mL ± 7.18 vs 20.3 pg/mL ± 4.39; p=0.01; 43.9 pg/mL ± 5.38 vs 21.5 pg/mL ± 3.57; p=0.007). Treatment with GRT™ blunted this effect (p= NS) (Figure 24).

At basal glucose levels, higher amylin concentrations were observed in the HG-GRT™ compared to the NG and the HG groups (30.2 pg/mL ± 1.43 vs 21.5 pg/mL ± 3.57; p=0.05 and 20.3 pg/mL ± 4.39; p=0.05) (Figure 24).

At stimulated glucose levels, amylin levels were higher in the HG, HG-GRT™ and HG-BACE groups compared to the NG (41.7 pg/mL ± 7.18; 32.5 pg/mL ± 7.19 and 43.9 pg/mL ± 5.38 vs 12.8 pg/mL ± 3.08; p<0.05, respectively).

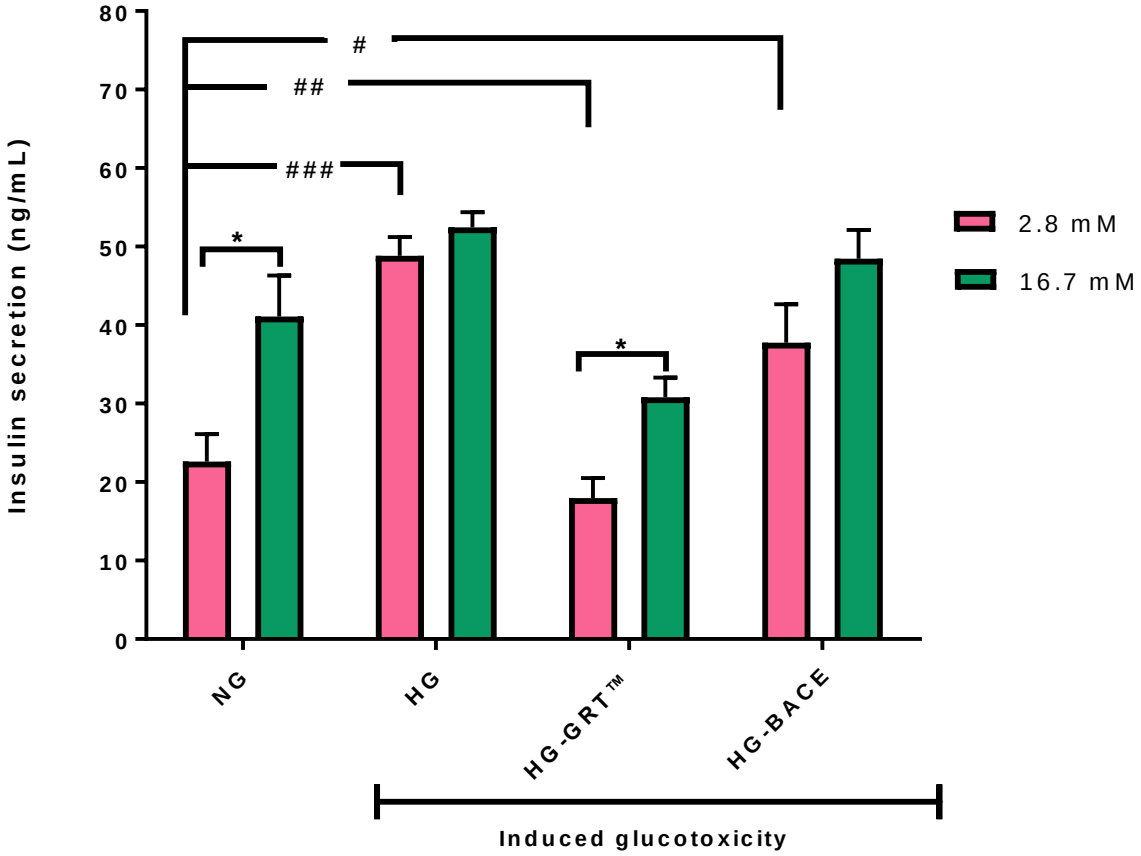

Figure 23: Glucose stimulated insulin secretion of treated INS-1 spheroids. Insulin secretion was measured in response to basal glucose levels (2.8 mM) and stimulation levels (16.7 mM) under different treatment conditions: normal glucose control (NG-11 mM glucose), high glucose control (HG-33 mM glucose), high glucose treated with GRT™ (HG-GRT™) and high glucose treated with BACE inhibitor LY2886721 (HG-BACE). Insulin was quantified spectrophotometrically using ELISA (630 nm).

Data is presented is the mean ± SEM of three independent experimental repeats (n=3) relative to the control. Two-way ANOVA was used for analysis (Sidak's multiple comparisons test); followed by a Student T-test where appropriate; * = p< 0.05 vs basal glucose levels at that specific treatment group, # = p< 0.01, ## = p<0.001 , ### = p <0.0001 vs basal NG.

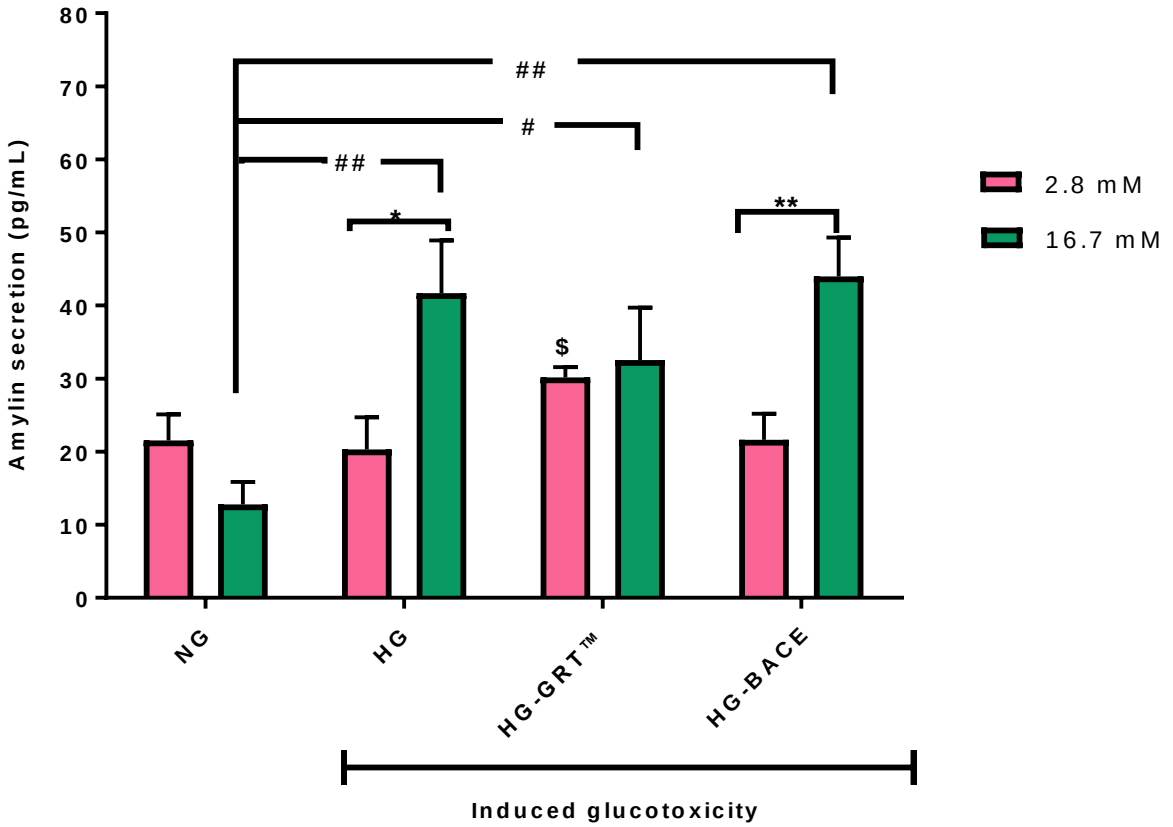

Figure 24: Amylin secretion profile of INS-1 spheroids. Effect of the treatments on glucose stimulated amylin secretion was determined in the spheroids following treatments as follows: Normal glucose control (NG-11 mM glucose), high glucose control (HG-33 mM glucose), high glucose treated with GRT™ (HG-GRT™) and high glucose treated with BACE inhibitor LY2886721 (HG-BACE). Amylin secretion was significantly reduced in the NG after stimulation while in the HG, HG-GRT™ and HG-BACE, amylin secretion was increased compared to basal glucose levels. Amylin was quantified spectrophotometrically using the Spectra-max (450 nm).

Data is presented is the mean ± SEM of three independent experiments (n=3), relative to the control. Analysis was conducted using Two-way ANOVA (Sidak's multiple comparisons test); followed by a Student T-test where fitting; * = p< 0.05 and ** = p<0.001 vs basal glucose levels at that specific treatment group, # = p< 0.05 and ## = p<0.001 vs stimulated NG levels, $ = p< 0.05 vs basal NG levels.

4.1.8.3. Insulin to Amylin Ratio

Glucose stimulation had no effect on the insulin/amylin ratio in the NG group. However, in the HG group, the basal insulin/ amylin ratio was significantly increased compared to the stimulated insulin/ amylin ratio (168.8% ± 33.37 vs 28.1% ± 5.82; p=0002) while the glucose stimulated ratio was reduced compared to the NG group (28.1% ± 5.82 vs 64.4% ± 16.86; p=0.02). The GRT™ treatment significantly reduced the basal insulin/ amylin ratio compared to NG and HG groups (34.7% ± 5.16 vs 100% ± 26.43 and 168.8% ± 33.37; respectively), while BACE had no effect (Figure 25). Moreover, compared to the HG group, HG-GRT™ had a lower basal insulin / amylin ratio (168.8% ± 33.37 vs 34.7% ± 5.16; p= 0.004).

Using Pearson r correlation coefficient, positive correlation at basal insulin and amylin secretion in the NG group was observed [r =-0.86, p =0.003] (Table 6). While at stimulated glucose levels, a positive correlation was only observed for the HG-GRT™ group (r=0.73, p=0.03) (Table 6).

Table 6: The relationship between insulin and amylin secretion in response to basal and stimulation glucose levels

Basal				Stimulation			
Group	r	P value	P value summary	Group	r	P value	P value summary
NG	0.8567	0.0032	**	NG	-0.1505	0.6991	ns
HG	0.3439	0.6480	ns	HG	0.0171	0.9651	ns
HG-GRT™	058862	0.0972	ns	HG-GRT™	0.7289	0.0259	*
HG-BACE	0.3931	0.2952	ns	HG-BACE	0.1317	0.7356	ns

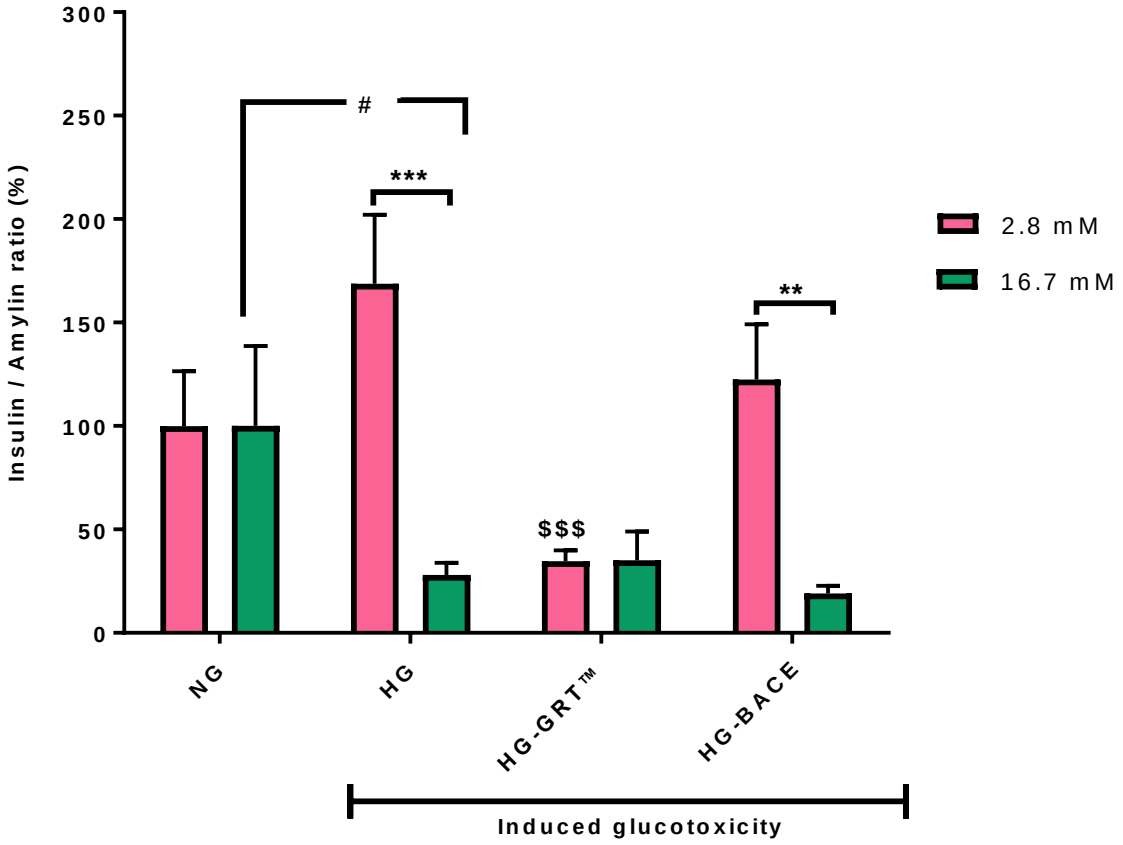

Figure 25: Insulin/amylin secretion ratio. Insulin to amylin ratio was determined as an indicator of the function of the spheroids following basal (2.8 mM) and stimulation (16.7 mM) glucose levels treatments in the groups: Normal glucose control (NG-11 mM glucose), high glucose control (HG-33 mM glucose), high glucose treated with GRT™ (HG-GRT™) and high glucose treated with BACE inhibitor LY2886721 (HG-BACE). Insulin and Amylin were quantified spectrophotometrically using an ELISA (630 /450 nm). The percentage of amylin to insulin ratio was calculated by averaging the respective technical repeats of each end point assay.

Data is presented is the mean ± SEM of three independent experiments (n=3), relative to the control. Analysis was conducted using Two-way ANOVA (Sidak's multiple comparisons test); followed by a Student T-test where fitting; ** = p< 0.05, *** = p<0.001 vs same group at 16.7 mM; ## = p<0.001 vs HG, $$$ = p<0.001 vs basal NG and HG respectively.

4.1.9. The effect of GRT™ extract and BACE inhibitor on HG induced inflammation

We assessed the secretion of the pro-inflammatory cytokines, interleukin 6 (IL-6) and 10 (IL-10) and tumour necrosis factor alpha (TNF-α) by spheroids at week 1 and week 2 after glucotoxicity induction and subsequent treatments.

4.1.9.1. Effects of GRT™ and BACE inhibitor on TNF- α and IL-6 levels

After 1 week of glucotoxicity induction, higher TNF-α levels in the HG and HG-GRT™ were observed compared to the NG group (2.4 pg/mL ± 0.24; p= 0.001 and 2.3 pg/mL ± 0.33; p= 0.01 vs 1.1 pg/mL ± 0.23, respectively). The HG-BACE group had significantly lower TNF-α levels compared to HG group (2.4 pg/mL ± 0.24, 0.67 pg/mL ± 0.15; p< 0.0001) (Figure 26A).

After 2 weeks, increased levels of TNF-α persisted in the HG group while in the HG-GRT™ group, these levels were reduced (1.6 pg/mL ± 0.16 vs 2.6 pg/mL ± 0.33; p= 0.02). Interestingly, TNF-α levels increased in the HG-BACE group after 2 weeks (2.4 pg/mL ± 0.24 vs 0.9 pg/mL ± 0.20; p= 0.0001).

IL-6 levels were not detectable in the NG and BACE group while low levels were detectable for HG and HG-GRT™ following week 1 of glucotoxicity induction (Figure 26B). After 2 weeks, IL-6 levels had increased but these differences were not significant across the groups (Figure 26B).

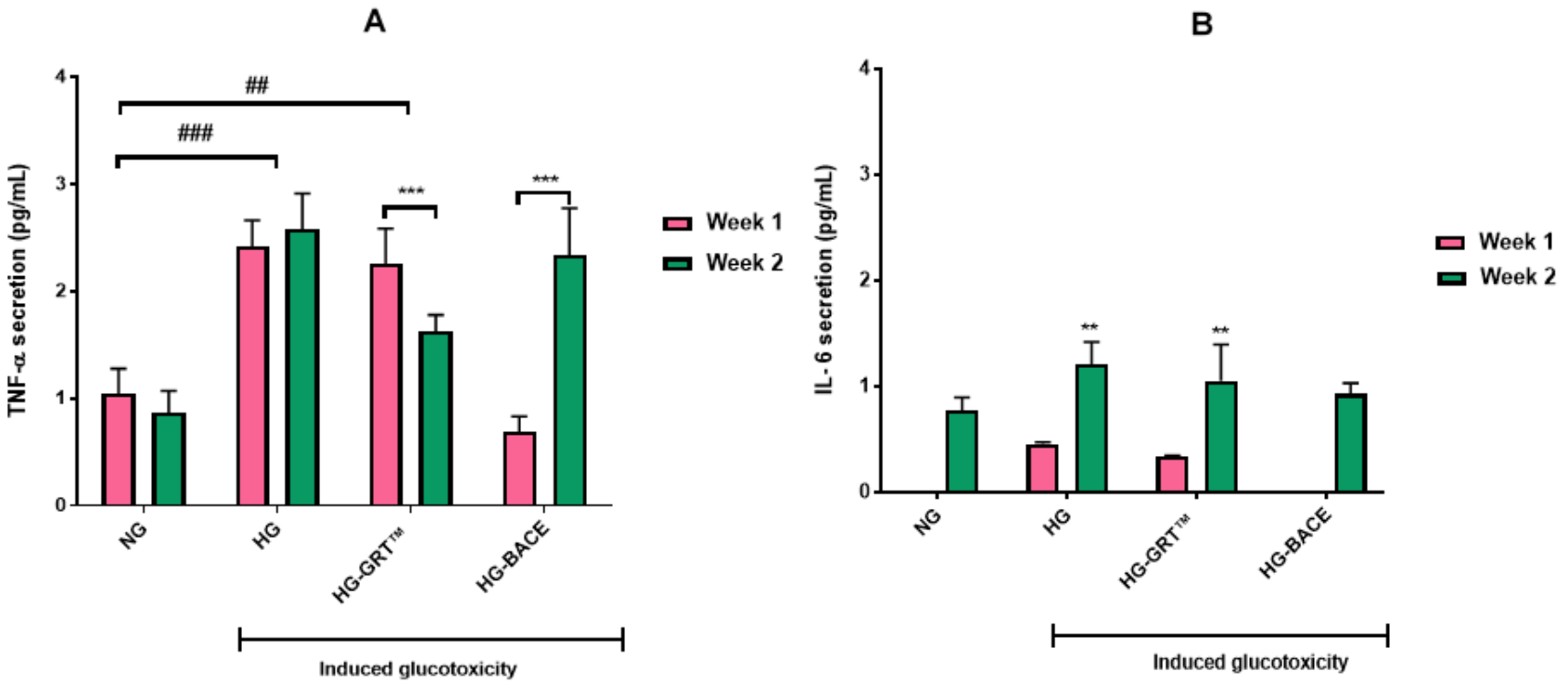

Figure 26: Pro-inflammatory cytokine levels in treated INS-1 spheroids following glucotoxicity induction. Effects of HG, HG-GRT™ and HG-BACE inhibitor on the secretion of TNF-α levels (A) and IL-6 levels (B) in the spheroids. TNF-α and IL-6 were quantified spectrophotometrically using an ELISA (630 nm).

Data is presented as the mean ± SEM of three independent experiments (n=3), relative to the control. Analysis was conducted using Two-way ANOVA (Sidak's multiple comparisons test); followed by a Student T-test where appropriate; * = p<0.05, ** = p<0.001, *** = p<0.0001 vs same group at week 1; # = p<0.05, ## = p<0.001, ### =p<0.0001 vs. NG.

4.1.10. Western blot analysis

Although not statistically significant, fold expression changes were observed in TMEM27 expression in the HG, HG-GRT™ and HG-BACE groups (3-, 7- and 4-fold increase, respectively) compared to NG group (3.15 ± 2.44; 7.11 ± 5.95 and 4.38 ± 2.41vs. 1.0 ± 0.54, respectively) (Figure 26A). Similarly, 4 and 1.7-fold increases in BACE was observed in the HG-GRT™ and HG-BACE group compared to the NG group (2- and 1.7-fold increase, respectively) compared to NG group (2.12 ± 0.91 and 1.74 ± 0.84 vs. 1.0 ± 0.82, respectively) (Figure 27B).

No fold change in PDX-1 expression was observed (Figure 27C) while Ki-67 expression increased 2-fold in HG-GRT™ compared to NG group (2.72 ± 0.88 and vs 1.0 ± 0.31) (Figure 27D). Additionally, no significant fold changes were observed in IR, GLUT-2 (Figure 27E&F), p-38, ERK1/2 (Figure 27G&H), LC3A/B and AKT protein expression levels in HG, HG-GRT™ and HG-BACE compared to NG groups (Figure 27I&J).

Moreover, we were unable to detect amylin and caspase-3 expression in the spheroids after various optimizations.

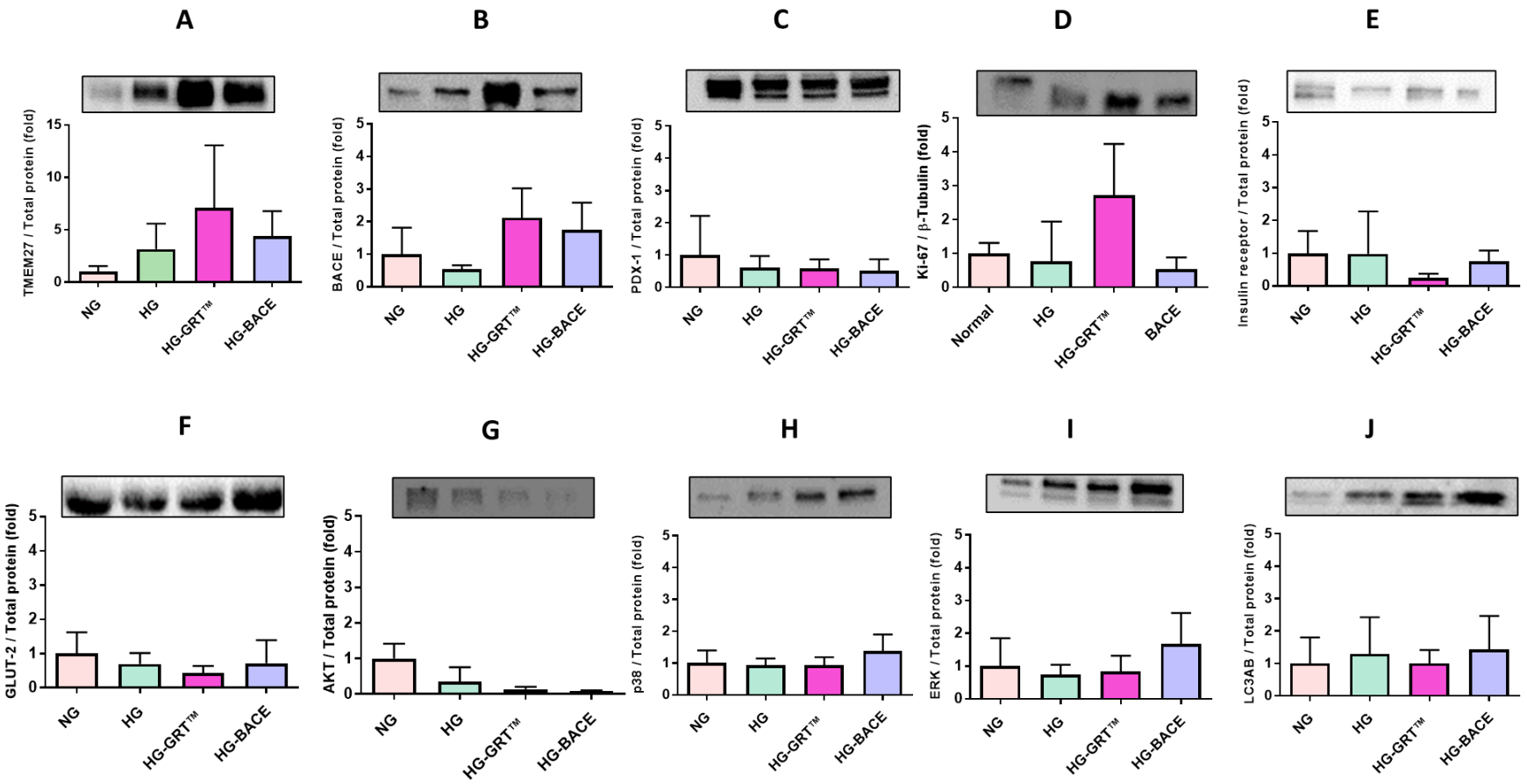

Figure 27: Functional protein expression in treated INS-1 spheroids. Expression of BACE2 (A), TMEM27 (B), PDX-1 (C), Ki-67 (D), IR (E), GLUT-2 (F), AKT G), p38 (H), ERK (I), LC3AB (J). Chemiluminescent images were obtained on the ChemiDoc to quantify protein expression. Data presented is the mean ± SEM of three independent experiments and normalised to total protein (n=3) and expressed relative to the control (NG); One-way ANOVA (Tukey post-hoc test).

4.1.2. Summary of Results

Table 6: Summary of the effect of HG- GRT™ and HG-BACE on viability, cell function, inflammation in the spheroids.

	NG	HG	HG-GRT™	HG-BACE
Viability and cell growth				
Size profiling	-	↓	↑↑	↑↑
ATP content	-	↓↓	↑↑	↑↑
Glucose utilization	-	Θ	Θ	Θ
Function				
Insulin secretion	-	Dysfunctional	↑↑	↑↑
Amylin secretion	-	↑	↑	↑
Insulin/Amylin ratio	-	↑↑	↓↓	↑
Correlation insulin and amylin	+ only at basal glucose levels	Θ	+ only stimulatory glucose levels	Θ
TNF-α secretion	-	↑↑	↓↓ at week 2	↓ at week 1
IL-6 secretion	-	↑↑	↑↑	↓ at week 1
IL-10 secretion	ND	ND	ND	ND
Western blots				
Amylin	ND	ND	ND	ND
BACE2	-	Θ	↑↑ fold increase	↑↑ fold increase
Caspase 3	ND	ND	ND	ND
TMEM27	-	↑↑	↑↑	↑↑
ERK1/2	-	Θ	Θ	Θ
LC3A/B	-	Θ	Θ	Θ
p38	-	Θ	Θ	Θ
PDX-1	-	Θ	Θ	Θ
GLUT-2	-	Θ	Θ	Θ
AKT	-	Θ	Θ	Θ
IR	-	Θ	Θ	Θ
Ki-67	-	Θ	↑↑ fold increase	Θ

** Arrow represents ↓decrease, ↑ increase / improved, ND= Not detectable, += Positive correlation, Θ= No effect / No correlation.

4.2. *In vivo* results

The efficacy of GRT™ and BACE inhibitor to ameliorate hyperglycemia induced changes in the pancreas was investigated in six-week-old C57BLKS homozygous obese diabetic Lepr *db/db* and heterozygous lean non-diabetic *db*+ mice. In this study, we used male mice on the basis of avoiding hormonal interplay which would render the results uninterpretable and female animals are quite protective in several diseases. The study was divided into three phases: phase I (10 weeks treatment), phase II (16 weeks treatment) and phase III (32 weeks treatment) as detailed in the methods section. An insulin sensitizing anti-diabetic drug, pioglitazone was used as treatment control (positive control). A low and high dose of GRT™ extract (GRT™-1 and GRT™-2, respectively) and a BACE inhibitor (β-secretase inhibitor IV) were used in each phase.

Physiological parameters such as calorie intake and body weights were assessed, while biochemical parameters assessed included: fasting blood glucose, oral glucose tolerance, fasting serum insulin, C-peptide and amylin levels. Insulin resistance and β-cell function were assessed by calculating HOMA-IR and HOMA-β respectively. Immunohistochemistry was used to assess the effect of treatment on the pancreatic islets.

4.2.1. Morbidity and Mortality

None of the non-diabetic *db*+ treatment groups exhibited adverse effects or caused mortality. In the diabetic *db/db* mice, apart from the anticipated pathophysiological phenotypic traits, such as hyperphagia, hyperglycemia, and increased body weight, treatments did not induce any adverse effects.

4.2.2. Calorie intake and body weight

In phase I, statistically significant increases in calorie intake and body weight were observed in *db/db* mice compared to *db*+ mice over the 10-week period ($p<0.05$) (Figure 28A & B). A similar effect was observed in phase II ($p<0.05$) (Figure 29 A & B). In the *db*+ mice, no apparent changes in body weight and calorie intake throughout the phases were observed, except at the end of each respective phase (phase I, II, III) (Figure 28A, Figure 29A & Figure 30).

In phase I *db*+ mice, a decrease in calorie intake in BACE inhibitor and an increase in GRT™-2 groups respectively was observed compared to the NC group (4056 ± 52.1; p=0.003 and 4690 ± 2.5; p=0.02 vs 4417 ± 52.0). In phase II, increases in calorie intake for BACE inhibitor, GRT™-1 and GRT™-2 were observed (4685 ± 2.5; p=0.02; 4417 ± 52.0; p=0.01 and 4237 ± 52.0; p=0.03 vs 3245 ± 471.3, respectively). Additionally, all treatments had higher body weight and calorie intake compared to phase I and phase II (p>0.05) (Figure 28A & Figure 29A).

In the *db/db* mice, all treatment groups had no significant effect on calorie intake except for GRT™-1, which increased calorie intake only in phase I (5767 ± 2.5 vs 5411 ± 2; p=0.002) (Figure 29B).

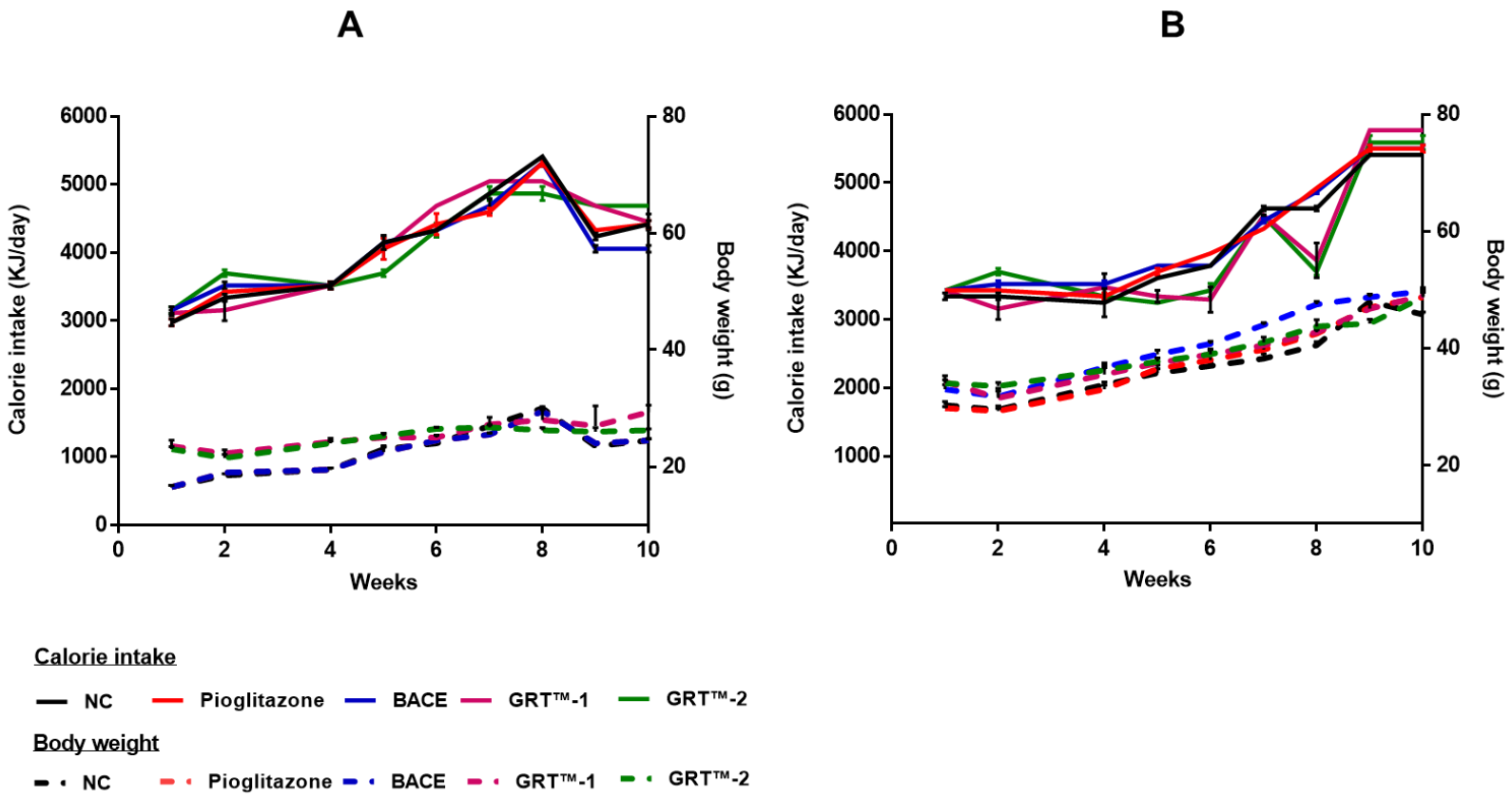

Figure 28: Body weight and calorie intake in phase I. Body weights and calorie intake were monitored during 10 weeks of treatment in non-diabetic *db*+ mice (A) and diabetic *db/db* mice (B). NC: Normal control, BACE: β-secretase inhibitor, GRT™-1: low dose, GRT™-2: high dose.

The results are expressed as the mean ± SEM (n = 4 per group) (Two-way ANOVA)

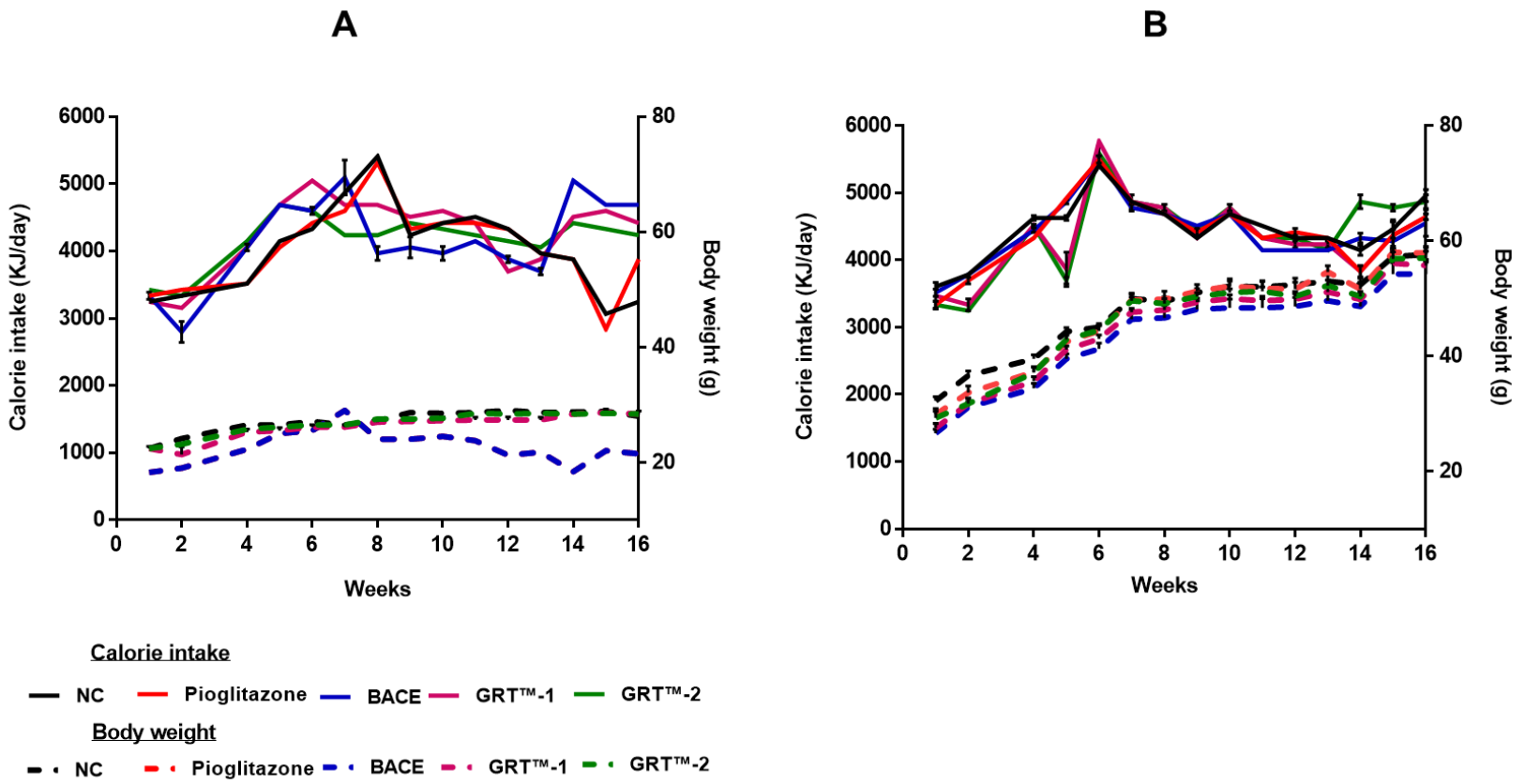

Figure 29: Body weight and calorie intake in phase II. Body weights and calorie intake were monitored during 16 weeks of treatment in heterozygous *db*+ mice (A) and homozygous *db/db* mice (B). NC: Normal control, BACE: β-secretase inhibitor, GRT™-1: low dose, GRT™-2: high dose.

The results are expressed as the mean ± SEM (n=7-8 per group) (Two-way ANOVA).

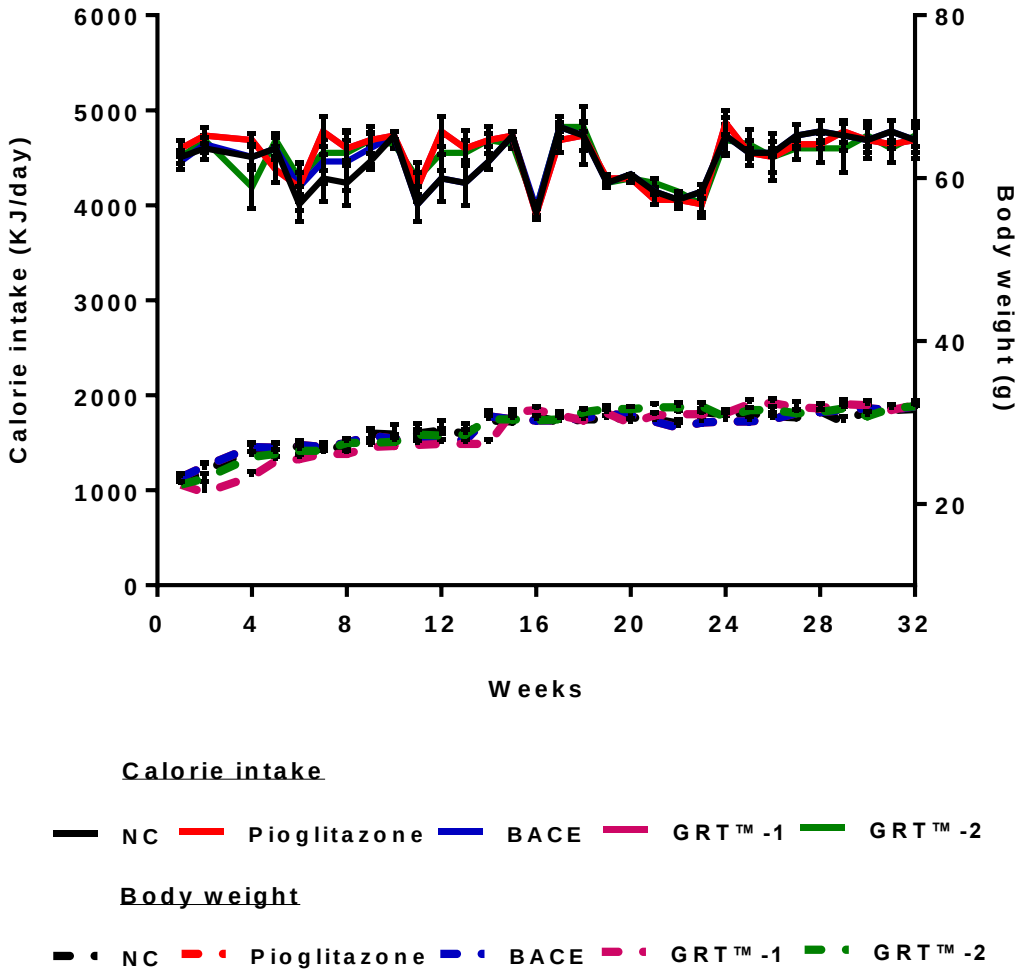

Figure 30: Body weight and calorie intake in phase III. Body weights and calorie intake were monitored during 32 weeks of treatment in heterozygous *db*+. NC: Normal control, BACE: β-secretase inhibitor, GRT™-1: low dose, GRT™-2: high dose.

The results are expressed as the mean ± SEM (n=8).

4.2.3. Fasting blood glucose and glucose tolerance

Fasting blood glucose (FBG) levels were higher in the *db/db* mice in both phase I and phase II compared to their *db*+ littermates ($p<0.05$) (Table 8 & Table 9).

4.2.3.1. Heterozygous *db*+ mice results in phase I, II and III

Fasting blood glucose levels were increased in all treatment groups of phase II compared to the same groups of phase I ($p<0.05$), followed by a gradual decrease in phase III (Table 8). Oral glucose tolerance remained comparable throughout the phases (Table 8).

Table 7: Impact of treatments on fasting blood glucose and oral glucose tolerance in phase I, II, III heterozygous *db*+ mice.

Fasting blood glucose levels increased in phase II compared to phase I, followed by a gradual decline in phase III.

	Group	Mean ± SEM	Mean ± SEM	Mean ± SEM
		Phase I	Phase II	Phase III
FBG (mmol/L)	NC	7.8±0.6	12.6±3.9 *	6.3±0.2 †
	Pioglitazone	6.5±1.1	9.1±1.7 *	7.2±0.4 †
	BACE	7.5±0.1	12.1±3.5 *	7.0±0.2 †
	GRT™-1	7.5±0.1	11.1±2.5 *	7.6±0.2 †
	GRT™-2	8.5±0.3	9.5±3.7 *	7.6±0.5 †
OGTT (AUC)	NC	1210±55	1064±69	1058±21.9
	Pioglitazone	991±92	1124±41	1039±29.7
	BACE	1034±47	1232±72	1232±72.2
	GRT™-1	1138±197	1242±51	1102±48.7
	GRT™-2	1195±93	1156±66	1008±30.3

NC: Normal control, BACE: β-secretase inhibitor, GRT™-1: low dose, GRT™-2: high dose.

Data is expressed as mean ± SEM (n=4-8); *$p<0.05$ vs. phase I and † $p<0.05$ vs phase II, (One-Way ANOVA, Tukey post-test).

4.2.3.2. Homozygous *db/db* mice results in phase I and II

Decreased FBG levels were observed at the end of phase I and phase II in the pioglitazone group compared to NC (Table 9). Additionally, BACE inhibitor and GRT™-2 improved glucose tolerance of the mice in phase I (2412 ± 121.0; p=0.01 and 2293 ± 105.6, p= 0.02 vs 2970 ± 95.62, respectively) (Figure 31A and Figure 31B).

In phase II, only pioglitazone improved glucose tolerance of the mice (1884 ± 296.0 vs 3238 ± 260.5; p= 0.004) (Figure 32A and Figure 32B), however FBG levels were not affected (Table 9).

Table 8: FBG levels of treatment groups in homozygous *db/db* mice of phase I and II.

Pioglitazone decreased FBG levels in both phase I and II compared to other treatments.

	Group	Mean ± SEM	Mean ± SEM
		Phase I	Phase II
FBG (mmol/L)	NC	14.1 ± 1.9	12.3 ± 1.8
	Pioglitazone	10.5 ± 1.0	9.3 ± 1.4
	BACE	12.5 ± 2.1	11.4 ± 0.5
	GRT™-1	12.4 ± 2.3	14.6 ± 2.5
	GRT™-2	11.8 ± 0.8	12.8 ± 2.5

NC: Normal control, BACE: β-secretase inhibitor, GRT™-1: low dose, GRT™-2: high dose.

Data is expressed as mean ± SEM (n=4-8), (One-Way ANOVA, Tukey post-test).

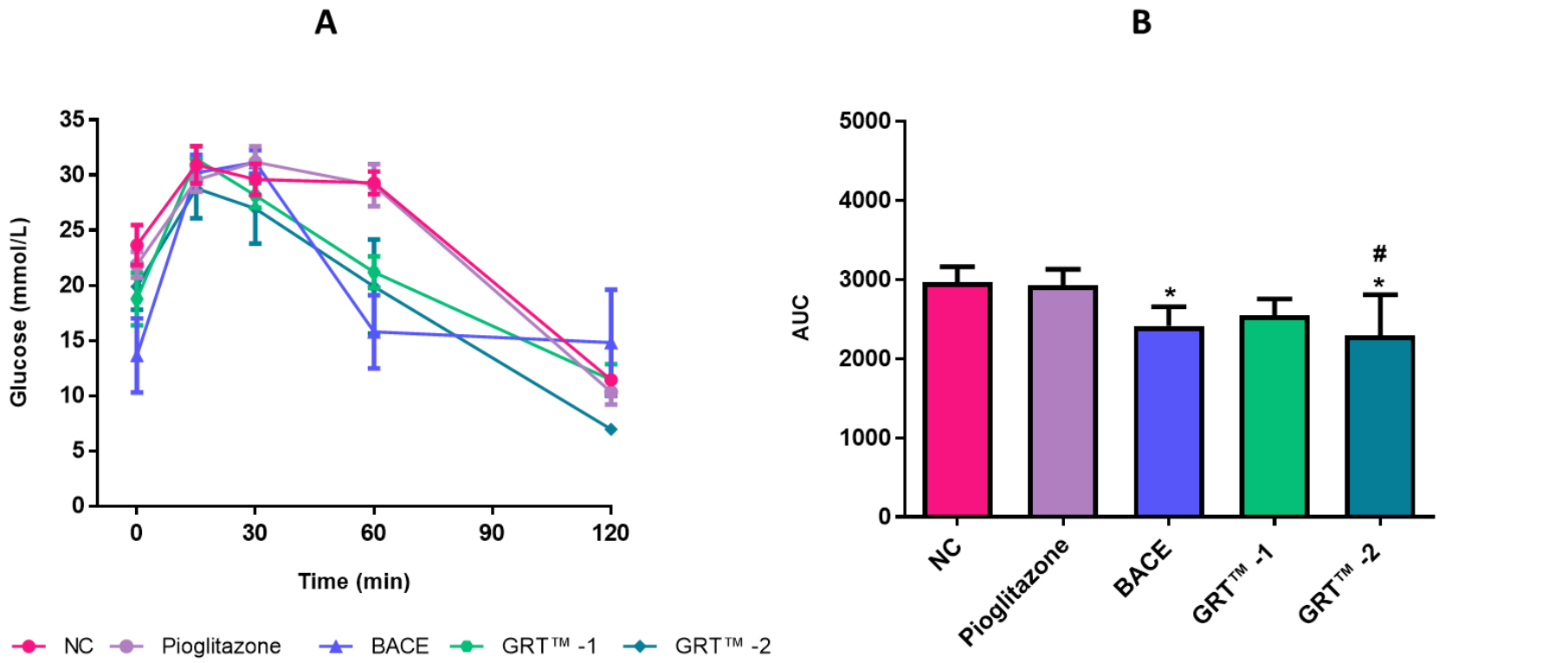

Figure 31: OGTT of *db/db* mice at the end of phase I. Oral glucose tolerance of *db/db* mice, where mice were fasted for 16 hours. Thereafter treatments were gavaged and an hour later glucose (2 g/kg) was administered to the mice and blood glucose levels were measured at 0 min, 15, 30, 60 and 120 minute (A), and area under the curve thereof (B). NC: Normal control, BACE: β-secretase inhibitor, GRT™-1: low dose, GRT™-2: high dose.

The results are expressed as the means ± SEM (n=4). *p< 0.05 and ***p< 0.0001 vs. the NC group, #p< 0.05 vs. pioglitazone (One-way ANOVA and Tukey post-test).

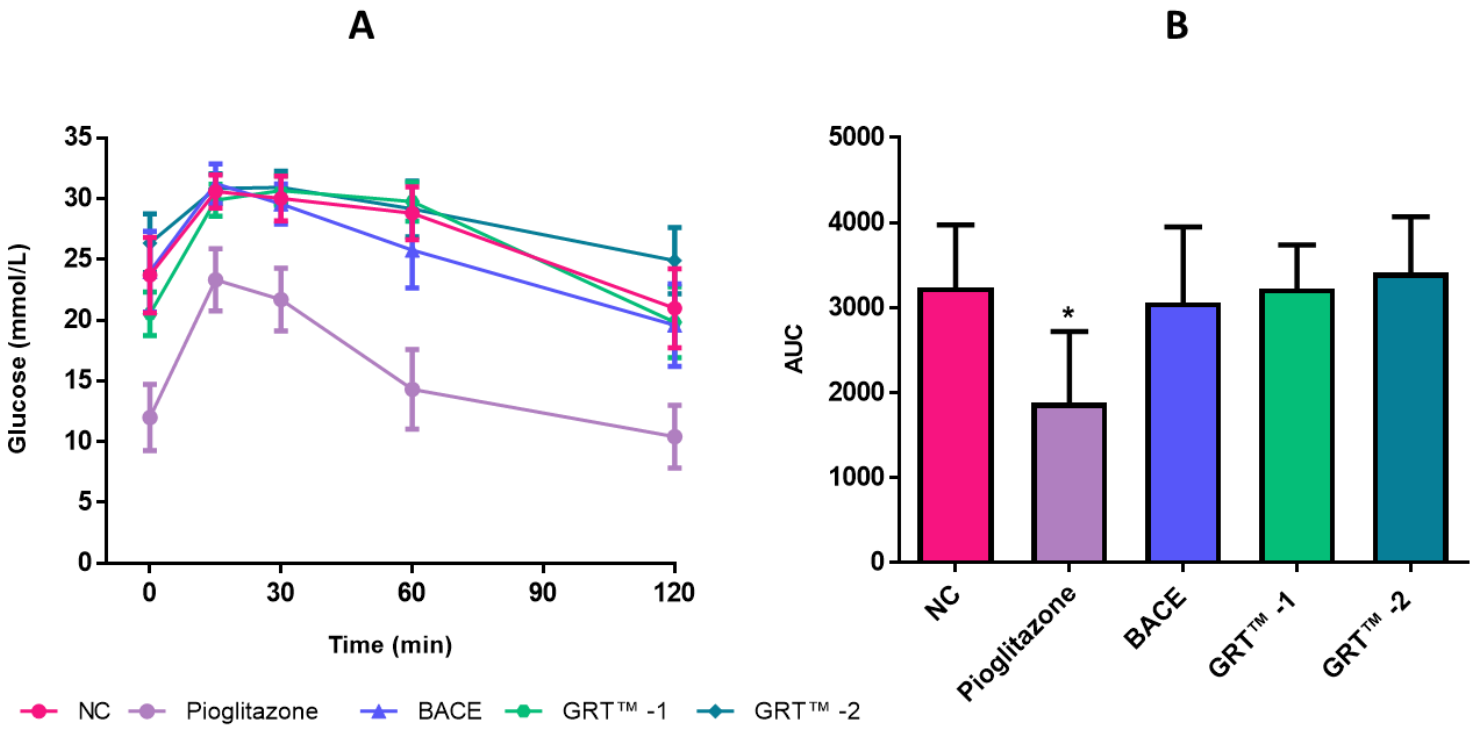

Figure 32: OGTT of *db/db* mice at the end of phase II. Oral glucose tolerance of *db/db* mice, where mice were fasted for 16 hours. Thereafter treatments were gavaged and an hour later glucose (2 g/kg) was administered to the mice and blood glucose levels were measured at 0 min, 15, 30, 60 and 120 minute (A), and area under the curve thereof (B). NC: Normal control, BACE: β-secretase inhibitor, GRT™-1: low dose, GRT™-2: high dose.

The results are expressed as the means ± SEM (n=7-8). *p< 0.05 vs. the NC group (One-way ANOVA and Tukey post-test).

Table 9: Summary of the effect of BACE inhibitor and GRT™ on fasting blood glucose and glucose tolerance of *db*+ and *db/db* mice in phases I, II and III.

In the *db/db* mice, BACE inhibitor and GRT™-2 were able to improve glucose tolerance in phase I while in phase II, only pioglitazone improved glucose tolerance.

	NC	Pioglitazone	BACE	GRT™-1	GRT™-2
Fasting blood glucose of *db*+					
Phase I	-	Θ	Θ	Θ	Θ
Phase II	-	Θ	Θ	Θ	Θ
Phase III	-	Θ	Θ	Θ	Θ
Glucose tolerance of *db*+					
Phase I	-	Θ	Θ	Θ	Θ
Phase II	-	Θ	Θ	Θ	Θ
Phase III	-	Θ	Θ	Θ	Θ
Fasting blood glucose of *db/db*					
Phase I	-	Θ	Θ	Θ	Θ
Phase II	-	Θ	Θ	Θ	Θ
Glucose tolerance of *db/db*					
Phase I	-	Θ	Improved	Θ	Improved
Phase II	-	Improved	Θ	Θ	Θ

NC: Normal control, BACE: β-secretase inhibitor, GRT™-1: low dose, GRT™-2: high dose.

Θ = No effect

4.2.4. Biochemical analysis

Plasma insulin, C-peptide and amylin levels were 2-fold to 4-fold higher in the *db/db* mice vs the *db*+ controls for all phases and treatment groups (Table 11 and Figure 33A & Figure 34A). Amylin levels were increased in phase II vs phase I in both *db/db* and *db*+ mice.

4.2.4.1. Serum insulin, C-peptide and amylin levels in *db*+ mice

Lower C-peptide levels were observed in phase III compared to both phase I and II in all treatments ($p<0.05$) (Table 11). BACE inhibitor significantly reduced amylin levels in phase II compared to the control groups ($p<0.05$). Moreover, amylin levels were significantly higher in all treatment groups except BACE inhibitor in phase II compared to phase I (Table 11). Insulin levels in BACE group had no outliers, BACE may have an effect on insulin secretion but would require prolonged treatment.

Due to serum constraints, insulin, C-peptide and amylin levels were only assessed in the following groups: NC, pioglitazone, BACE and GRT™-2 of both *db/db* and *db*+ mice (phase I and II).

4.2.4.2. Serum insulin, C-peptide and amylin concentrations of *db/db* mice

In phase I, insulin, amylin and insulin / C-peptide ratio levels tended to be slightly higher in the BACE inhibitor group (2.56 ng/mL ± 0.57 vs 1.27 ng/mL ± 0.28, $p=0.16$; 0.81 ng/mL ± 0.25 vs 0.59 ng/mL ± 0.26 and 22.83 ng/mL ± 4.81 vs 14.6 ng/mL ± 3.18; respectively) (Figure 34A and 34B), while C-peptide levels remained unchanged (Figure 33A & B).

In phase II, lower C-peptide levels were observed (0.15 ng/mL ± 0.02 vs 0.23 ng/mL ± 0.00; $p=0.009$) (Figure 34A) whereas insulin levels, insulin / C-peptide and insulin / amylin ratios were relatively unchanged (Figure 35A & 35B).

Table 10: The effects of treatments on biochemical parameters in phase I, II and III heterozygous *db*+ mice.

Serum C-peptide levels were lower in phase III compared to phase I and II. Amylin levels were significantly decreased by BACE inhibitor in phase II compared to the NC, whereas overall amylin levels were higher in phase II compared to phase I.

	Group	Mean ± SEM	Mean ± SEM	Mean ± SEM
		Phase I	Phase II	Phase III
Insulin (ng/mL)	NC	0.17±0.01	0.15±0.04	0.19±0.07
	Pioglitazone	0.15±0.02	0.19±0.06	0.22±0.03
	BACE	0.37±0.17	0.11±0.01	0.14±0.08
	GRT™-2	0.09±0.03	0.16±0.06	0.24±0.07
C-peptide (ng/mL)	NC	0.11±0.003	0.12±0.009	0.01±0.0003 †
	Pioglitazone	0.12±0.002	0.12±0.005	0.01±0.0003 †
	BACE	0.14±0.013	0.11±0.004	0.01±0.0004 †
	GRT™-2	0.12±0.004	0.12±0.005	0.01±0.0002 †
Amylin (ng/mL)	NC	0.08±0.03	0.36±0.18 †	-
	Pioglitazone	0.06±0.003	0.11±0.02 †	-
	BACE	0.11±0.07	0.06±0.02*****†	-
	GRT™-2	0.04±0.01	0.09±0.01 †	-
Insulin/C-peptide (ratio)	NC	1.45±0.11	1.24±0.34	2.63±0.27†
	Pioglitazone	1.27±0.22	1.65±0.54	2.78±0.05†
	BACE	2.54±0.91	1.06±0.16	2.31±0.31
	GRT™-2	0.77±0.24	1.35±0.55	3.12±0.50†
Insulin/Amylin (ratio)	NC	0.08±0.03	0.36±0.18	-
	Pioglitazone	0.06±0.003	0.11±0.02	-
	BACE	0.04±0.014	0.06±0.02	-
	GRT™-2	0.04±0.011	0.09±0.01	-

NC: Normal control, BACE: β-secretase inhibitor, GRT™-1: low dose, GRT™-2: high dose.

Data is expressed as mean ± SEM; *p<0.05 vs NC; † p<0.05 vs phase I and phase II.

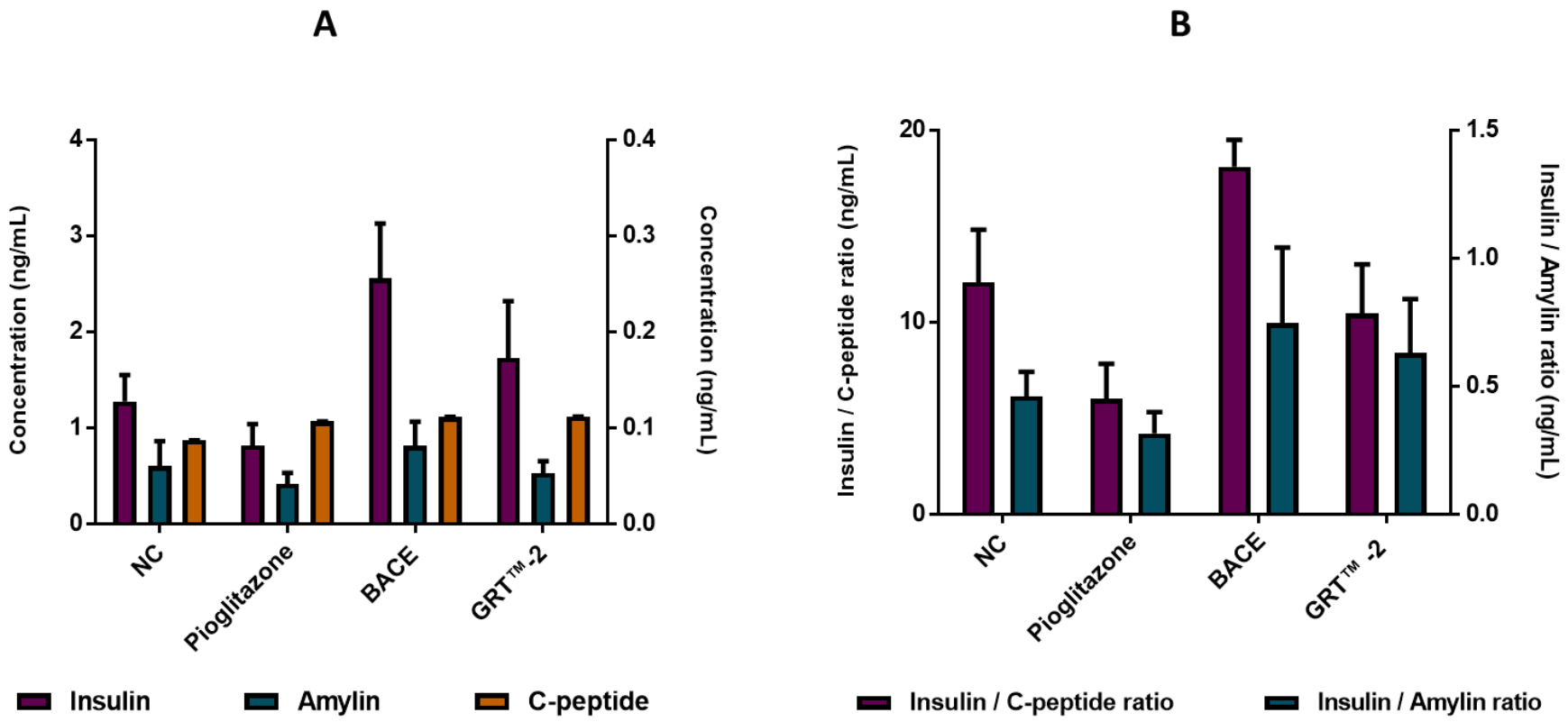

Figure 33: Serum insulin, C-peptide and amylin level profiles of the homozygous *db/db* mice in phase I. Fasted serum insulin levels were determined from blood collected at termination, following a 16 hour overnight fast. Serum insulin, C-peptide and amylin concentrations (A), Insulin / C-peptide ratio and Insulin / amylin ratio (B). NC: Normal control, BACE: β-secretase inhibitor, GRT™-1: low dose, GRT™-2: high dose.

The results are expressed as the mean ± SEM (n=9) (Two-way ANOVA).

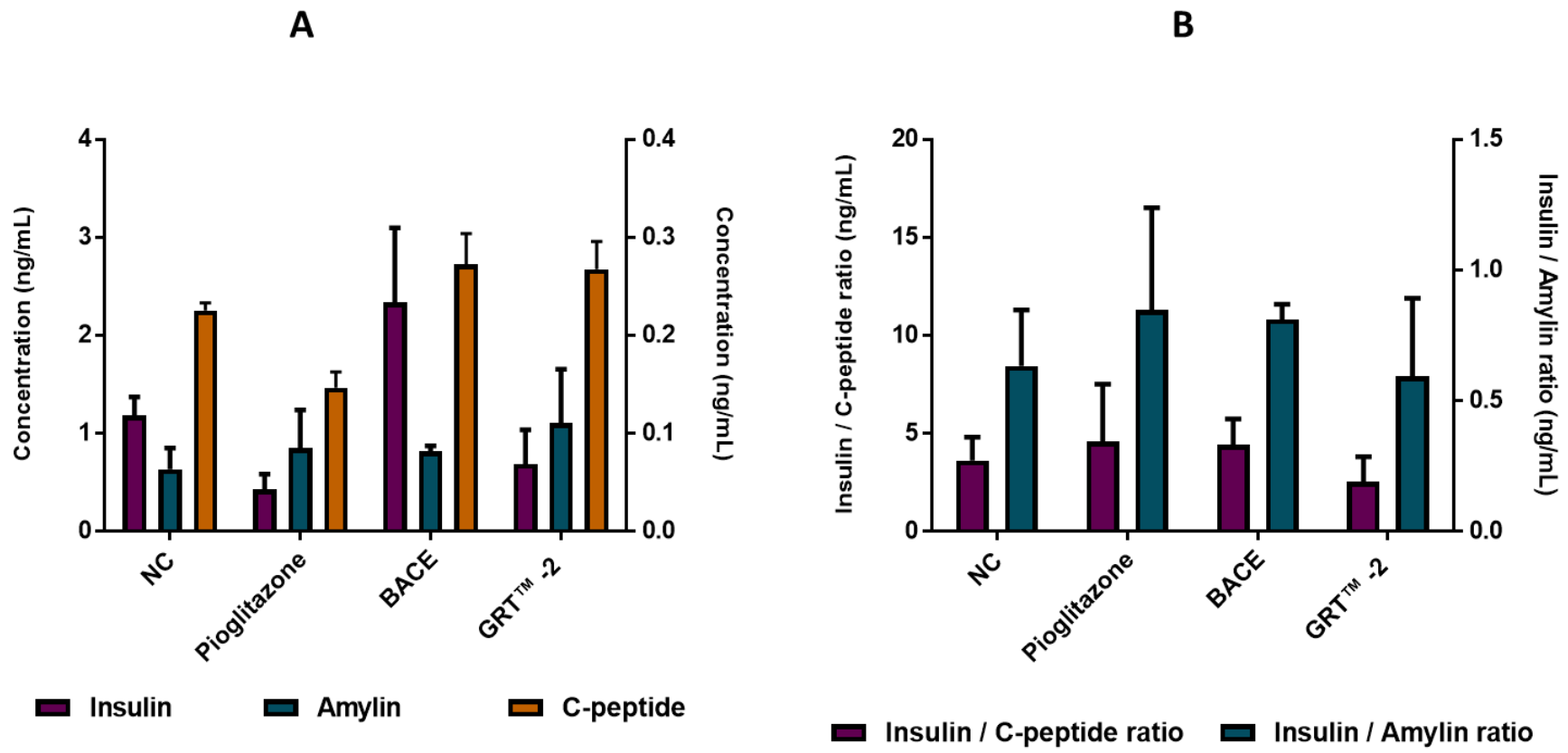

Figure 34: Serum Insulin, C-peptide and amylin level profiles of the homozygous *db/db* mice in phase II. Fasted serum insulin levels were determined from blood collected at termination, following a 16 hour overnight fast. Serum insulin, C-peptide and amylin concentrations (A), Insulin / C-peptide ratio and Insulin / amylin ratio (B). NC: Normal control, BACE: β-secretase inhibitor, GRT™-1: low dose, GRT™-2: high dose.

The results are expressed as the mean ± SEM (n=9) (Two-way ANOVA).

4.2.5. HOMA-β and HOMA-IR assessment

HOMA-IR was significantly increased in NC groups in *db/db* mice compared to *db*+ mice in both phase I (97.3 ± 14.4 vs 16.0 ± 6.5; $p<0.05$) and phase II (92.66 ± 28.5 vs 7.0 ± 2.7; $p<0.05$). Moreover, HOMA-β was higher in *db/db* mice of phase I compared to *db*+ mice (301.9 ± 95.3 vs 50.9 ± 19.1, $p<0.05$), while in phase II, a decrease in HOMA- β was observed in *db*+ mice compared to *db/db* mice (275.5 ± 36.65 vs 293.1 ± 221.4).

BACE inhibitor had lower HOMA-IR levels in both phase II and III compared to phase I in the *db*+ mice ($p<0.05$) (Figure 35B).

In contrast, in the *db/db* mice, pioglitazone and GRT™-2 tended to have lower HOMA-IR and HOMA-β in phase II compared to phase I, although these decreases were not statistically significant (Figure 36A & Figure 36B). While BACE inhibitor showed to have higher HOMA-IR in both phase I and II compared to respective controls (Figure 36B).

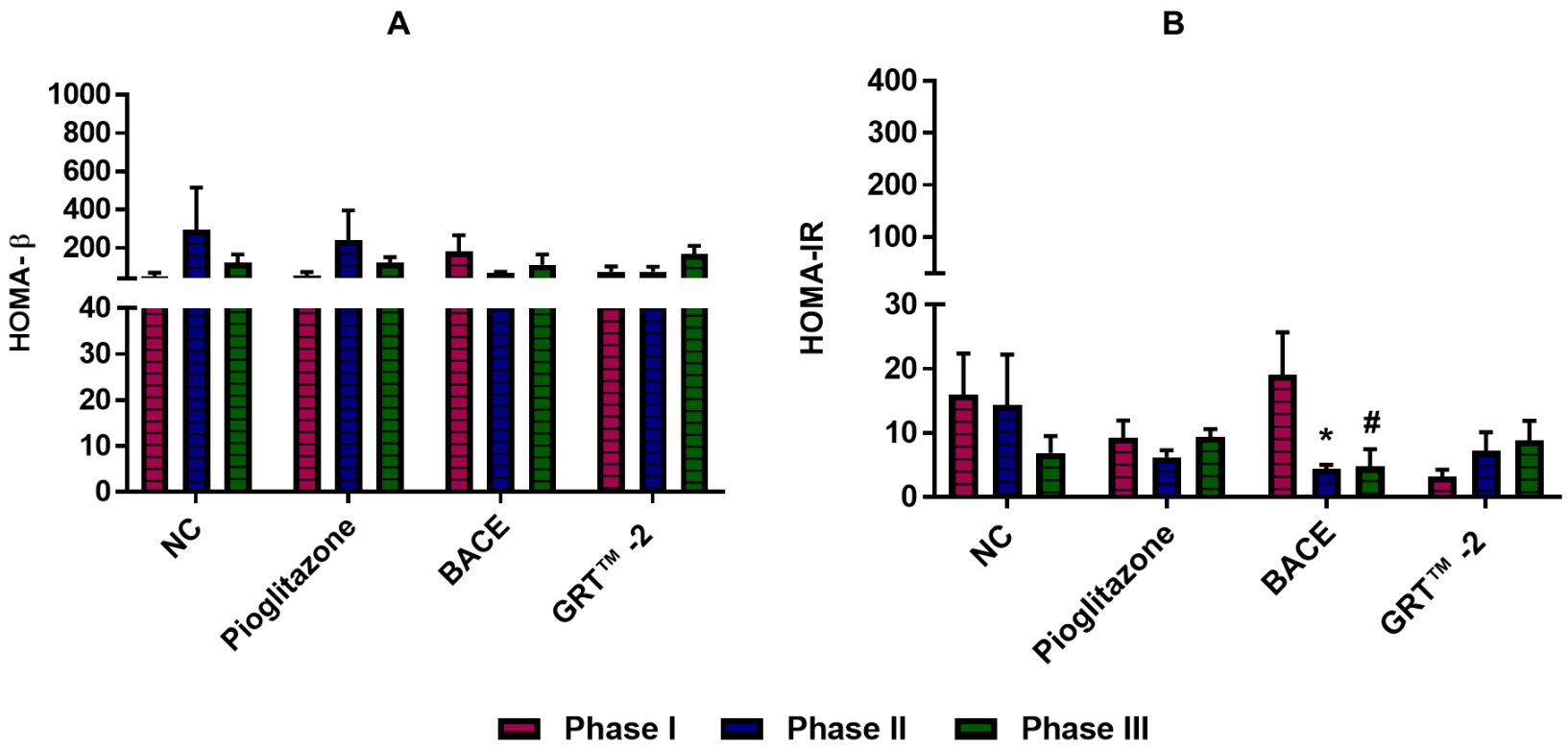

Figure 35: β-cell function and Insulin sensitivity of heterozygous *db*+ mice in phase I, II and III. β-cell function measured by HOMA-β (A) and insulin sensitivity measured by the HOMA-IR index (B). Fasted serum insulin levels were determined from blood collected at termination, following a 16 hour overnight fast of each respective phase and HOMA-IR and HOMA-β indexes were calculated. NC: Normal control, BACE: β-secretase inhibitor, GRT™-1: low dose, GRT™-2: high dose.

The results are expressed as the mean ± SEM (n=4-8); *p< 0.05 vs phase I in the same phase, #p<0.05 vs phase I (Two-way ANOVA and Dunnett's test).

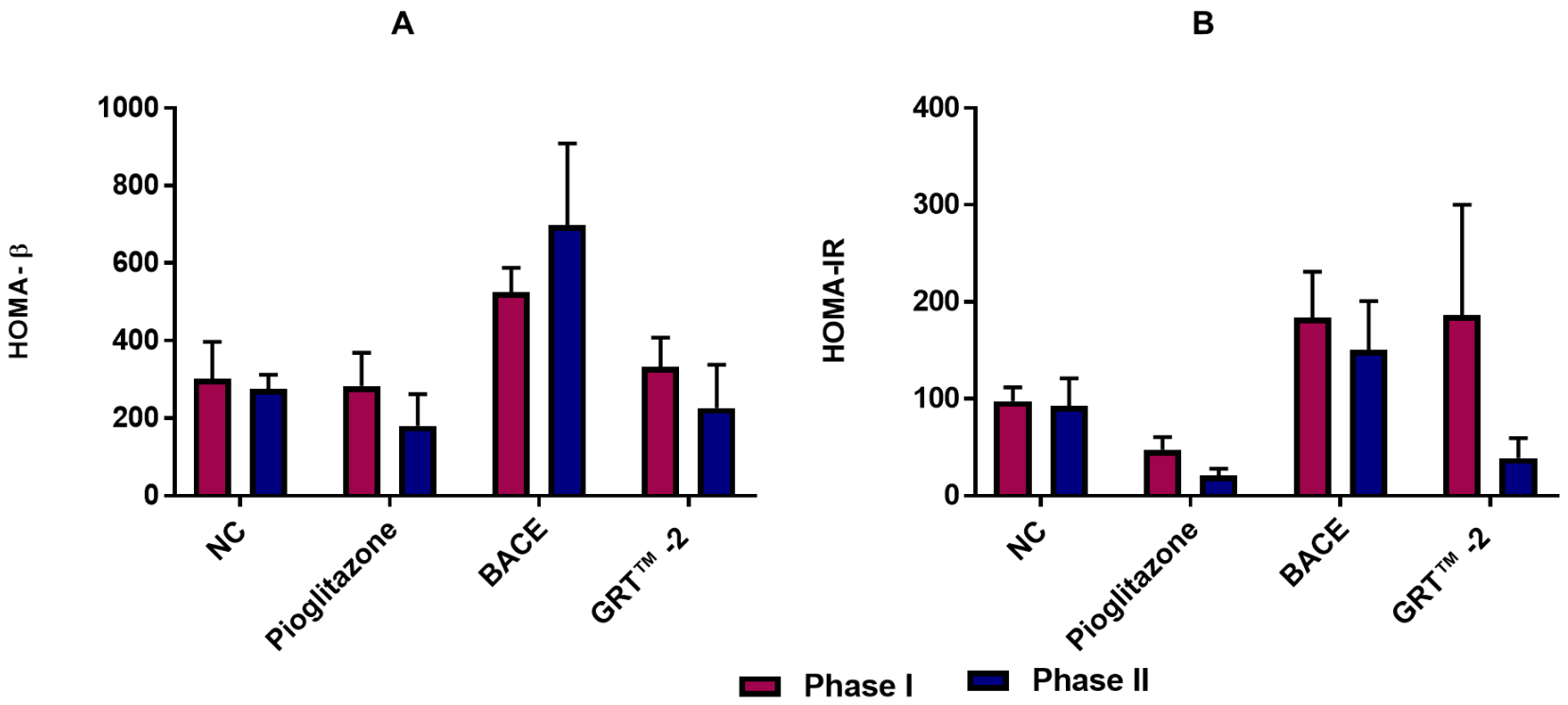

Figure 36: β-cell function and Insulin sensitivity of diabetic *db/db* mice in phase I and II. β-cell function measured by HOMA-β (A) and insulin sensitivity measured by the HOMA-IR index (B). Fasted serum insulin levels were determined from blood collected at termination, following a 16 hour overnight fast of each respective phase and HOMA-IR and HOMA- β indexes were calculated. NC: Normal control, BACE: β-secretase inhibitor, GRT™-1: low dose, GRT™-2: high dose.

The results are expressed as the mean ± SEM, (Two-way ANOVA and Dunnett's test).

Table 11: Summary of the effect of BACE inhibitor and GRT™ on serum insulin, C-peptide and amylin concentrations of *db*+ and *db/db* mice in Phase I, II and III.

In phase II, reduced amylin levels were observed in the BACE inhibitor group in *db*+ mice peptide levels were decreased in pioglitazone in phase II *db/db* mice

	NC	Pioglitazone	BACE Inhibitor	GRT™-1	GRT™-2
Insulin concentrations in *db*+					
Phase I	-	Θ	Θ	-	Θ
Phase II	-	Θ	Θ	-	Θ
Phase III	-	Θ	Θ	-	Θ
C-peptide levels in *db*+					
Phase I	-	Θ	Θ	-	Θ
Phase II	-	Θ	Θ	-	Θ
Phase III	-	Θ	Θ	-	Θ
Insulin / C-peptide ratio in *db*+					
Phase I	-	Θ	Θ	-	Θ
Phase II	-	Θ	Θ	-	Θ
Phase III	-	Θ	Θ	-	Θ
Amylin levels in *db*+					
Phase I	-	Θ	Θ	-	Θ
Phase II	-	Θ	↓	-	Θ
Insulin concentrations in *db/db*					
Phase I	-	Θ	Θ	-	Θ
Phase II	-	Θ	Θ	-	Θ
C-peptide levels in *db/db*					
Phase I	-	Θ	Θ	-	Θ
Phase II	-	↓	Θ	-	Θ
Insulin / C-peptide ratio in *db/db*					
Phase I	-	Θ	Θ	-	Θ
Phase II	-	Θ	Θ	-	Θ
Amylin levels in *db/db*					
Phase I	-	Θ	Θ	-	Θ

Phase II	-	Θ	Θ	-	Θ

NC: Normal control, BACE: β-secretase inhibitor, GRT™-1: low dose, GRT™-2: high dose. Arrow represents ↓ decrease and ↑ increase/ improvement, Θ= No effect.

4.2.6. Pancreatic islets morphology

Micrographs of small, medium and large pancreatic islets, in figures 37, 38 and 39, respectively display changes in pancreatic architecture of *db*+ mice in phase I (A-E), phase II (F-J) and *db/db* mice in phase I (K-O) and phase II (P-T). Islets of *db*+ mice characteristically contained a majority of β-cells, centrally localized within the islet. β-cells were identified by a consistent cytoplasmic intensity of insulin immunostaining (red/pink). Few, dispersed glucagon positive α-cells (brown) were present at the periphery of the islet (Figure 37A-E). In contrast, the islets of *db/db* mice showed several morphological anomalies, including derangement of the islet α- and β-cell distribution, α-cell hyperplasia and inconsistent β-cell cytoplasmic intensity of insulin immunostaining (red) (Figure 37K-T). Additionally, an increase in the number and distribution of α- to β-cells was more prevalent in phase I (Figure 37, 38, 39K-O). In phase II, irregular insulin immunostaining of β-cells was a consistent feature (Figure 37, 38, 39P-T). Overall, assessment of sections revealed *db*+ and *db/db* changes as quantified in sub-sections (4.5.1.1 and 4.5.1.2).

4.2.6.1. Quantified morphological changes in non-diabetic *db*+ mice

In phase I, BACE inhibitor and GRT™ -1 decreased β-cell size compared to the NC, while in phase II, only GRT™-2 reduced β-cell size (Figure 41A). Average α-cell size was decreased in pioglitazone and BACE inhibitor in phase I compared to NC ($p<0.0001$) (Figure 40B). Furthermore, islet sizes of *db*+ mice were smaller in the BACE inhibitor, GRT™-1 and GRT™-2 groups compared to both NC and pioglitazone in phase I (Figure 37A-E). In phase II, BACE inhibitor increased islet size compared to the NC (Figure 37F & H).

4.2.6.2. Quantified morphological changes in diabetic *db/db* mice

In the *db/db* mice, decreases in average α-cell size were observed in BACE inhibitor, GRT™-1 and GRT™-2 groups in phase II compared to NC group ($p<0.05$) (Figure 41B). Islet size was increased by the BACE inhibitor in phase I compared to the NC (Figure 39K & M) and islet area was increased in phase II compared to phase I in the pioglitazone group (Figure 42B).

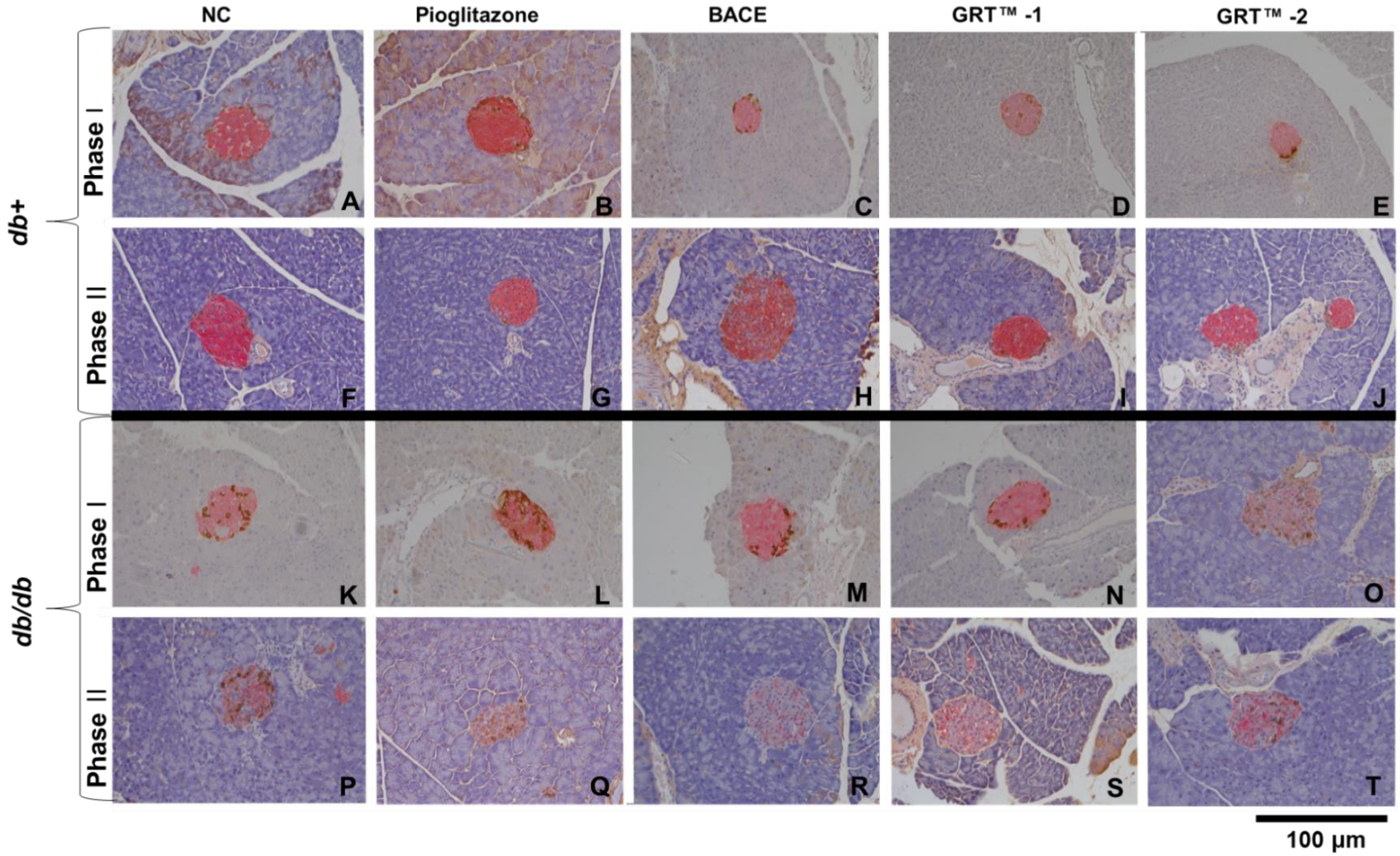

Figure 37: Histology of mouse pancreatic small islets in phase I and phase II using double antibody labelling with anti-glucagon (brown) and anti-insulin (red). Top part: heterozygous *db*+ micrographs of both phase I and II, bottom part: homozygous *db/db* micrographs of phase I and phase II.

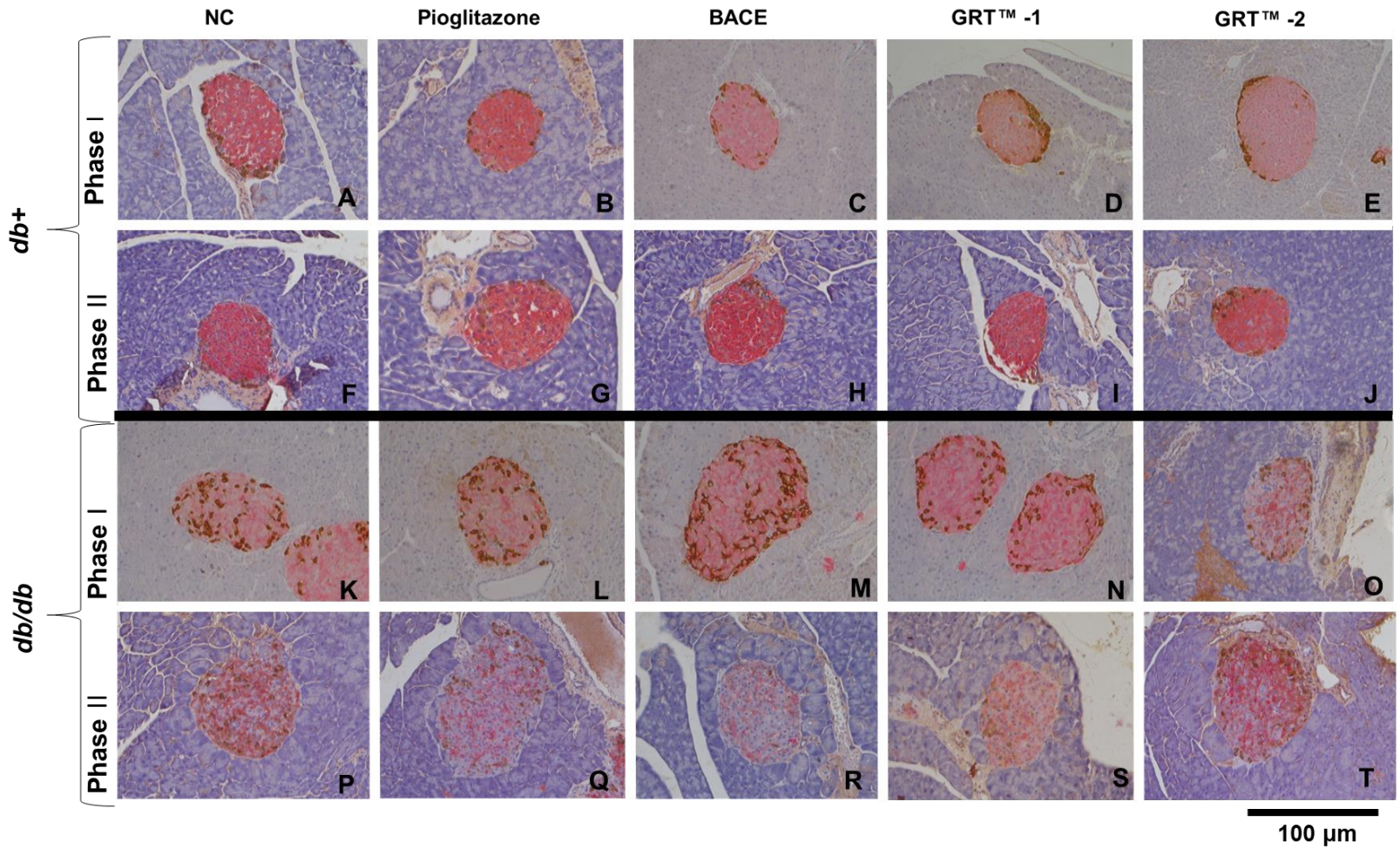

Figure 38: Histology of mouse pancreatic medium islets in phase I and phase II using double antibody labelling with anti-glucagon (brown) and anti-insulin (red). Top part: heterozygous *db*+ micrographs of both phase I and II, bottom part: homozygous *db/db* micrographs of phase I and phase II.

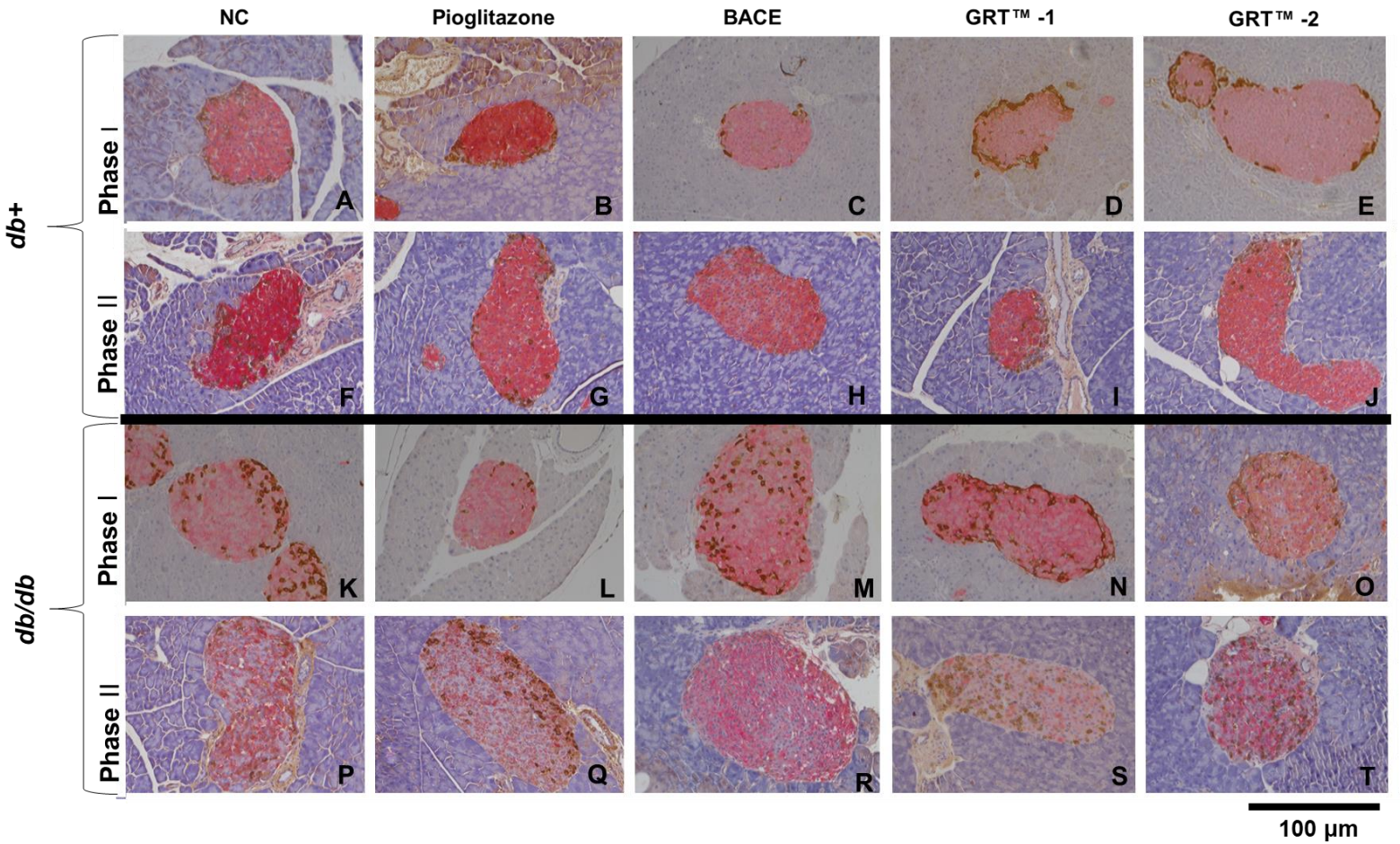

Figure 39: Histology of mouse pancreatic medium islets in phase I and phase II using double antibody labelling with anti-glucagon (brown) and anti-insulin (red). Top part: heterozygous *db*+ micrographs of both phase I and II, bottom part: homozygous *db/db* micrographs of phase I and phase II.

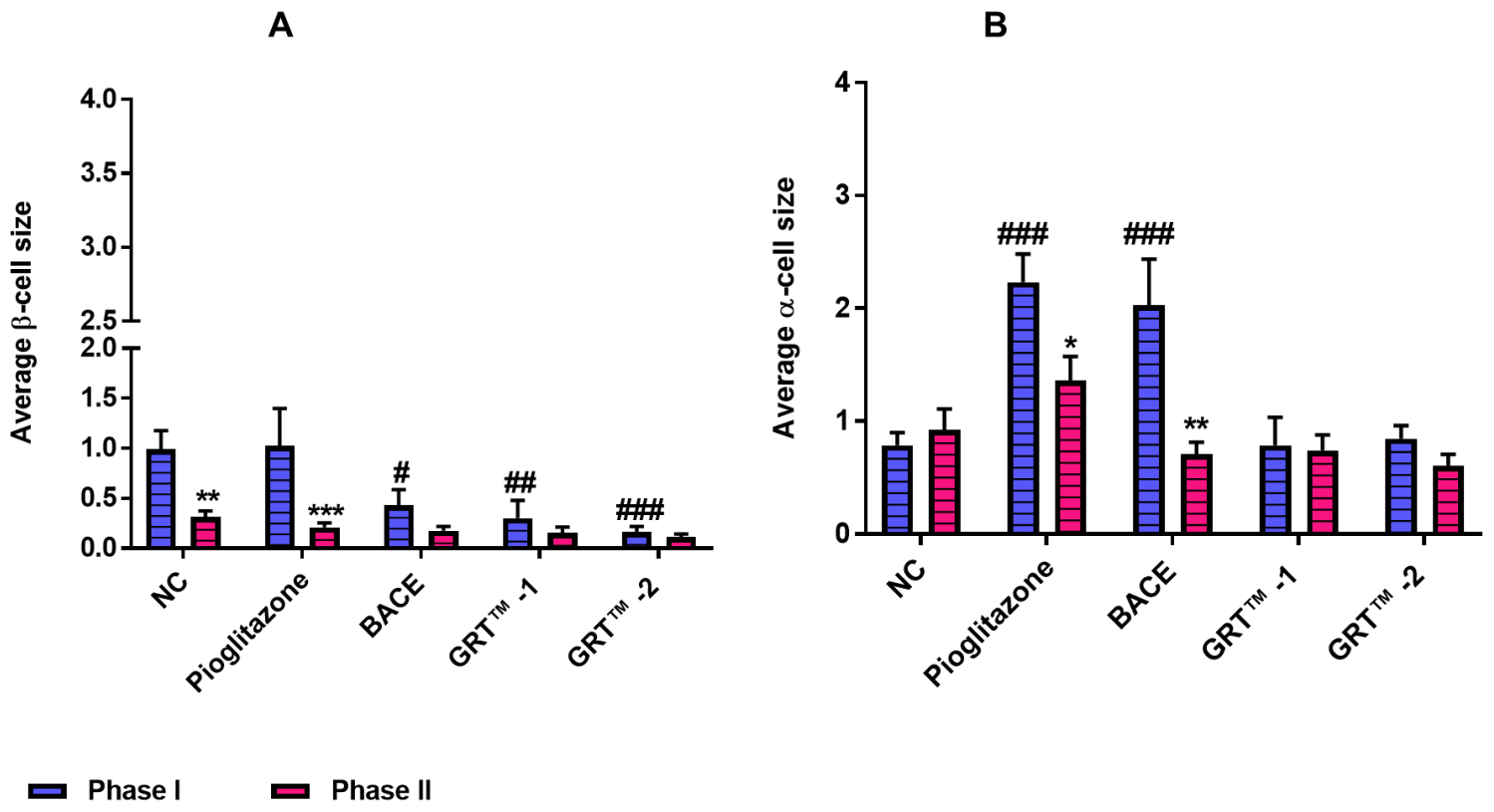

Figure 40: Average β and α-cell size in *db*+ mice of phase I and phase II. Average β-cell size (A) and average α-cell sizes (B) of heterozygous *db*+ mice in phase I, II and III.

Data is expressed as mean ± SEM (4-8); *=p<0.05, **= p<0.001 , ***p<0.0001 vs phase I of the same treatment group, #p<0.05; ##p<0.001; ###p<0.0001 vs NC of phase I (Two-way ANOVA and Dunnett's test).

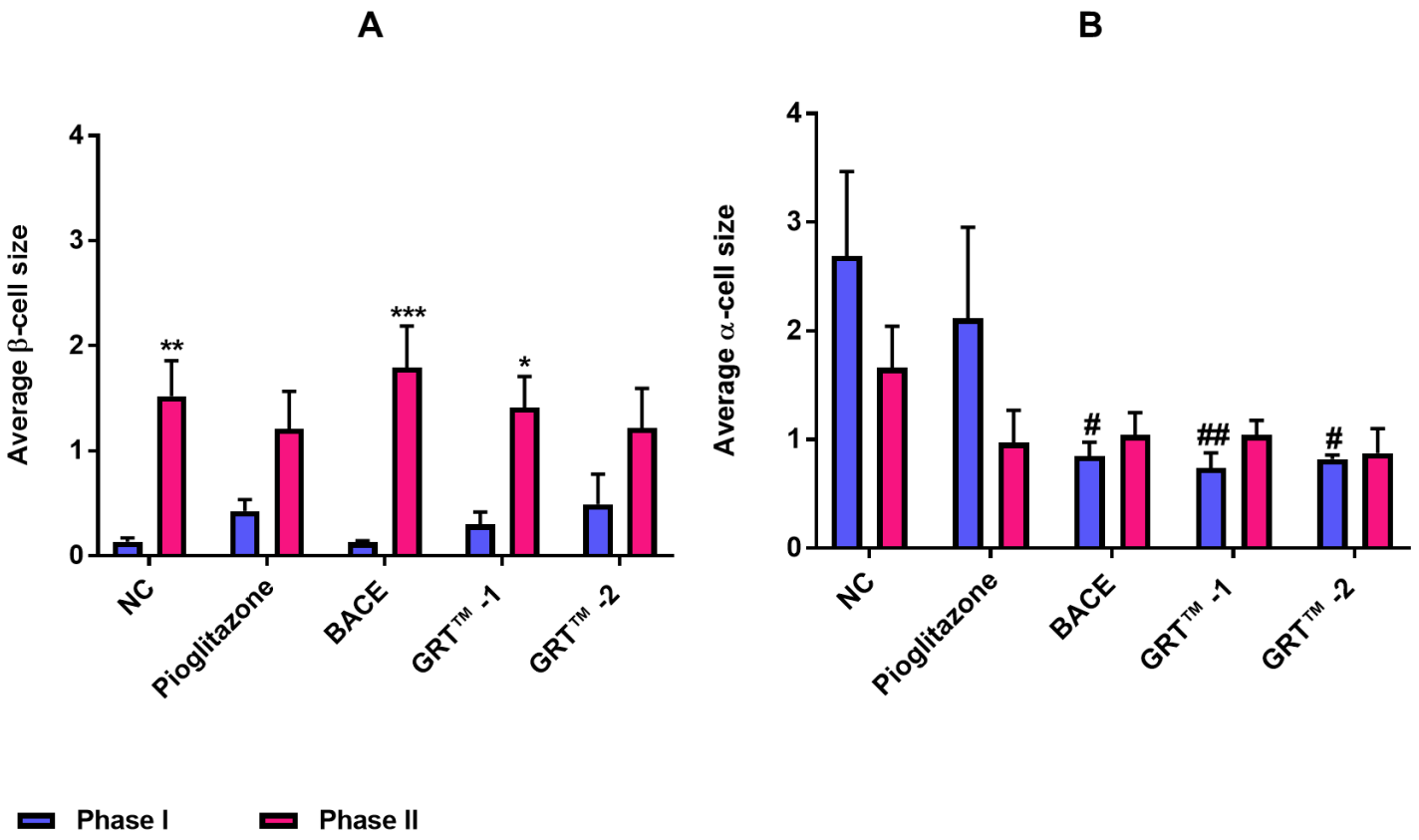

Figure 41: Average β and α-cell size in *db/db* mice in phase I and phase II. Average β-cell size (A) and average α-cell sizes (B) of homozygous *db/db* mice in phase I and II.

Data is expressed as mean ± SEM (4-8), *=p<0.05; **= p<0.001; ***= p<0.001 vs phase I of the same treatment group, #p<0.05; ##p<0.001 vs NC of phase I (Two-way ANOVA and Dunnett's test).

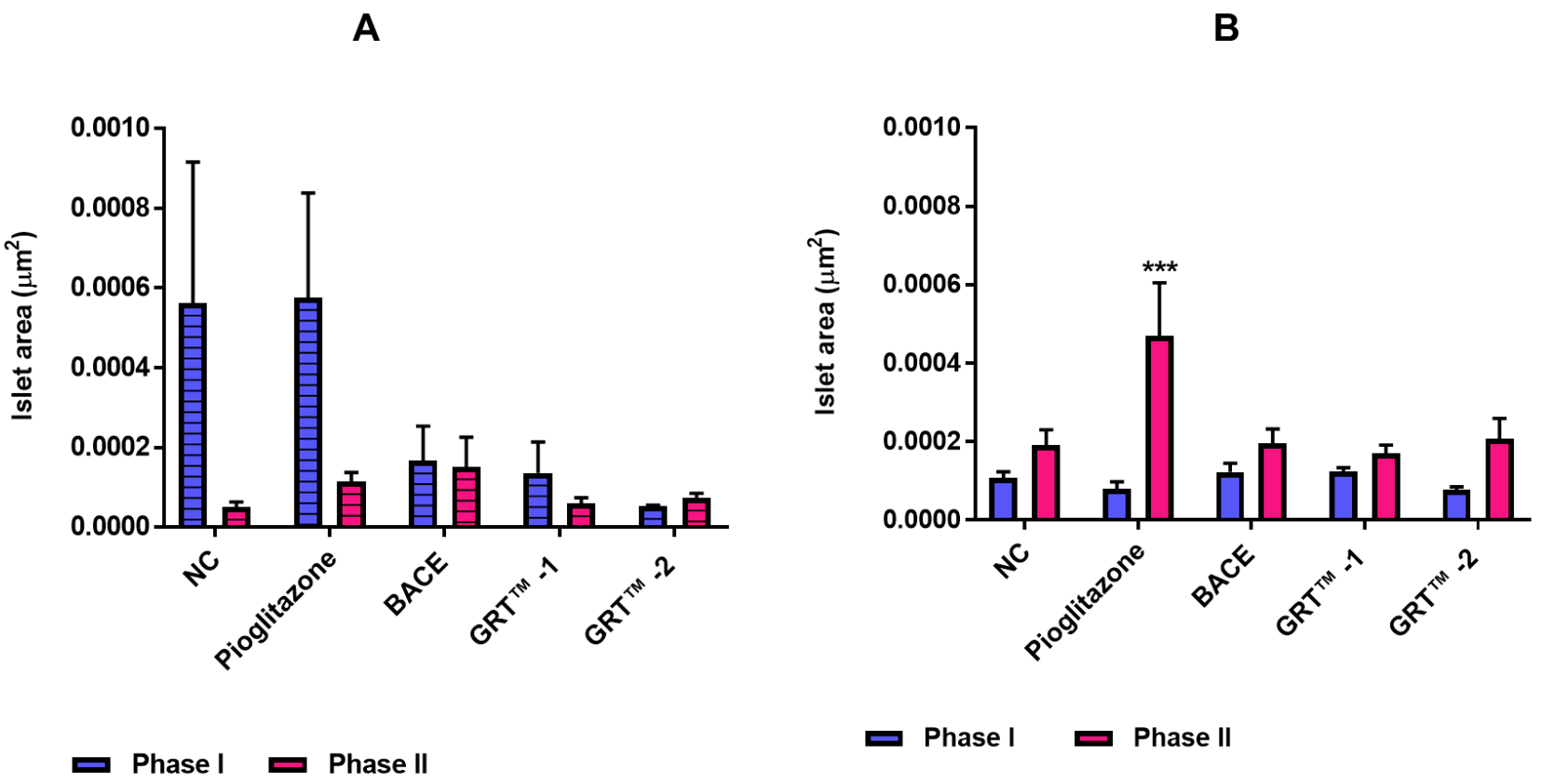

Figure 42: Average islet area of *db*+ and db/*db* mice in phase I and phase II. Average islet area of *db*+ mice (A) and average islet area of *db/db* mice (B).

Data is expressed as mean ± SEM (4-8), ***= p<0.001 vs phase I of the same treatment group (Two-way ANOVA and Dunnett's test).

Table 12: Summary of *in vivo* results in HOMA-IR, HOMA-β and pancreatic islets morphometrics. BACE inhibitor exacerbated insulin resistance in phase I *db/db* mice while Pioglitazone improved β-cell function in phase II *db/db* mice.

	NC	Pioglitazone	BACE Inhibitor	GRT™-1	GRT™-2
HOMA-IR *db+*					
Phase I	-	Θ	Θ	-	Θ
Phase II	-	Θ	Θ	-	Θ
Phase III	-	Θ	Θ	-	Θ
HOMA- β *db+*					
Phase I	-	Θ	Θ	-	Θ
Phase II	-	Θ	Θ	-	Θ
Phase III	-	Θ	Θ	-	Θ
β -cell size *db+*					
Phase I	-	-	↓	↓	↓
Phase II	-	Θ	Θ	-	↓
Phase III	-	-	-	-	-
α-cell size in *db+*					
Phase I	-	↑	↑	-	-
Phase II	-	Θ	Θ	-	-
HOMA-IR in *db/db*					
Phase I	-	Θ	↑	-	Θ
Phase II	-	Θ	Θ	-	Θ
HOMA- β in *db/db*					
Phase I	-	Θ	Θ	-	Θ
Phase II	-	↓	Θ	-	Θ
β-cell size in *db/db*					
Phase I	-	Θ	Θ	Θ	Θ
Phase II	-	Θ	Θ	Θ	Θ
α-cell size in *db/db*					
Phase I	-	Θ	↓	↓	↓
Phase II	-	Θ	Θ	Θ	Θ

Arrow represents ↓ decrease and ↑ increase, Θ= No Effect, += Positive correlation

CHAPTER FIVE

Discussion

Prolonged/ chronic high glucose (HG) exposure both *in vitro* and *in vivo* exerts deleterious effects on β-cells phenotype and function. However, the effect of elevated glucose concentration exposure in aging β-cells remains not fully elucidated. The interest in 3D cell culture systems is increasing widely as these offer more physiological relevant features than conventional 2D cultures systems. Evidence suggests that glucotoxicity correlates with increases in amylin levels which may later aggregate to form toxic amyloid plaques, a hallmark of the T2D in humans (Del Prato, 2009; Hull *et al*., 2004; Konarkowska *et al*., 2006 Alcarraz-Vizán *et al*., 2017). Increased amyloid plaque formation is positively correlated with BACE2 levels in the pancreas, a protease that cleaves IAPP (Alcarraz-Vizán *et al*., 2017; Esterházy *et al*., 2011). Additionally, BACE levels are perceived to offer both detrimental and beneficial effects by increasing amyloid plaque formation and regulating insulin secretion via TMEM27 cleavage (a known β-cell marker) (Alcarraz-Vizán et al., 2017; Esterházy *et al*., 2011). Literature indicates that polyphenols may act as BACE inhibitors to inhibit β-amyloid plaque formation (Shimmyo *et al*., 2008). Thus, understanding the effects of chronic glucotoxicity on amylin and BACE activities could decipher an opportunity for the development of novel therapeutic strategy to protect β-cell functional mass against hyperglycemia and T2D. In this study, the potential effect of a BACE inhibitor and an aspalathin-rich Rooibos extract Afriplex GRT™ to ameliorate glucotoxicity was studied.

5.1.1. Characterization of the spheroids

Unlike the distinct rounded shape of the C3A spheroids described by Wrzesinski and Fey (2013), the INS-1 spheroids had cellular protrusions. Literature describes that cells with higher doubling time are more likely to form round spheroids (Ivascu and Kubbies, 2006; Jagiella *et al*., 2016), thus the lower doubling time of INS-1 cells compared to the C3A cells may be an attributing factor. Generally, cellularity (size and shape) and stress tolerance levels (reflection of spheroids response against internal forces within the spheroid such as division and entering quiescence state) contributes to the spheroid's compactness. While the work done by Wrzesinski and Fey, (2013) has shown that C3A liver spheroids regain functionality and ultrastructural features 18 days after trypsinization,

our spheroids had distinct ultrastructural features and reached an equilibrium plateau, four days earlier than it took C3A liver spheroids (Wrzesinski and Fey, 2013).

5.1.2. Ultrastructural characterization of the spheroids

Transmission electron microscopy (TEM) micrographs of INS-1 spheroids demonstrated the typical presence of neuroendocrine cells with ultrastructural features synonymous with those of pancreatic β-cells including prominent RER, Golgi apparatus, euchromatic nuclei and prominent nucleoli, indicative of active cellular protein synthesis (Figure 15-17) (Sato *et al*., 1966 ; Stevens and Lowe's., 2015). A well-developed RER is vital for insulin production, modification and secretion via the trans Golgi network (Golgi apparatus and secretory granules). Euchromatic nuclei, multiple nucleoli and mitochondria confirm normal cell functionality including integration and generation of metabolic signals for glucose homeostasis (Jin and Diano, 2018; Kaufman *et al*., 2009). The presence of apoptotic and mitotic cell was indicative of active cell turnover (Figure 18). As further confirmation of cellular specialization of spheroids, functional endocrine cells containing many insulin-like secretory β-granules which were membrane-bound granules of approximately 300 nm in diameter with an electron-dense central core resembling crystalline were observed. The number, size and content of insulin secretory β-granules, which are complex intracellular organelles, that apart from proinsulin are composed of many proteins including Islet amyloid polypeptide (IAPP) also called amylin, syncollin and granule membrane associated proteins such as phogrin, play an important role in the physiology of pancreatic β-cells (Ferri *et al*., 2019; Hutton, 1989). In contrast with 2D culture, where the monolayer growth dynamics is related passaging before reaching confluence keeps cells at a proliferative phase with minimal phenotypical differentiation before the next passage. In 3D culture systems, cells are usually found in various stages, such as proliferating, quiescent, apoptotic, hypoxic, and necrotic cells (Khaitan *et al*., 2006; Mehta *et al*., 2012). The central core of the spheroids comprise an area of dead cells, apoptotic cells and cellular debris (TEM and TB stain) indicative of ischemic stress and/or nutrient deficiency (Figure 18 and Figure 14, respectively). The outer area in 3D spheroids, due to the proximity surface and adequate gaseous exchange and nutrient diffusion, are comprised of viable proliferating cells. The toluidine blue section clearly

demonstrated that the outer mantel of the spheroids had cells that were less vacuolized and morphologically more viable than the central core (Figure 14), agreeing with previous reports (Khaitan *et al*., 2006; Mehta *et al*., 2012).

5.1.3. Amelioration of glucotoxicity by GRT™ and BACE activity inhibition

INS-1 spheroids grown in NG conditions simulated a growth pattern that produced stable spheroids without visible cellular debris in the media. The spheroids were morphologically compact and tended to be larger in size (Figure 13 & 19). From day 10, the spheroids appeared to reach an equilibrium plateau i.e. the cell turnover within the mantel of the spheroid remained stable and growth of the spheroid slowed without changes in ATP content, showing that the spheroids were still metabolically active (Khaitan *et al*., 2006; Bussador do Amaral *et al*., 2010; Mehta *et al*., 2012). During this phase, the size of the spheroids decreased slightly which we postulate is due to late apoptotic cellular shrinkage (pyknosis), karyorrhexes within the core and cytoskeleton intercellular proteins contraction observed by the presence of more cell-cell junctions within the viable mantle, may have contributed to the size reduction (Figure 16) (Papadopoulos *et al*., 2000; Cheng *et al*., 2009; Sodek *et al*., 2009).

Exposing the spheroids to HG concentrations (HG-33 mM) adversely affected the shape, size and surface morphology of the spheroids. Visually, increased cellular debris in the media was observed. Alterations in the macroscopic appearances of the spheroids were evident by the drastic reduction in size and ATP content (Figure 19 & 20) compared to the NG group (7185 μm^2 vs 25030 μm^2) after 1 week of glucotoxicity induction. These reductions are related to the HG toxic effects on the spheroid viability, similar to *in vitro* and *in vivo* studies suggesting that, intermittent and chronic HG reduces pancreatic β-cell mass and causes β-cell dysfunction owing to increased apoptosis (Butler *et al*., 2007; Shi *et al*., 2014). Two weeks later, the spheroids recovered from the glucotoxicity effect proven by an increase in size compared to 1 week of glucotoxicity induction (22658 μm^2 vs 7185 μm^2). Pancreatic β-cells have well-coordinated mechanisms conferring the ability to adapt to varying glucose concentrations using several mechanisms involved in oxidative stress and inflammation which sequentially decreases β-cell apoptosis, hence the improvement in viability (Kamimura *et al*., 2004; Hou *et al*., 2008). Subsequent

treatment, with either GRT™ extract (HG-GRT™) or a BACE inhibitor (HG-BACE), respectively, improved the viability of the spheroids as less cellular debris was observed in the media. Potential mechanisms to validate that the treatments improved viability may involve the inhibition of protein kinase C, NAD(P)H-oxidase activities, which are inducers of oxidative stress and NF-κB pathway, which inhibits β-cell proliferation which themselves causes β-cell dysfunction (Pi *et al*., 2007; Chen *et al*., 2011; Sun *et al*., 2012; Zhang *et al*., 2016). Furthermore, an improvement in the spheroid sizes was observed as early as 1 week of treatment compared to the HG group (13308 μm^2 and 10812 μm^2 vs 7185 μm^2, respectively) (Figure 20). Pronounced improvements were evident by week 2 of treatment (24992 μm^2 and 23593 μm^2 vs 22658 μm^2, respectively). ATP content was improved by GRT™ and BACE inhibitor (Figure 20). These positive effects on size and ATP content thus suggests that GRT™ and BACE inhibitor improves spheroid viability in this glucotoxic induced INS-1 spheroid model. These effects were correlated with protein expression levels of BACE and TMEM27, where 4-fold increases were observed (Figure 27 A & B). Increased BACE1 expression in response to hyperglycemia has been shown in ZDF rats (Lee *et al*., 2016). In this study, the BACE inhibitor induced a compensatory overexpression of BACE protein expression, however, gene expression is necessary to verify this. While it has been shown that insulin-producing β-cells express higher levels of BACE, expression levels in NG were comparable to treatment groups (Figueroa *et al*., 2001).

Glucose utilization in the INS-1 spheroids: HG, HG-GRT™ and HG-BACE were comparable to the NG group (Figure 22), suggesting that the increase in spheroid sizes had no impact on glucose usage. We postulate that, this could be further evidence that the spheroids had reached a stable cellular equilibrium. Basically, glucose levels were sufficient to sustain the outer mantel of the spheroids which contained viable cells, and the necrotic core did not utilize any nutrients. This result contrasts with previous reports stating that an increase in spheroid size is likely to result in enhanced glucose usage accompanied by anaerobic glycolysis, comparatively responsible for alterations in oxidative status (Khaitan *et al*., 2006).

5.1.4. Improvement of insulin secretory profile by GRT™ and BACE inhibitor in spheroids exposed to glucotoxicity

The exposure of pancreatic islets to HG levels is one of the causal factors for the progressive lowering of insulin secretion during the development of T2D (Kahn, 2001; Zhang *et al*., 2016; Ottosson-Laakso *et al*., 2017). Herein, insulin secretion was assessed at basal glucose levels (2.8 mM) meant to mimic a fasted condition and under stimulation (16.7 mM) glucose concentrations, representing the post-prandial condition. In the NG group spheroids, higher stimulated insulin secretion was observed compared to basal insulin secretion (Figure 23). These results are parallel with many studies conducted in 2D cultures, *in vivo* models and human studies, suggestive of the ability of the developed spheroids to retain normal β-cell function (Zhang *et al*.,2004; Moynihan *et al*., 2005; Pi *et al*., 2007; Saadeh *et al*. 2012). Glucotoxicity (HG- 33 mM) resulted in increased basal insulin secretion compared to the NG group (Figure 23) which recapitulates β-cell compensation as seen in early T2D/IR (Nolan et al., 2006a). Increases in basal insulin secretion following HG exposure have previously been shown in rodent islets and purified β-cells (Fu *et al*., 2006, 2017; Rebelato *et al*., 2018). As a result of chronic hyperstimulation by supraphysiological glucose levels, insulin secretion was lost at stimulated glucose levels compared to basal levels (Figure 23). This could be in line with the notion that chronic HG causes excessive depletion of intracellular insulin stores and impairs the maximum insulin secretory capacity of β-cells upon glucose stimulation (Chen *et al*., 1996; Wali *et al*., 2014; Fu *et al*., 2017; Rebelato *et al*., 2018). Furthermore, we showed that GRT™ and BACE inhibitor in chronic HG conditions reduced basal insulin secretion (Figure 23) and this is corroborated by findings suggesting that BACE silencing improves glucose homeostasis (Visa *et al*., 2015). These results potentiate GRT™ extract and BACE inhibition ameliorating toxic effects of chronic HG exposure by promoting β-cell rest by means of a reduction in insulin hypersecretion, similar to the effect of bromocriptine (a dopamine agonist) in β-cells (de Leeuw van Weenen *et al*., 2010). Others have shown that aspalathin (Rooibos bioactive constituent) increases insulin secretion from several β-cell lines not exposed to stressors (Kawano *et al* ., 2009; Fu *et al*., 2017). The reduction in GSIS induced by GRT™ and BACE inhibitor in the spheroids exposed to glucotoxicity is most probably due to an improvement in cellular function,

glucose sensing and related insulin response in the HG (Figure 23). A differential expression can be regarded biologically significant (meaningful) when a fold change is greater than 1.5 compared to the control (McCarthy and Smyth, 2009), even when not deemed statistically significant by one-way ANOVA analysis. Literature suggests that BACE2, highly expressed in pancreatic β-cells, regulates insulin secretion through TMEM27 cleavage (Visa *et al*., 2015; Alcarraz-Vizán *et al*., 2017). In this study, 3- and 7-fold increases in BACE and TMEM27 protein expression observed (Figure 27A & B), respectively, are associated with improved insulin secretion conferred by GRT™ and the BACE inhibitor. However, noteworthy is that the BACE inhibitor used here was not specific to either BACE1 or BACE2 leaving room for discrepancies. As previously stated, chronic glucose exposure impairs insulin secretion and dysregulates insulin receptor (IR) (Chen et al., 1996b; Hribal et al., 2003; Wali et al., 2014). Despite having demonstrated an impairment in HG group insulin secretion (Figure 23), this defect could not be associated with IR protein expression. More so, no changes were observed in GLUT-2 expression, a molecule involved in glucose sensing, is suggestive of the insulin secretion defects not necessarily brought about by altered protein expression but rather by alterations in GSIS intracellular mechanisms. So overall, GRT™ and BACE inhibitor appear to protect against deleterious effects of chronic HG exposure as seen through improved INS-1 spheroid function.

5.1.5. GRT™ and BACE inhibitor improves amylin secretion profiles

Amylin secretion was used as an indicator of β-cell function. Here, an increase in basal amylin secretion in the NG group was observed similar to that of the insulin secretory response while, surprisingly, a decrease in stimulatory amylin secretion was observed (Figure 24). In normal physiology, amylin secretion should be similar to insulin secretion at a ratio of 1:100 (Moore and Cooper, 1991; Zhang et al., 2016a). Regarding this discrepancy with stimulated amylin secretion, we postulate that basal amylin secretion is under feed-back control by insulin hence, at stimulated levels, insulin has an inhibitory effect on amylin secretion (Figure 24). However, others have also reported the lack of co-secretion between insulin and amylin from isolated pancreatic islets *in vitro* (Dégano *et al*., 1993; Stridsberg *et al*., 1993). A Pearson's correlation coefficient was computed to

assess the relationship between insulin and amylin secretion in the spheroids, where positive correlation was attained in the NG group indicative of normal function with no correlation in the other treatment groups (Table 6). Consistent with insulin data, an increase in amylin secretion in the HG group compared to the NG group was observed whereas the presence of GRT™ and BACE inhibitor in chronic HG, blunted the glucotoxic effects on amylin hypersecretion, correlating with the insulin secretory profile (Figure 24). The possibility that amylin levels may have already been depleted at basal levels, as seen in the insulin secretion results, cannot be ignored. Insulin to amylin ratio was higher in the HG group with no Pearson's correlation, clearly suggestive of a dysfunction, while insulin to amylin ratio was completely inverted in the presence of GRT™. Insulin to amylin ratio of the HG-BACE group closely resembled that of the NG group suggestive of normal functionality (Figure 25). In this study, amylin/ IAPP protein expression could not be detected, despite literature describing otherwise in *in vitro* pancreatic β-cell lines and diabetic heart tissue (Cai *et al*., 2011; Despa *et al*., 2012; Kulas *et al*., 2017). As such, we were unable to confirm the potential direct effect of BACE inhibition on amylin expression despite several speculations that amylin is a substrate of BACE (Alcarraz-Vizán *et al*., 2017) and this may be potentially regulated by BACE inhibition.

5.1.6. The effect of GRT™ and BACE inhibitor on spheroid inflammation

Inflammation is a hallmark for β-cell dysfunction in T2D (McCarthy and Smyth, 2009; Keane *et al*., 2015). Secreted inflammatory markers, such as TNF-α, IL-6 and IL-10 in the spheroids were quantified by ELISA. Chronic HG exposure (HG) resulted in higher levels of TNF-α and IL-6 compared to the NG group (Figure 26A), consistent with previous studies proposing that HG levels can actively induce inflammation in β-cells (Shi *et al*., 2014; Wali *et al*., 2014; Ku *et al*., 2015). Literature suggests that IL-6 exerts both pro-inflammatory and anti-inflammatory effects (Xing *et al*., 1998; Perini *et al*., 2001; Keane *et al*., 2015). Others have shown that IL-6 protects pancreatic β-cells from pro-inflammatory cytokine-induced cell death and functional impairment *in vitro* and *in vivo* (Choi *et al*., 2004). Here, after 1 week of glucotoxicity, IL-6 levels were only detectable in the HG and HG-GRT™ groups (Figure 26B), and two-weeks later, the IL-6 levels in the HG and HG- GRT™ groups were increased (Figure 26B). This result is corroborated by

a study where an addition of Rooibos in whole blood cultures induced higher IL-6 and IL-10 levels (Hendricks and Pool, 2010). Unfortunately, in this study, IL-10 levels could not be detected.

TNF-α is a renowned death effector molecule (Beg and Baltimore, 1996; Van Antwerp et al., 1996b). High TNF-α levels were observed in HG and HG-GRT™ groups compared to the NG group following 1 week of glucotoxicity (Figure 26A). After 2 weeks of glucotoxicity, a significant decrease in TNF-α levels was observed in the HG-GRT™ indicative of inhibition of the induced inflammatory response by GRT™ extract (Figure 26A). This finding correlates with previous studies where male Wistar rats that consumed fermented Rooibos extract for 4 weeks in an LPS-stimulated macrophage model had decreased levels of TNF-α and IL-6 (Ajuwon *et al*., 2014). Furthermore, in RAW 264.7 macrophages and adrenal cortical tissue, Rooibos decreased IL-6 levels (Mueller *et al*., 2010; Smith and Swart, 2016; Hoosen, 2019). However, more investigation needs to be done to confirm the possibility that GRT™ has an anti-inflammatory effect in a chronic HG condition in a time dependent manner. Interestingly, direct inhibition of BACE activity (HG-BACE) resulted in lower levels of both TNF-α and IL-6 compared to HG group, however this effect was somehow lost after 2 weeks of glucotoxicity (Figure 26A & B). Literature has shown that inflammation results in increased Aβ amyloid generation via BACE thus, it can be postulated that inhibiting the activity of BACE may reduce inflammation (Sastre *et al*., 2008), as we have demonstrated here. These results showed that GRT™ and BACE inhibitor possess anti-inflammatory properties by reducing TNF-α and IL-6 levels following chronic and short-term treatment periods in INS-1 spheroids, respectively. Data from purified non-cell based BACE enzyme assay, showed that the highest GRT™ concentration seemed to have activity against BACE inhibition (Figure 10). Although the effect seen in the purified assay is not indicative of what happens *in vitro*, it potentiates the efficacy of GRT™ as BACE activity inhibitor, in addition to other known biological activities, such as anti-diabetic, anti-inflammatory and anti-hyperglycemic in pancreatic β-cells (Kawano *et al*., 2009; Muller *et al*., 2012; Ajuwon *et al*., 2014; Ayeleso *et al*., 2014; Kamakura *et al*., 2015). Others have confirmed the ability of an ethyl acetate soluble fraction of green tea that is rich in catechins to have BACE1 inhibitory activity (Jeon *et al*., 2003).

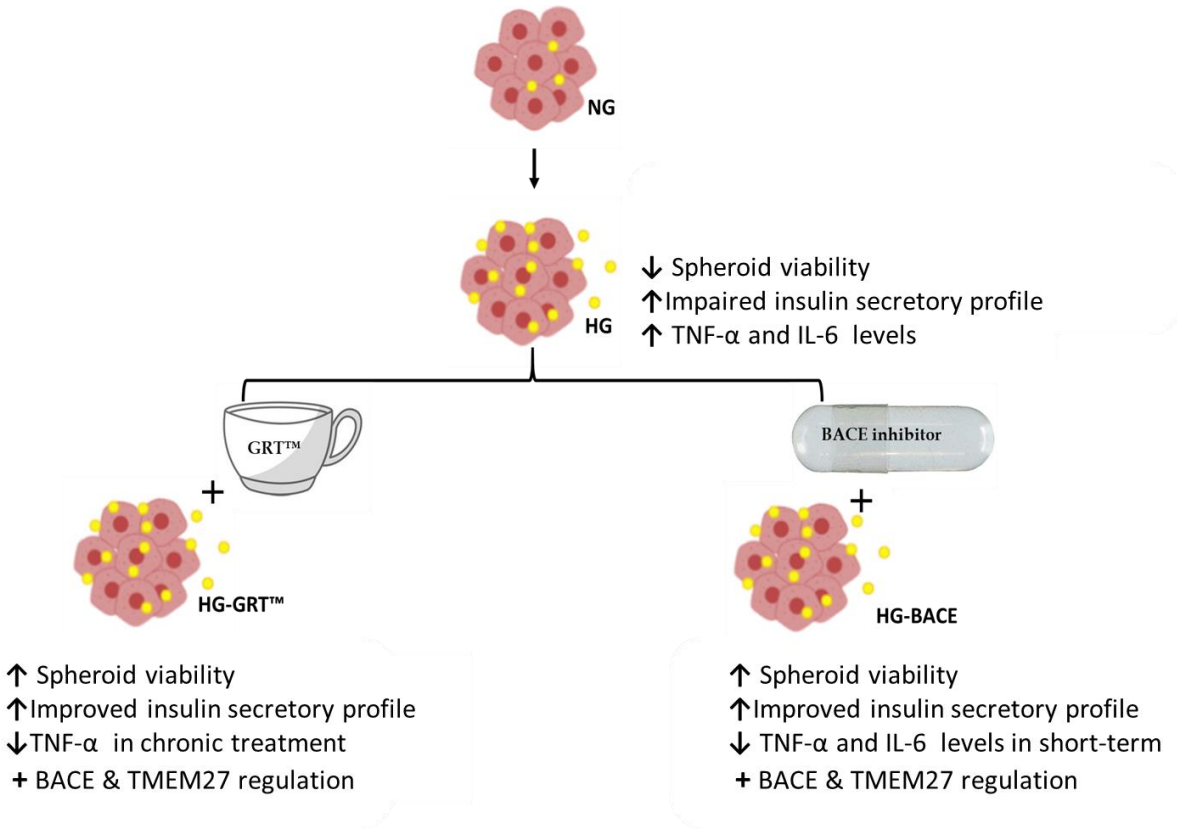

Figure 43: Proposed effects of chronic glucotoxicity in pancreatic β-cell spheroids. Glucotoxicity (HG) reduced viability (ATP content & size profile), impaired GSIS and induced higher TNF-α and IL-6 cytokines. Treatment with an aspalathin rich green Rooibos extract (GRT™) and a BACE inhibitor improved both viability and functionality of the spheroids through increased ATP content, size profile and GSIS, additionally, the treatments lowered TNF-α during long-term and short-term treatments, respectively. BACE was able to lower IL-6 levels. Both GRT™ and BACE modulated TMEM27 and BACE activity.

Six-week old C57BL/Ks diabetic *db/db* mice were used to the elucidate age-dependent impact of treatments after 10 weeks (phase I) and 16 weeks (phase II). Additionally, non-diabetic *db*+ littermates were used to substantiate effects of the treatments after 10 weeks (Phase I), 16 weeks (Phase II) and 32 weeks (Phase III). The *db/db* model is the most commonly used mouse model for type 2 diabetes (T2D) due to its deleterious point mutation in the leptin receptor gene (Ritchie *et al*., 2008; Patton and DeGolier, 2010; Belke and Severson, 2012; King, 2012). This gene disruption is associated with hyperphagia, obesity, hyperglycemia, hyperinsulinemia and reduced metabolism (Kawano *et al*., 2009; Patton and DeGolier, 2010; Ernst *et al*., 2013; Wang *et al*., 2014; Zheng *et al*., 2015). Changes observed in and associated with mouse pancreatic islets were compared to what was found *in vitro* INS-1 spheroids.

5.2.1. Pathophysiological changes in *db/db* mice

Increased calorie intake, as a result of hyperphagia, resulted in substantial increases in body weight (Figure 28 B & 29 B). Literature substantiates that excess calories and adiposity leads to obesity induced insulin resistance and T2D through direct inhibition of insulin receptor substrate phosphorylation in insulin target tissues (Capurso and Capurso, 2012; White, 2006). As expected, glucose concentrations remained high in both phases during OGTT (Figure 31 & 32, respectively), confirming impaired glucose tolerance on basis of the World Health Organization criteria (WHO) (Gomez-Perez *et al* ., 1998; WHO, 1985). Hyperinsulinemia and increased amylin levels concurrent with hypertrophic islets (Figure 33, 34, 40, 41) were observed suggestive of β-cell compensation. It is known that β-cells are capable of increasing their mass and function to compensate for increased glucose levels to maintain normoglycemia (Bernard *et al*., 1999; Nolan *et al*., 2006; Prentki, 2006; Chen *et al*., 2016). Morphometric analysis showed increases in the number and distribution of α-cells in the *db/db* mice as well as irregular staining, which is an indication of degranulation due to hyperglycemia (Figure 37, 38 & 39). These findings agree with available literature on the pathophysiological and morphometric changes seen in rodents and T2D subjects (Leiter, 1988; Leiter *et al*., 1988; Clark *et al*., 2001; Yoon *et al*., 2003; Zibolka *et al*., 2018).

5.2.2. Aging in *db*+ and *db/db* mice

Calorie intake has been shown to increase with age (Weindruch and Sohal, 1997) and this was confirmed when *db*+ mice of phase III (approximately 8.7 months old) had higher calorie intake compared to phase II (5 months old) and I (3.6 months old) (Figure 28A, 29A & 30). These changes represent normal aging with respect to caloric intake in *db*+, as opposed to what was seen in *db/db* mice with metabolic disturbances. Glucose tolerance remained comparable across all phases (Table 8), suggesting that increased calories were not sufficient to induce glucose metabolic impairments, which is in contrast with human studies where aging is occasionally associated with progressive impairments in glucose metabolism (Leiter *et al*., 1988). This may be due to rodent islet compensation capacity. In fact, modest decreases in FBG were observed in older animals (phase III), compared to phase II (Table 8). Although insulin levels were higher with age, they could not be categorized as hyperinsulinemic (Table 11). Importantly, although neither hyperglycemia nor hyperinsulinemia occurred, C-peptide levels were elevated with age (phase III) (Table 11), correlating with rodent islet compensation capacity as C-peptide levels represent insulin secretion (Haffner *et al*., 1995; Okereke *et al*., 2005; De Tata, 2014; Sandovici *et al*., 2016). Amylin levels were elevated with age (phase II) compared to phase I (Table 11), aligning with previous studies, where an increase in amylin has been reported in older humans (Dechenes *et al*., 1998). Because amylin is co-secreted with insulin, and increases in insulin signify impaired β-cell function, increased amylin may be suggestive of the same and are associated with cognitive impairments and susceptibility to T2D through increased amyloid deposition (Srodulski *et al*., 2014; Rasheedy *et al*., 2019).

Hyperinsulinemia, hyperglycemia and glucose intolerance were evident as early as 3.6 months old (phase I) in *db/db* mice (Figure 33 &31, Table 9), consistent with various human and rodent studies (Dalbøge *et al*., 2013; Crofts *et al*., 2016). Elevated insulin levels and hyperglycemia substantiate the increased body weight observed and are known risk factors of many metabolic disorders including IR and obesity (DeFronzo *et al*., 1987; Odeleye *et al*., 1997; Shanik *et al*., 2008; Mehran *et al*., 2012). Persistent hyperinsulinemia seems to explain the dramatic increase in body weight with aging (phase II), as insulin is known to influence body weight and adiposity in mouse and Zucker rat models (Alemzadeh et al., 2008; Burke et al., 2017). The increase in body weight causes increased insulin secretion due to β-compensation as seen by

hypertrophic islets, this interaction can be a negative feedback further exacerbating weight gain. Hypertrophic islets with increased α-cell size were evident already in phase I (Figure 38K-T), corroborating hyperinsulinemia suggestive of β-cell compensation (Figure 33A). In particular these characteristics recapitulate the progression of T2D in humans which involves deterioration in glucose tolerance and insulin sensitivity (Dalbøge *et al*., 2013). Since amylin and insulin are co-stored and co-secreted from the β-cells in response to glucose / other secretagogues (Lukinius *et al*., 1989; Butler *et al*., 1990; Cooper, 1994), it can be expected that insulin resistance would modulate both insulin and amylin secretion simultaneously. Indeed, elevated amylin levels concomitant with hyperinsulinemia were observed in the older *db/db* animals (phase II) (Figure 34A), while in *db*+ mice, higher insulin levels with amylin levels were observed but mice were not hyperinsulinemic (Table 11). Studies have shown that amylin secretion increases with body size and IR in human studies (Kahn, 2003; Kautzky-Willer et al., 1994), with the same being observed in this study for both *db/db* and *db*+ mice. Hypertrophic islets persisted with age (phase II) together with increased α-cell size, decreased β-cell size, irregular staining and disruption of islet architecture, suggesting β-and α-cell degranulation typical of hyperglycemia (Figure 370-S) and dysfunctional β-cells (Figure 36A). These findings align with available literature showing that elevated glucagon levels are a known feature of uncontrolled diabetes as they inhibit β-cell insulin secretion and that pancreatic islet β-cells from T2D patients display markers of dedifferentiation, from β- to α-cells (Unger and Orci, 1975; Bernard *et al*., 1999; Sone and Kagawa, 2005; Weir *et al*., 2001; Dalbøge *et al*., 2013; Weir and Bonner-Weir, 2013). The reduction in insulin to C-peptide ratio with aging, is expected and may be a consequence of severe decompensation, as both insulin and C-peptide levels are initially increased and then deteriorates depending on the duration of diabetes (Weir and Bonner-Weir, 2004; Genuth, 2013; Qiu *et al*., 2014). As proven, aging is associated with changes in glucose metabolism including increased insulin and amylin secretion, reported in both rodent and human studies (Dechenes et al., 1998; Mather et al., 2002; Zhang et al., 2016b). For this reason, it can be reasonable to assume that amylin, like insulin, acts as a β-cell functional marker, where supra-physiological elevations are indicative of impaired β-cell function and thus dysregulated glucose metabolism (Figure 33A & 34A).

5.2.3. BACE Inhibitor improves insulin sensitivity in *db*+ mice

In phase II, BACE inhibitor decreased calorie intake concurrently with body weight while improving insulin sensitivity as measured by HOMA-IR (Figure 35A & 35B). Improved insulin sensitivity correlates with lower insulin / C-peptide and insulin / amylin ratios (Table 11) which may be as a result of BACE inhibition regulating hypothalamic leptin sensitivity, as has been shown by Meakin and co-workers to improve body weight, however this requires intact leptin signaling (Meakin *et al*., 2012). Inflammation has been linked with hypothalamic leptin resistance which causes disruptions in energy and glucose homeostasis as has been linked with functional interactions with metabolism elements including insulin (Pan et al., 2014; Park and Ahima, 2014). Glucose homeostasis disruptions have deleterious effects on insulin function which in turn may cause glucotoxicity. Our in vitro results showed that BACE inhibition in β-cell spheroids exposed to glucotoxicity inhibited pro-inflammatory cytokines secretion, suggesting anti-inflammatory activity which may have resulted in the reduction of leptin resistance and/or stimulation of residual leptin receptors (Figure 25A). On a morphometric level, an increase in islet size with a dramatic decrease in α-cell size was observed (Figure 40 & 42), taken as a positive compensation mechanism since literature suggests that increases in glucagon and insulin levels are tightly coupled with insulin resistance (Ahren *et al*., 2006; Ahrén, 2006; Nolan *et al*., 2006b; Weir and Bonner-Weir, 2007). This further supports the improved insulin sensitivity observed. Taken together, these results suggest the ability of BACE inhibition to prevent adiposity and improve insulin sensitivity in aged *db*+ rodent model.

5.2.4. GRT™-2 stimulates appetite and has insulin-sensitizing effects in short-term in *db*+ mice

Treatment with a high dose of aspalathin-rich Rooibos extract (GRT™-2) increased calorie intake corresponding with increased body weight (Figure 28A), agreeing with reports stating that Rooibos stimulates appetite (Fiddian-Green and Silen, 1975; Schulz *et al*., 2003; Dmowski *et al*., 2017; Hoosen *et al*., 2019). Although body weight was increased, it is important to note that the insulin-sensitizing effects of GRT™-2 were observed at a biochemical level (Table 12), linked with morphometric evidence which supports β-cell expansion and compensation to regulate insulin (Figure 37,38 &39). The increases in insulin sensitivity in normal db+ mice may have the potential to

induce hypoglycemia. However, increased appetite stimulation may have compensated for insulin sensitizing effect as FBG levels were not significantly changed (Figure 35B). Mazibuko-Mbeje and co-workers (2019) have shown that Rooibos improves insulin sensitivity in high-fat diet induced obese Wistar rat model (Mazibuko-Mbeje et al., 2019). The effects of GRT™-1 and pioglitazone were negligible in *db*+ mice.

5.2.5. Long-term pioglitazone treatment improves insulin sensitivity in *db/db* mice

The insulin sensitizing effect of pioglitazone is well established and has been reported in various studies (Pavo *et al*., 2003; Ishida *et al*., 2004; Miyazaki *et al*., 2004). In this study, long-term treatment (phase II) with pioglitazone lowered FBG (Table 9) and improved glucose intolerance (Figure 32), while correlating with higher insulin sensitivity (Figure 34A). These results are consistent with available literature in diabetic *db/db* mice which showed that pioglitazone improved glycemic control and decreased HOMA-IR, thereby improving insulin sensitivity (Kemnitz *et al*., 1994; Kobayashi *et al*., 2000; Ishida *et al*., 2004; Miyazaki *et al*., 2004). Thus, because the effect of pioglitazone in the present study was seen during long-term treatment, it should preferentially be used in combination with other oral anti-diabetes drugs that are known to have acute glucose lowering effects, such as glucagon-like peptide-1 receptor agonist (Fadini *et al*., 2019). However, caution should be taken when choosing the combination therapy, where a drug that is not associated with the risk of hypoglycemia should be considered. The effect of pioglitazone in the *db/db* mice shows that the model is responsive to anti-diabetic therapies, despite the leptin receptor deficiency. Although *db/db* mice are known to have a short life span, the sequence of events leading to occurrence of T2D closely mimics human T2D.

5.2.6. BACE inhibitor confers short-term glucose modulatory effects in *db/db* mice

In phase I, treatment with BACE inhibitor improved glucose tolerance and increased insulin to C-peptide ratio (Figure 31 & 33A), correlated with higher β-cell function (HOMA-β) and elevated insulin secretion (Figure 36A & 33A). This data signifies β-compensation underpinning improved glucose tolerance, differing with a study where BACE1 inhibition action was suggested to require intact leptin signaling to improve

glucose homeostasis (Meakin *et al*., 2012). BACE activity elicits positive effects through improvement of inflammation (Peña-Altamira *et al*., 2017), as was observed in our *in vitro* INS-1 spheroids induced with glucotoxicity, which subsequently reduced pro-inflammatory markers and improved GSIS (Figure 25A & 22). BACE inhibition may have improved glucose tolerance by reducing pro-inflammatory cytokine secretion, as seen in the *in vitro* component of this study (Figure 25A), which is associated with improved leptin resistance. Flavonoids from citrus, garlic, and tea attenuate and reverse Aβ25-35 fibril formation in vitro indicating that this action might be related to their free-radical scavenger activity and might suppress neurotoxicity (Jeon *et al*., 2007; Abdul *et al*., 2018). With aging and long-term treatment (phase II), BACE inhibitor lost its efficacy in improving glucose tolerance (Figure 32), allowing us to speculate that, BACE inhibition activity is age-dependent, may be lost due to the severity of the disease, corresponding with *in vitro* findings where BACE inhibition reduced inflammatory cytokine secretion, however, this effect was lost over time. As following 1 week of glucotoxicity induction, TNF-α and IL-6 were reduced during treatment with BACE inhibitor, while after week 2, a slight elevation in TNF-α was observed (Figure 25A & B). Regarding the differences in the levels of pro-inflammatory cytokines observed in week 1 and 2, we postulate they may be due to the in-culture conditions, where during week 1, normal physiological responses needed to stabilise as spheroids were transferred into new clinostatic bioreactors. More so, during media changes, only 50% of the media is replaced which may have resulted in the accumulation of TNF-α levels, hence the increase by week 2. Although, glucose intolerance transpired, improvements in islet architecture together with improved β-cell function (HOMA-β) were observed, indicative of somewhat, sustained normal β-cell functioning (Figure 36A & 39). Literature has reported *in vitro* BACE1 inhibitory activity in a range of natural plant products, particularly those having a polyphenolic structure. Jeon and co-workers have shown that flavonoid from Smilax china L. plant inhibited BACE1 activity in a dose-dependent manner (Jeon *et al*., 2007).

5.2.7. GRT™-2 has gluco-regulatory activity in *db/db* mice

Rooibos has numerous biological activities associated with gluco-metabolic regulation (Kawano *et al*., 2009; Muller *et al*., 2012; Ajuwon *et al*., 2014; Ayeleso *et al*., 2014; Kamakura *et al*., 2015). Short-term (phase I) treatment with GRT™-2 decreased FBG levels in *db/db* mice similar to the effect of pioglitazone (Table 9). This is associated

with increased insulin levels, improved glucose tolerance and slightly higher β-cell size (Figure 31 & 42). The fact that these effects were observed during short-term treatment may be due the low-bioavailability status of aspalathin, previously reported in an *in vitro* intestinal epithelial monolayer (Caco-2) transport model (Bowles et al., 2017). It is well-documented that the beneficial effects of Rooibos are attributed to its abundant polyphenolic content, particularly aspalathin`s hypoglycemic effect (Kawano *et al*., 2009; Dludla *et al*., 2018; Mazibuko-Mbeje *et al*., 2019). The fact that no measurable effect on calorie intake and body weight was observed (Figure 28B), may be corroborated with the appetite stimulatory effect of Rooibos (Fiddian-Green and Silen, 1975; Schulz *et al*., 2003; Dmowski *et al*., 2017; Hoosen *et al*., 2019). However, with long-term treatment, GRT™-2 lost its moderate glucose modulatory effects, as shown by glucose intolerance (Figure 32). Surprisingly, although glucose intolerance persisted, moderate decreases in insulin to C-peptide ratio and HOMA-IR showing some improvement in insulin sensitivity (Figure 34A & 36B). Literature substantiates that low-grade inflammation causes dysfunctional insulin receptor signaling which impairs insulin biogenesis (Sivitz et al., 2010). In our *in vitro* model, GRT™ significantly decreased TNF-α levels following 2 weeks treatment, suggesting decreased inflammation (Figure 25A). This anti-inflammatory effect *in vivo*, as discussed for pioglitazone and BACE inhibitor, may have induced the improvement in GSIS (Figure 22), in conjunction with aspalathin's known insulin stimulatory effect (Kawano *et al*., 2009). Insulin secretion is reported to decrease with age and the strong argument for the occurrence of an inflammatory process in islets cannot be ignored as may have been the contributing factor to the glucose intolerance phenotype observed in *db/db* mice (Muller *et al*., 1996; Donath *et al*., 1999; Ehses *et al*., 2009). Because leptin inhibits insulin secretion through PI3K-dependent PDE3B activation in β-cell lines and isolated islets (Seufert *et al*., 1999; Kieffer and Habener, 2000; Lee *et al*., 2001; Morioka *et al*., 2007), the lack of leptin signaling may explain the elevated insulin and fasted glucose levels observed.

CHAPTER SIX

Conclusion

5. Conclusions

Improved glucose tolerance induced by both BACE inhibitor and GRT™ in diabetic *db/db* was comparable with the effect of a known anti-diabetic drug, pioglitazone. These gluco-modulatory effects were supported by concomitant changes in pancreatic islet architecture, with increased β-cell sizes correlating with increased cell viability induced by the treatments in the INS-1 spheroids. Both *in vitro* and *in vivo* data support improvements in insulin secretory profiles, with BACE and TMEM27 implicated in regulation in the novel INS-1 spheroids. HOMA-IR and HOMA-β data support the notion that both treatments used in this study have the potential to improve both insulin resistance β-cell function.

In conclusion, this study demonstrates for the first time the gluco-modulatory effects of Afriplex aspalathin rich-green rooibos extract (GRT™) and chemical BACE inhibitor (LY2886721), where glucose tolerance was improved by regulating both insulin resistance and β-cell survival, and preserved function in both an *in vitro* and *in vivo* model. Taken together, this study makes a strong case for the prospective use of either/or both treatments as an adjunctive therapy in the management of T2D.

CHAPTER SEVEN

Limitations and Future work

Study shortcomings and future work

In vitro

The major limitation to the *in vitro* study was the inability to create more defined, rounded INS-1 spheroids. This may have affected the response to treatments, since sphericity, among other things, has been described to affect the response of tumor-derived spheroids to drugs (Michelson and Leith, 1997; Kelm and Fussenegger, 2004; Cheng *et al*., 2009; Zanoni *et al*., 2016). Modifications of the culturing of the spheroids such as the co-culturing of the β-cell spheroids with endothelial cells to allow for exploration of vasculogenesis would be beneficial (Figliolini *et al*., 2014).
In this study proliferation and apoptosis / necrosis were measured only by detecting the protein expression of proliferation marker BrdU and apoptosis markers BAX (which we were unable to detect) in order to understand the changes in β-cell spheroid viability and animals. In order to attain further information regarding changes in neogenesis, apoptosis and/or necrosis, proliferation stains and flow cytometry analysis of single cell spheroid suspensions will need to be used to measure the incorporation of BrdU stain as an indicator of proliferation as well as annexin-V and propidium iodide to assess cell death. In addition, other proteins (e.g. p53, BCL-2) involved in intrinsic and extrinsic apoptotic pathways need to be further investigated.

The inability to detect amylin expression by western blotting in the spheroids was another short coming of the *in vitro* study and warrants further investigation by immunocytochemical analysis, since amylin is an important hormone that plays an important role in glucose homeostasis (Westermark et al., 1986, Clark et al., 1987, Cooper *et al*., 1987; Stridsberg *et al*., 1993, Clark *et al*., 1996, Cao *et al*., 2013; Zhang *et al*. 2016). Furthermore, in humans, amylin aggregation is associated with the development of T2D (Zhang *et al*., 2016). As such incorporation of human IAPP in the spheroids would present with benefits for a model that will be able to recapitulate amylin aggregation *in vitro*.

Since GRT™ and BACE inhibitor treatments of the spheroids exposed to glucotoxic conditions lowered the secretion of these pro-inflammatory cytokines, co-treatment may prove to be beneficial to understand any synergistic activities and the molecular mechanisms underlying their amelioration of toxic effects of these cytokines would need to be further elucidated through protein studies.

In vivo

Since this was a rodent study and we could not fully explore the aggregation of amylin into toxic amyloid plaques as the hormone is known to only aggregate in humans, we could not conclude on the effect of direct BACE inhibition in preventing amyloid plaque formation associated with T2D. The use of transgenic mice that express human IAPP will be necessary for future studies to elucidate BACE inhibition activity.

The effects of BACE inhibitor and GRT™ could not be assessed at a protein or gene level using Western blot or PCR since in the total pancreas, pancreatic islets account only for about 2% of the total endocrine cells of the pancreas (Stefan *et al*., 1982; Kobayashi *et al*., 2010) thus protein and/or gene expression specifically associated with the islets is masked by the rest of the exocrine tissue.

Since we propose that GRT™ and BACE inhibitor may be beneficial as adjunctive therapies in T2D, further investigations to validate their effects as co-administered therapies in the presence of each other and other currently used anti-diabetic drugs will be necessary.

CHAPTER EIGHT

References

References

Abdul-Ghani, M.A., Tripathy, D., DeFronzo, R.A., 2006. Contributions of -Cell Dysfunction and Insulin Resistance to the Pathogenesis of Impaired Glucose Tolerance and Impaired Fasting Glucose. Diabetes Care 29, 1130–1139. https://doi.org/10.2337/dc05-2179

Abedini, A., Schmidt, A.M., 2013. Mechanisms of islet amyloidosis toxicity in type 2 diabetes. FEBS Letters 587, 1119–1127. https://doi.org/10.1016/j.febslet.2013.01.017

Ahrén, B., 2006. Glucagon secretion in relation to insulin sensitivity in healthy subjects. Diabetologia 49, 117–122. https://doi.org/10.1007/s00125-005-0056-8

Ahren, B., Wierup, N., Sundler, F., 2006. Neuropeptides and the Regulation of Islet Function. Diabetes 55, S98–S107. https://doi.org/10.2337/db06-S013

Ajuwon, O.R., Katengua-Thamahane, E., Van Rooyen, J., Oguntibeju, O.O., Marnewick, J.L., 2013. Protective Effects of Rooibos (*Aspalathus linearis*) and/or Red Palm Oil (*Elaeis guineensis*) Supplementation on *tert* -Butyl Hydroperoxide-Induced Oxidative Hepatotoxicity in Wistar Rats. Evidence-Based Complementary and Alternative Medicine 2013, 1–19. https://doi.org/10.1155/2013/984273

Ajuwon, O.R., Oguntibeju, O.O., Marnewick, J.L., 2014. Amelioration of lipopolysaccharide-induced liver injury by aqueous rooibos (Aspalathus linearis) extract via inhibition of pro-inflammatory cytokines and oxidative stress. BMC Complementary and Alternative Medicine 14, 392. https://doi.org/10.1186/1472-6882-14-392

Alcarraz-Vizán, G., Castaño, C., Visa, M., Montane, J., Servitja, J.-M., Novials, A., 2017. BACE2 suppression promotes β-cell survival and function in a model of type 2 diabetes induced by human islet amyloid polypeptide overexpression. Cellular and Molecular Life Sciences 74, 2827–2838. https://doi.org/10.1007/s00018-017-2505-1

Alemzadeh, R., Kichler, J., Babar, G., Calhoun, M., 2008. Hypovitaminosis D in obese children and adolescents: relationship with adiposity, insulin sensitivity, ethnicity, and season. Metabolism 57, 183–191. https://doi.org/10.1016/j.metabol.2007.08.023

Alnahdi, A., John, A., Raza, H., 2019. Augmentation of Glucotoxicity, Oxidative Stress, Apoptosis and Mitochondrial Dysfunction in HepG2 Cells by Palmitic Acid. Nutrients 11, 1979. https://doi.org/10.3390/nu11091979

American Diabetes Association, 2019. 12. Older Adults: *Standards of Medical Care in Diabetes.,* 2019. Diabetes Care 42, S139–S147. https://doi.org/10.2337/dc19-S012

Ashcroft, F.M., Rorsman, P., 2012. Diabetes Mellitus and the β Cell: The Last Ten Years. Cell 148, 1160–1171. https://doi.org/10.1016/j.cell.2012.02.010

Assmann, A., Ueki, K., Winnay, J.N., Kadowaki, T., Kulkarni, R.N., 2009. Glucose Effects on Beta-Cell Growth and Survival Require Activation of Insulin Receptors and Insulin Receptor Substrate 2. Molecular and Cellular Biology 29, 3219–3228. https://doi.org/10.1128/MCB.01489-08

Augstein, P., Elefanty, A.G., Allison, J., Harrison, L.C., 1998. Apoptosis and beta-cell destruction in pancreatic islets of NOD mice with spontaneous and cyclophosphamide-

accelerated diabetes. Diabetologia 41, 1381–1388. https://doi.org/10.1007/s001250051080

Ayeleso, A., Brooks, N., Oguntibeju, O., 2014. Modulation of antioxidant status in streptozotocin-induced diabetic male wistar rats following intake of red palm oil and/or rooibos. Asian Pacific Journal of Tropical Medicine 7, 536–544. https://doi.org/10.1016/S1995-7645(14)60090-0

Badman, M.K., Shennan, K.I.J., Jermany, J.L., Docherty, K., Clark, A., 1996. Processing of pro-islet amyloid polypeptide (proIAPP) by the prohormone convertase PC2. FEBS Letters 378, 227–231. https://doi.org/10.1016/0014-5793(95)01460-8

Baetta, R., Corsini, A., 2011. Pharmacology of Dipeptidyl Peptidase-4 Inhibitors: Similarities and Differences. Drugs 71, 1441–1467. https://doi.org/10.2165/11591400-000000000-00000

Baharvand, H., Hashemi, S.M., Kazemi Ashtiani, S., Farrokhi, A., 2006. Differentiation of human embryonic stem cells into hepatocytes in 2D and 3D culture systems in vitro. The International Journal of Developmental Biology 50, 645–652. https://doi.org/10.1387/ijdb.052072hb

Bailey-Bucktrout, S.L., Martinez-Llordella, M., Zhou, X., Anthony, B., Rosenthal, W., Luche, H., Fehling, H.J., Bluestone, J.A., 2013. Self-antigen-Driven Activation Induces Instability of Regulatory T Cells during an Inflammatory Autoimmune Response. Immunity 39, 949–962. https://doi.org/10.1016/j.immuni.2013.10.016

Banday, A.A., Marwaha, A., Tallam, L.S., Lokhandwala, M.F., 2005. Tempol Reduces Oxidative Stress, Improves Insulin Sensitivity, Decreases Renal Dopamine D1 Receptor Hyperphosphorylation, and Restores D1 Receptor-G-Protein Coupling and Function in Obese Zucker Rats. Diabetes 54, 2219–2226. https://doi.org/10.2337/diabetes.54.7.2219

Barré-Sinoussi, F., Montagutelli, X., 2015. Animal models are essential to biological research: issues and perspectives. Future Science OA 1, fso.15.63. https://doi.org/10.4155/fso.15.63

Barzilai, N., Huffman, D.M., Muzumdar, R.H., Bartke, A., 2012. The Critical Role of Metabolic Pathways in Aging. Diabetes 61, 1315–1322. https://doi.org/10.2337/db11-1300

Beg, A.A., Baltimore, D., 1996. An Essential Role for NF-kappa B in Preventing TNF-alpha - Induced Cell Death. Science 274, 782–784. https://doi.org/10.1126/science.274.5288.782

Belgardt, B.F., Mauer, J., Wunderlich, F.T., Ernst, M.B., Pal, M., Spohn, G., Bronneke, H.S., Brodesser, S., Hampel, B., Schauss, A.C., Bruning, J.C., 2010. Hypothalamic and pituitary c-Jun N-terminal kinase 1 signaling coordinately regulates glucose metabolism. Proceedings of the National Academy of Sciences 107, 6028–6033. https://doi.org/10.1073/pnas.1001796107

Belke, D.D., Severson, D.L., 2012. Diabetes in Mice with Monogenic Obesity: The db/db Mouse and Its Use in the Study of Cardiac Consequences, in: Joost, H.-G., Al-Hasani, H., Schürmann, A. (Eds.), Animal Models in Diabetes Research. Humana Press, Totowa, NJ, pp. 47–57. https://doi.org/10.1007/978-1-62703-068-7_4

Beltrán-Debón, R., Rull, A., Rodríguez-Sanabria, F., Iswaldi, I., Herranz-López, M., Aragonès, G., Camps, J., Alonso-Villaverde, C., Menéndez, J.A., Micol, V., Segura-Carretero, A., Joven, J., 2011. Continuous administration of polyphenols from aqueous rooibos (Aspalathus linearis) extract ameliorates dietary-induced metabolic disturbances in hyperlipidemic mice. Phytomedicine 18, 414–424. https://doi.org/10.1016/j.phymed.2010.11.008

Bennett, B.D., Babu-Khan, S., Loeloff, R., Louis, J.-C., Curran, E., Citron, M., Vassar, R., 2000. Expression Analysis of BACE2 in Brain and Peripheral Tissues. Journal of Biological Chemistry 275, 20647–20651. https://doi.org/10.1074/jbc.M002688200

Bensellam, M., Laybutt, D.R., Jonas, J.-C., 2012. The molecular mechanisms of pancreatic β-cell glucotoxicity: Recent findings and future research directions. Molecular and Cellular Endocrinology 364, 1–27. https://doi.org/10.1016/j.mce.2012.08.003

Bernard, C., Berthault, M.-F., Saulnier, C., Ktorza, A., 1999. Neogenesis vs. apoptosis as main components of pancreatic β cell mass changes in glucose-infused normal and mildly diabetic adult rats. The FASEB Journal 13, 1195–1205. https://doi.org/10.1096/fasebj.13.10.1195

Bhattacharya, B., Low, S.H.H., Soh, C., Kamal Mustapa, N., Beloueche-Babari, M., Koh, K.X., Loh, J., Soong, R., 2014. Increased drug resistance is associated with reduced glucose levels and an enhanced glycolysis phenotype: Chemoresistance and hypoglycaemia and glycolysis. British Journal of Pharmacology 171, 3255–3267. https://doi.org/10.1111/bph.12668

Blaser, H., Dostert, C., Mak, T.W., Brenner, D., 2016. TNF and ROS Crosstalk in Inflammation. Trends in Cell Biology 26, 249–261. https://doi.org/10.1016/j.tcb.2015.12.002

Blouet, C., Mariotti, F., Azzout-Marniche, D., Mathé, V., Mikogami, T., Tomé, D., Huneau, J.-F., 2007. Dietary cysteine alleviates sucrose-induced oxidative stress and insulin resistance. Free Radical Biology and Medicine 42, 1089–1097. https://doi.org/10.1016/j.freeradbiomed.2007.01.006

Bollheimer, L.C., Skelly, R.H., Chester, M.W., McGarry, J.D., Rhodes, C.J., 1998. Chronic exposure to free fatty acid reduces pancreatic beta cell insulin content by increasing basal insulin secretion that is not compensated for by a corresponding increase in proinsulin biosynthesis translation. Journal of Clinical Investigation 101, 1094–1101. https://doi.org/10.1172/JCI420

Bowles, S., Joubert, E., de Beer, D., Louw, J., Brunschwig, C., Njoroge, M., Lawrence, N., Wiesner, L., Chibale, K., Muller, C., 2017. Intestinal Transport Characteristics and Metabolism of C-Glucosyl Dihydrochalcone, Aspalathin. Molecules 22, 554. https://doi.org/10.3390/molecules22040554

Bradford, M.M., 1976. A rapid and sensitive method for the quantitation of microgram quantities of protein utilizing the principle of protein-dye binding. Analytical Biochemistry 72, 248–254. https://doi.org/10.1016/0003-2697(76)90527-3

Bradshaw, D., Norman, R., Pieterse, D., Levitt, N.S., 2007. Estimating the burden of disease attributable to diabetes in South Africa in 2000. South African medical journal 97, 700–706.

Bravo, J., Arbillaga, L., de Peña, M.P., Cid, C., 2013. Antioxidant and genoprotective effects of spent coffee extracts in human cells. Food and Chemical Toxicology 60, 397–403. https://doi.org/10.1016/j.fct.2013.08.002

Bravo, R., Parra, V., Gatica, D., Rodriguez, A.E., Torrealba, N., Paredes, F., Wang, Z.V., Zorzano, A., Hill, J.A., Jaimovich, E., Quest, A.F.G., Lavandero, S., 2013. Endoplasmic Reticulum and the Unfolded Protein Response, in: International Review of Cell and Molecular Biology. Elsevier, pp. 215–290. https://doi.org/10.1016/B978-0-12-407704-1.00005-1

Breslin, S., O'Driscoll, L., 2013. Three-dimensional cell culture: the missing link in drug discovery. Drug Discovery Today 18, 240–249. https://doi.org/10.1016/j.drudis.2012.10.003

Buchanan, T.A., 2003. Pancreatic beta-cell loss and preservation in type 2 diabetes. Clinical Therapeutics 25, B32–B46. https://doi.org/10.1016/S0149-2918(03)80241-2

Bunprajun, T., Henriksen, T.I., Scheele, C., Pedersen, B.K., Green, C.J., 2013. Lifelong Physical Activity Prevents Aging-Associated Insulin Resistance in Human Skeletal Muscle Myotubes via Increased Glucose Transporter Expression. PLoS ONE 8, e66628. https://doi.org/10.1371/journal.pone.0066628

Burcelin, R., Crivelli, V., Perrin, C., Costa, A.D., Mu, J., Kahn, B.B., Birnbaum, M.J., Kahn, C.R., Vollenweider, P., Thorens, B., 2003. GLUT4, AMP kinase, but not the insulin receptor, are required for hepatoportal glucose sensor–stimulated muscle glucose utilization. Journal of Clinical Investigation 111, 1555–1562. https://doi.org/10.1172/JCI200316888

Burke, S.J., Batdorf, H.M., Burk, D.H., Noland, R.C., Eder, A.E., Boulos, M.S., Karlstad, M.D., Jason Collier, J., 2017. *db* / *db* Mice Exhibit Features of Human Type 2 Diabetes That Are Not Present in Weight-Matched C57BL/6J Mice Fed a Western Diet. Journal of Diabetes Research 2017, 1–17. https://doi.org/10.1155/2017/8503754

Burks, D.J., White, M.F., 2001. IRS proteins and beta-cell function. Diabetes 50, S140–S145. https://doi.org/10.2337/diabetes.50.2007.S140

Bussador do Amaral, J., Shiniti Urabayashi, M., Maria Machado-Santelli, G., 2010. Cell death and lumen formation in spheroids of MCF-7 cells. Cell Biology International 34, 267–274. https://doi.org/10.1042/CBI20090024

Butler, A.E., Galasso, R., Meier, J.J., Basu, R., Rizza, R.A., Butler, P.C., 2007. Modestly increased beta cell apoptosis but no increased beta cell replication in recent-onset type 1 diabetic patients who died of diabetic ketoacidosis. Diabetologia 50, 2323–2331. https://doi.org/10.1007/s00125-007-0794-x

Butler, P.C., Chou, J., Carter, W.B., Wang, Y.-N., Bu, B.-H., Chang, D., Chang, J.-K., Rizza, R.A., 1990. Effects of Meal Ingestion on Plasma Amylin Concentration in NIDDM and Nondiabetic Humans. Diabetes 39, 752–756. https://doi.org/10.2337/diab.39.6.752

Cai, K., Qi, D., Wang, O., Chen, J., Liu, X., Deng, B., Qian, L., Liu, X., Le, Y., 2011. TNF-α acutely upregulates amylin expression in murine pancreatic beta cells. Diabetologia 54, 617–626. https://doi.org/10.1007/s00125-010-1972-9

Canda, B.D., Oguntibeju, O.O., Marnewick, J.L., 2014. Effects of Consumption of Rooibos (*Aspalathus linearis*) and a Rooibos-Derived Commercial Supplement on Hepatic Tissue Injury by *tert* -Butyl Hydroperoxide in Wistar Rats. Oxidative Medicine and Cellular Longevity 2014, 1–9. https://doi.org/10.1155/2014/716832

Cao, P., Abedini, A., Wang, H., Tu, L.-H., Zhang, X., Schmidt, A.M., Raleigh, D.P., 2013. Islet amyloid polypeptide toxicity and membrane interactions. Proceedings of the National Academy of Sciences 110, 19279–19284. https://doi.org/10.1073/pnas.1305517110

Capurso, C., Capurso, A., 2012. From excess adiposity to insulin resistance: The role of free fatty acids. Vascular Pharmacology 57, 91–97. https://doi.org/10.1016/j.vph.2012.05.003

Casas, S., Casini, P., Piquer, S., Altirriba, J., Soty, M., Cadavez, L., Gomis, R., Novials, A., 2010. BACE2 plays a role in the insulin receptor trafficking in pancreatic β-cells. American Journal of Physiology-Endocrinology and Metabolism 299, E1087–E1095. https://doi.org/10.1152/ajpendo.00420.2010

Cernea, S., Dobreanu, M., 2013. Diabetes and beta cell function: from mechanisms to evaluation and clinical implications. Biochemia Medica 266–280. https://doi.org/10.11613/BM.2013.033

Chang, L., Chiang, S.-H., Saltiel, A.R., 2004. Insulin Signaling and the Regulation of Glucose Transport. Molecular Medicine 10, 65–71. https://doi.org/10.2119/2005-00029.Saltiel

Chang, T.T., Hughes-Fulford, M., 2009. Monolayer and Spheroid Culture of Human Liver Hepatocellular Carcinoma Cell Line Cells Demonstrate Distinct Global Gene Expression Patterns and Functional Phenotypes. Tissue Engineering Part A 15, 559–567. https://doi.org/10.1089/ten.tea.2007.0434

Chen, C., Chmelova, H., Cohrs, C.M., Chouinard, J.A., Jahn, S.R., Stertmann, J., Uphues, I., Speier, S., 2016. Alterations in β-Cell Calcium Dynamics and Efficacy Outweigh Islet Mass Adaptation in Compensation of Insulin Resistance and Prediabetes Onset. Diabetes 65, 2676–2685. https://doi.org/10.2337/db15-1718

Chen, F., Sha, M., Wang, Y., Wu, T., Shan, W., Liu, J., Zhou, W., Zhu, Y., Sun, Y., Shi, Y., Bleich, D., Han, X., 2016. Transcription factor Ets-1 links glucotoxicity to pancreatic beta cell dysfunction through inhibiting PDX-1 expression in rodent models. Diabetologia 59, 316–324. https://doi.org/10.1007/s00125-015-3805-3

Chen, H., Charlat, O., Tartaglia, L.A., Woolf, E.A., Weng, X., Ellis, S.J., Lakey, N.D., Culpepper, J., More, K.J., Breitbart, R.E., Duyk, G.M., Tepper, R.I., Morgenstern, J.P., 1996a. Evidence That the Diabetes Gene Encodes the Leptin Receptor: Identification of a Mutation in the Leptin Receptor Gene in db/db Mice. Cell 84, 491–495. https://doi.org/10.1016/S0092-8674(00)81294-5

Chen, T., Liu, W., Chao, X., Qu, Y., Zhang, L., Luo, P., Xie, K., Huo, J., Fei, Z., 2011. Neuroprotective effect of osthole against oxygen and glucose deprivation in rat cortical neurons: involvement of mitogen-activated protein kinase pathway. Neuroscience 183, 203–211. https://doi.org/10.1016/j.neuroscience.2011.03.038

Cheng, G., Tse, J., Jain, R.K., Munn, L.L., 2009a. Micro-Environmental Mechanical Stress Controls Tumor Spheroid Size and Morphology by Suppressing Proliferation and

Inducing Apoptosis in Cancer Cells. PLoS ONE 4, e4632. https://doi.org/10.1371/journal.pone.0004632

Cho, N.H., Shaw, J.E., Karuranga, S., Huang, Y., da Rocha Fernandes, J.D., Ohlrogge, A.W., Malanda, B., 2018. IDF Diabetes Atlas: Global estimates of diabetes prevalence for 2017 and projections for 2045. Diabetes Research and Clinical Practice 138, 271–281. https://doi.org/10.1016/j.diabres.2018.02.023

Choi, S.E., Choi, K.M., Yoon, I.H., Shin, J.Y., Kim, J.S., Park, W.Y., Han, D.J., Kim, S.C., Ahn, C., Kim, J.Y., Hwang, E.S., Cha, C.Y., Szot, G.L., Yoon, K.H., Park, C.G., 2004. IL-6 protects pancreatic islet beta cells from pro-inflammatory cytokines-induced cell death and functional impairment in vitro and in vivo. Transplant Immunology 13, 43–53. https://doi.org/10.1016/j.trim.2004.04.001

Christensen, A.A., Gannon, M., 2019. The Beta Cell in Type 2 Diabetes. Current Diabetes Reports 19, 81. https://doi.org/10.1007/s11892-019-1196-4

Christensen, K., Doblhammer, G., Rau, R., Vaupel, J.W., 2009. Ageing populations: the challenges ahead. The Lancet 374, 1196–1208. https://doi.org/10.1016/S0140-6736(09)61460-4

Chung, J.H., Seo, A.Y., Chung, S.W., Kim, M.K., Leeuwenburgh, C., Yu, B.P., Chung, H.Y., 2008. Molecular mechanism of PPAR in the regulation of age-related inflammation. Ageing Research Reviews 7, 126–136. https://doi.org/10.1016/j.arr.2008.01.001

Clark, A., Edwards, CatherineA., Ostle, LynneR., Sutton, R., Rothbard, JonathanB., Morris, JohnF., Turner, RobertC., 1989. Localisation of islet amyloid peptide in lipofuscin bodies and secretory granules of human B-cells and in islets of type-2 diabetic subjects. Cell and Tissue Research 257. https://doi.org/10.1007/BF00221649

Clark, A., Jones, L., de Koning, E., Hansen, B.C., Matthews, D.R., 2001. Decreased insulin secretion in type 2 diabetes: a problem of cellular mass or function? Diabetes 50, S169–S171. https://doi.org/10.2337/diabetes.50.2007.S169

Clark, M., Hampson, S.E., Avery, L., Simpson, R., 2004. Effects of a tailored lifestyle self-management intervention in patients with Type 2 diabetes. British Journal of Health Psychology 9, 365–379. https://doi.org/10.1348/1359107041557066

Cooper, G.J.S., 1994. Amylin Compared with Calcitonin Gene-Related Peptide: Structure, Biology, and Relevance to Metabolic Disease. Endocrine Reviews 15, 163–201. https://doi.org/10.1210/edrv-15-2-163

Courtade, J.A., Wang, E.Y., Yen, P., Dai, D.L., Soukhatcheva, G., Orban, P.C., Verchere, C.B., 2017. Loss of prohormone convertase 2 promotes beta cell dysfunction in a rodent transplant model expressing human pro-islet amyloid polypeptide. Diabetologia 60, 453–463. https://doi.org/10.1007/s00125-016-4174-2

Cowie, C.C., Rust, K.F., Ford, E.S., Eberhardt, M.S., Byrd-Holt, D.D., Li, C., Williams, D.E., Gregg, E.W., Bainbridge, K.E., Saydah, S.H., Geiss, L.S., 2009. Full Accounting of Diabetes and Pre-Diabetes in the U.S. Population in 1988-1994 and 2005-2006. Diabetes Care 32, 287–294. https://doi.org/10.2337/dc08-1296

Cox, C.J., Choudhry, F., Peacey, E., Perkinton, M.S., Richardson, J.C., Howlett, D.R., Lichtenthaler, S.F., Francis, P.T., Williams, R.J., 2015. Dietary (−)-epicatechin as a potent inhibitor of βγ-secretase amyloid precursor protein processing. Neurobiology of Aging 36, 178–187. https://doi.org/10.1016/j.neurobiolaging.2014.07.032

Crofts, C., Schofield, G., Zinn, C., Wheldon, M., Kraft, J., 2016. Identifying hyperinsulinaemia in the absence of impaired glucose tolerance: An examination of the Kraft database. Diabetes Research and Clinical Practice 118, 50–57. https://doi.org/10.1016/j.diabres.2016.06.007

da Rocha Fernandes, J., Ogurtsova, K., Linnenkamp, U., Guariguata, L., Seuring, T., Zhang, P., Cavan, D., Makaroff, L.E., 2016. IDF Diabetes Atlas estimates of 2014 global health expenditures on diabetes. Diabetes Research and Clinical Practice 117, 48–54. https://doi.org/10.1016/j.diabres.2016.04.016

Dalbøge, L.S., Almholt, D.L.C., Neerup, T.S.R., Vassiliadis, E., Vrang, N., Pedersen, L., Fosgerau, K., Jelsing, J., 2013. Characterisation of Age-Dependent Beta Cell Dynamics in the Male db/db Mice. PLoS ONE 8, e82813. https://doi.org/10.1371/journal.pone.0082813

D'Avanzo, C., Aronson, J., Kim, Y.H., Choi, S.H., Tanzi, R.E., Kim, D.Y., 2015. Alzheimer's in 3D culture: Challenges and perspectives: Alzheimer's in 3D culture. BioEssays 37, 1139–1148. https://doi.org/10.1002/bies.201500063

D'Cruz, S.C., Jubendradass, R., Mathur, P.P., 2012. Bisphenol A Induces Oxidative Stress and Decreases Levels of Insulin Receptor Substrate 2 and Glucose Transporter 8 in Rat Testis. Reproductive Sciences 19, 163–172. https://doi.org/10.1177/1933719111415547

de Leeuw van Weenen, J.E., Parlevliet, E.T., Maechler, P., Havekes, L.M., Romijn, J.A., Ouwens, D.M., Pijl, H., Guigas, B., 2010. The dopamine receptor D2 agonist bromocriptine inhibits glucose-stimulated insulin secretion by direct activation of the α2-adrenergic receptors in beta cells. Biochemical Pharmacology 79, 1827–1836. https://doi.org/10.1016/j.bcp.2010.01.029

De Tata, V., 2014. Age-Related Impairment of Pancreatic Beta-Cell Function: Pathophysiological and Cellular Mechanisms. Frontiers in Endocrinology 5. https://doi.org/10.3389/fendo.2014.00138

Dechenes, C.J., Verchere, C.B., Andrikopoulos, S., Kahn, S.E., 1998. Human aging is associated with parallel reductions in insulin and amylin release. American Journal of Physiology-Endocrinology and Metabolism 275, E785–E791. https://doi.org/10.1152/ajpendo.1998.275.5.E785

DeFronzo, R.A., 1981. Glucose Intolerance and Aging. Diabetes Care 4, 493–501. https://doi.org/10.2337/diacare.4.4.493

DeFronzo, R.A., Sherwin, R.S., Kraemer, N., 1987. Effect of Physical Training on Insulin Action in Obesity. Diabetes 36, 1379–1385. https://doi.org/10.2337/diab.36.12.1379

Dégano, P., Silvestre, R.A., Salas, M., Peiró, E., Marco, J., 1993. Amylin inhibits glucose-induced insulin secretion in a dose-dependent manner. Study in the perfused rat

pancreas. Regulatory Peptides 43, 91–96. https://doi.org/10.1016/0167-0115(93)90411-Z

Del Prato, S., 2009. Role of glucotoxicity and lipotoxicity in the pathophysiology of Type 2 diabetes mellitus and emerging treatment strategies: Glucotoxicity and lipotoxicity in Type 2 diabetes. Diabetic Medicine 26, 1185–1192. https://doi.org/10.1111/j.1464-5491.2009.02847.x

Despa, S., Margulies, K.B., Chen, L., Knowlton, A.A., Havel, P.J., Taegtmeyer, H., Bers, D.M., Despa, F., 2012. Hyperamylinemia Contributes to Cardiac Dysfunction in Obesity and Diabetes: A Study in Humans and Rats. Circulation Research 110, 598–608. https://doi.org/10.1161/CIRCRESAHA.111.258285

Dimitriadis, G., Mitrou, P., Lambadiari, V., Maratou, E., Raptis, S.A., 2011. Insulin effects in muscle and adipose tissue. Diabetes Research and Clinical Practice 93, S52–S59. https://doi.org/10.1016/S0168-8227(11)70014-6

Dludla, P.V., Gabuza, K.B., Muller, C.J.F., Joubert, E., Louw, J., Johnson, R., 2018. Aspalathin, a C-glucosyl Dihydrochalcone From Rooibos Improves the Hypoglycemic Potential of Metformin in Type 2 Diabetic (db/db) Mice. Physiological Research 813–818. https://doi.org/10.33549/physiolres.933891

Donath, M.Y., 2014. Targeting inflammation in the treatment of type 2 diabetes: time to start. Nature Reviews Drug Discovery 13, 465–476. https://doi.org/10.1038/nrd4275

Donath, M.Y., Ehses, J.A., Maedler, K., Schumann, D.M., Ellingsgaard, H., Eppler, E., Reinecke, M., 2005. Mechanisms of -Cell Death in Type 2 Diabetes. Diabetes 54, S108–S113. https://doi.org/10.2337/diabetes.54.suppl_2.S108

Donath, M.Y., Gross, D.J., Cerasi, E., Kaiser, N., 1999. Hyperglycemia-induced beta-cell apoptosis in pancreatic islets of Psammomys obesus during development of diabetes. Diabetes 48, 738–744. https://doi.org/10.2337/diabetes.48.4.738

Ehses, J.A., Lacraz, G., Giroix, M.-H., Schmidlin, F., Coulaud, J., Kassis, N., Irminger, J.-C., Kergoat, M., Portha, B., Homo-Delarche, F., Donath, M.Y., 2009. IL-1 antagonism reduces hyperglycemia and tissue inflammation in the type 2 diabetic GK rat. Proceedings of the National Academy of Sciences 106, 13998–14003. https://doi.org/10.1073/pnas.0810087106

Eizirik, D.L., Mandrup-Poulsen, T., 2001. A choice of death - the signal-transduction of immune-mediated beta-cell apoptosis. Diabetologia 44, 2115–2133. https://doi.org/10.1007/s001250100021

Ekor, M., 2014. The growing use of herbal medicines: issues relating to adverse reactions and challenges in monitoring safety. Frontiers in Pharmacology 4. https://doi.org/10.3389/fphar.2013.00177

Ernst, A., Sharma, A.N., Elased, K.M., Guest, P.C., Rahmoune, H., Bahn, S., 2013a. Diabetic db/db mice exhibit central nervous system and peripheral molecular alterations as seen in neurological disorders. Translational Psychiatry 3, e263–e263. https://doi.org/10.1038/tp.2013.42

Esposito, K., Giugliano, D., 2004. The metabolic syndrome and inflammation: association or causation? Nutrition, Metabolism and Cardiovascular Diseases 14, 228–232. https://doi.org/10.1016/S0939-4753(04)80048-6

Esser, N., Legrand-Poels, S., Piette, J., Scheen, A.J., Paquot, N., 2014. Inflammation as a link between obesity, metabolic syndrome and type 2 diabetes. Diabetes Research and Clinical Practice 105, 141–150. https://doi.org/10.1016/j.diabres.2014.04.006

Esterházy, D., Stützer, I., Wang, H., Rechsteiner, M.P., Beauchamp, J., Döbeli, H., Hilpert, H., Matile, H., Prummer, M., Schmidt, A., Lieske, N., Boehm, B., Marselli, L., Bosco, D., Kerr-Conte, J., Aebersold, R., Spinas, G.A., Moch, H., Migliorini, C., Stoffel, M., 2011a. Bace2 Is a β Cell-Enriched Protease that Regulates Pancreatic β Cell Function and Mass. Cell Metabolism 14, 365–377. https://doi.org/10.1016/j.cmet.2011.06.018

Farzan, M., Schnitzler, C.E., Vasilieva, N., Leung, D., Choe, H., 2000. BACE2, a beta -secretase homolog, cleaves at the beta site and within the amyloid-beta region of the amyloid-beta precursor protein. Proceedings of the National Academy of Sciences 97, 9712–9717. https://doi.org/10.1073/pnas.160115697

Fennema, E., Rivron, N., Rouwkema, J., van Blitterswijk, C., de Boer, J., 2013. Spheroid culture as a tool for creating 3D complex tissues. Trends in Biotechnology 31, 108–115. https://doi.org/10.1016/j.tibtech.2012.12.003

Ferrannini, E., Mari, A., Nofrate, V., Sosenko, J.M., Skyler, J.S., for the DPT-1 Study Group, 2010. Progression to Diabetes in Relatives of Type 1 Diabetic Patients: Mechanisms and Mode of Onset. Diabetes 59, 679–685. https://doi.org/10.2337/db09-1378

Ferri, G., Digiacomo, L., Lavagnino, Z., Occhipinti, M., Bugliani, M., Cappello, V., Caracciolo, G., Marchetti, P., Piston, D.W., Cardarelli, F., 2019. Insulin secretory granules labelled with phogrin-fluorescent proteins show alterations in size, mobility and responsiveness to glucose stimulation in living β-cells. Scientific Reports 9, 2890. https://doi.org/10.1038/s41598-019-39329-5

Ferriolli, E., Pessanha, F.P.A.S., Marchesi, J.C.L.S., 2014. Diabetes and Exercise in the Elderly, in: Goedecke, J.H., Ojuka, E.O. (Eds.), Medicine and Sport Science. S. KARGER AG, Basel, pp. 122–129. https://doi.org/10.1159/000357342

Fey, S.J., Wrzesinski, K., 2012. Determination of Drug Toxicity Using 3D Spheroids Constructed From an Immortal Human Hepatocyte Cell Line. Toxicological Sciences 127, 403–411. https://doi.org/10.1093/toxsci/kfs122

Fiddian-Green, R.G., Silen, W., 1975. Mechanisms of disposal of acid and alkali in rabbit duodenum. The American Journal of Physiology 229, 1641–1648. https://doi.org/10.1152/ajplegacy.1975.229.6.1641

Figliolini, F., Cantaluppi, V., De Lena, M., Beltramo, S., Romagnoli, R., Salizzoni, M., Melzi, R., Nano, R., Piemonti, L., Tetta, C., Biancone, L., Camussi, G., 2014. Isolation, Characterization and Potential Role in Beta Cell-Endothelium Cross-Talk of Extracellular Vesicles Released from Human Pancreatic Islets. PLoS ONE 9, e102521. https://doi.org/10.1371/journal.pone.0102521

Figueroa, D.J., Shi, X.-P., Gardell, S.J., Austin, C.P., 2001. Aβpp secretases are co-expressed with Aβpp in the pancreatic islets. Journal of Alzheimer's Disease 3, 393–396. https://doi.org/10.3233/JAD-2001-3405

Fluhrer, R., Capell, A., Westmeyer, G., Willem, M., Hartung, B., Condron, M.M., Teplow, D.B., Haass, C., Walter, J., 2002. A non-amyloidogenic function of BACE-2 in the secretory pathway: Distinct βAPP cleavage by BACE-1 and BACE-2. Journal of Neurochemistry 81, 1011–1020. https://doi.org/10.1046/j.1471-4159.2002.00908.x

Ford, E.S., 2003. The metabolic syndrome and C-reactive protein, fibrinogen, and leukocyte count: findings from the Third National Health and Nutrition Examination Survey. Atherosclerosis 168, 351–358. https://doi.org/10.1016/S0021-9150(03)00134-5

Frieboes, H.B., Zheng, X., Sun, C.-H., Tromberg, B., Gatenby, R., Cristini, V., 2006. An Integrated Computational/Experimental Model of Tumor Invasion. Cancer Research 66, 1597–1604. https://doi.org/10.1158/0008-5472.CAN-05-3166

Friedman, J.M., Halaas, J.L., 1998. Leptin and the regulation of body weight in mammals. Nature 395, 763–770. https://doi.org/10.1038/27376

Friedrichsen, B.N., Neubauer, N., Lee, Y.C., Gram, V.K., Blume, N., Petersen, J.S., Nielsen, J.H., Møldrup, A., 2006. Stimulation of pancreatic β-cell replication by incretins involves transcriptional induction of cyclin D1 via multiple signalling pathways. Journal of Endocrinology 188, 481–492. https://doi.org/10.1677/joe.1.06160

Fu, H., Li, W., Lao, Y., Luo, J., Lee, N.T.K., Kan, K.K.W., Tsang, H.W., Tsim, K.W.K., Pang, Y., Li, Z., Chang, D.C., Li, M., Han, Y., 2006. Bis(7)-tacrine attenuates β amyloid-induced neuronal apoptosis by regulating L-type calcium channels. Journal of Neurochemistry 98, 1400–1410. https://doi.org/10.1111/j.1471-4159.2006.03960.x

Fu, J., Cui, Q., Yang, B., Hou, Y., Wang, H., Xu, Y., Wang, D., Zhang, Q., Pi, J., 2017. The impairment of glucose-stimulated insulin secretion in pancreatic β-cells caused by prolonged glucotoxicity and lipotoxicity is associated with elevated adaptive antioxidant response. Food and Chemical Toxicology 100, 161–167. https://doi.org/10.1016/j.fct.2016.12.016

Gadot, M., Ariav, Y., Cerasi, E., Kaiser, N., Gross, D.J., 1995. Hyperproinsulinemia in the diabetic Psammomys obesus is a result of increased secretory demand on the beta-cell. Endocrinology 136, 4218–4223. https://doi.org/10.1210/endo.136.10.7664638

Garg, A.D., Kaczmarek, A., Krysko, O., Vandenabeele, P., Krysko, D.V., Agostinis, P., 2012. ER stress-induced inflammation: does it aid or impede disease progression? Trends in Molecular Medicine 18, 589–598. https://doi.org/10.1016/j.molmed.2012.06.010

Garlanda, C., Dinarello, C.A., Mantovani, A., 2013. The Interleukin-1 Family: Back to the Future. Immunity 39, 1003–1018. https://doi.org/10.1016/j.immuni.2013.11.010

Gastaldelli, A., Ferrannini, E., Miyazaki, Y., Matsuda, M., DeFronzo, R.A., 2004. Beta-cell dysfunction and glucose intolerance: results from the San Antonio metabolism (SAM) study. Diabetologia 47, 31–39. https://doi.org/10.1007/s00125-003-1263-9

Gauvin, R., Chen, Y.-C., Lee, J.W., Soman, P., Zorlutuna, P., Nichol, J.W., Bae, H., Chen, S., Khademhosseini, A., 2012. Microfabrication of complex porous tissue engineering

scaffolds using 3D projection stereolithography. Biomaterials 33, 3824–3834. https://doi.org/10.1016/j.biomaterials.2012.01.048

Gedulin, B.R., Jodka, C.M., Herrmann, K., Young, A.A., 2006. Role of endogenous amylin in glucagon secretion and gastric emptying in rats demonstrated with the selective antagonist, AC187. Regulatory Peptides 137, 121–127. https://doi.org/10.1016/j.regpep.2006.06.004

Genuth, S., 2003. Lowering the Criterion for Impaired Fasting Glucose Is in Order. Diabetes Care 26, 3331–3332. https://doi.org/10.2337/diacare.26.12.3331

Genuth, S., Kahn, R., 2008. A Step Backward--or Is it Forward? Diabetes Care 31, 1093–1096. https://doi.org/10.2337/dc07-2407

Genuth, S.M., 2013. How Does Pioglitazone Prevent Progression of Impaired Glucose Tolerance to Diabetes? Diabetes 62, 3663–3665. https://doi.org/10.2337/db13-1175

Gomez-Perez, F.J., Aguilar-Salinas, C.A., Lopez-Alvarenga, J.C., Perez-Jauregui, J., Guillen-Pineda, L.E., Rull, J.A., 1998. Lack of agreement between the World Health Organization Category of impaired glucose tolerance and the American Diabetes Association category of impaired fasting glucose. Diabetes Care 21, 1886–1888. https://doi.org/10.2337/diacare.21.11.1886

Greenberg, A.S., McDaniel, M.L., 2002. Identifying the links between obesity, insulin resistance and beta-cell function: potential role of adipocyte-derived cytokines in the pathogenesis of type 2 diabetes. European Journal of Clinical Investigation 32, 24–34. https://doi.org/10.1046/j.1365-2362.32.s3.4.x

Gual, P., Le Marchand-Brustel, Y., Tanti, J.-F., 2005. Positive and negative regulation of insulin signaling through IRS-1 phosphorylation. Biochimie 87, 99–109. https://doi.org/10.1016/j.biochi.2004.10.019

Gunasekaran, U., Gannon, M., 2011. Type 2 Diabetes and the Aging Pancreatic Beta Cell. Aging 3, 565–575. https://doi.org/10.18632/aging.100350

Haffner, S.M., Miettinen, H., Gaskill, S.P., Stern, M.P., 1995. Decreased Insulin Secretion and Increased Insulin Resistance Are Independently Related to the 7-Year Risk of NIDDM in Mexican-Americans. Diabetes 44, 1386–1391. https://doi.org/10.2337/diab.44.12.1386

Hampel, H., Shen, Y., Walsh, D.M., Aisen, P., Shaw, L.M., Zetterberg, H., Trojanowski, J.Q., Blennow, K., 2010. Biological markers of amyloid β-related mechanisms in Alzheimer's disease. Experimental Neurology 223, 334–346. https://doi.org/10.1016/j.expneurol.2009.09.024

Hampp, C., Borders-Hemphill, V., Moeny, D.G., Wysowski, D.K., 2014. Use of Antidiabetic Drugs in the U.S., 2003–2012. Diabetes Care 37, 1367–1374. https://doi.org/10.2337/dc13-2289

Handelsman, Y., 2011. Role of Bile Acid Sequestrants in the Treatment of Type 2 Diabetes. Diabetes Care 34, S244–S250. https://doi.org/10.2337/dc11-s237

Hasnain, S.Z., Lourie, R., Das, I., Chen, A.C.-H., McGuckin, M.A., 2012. The interplay between endoplasmic reticulum stress and inflammation. Immunology and Cell Biology 90, 260–270. https://doi.org/10.1038/icb.2011.112

Haycock, J.W., 2011. 3D Cell Culture: A Review of Current Approaches and Techniques, in: Haycock, J.W. (Ed.), 3D Cell Culture. Humana Press, Totowa, NJ, pp. 1–15. https://doi.org/10.1007/978-1-60761-984-0_1

Hendricks, R., Pool, E.J., 2010. THE *IN VITRO* EFFECTS OF ROOIBOS AND BLACK TEA ON IMMUNE PATHWAYS. Journal of Immunoassay and Immunochemistry 31, 169–180. https://doi.org/10.1080/15321811003617537

Higham, C.E., Hull, R.L., Lawrie, L., Shennan, K.I.J., Morris, J.F., Birch, N.P., Docherty, K., Clark, A., 2000. Processing of synthetic pro-islet amyloid polypeptide (proIAPP) 'amylin' by recombinant prohormone convertase enzymes, PC2 and PC3, in vitro: Pro-islet amyloid polypeptide proteolysis in vitro. European Journal of Biochemistry 267, 4998–5004. https://doi.org/10.1046/j.1432-1327.2000.01548.x

Hoosen, M., 2019. The Effects of Aspalathus linearis (Rooibos Tea) on Nitric Oxide (NO) and Cytokine Activity. International Journal of Human and Health Sciences (IJHHS) 3, 150. https://doi.org/10.31344/ijhhs.v3i3.93

Hotamisligil, G. k. S., Peraldi, P., Budavari, A., Ellis, R., White, M.F., Spiegelman, B.M., 1996. IRS-1-Mediated Inhibition of Insulin Receptor Tyrosine Kinase Activity in TNF-alpha- and Obesity-Induced Insulin Resistance. Science 271, 665–670. https://doi.org/10.1126/science.271.5249.665

Hotamisligil, G.S., Erbay, E., 2008. Nutrient sensing and inflammation in metabolic diseases. Nature Reviews Immunology 8, 923–934. https://doi.org/10.1038/nri2449

Hou, Z.Q., Li, H.L., Gao, L., Pan, L., Zhao, J.J., Li, G.W., 2008a. Involvement of chronic stresses in rat islet and INS-1 cell glucotoxicity induced by intermittent high glucose. Molecular and Cellular Endocrinology 291, 71–78. https://doi.org/10.1016/j.mce.2008.03.004

Houstis, N., Rosen, E.D., Lander, E.S., 2006. Reactive oxygen species have a causal role in multiple forms of insulin resistance. Nature 440, 944–948. https://doi.org/10.1038/nature04634

Hribal, M.L., Perego, L., Lovari, S., Andreozzi, F., Menghini, R., Perego, C., Finzi, G., Usellini, L., Placidi, C., Capella, C., Guzzi, V., Lauro, D., Bertuzzi, F., Davalli, A., Pozza, G., Pontiroli, A., Federici, M., Lauro, R., Brunetti, A., Folli, F., Sesti, G., 2003. Chronic hyperglycemia impairs insulin secretion by affecting insulin receptor expression, splicing, and signaling in RIN β cell line and human islets of Langerhans. The FASEB Journal 17, 1340–1342. https://doi.org/10.1096/fj.02-0685fje

Huang, G., Shi, L.Z., Chi, H., 2009. Regulation of JNK and p38 MAPK in the immune system: Signal integration, propagation and termination. Cytokine 48, 161–169. https://doi.org/10.1016/j.cyto.2009.08.002

Huh, D., Hamilton, G.A., Ingber, D.E., 2011. From 3D cell culture to organs-on-chips. Trends in Cell Biology 21, 745–754. https://doi.org/10.1016/j.tcb.2011.09.005

Hull, R.L., Andrikopoulos, S., Verchere, C.B., Vidal, J., Wang, F., Cnop, M., Prigeon, R.L., Kahn, S.E., 2003. Increased Dietary Fat Promotes Islet Amyloid Formation and -Cell Secretory Dysfunction in a Transgenic Mouse Model of Islet Amyloid. Diabetes 52, 372–379. https://doi.org/10.2337/diabetes.52.2.372

Hull, R.L., Westermark, G.T., Westermark, P., Kahn, S.E., 2004. Islet Amyloid: A Critical Entity in the Pathogenesis of Type 2 Diabetes. The Journal of Clinical Endocrinology & Metabolism 89, 3629–3643. https://doi.org/10.1210/jc.2004-0405

Hutton, J.C., 1989. The insulin secretory granule. Diabetologia 32, 271–281. https://doi.org/10.1007/BF00265542

Iizuka, K., Nakajima, H., Ono, A., Okita, K., Miyazaki, J., Miyagawa, J., Namba, M., Hanafusa, T., Matsuzawa, Y., 2000. Stable overexpression of the glucose-6-phosphatase catalytic subunit attenuates glucose sensitivity of insulin secretion from a mouse pancreatic beta-cell line. Journal of Endocrinology 164, 307–314. https://doi.org/10.1677/joe.0.1640307

Inzucchi, S.E., Bergenstal, R.M., Buse, J.B., Diamant, M., Ferrannini, E., Nauck, M., Peters, A.L., Tsapas, A., Wender, R., Matthews, D.R., 2012. Management of hyperglycaemia in type 2 diabetes: a patient-centered approach. Position statement of the American Diabetes Association (ADA) and the European Association for the Study of Diabetes (EASD). Diabetologia 55, 1577–1596. https://doi.org/10.1007/s00125-012-2534-0

Iozzo, P., Beck-Nielsen, H., Laakso, M., Smith, U., Yki-Järvinen, H., Ferrannini, E., 1999. Independent Influence of Age on Basal Insulin Secretion in Nondiabetic Humans. The Journal of Clinical Endocrinology & Metabolism 84, 863–868. https://doi.org/10.1210/jcem.84.3.5542

Ishida, H., Takizawa, M., Ozawa, S., Nakamichi, Y., Yamaguchi, S., Katsuta, H., Tanaka, T., Maruyama, M., Katahira, H., Yoshimoto, K., Itagaki, E., Nagamatsu, S., 2004. Pioglitazone improves insulin secretory capacity and prevents the loss of β-cell mass in obese diabetic db/db mice: possible protection of β cells from oxidative stress. Metabolism 53, 488–494. https://doi.org/10.1016/j.metabol.2003.11.021

Islam, Md.S., Wilson, R.D., 2012. Experimentally Induced Rodent Models of Type 2 Diabetes, in: Joost, H.-G., Al-Hasani, H., Schürmann, A. (Eds.), Animal Models in Diabetes Research. Humana Press, Totowa, NJ, pp. 161–174. https://doi.org/10.1007/978-1-62703-068-7_10

Ivascu, A., Kubbies, M., 2006. Rapid Generation of Single-Tumor Spheroids for High-Throughput Cell Function and Toxicity Analysis. Journal of Biomolecular Screening 11, 922–932. https://doi.org/10.1177/1087057106292763

Jackson, R.A., 1990. Mechanisms of Age-Related Glucose Intolerance. Diabetes Care 13, 9–19. https://doi.org/10.2337/diacare.13.2.S9

Jacobi, N., Seeboeck, R., Hofmann, E., Schweiger, H., Smolinska, V., Mohr, T., Boyer, A., Sommergruber, W., Lechner, P., Pichler-Huebschmann, C., Önder, K., Hundsberger, H., Wiesner, C., Eger, A., 2017. Organotypic three-dimensional cancer cell cultures mirror drug responses *in vivo*: lessons learned from the inhibition of EGFR signaling. Oncotarget 8. https://doi.org/10.18632/oncotarget.22475

Jagiella, N., Müller, B., Müller, M., Vignon-Clementel, I.E., Drasdo, D., 2016. Inferring Growth Control Mechanisms in Growing Multi-cellular Spheroids of NSCLC Cells from Spatial-Temporal Image Data. PLOS Computational Biology 12, e1004412. https://doi.org/10.1371/journal.pcbi.1004412

Jiang, T., Yu, J.T., Zhu, X.C., Wang, H.F., Tan, M.S., Cao, L., Zhang, Q.Q., Gao, L., Shi, J.Q., Zhang, Y.D., Tan, L., 2014. Acute metformin preconditioning confers neuroprotection against focal cerebral ischaemia by pre-activation of AMPK-dependent autophagy: Metformin preconditioning confers neuroprotection. British Journal of Pharmacology 171, 3146–3157. https://doi.org/10.1111/bph.12655

Jin, S., Diano, S., 2018. Mitochondrial Dynamics and Hypothalamic Regulation of Metabolism. Endocrinology 159, 3596–3604. https://doi.org/10.1210/en.2018-00667

Johnson, R., Dludla, P., Joubert, E., February, F., Mazibuko, S., Ghoor, S., Muller, C., Louw, J., 2016. Aspalathin, a dihydrochalcone *C* -glucoside, protects H9c2 cardiomyocytes against high glucose induced shifts in substrate preference and apoptosis. Molecular Nutrition & Food Research 60, 922–934. https://doi.org/10.1002/mnfr.201500656

Jonas, J.C., Guiot, Y., Rahier, J., Henquin, J.C., 2003. Haeme-oxygenase 1 expression in rat pancreatic beta cells is stimulated by supraphysiological glucose concentrations and by cyclic AMP. Diabetologia 46, 1234–1244. https://doi.org/10.1007/s00125-003-1174-9

Joubert, E., de Beer, D., 2011. Rooibos (Aspalathus linearis) beyond the farm gate: From herbal tea to potential phytopharmaceutical. South African Journal of Botany 77, 869–886. https://doi.org/10.1016/j.sajb.2011.07.004

Joubert, E., Manley, M., Botha, M., 2008. Evaluation of spectrophotometric methods for screening of green rooibos (Aspalathus linearis) and green honeybush (Cyclopia genistoides) extracts for high levels of Bio-active compounds. Phytochemical Analysis 19, 169–178. https://doi.org/10.1002/pca.1033

Kahn, B.B., 1998. Type 2 Diabetes: When Insulin Secretion Fails to Compensate for Insulin Resistance. Cell 92, 593–596. https://doi.org/10.1016/S0092-8674(00)81125-3

Kahn, S.E., 2003. The relative contributions of insulin resistance and beta-cell dysfunction to the pathophysiology of Type 2 diabetes. Diabetologia 46, 3–19. https://doi.org/10.1007/s00125-002-1009-0

Kahn, S.E., 2001. The Importance of β-Cell Failure in the Development and Progression of Type 2 Diabetes. The Journal of Clinical Endocrinology & Metabolism 86, 4047–4058. https://doi.org/10.1210/jcem.86.9.7713

Kahn, S.E., Cooper, M.E., Del Prato, S., 2014. Pathophysiology and treatment of type 2 diabetes: perspectives on the past, present, and future. The Lancet 383, 1068–1083. https://doi.org/10.1016/S0140-6736(13)62154-6

Kahn, S.E., D'Alessio, D.A., Schwartz, M.W., Fujimoto, W.Y., Ensinck, J.W., Taborsky, G.J., Porte, D., 1990. Evidence of Cosecretion of Islet Amyloid Polypeptide and Insulin by -Cells. Diabetes 39, 634–638. https://doi.org/10.2337/diab.39.5.634

Kahn, S.E., Hull, R.L., Utzschneider, K.M., 2006. Mechanisms linking obesity to insulin resistance and type 2 diabetes. Nature 444, 840–846. https://doi.org/10.1038/nature05482

Kamakura, R., Son, M.J., de Beer, D., Joubert, E., Miura, Y., Yagasaki, K., 2015. Antidiabetic effect of green rooibos (Aspalathus linearis) extract in cultured cells and type 2 diabetic model KK-Ay mice. Cytotechnology 67, 699–710. https://doi.org/10.1007/s10616-014-9816-y

Kamimura, D., Ishihara, K., Hirano, T., 2004. IL-6 signal transduction and its physiological roles: the signal orchestration model, in: Reviews of Physiology, Biochemistry and Pharmacology. Springer Berlin Heidelberg, Berlin, Heidelberg, pp. 1–38. https://doi.org/10.1007/s10254-003-0012-2

Kaneto, H., Matsuoka, T., Nakatani, Y., Kawamori, D., Matsuhisa, M., Yamasaki, Y., 2005a. Oxidative Stress and the JNK Pathway in Diabetes. Current Diabetes Reviews 1, 65–72. https://doi.org/10.2174/1573399052952613

Kaneto, H., Nakatani, Y., Kawamori, D., Miyatsuka, T., Matsuoka, T., Matsuhisa, M., Yamasaki, Y., 2005b. Role of oxidative stress, endoplasmic reticulum stress, and c-Jun N-terminal kinase in pancreatic β-cell dysfunction and insulin resistance. The International Journal of Biochemistry & Cell Biology 37, 1595–1608. https://doi.org/10.1016/j.biocel.2005.04.003

Kaufman, M., Nikitin, A.Yu., Sundberg, J.P., 2009. Histologic Basis of Mouse Endocrine System Development: A Comparative Analysis. CRC Press, Inc., Boca Raton, FL, USA.

Kautzky-Willer, A., Thomaseth, K., Pacini, G., Clodi, M., Ludvik, B., Streli, C., Waldhäusl, W., Prager, R., 1994. Role of islet amyloid polypeptide secretion in insulin-resistant humans. Diabetologia 37, 188–194. https://doi.org/10.1007/s001250050092

Kawano, A., Nakamura, H., Hata, S., Minakawa, M., Miura, Y., Yagasaki, K., 2009a. Hypoglycemic effect of aspalathin, a rooibos tea component from Aspalathus linearis, in type 2 diabetic model db/db mice. Phytomedicine 16, 437–443. https://doi.org/10.1016/j.phymed.2008.11.009

Kawasaki, F., Matsuda, M., Kanda, Y., Inoue, H., Kaku, K., 2005. Structural and functional analysis of pancreatic islets preserved by pioglitazone in *db/db* mice. American Journal of Physiology-Endocrinology and Metabolism 288, E510–E518. https://doi.org/10.1152/ajpendo.00128.2004

Kawasaki, N., Asada, R., Saito, A., Kanemoto, S., Imaizumi, K., 2012. Obesity-induced endoplasmic reticulum stress causes chronic inflammation in adipose tissue. Scientific Reports 2, 799. https://doi.org/10.1038/srep00799

Kayed, R., 2003. Common Structure of Soluble Amyloid Oligomers Implies Common Mechanism of Pathogenesis. Science 300, 486–489. https://doi.org/10.1126/science.1079469

Keane, K.N., Cruzat, V.F., Carlessi, R., de Bittencourt, P.I.H., Newsholme, P., 2015. Molecular Events Linking Oxidative Stress and Inflammation to Insulin Resistance and *β* -Cell

Dysfunction. Oxidative Medicine and Cellular Longevity 2015, 1–15. https://doi.org/10.1155/2015/181643

Kelm, J.M., Fussenegger, M., 2004. Microscale tissue engineering using gravity-enforced cell assembly. Trends in Biotechnology 22, 195–202. https://doi.org/10.1016/j.tibtech.2004.02.002

Kemnitz, J.W., Elson, D.F., Roecker, E.B., Baum, S.T., Bergman, R.N., Meglasson, M.D., 1994. Pioglitazone Increases Insulin Sensitivity, Reduces Blood Glucose, Insulin, and Lipid Levels, and Lowers Blood Pressure, in Obese, Insulin-Resistant Rhesus Monkeys. Diabetes 43, 204–211. https://doi.org/10.2337/diab.43.2.204

Khaitan, D., Chandna, S., Arya, M., Dwarakanath, B., 2006. Establishment and characterization of multicellular spheroids from a human glioma cell line; Implications for tumor therapy. Journal of Translational Medicine 4, 12. https://doi.org/10.1186/1479-5876-4-12

Kieffer, T.J., Habener, J.F., 2000. The adipoinsular axis: effects of leptin on pancreatic β-cells. American Journal of Physiology-Endocrinology and Metabolism 278, E1–E14. https://doi.org/10.1152/ajpendo.2000.278.1.E1

Kilpatrick, E.D., Robertson, R.P., 1998. Differentiation between glucose-induced desensitization of insulin secretion and beta-cell exhaustion in the HIT-T15 cell line. Diabetes 47, 606–611. https://doi.org/10.2337/diabetes.47.4.606

Kim, D.H., Kim, C.H., Kim, M.-S., Kim, J.Y., Jung, K.J., Chung, J.H., An, W.G., Lee, J.W., Yu, B.P., Chung, H.Y., 2007. Suppression of age-related inflammatory NF-κB activation by cinnamaldehyde. Biogerontology 8, 545–554. https://doi.org/10.1007/s10522-007-9098-2

Kim, E.K., Choi, E.-J., 2010. Pathological roles of MAPK signaling pathways in human diseases. Biochimica et Biophysica Acta (BBA) - Molecular Basis of Disease 1802, 396–405. https://doi.org/10.1016/j.bbadis.2009.12.009

Kim, M.S., Hur, H.J., Kwon, D.Y., Hwang, J.-T., 2012. Tangeretin stimulates glucose uptake via regulation of AMPK signaling pathways in C2C12 myotubes and improves glucose tolerance in high-fat diet-induced obese mice. Molecular and Cellular Endocrinology 358, 127–134. https://doi.org/10.1016/j.mce.2012.03.013

Kim, Y.H., Choi, S.H., D'Avanzo, C., Hebisch, M., Sliwinski, C., Bylykbashi, E., Washicosky, K.J., Klee, J.B., Brüstle, O., Tanzi, R.E., Kim, D.Y., 2015. A 3D human neural cell culture system for modeling Alzheimer's disease. Nature Protocols 10, 985–1006. https://doi.org/10.1038/nprot.2015.065

King, A.J., 2012. The use of animal models in diabetes research: Animal models of diabetes. British Journal of Pharmacology 166, 877–894. https://doi.org/10.1111/j.1476-5381.2012.01911.x

Kirkwood, T.B.L., 2005. Understanding the Odd Science of Aging. Cell 120, 437–447. https://doi.org/10.1016/j.cell.2005.01.027

Kobayashi, K., Forte, T.M., Taniguchi, S., Ishida, B.Y., Oka, K., Chan, L., 2000. The db/db mouse, a model for diabetic dyslipidemia: Molecular characterization and effects of

western diet feeding. Metabolism 49, 22–31. https://doi.org/10.1016/S0026-0495(00)90588-2

Kobayashi, T., Manivel, J.C., Bellin, M.D., Carlson, A.M., Moran, A., Freeman, M.L., Hering, B.J., Sutherland, D.E.R., 2010. Correlation of Pancreatic Histopathologic Findings and Islet Yield in Children With Chronic Pancreatitis Undergoing Total Pancreatectomy and Islet Autotransplantation: Pancreas 39, 57–63. https://doi.org/10.1097/MPA.0b013e3181b8ff71

Konarkowska, B., Aitken, J.F., Kistler, J., Zhang, S., Cooper, G.J.S., 2006. The aggregation potential of human amylin determines its cytotoxicity towards islet β-cells. FEBS Journal 273, 3614–3624. https://doi.org/10.1111/j.1742-4658.2006.05367.x

Kowal, P., Chatterji, S., Naidoo, N., Biritwum, R., Fan, W., Lopez Ridaura, R., Maximova, T., Arokiasamy, P., Phaswana-Mafuya, N., Williams, S., Snodgrass, J.J., Minicuci, N., D'Este, C., Peltzer, K., Boerma, J.T., the SAGE Collaborators, Yawson, A., Mensah, G., Yong, J., Guo, Y., Zheng, Y., Parasuraman, P., Lhungdim, H., Sekher, T., Rosa, R., Belov, V., Lushkina, N., Peltzer, K., Makiwane, M., Zuma, K., Ramlagan, S., Davids, A., Mbelle, N., Matseke, G., Schneider, M., Tabane, C., Tollman, S., Kahn, K., Ng, N., Juvekar, S., Sankoh, O., Debpuur, C., Nguyen, T.C., Gomez-Olive, F., Hakimi, M., Hirve, S., Abdullah, S., Hodgson, A., Kyobutungi, C., Egondi, T., Mayombana, C., Minh, H., Mwanyangala, M., Razzaque, A., Wilopo, S., Streatfield, P., Byass, P., Wall, S., Scholten, F., Mugisha, J., Seeley, J., Kinyanda, E., Nyirenda, M., Mutevedzi, P., Newell, M.-L., 2012. Data Resource Profile: The World Health Organization Study on global AGEing and adult health (SAGE). International Journal of Epidemiology 41, 1639–1649. https://doi.org/10.1093/ije/dys210

Krishnamurthy, S., Nör, J.E., 2013. Orosphere assay: A method for propagation of head and neck cancer stem cells. Head Neck 35, 1015–1021. https://doi.org/10.1002/hed.23076

Ku, S.K., Kwak, S., Kim, Y., Bae, J.-S., 2015. Aspalathin and Nothofagin from Rooibos (Aspalathus linearis) Inhibits High Glucose-Induced Inflammation In Vitro and In Vivo. Inflammation 38, 445–455. https://doi.org/10.1007/s10753-014-0049-1

Kulas, J.A., Puig, K.L., Combs, C.K., 2017. Amyloid precursor protein in pancreatic islets. Journal of Endocrinology 235, 49–67. https://doi.org/10.1530/JOE-17-0122

Kulkarni, R.N., Winnay, J.N., Daniels, M., Brüning, J.C., Flier, S.N., Hanahan, D., Kahn, C.R., 1999. Altered function of insulin receptor substrate-1–deficient mouse islets and cultured β-cell lines. Journal of Clinical Investigation 104, R69–R75. https://doi.org/10.1172/JCI8339

Kwon, H., Pessin, J.E., 2018. Adipokines, Inflammation, and Insulin Resistance in Obesity, in: Nillni, E.A. (Ed.), Textbook of Energy Balance, Neuropeptide Hormones, and Neuroendocrine Function. Springer International Publishing, Cham, pp. 225–252. https://doi.org/10.1007/978-3-319-89506-2_9

Lally, F.J., Ratcliff, H., Bone, A.J., 2001. Apoptosis and disease progression in the spontaneously diabetic BB/S rat. Diabetologia 44, 320–324. https://doi.org/10.1007/s001250051621

Lee, H.J., Ryu, J.M., Jung, Y.H., Lee, S.-J., Kim, J.Y., Lee, S.H., Hwang, I.K., Seong, J.K., Han, H.J., 2016. High glucose upregulates BACE1-mediated Aβ production through

ROS-dependent HIF-1α and LXRα/ABCA1-regulated lipid raft reorganization in SK-N-MC cells. Scientific Reports 6, 36746. https://doi.org/10.1038/srep36746

Lee, K.N., Jeong, I.C., Lee, S.J., Oh, S.H., Cho, M.Y., 2001. Regulation of leptin gene expression by insulin and growth hormone in mouse adipocytes. Experimental & Molecular Medicine 33, 234–239. https://doi.org/10.1038/emm.2001.38

Leighton, B., Cooper, G.J.S., 1988. Pancreatic amylin and calcitonin gene-related peptide cause resistance to insulin in skeletal muscle in vitro. Nature 335, 632–635. https://doi.org/10.1038/335632a0

Leiter, E.H., 1988. Control of spontaneous glucose intolerance, hyperinsulinemia, and islet hyperplasia in nonobese C3H.SW male mice by Y-linked locus and adrenal gland. Metabolism 37, 689–696. https://doi.org/10.1016/0026-0495(88)90092-3

Leiter, E.H., Premdas, F., Harrison, D.E., Lipson, L.G., 1988. Aging and glucose homeostasis in C57BL/6J male mice. The FASEB Journal 2, 2807–2811. https://doi.org/10.1096/fasebj.2.12.3044905

Levenberg, S., Huang, N.F., Lavik, E., Rogers, A.B., Itskovitz-Eldor, J., Langer, R., 2003. Differentiation of human embryonic stem cells on three-dimensional polymer scaffolds. Proceedings of the National Academy of Sciences 100, 12741–12746. https://doi.org/10.1073/pnas.1735463100

Lewis, J.D., Habel, L.A., Quesenberry, C.P., Strom, B.L., Peng, T., Hedderson, M.M., Ehrlich, S.F., Mamtani, R., Bilker, W., Vaughn, D.J., Nessel, L., Van Den Eeden, S.K., Ferrara, A., 2015. Pioglitazone Use and Risk of Bladder Cancer and Other Common Cancers in Persons With Diabetes. JAMA 314, 265. https://doi.org/10.1001/jama.2015.7996

Li, L., Hölscher, C., 2007. Common pathological processes in Alzheimer disease and type 2 diabetes: A review. Brain Research Reviews 56, 384–402. https://doi.org/10.1016/j.brainresrev.2007.09.001

Li, Y., Shen, R., Wen, G., Ding, R., Du, A., Zhou, J., Dong, Z., Ren, X., Yao, H., Zhao, R., Zhang, G., Lu, Y., Wu, X., 2017. Effects of Ketamine on Levels of Inflammatory Cytokines IL-6, IL-1β, and TNF-α in the Hippocampus of Mice Following Acute or Chronic Administration. Frontiers in Pharmacology 8. https://doi.org/10.3389/fphar.2017.00139

Ling, P.-R., Mueller, C., Smith, R.J., Bistrian, B.R., 2003. Hyperglycemia induced by glucose infusion causes hepatic oxidative stress and systemic inflammation, but not STAT3 or MAP kinase activation in liver in rats. Metabolism 52, 868–874. https://doi.org/10.1016/S0026-0495(03)00057-X

Lukinius, A., Korsgren, O., Grimelius, L., Wilander, E., 1996. Expression of islet amyloid polypeptide in fetal and adult porcine and human pancreatic islet cells. Endocrinology 137, 5319–5325. https://doi.org/10.1210/endo.137.12.8940352

Lukinius, A., Wilander, E., Westermark, G.T., Engstrom, U., Westermark, P., 1989. Co-localization of islet amyloid polypeptide and insulin in the B cell secretory granules of the human pancreatic islets. Diabetologia 32, 240–244. https://doi.org/10.1007/BF00285291

Lundberg, I.E., 2000. The role of cytokines, chemokines, and adhesion molecules in the pathogenesis of idiopathic inflammatory myopathies. Current Rheumatology Reports 2, 216–224. https://doi.org/10.1007/s11926-000-0082-y

Lundberg, J.O., Carlström, M., Weitzberg, E., 2018. Metabolic Effects of Dietary Nitrate in Health and Disease. Cell Metabolism 28, 9–22. https://doi.org/10.1016/j.cmet.2018.06.007

Maassen, J.A., Romijn, J.A., Heine, R.J., 2007. Fatty acid-induced mitochondrial uncoupling in adipocytes as a key protective factor against insulin resistance and beta cell dysfunction: a new concept in the pathogenesis of obesity-associated type 2 diabetes mellitus. Diabetologia 50, 2036–2041. https://doi.org/10.1007/s00125-007-0776-z

Macdonald, C., 1990. Development of New Cell Lines for Animal Cell Biotechnology. Critical Reviews in Biotechnology 10, 155–178. https://doi.org/10.3109/07388559009068265

Maedler, K., Sergeev, P., Ris, F., Oberholzer, J., Joller-Jemelka, H.I., Spinas, G.A., Kaiser, N., Halban, P.A., Donath, M.Y., 2002. Glucose-induced β cell production of IL-1β contributes to glucotoxicity in human pancreatic islets. Journal of Clinical Investigation 110, 851–860. https://doi.org/10.1172/JCI200215318

Marnewick, J., Joubert, E., Joseph, S., Swanevelder, S., Swart, P., Gelderblom, W., 2005. Inhibition of tumour promotion in mouse skin by extracts of rooibos (Aspalathus linearis) and honeybush (Cyclopia intermedia), unique South African herbal teas. Cancer Letters 224, 193–202. https://doi.org/10.1016/j.canlet.2004.11.014

Marzban, L., Rhodes, C.J., Steiner, D.F., Haataja, L., Halban, P.A., Verchere, C.B., 2006. Impaired NH2-Terminal Processing of Human Proislet Amyloid Polypeptide by the Prohormone Convertase PC2 Leads to Amyloid Formation and Cell Death. Diabetes 55, 2192–2201. https://doi.org/10.2337/db05-1566

Mather, K.J., Mirzamohammadi, B., Lteif, A., Steinberg, H.O., Baron, A.D., 2002. Endothelin Contributes to Basal Vascular Tone and Endothelial Dysfunction in Human Obesity and Type 2 Diabetes. Diabetes 51, 3517–3523. https://doi.org/10.2337/diabetes.51.12.3517

Matsuoka, T., Kajimoto, Y., Watada, H., Kaneto, H., Kishimoto, M., Umayahara, Y., Fujitani, Y., Kamada, T., Kawamori, R., Yamasaki, Y., 1997. Glycation-dependent, reactive oxygen species-mediated suppression of the insulin gene promoter activity in HIT cells. Journal of Clinical Investigation 99, 144–150. https://doi.org/10.1172/JCI119126

Mayer, J.P., Zhang, F., DiMarchi, R.D., 2007. Insulin structure and function. Biopolymers 88, 687–713. https://doi.org/10.1002/bip.20734

Mayosi, B.M., Flisher, A.J., Lalloo, U.G., Sitas, F., Tollman, S.M., Bradshaw, D., 2009. The burden of non-communicable diseases in South Africa. The Lancet 374, 934–947. https://doi.org/10.1016/S0140-6736(09)61087-4

Mazibuko, S.E., Muller, C.J.F., Joubert, E., de Beer, D., Johnson, R., Opoku, A.R., Louw, J., 2013. Amelioration of palmitate-induced insulin resistance in C2C12 muscle cells by rooibos (Aspalathus linearis). Phytomedicine 20, 813–819. https://doi.org/10.1016/j.phymed.2013.03.018

Mazibuko-Mbeje, S., Dludla, P., Roux, C., Johnson, R., Ghoor, S., Joubert, E., Louw, J., Opoku, A., Muller, C., 2019. Aspalathin-Enriched Green Rooibos Extract Reduces Hepatic Insulin Resistance by Modulating PI3K/AKT and AMPK Pathways. International Journal of Molecular Sciences 20, 633. https://doi.org/10.3390/ijms20030633

McCarthy, D.J., Smyth, G.K., 2009. Testing significance relative to a fold-change threshold is a TREAT. Bioinformatics 25, 765–771. https://doi.org/10.1093/bioinformatics/btp053

McClean, P.L., Gault, V.A., Harriott, P., Hölscher, C., 2010. Glucagon-like peptide-1 analogues enhance synaptic plasticity in the brain: A link between diabetes and Alzheimer's disease. European Journal of Pharmacology 630, 158–162. https://doi.org/10.1016/j.ejphar.2009.12.023

Meakin, P.J., Harper, A.J., Hamilton, D.L., Gallagher, J., McNeilly, A.D., Burgess, L.A., Vaanholt, L.M., Bannon, K.A., Latcham, J., Hussain, I., Speakman, J.R., Howlett, D.R., Ashford, M.L.J., 2012. Reduction in BACE1 decreases body weight, protects against diet-induced obesity and enhances insulin sensitivity in mice. Biochemical Journal 441, 285. https://doi.org/10.1042/BJ20110512

Mehran, A.E., Templeman, N.M., Brigidi, G.S., Lim, G.E., Chu, K.-Y., Hu, X., Botezelli, J.D., Asadi, A., Hoffman, B.G., Kieffer, T.J., Bamji, S.X., Clee, S.M., Johnson, J.D., 2012. Hyperinsulinemia Drives Diet-Induced Obesity Independently of Brain Insulin Production. Cell Metabolism 16, 723–737. https://doi.org/10.1016/j.cmet.2012.10.019

Mehta, G., Hsiao, A.Y., Ingram, M., Luker, G.D., Takayama, S., 2012. Opportunities and challenges for use of tumor spheroids as models to test drug delivery and efficacy. Journal of Controlled Release 164, 192–204. https://doi.org/10.1016/j.jconrel.2012.04.045

Meier, D.T., Morcos, M., Samarasekera, T., Zraika, S., Hull, R.L., Kahn, S.E., 2014. Islet amyloid formation is an important determinant for inducing islet inflammation in high-fat-fed human IAPP transgenic mice. Diabetologia 57, 1884–1888. https://doi.org/10.1007/s00125-014-3304-y

Meijssen, S., Cabezas, M.C., Ballieux, C.G.M., Derksen, R.J., Bilecen, S., Erkelens, D.W., 2001. Insulin Mediated Inhibition of Hormone Sensitive Lipase Activity *in Vivo* in Relation to Endogenous Catecholamines in Healthy Subjects. The Journal of Clinical Endocrinology & Metabolism 86, 4193–4197. https://doi.org/10.1210/jcem.86.9.7794

Michael, M.D., Kulkarni, R.N., Postic, C., Previs, S.F., Shulman, G.I., Magnuson, M.A., Kahn, C.R., 2000. Loss of Insulin Signaling in Hepatocytes Leads to Severe Insulin Resistance and Progressive Hepatic Dysfunction. Molecular Cell 6, 87–97. https://doi.org/10.1016/S1097-2765(05)00015-8

Michelson, S., Leith, J.T., 1997. Tumor Heterogeneity and Growth Control, in: Adam, J.A., Bellomo, N. (Eds.), A Survey of Models for Tumor-Immune System Dynamics. Birkhäuser Boston, Boston, MA, pp. 295–333. https://doi.org/10.1007/978-0-8176-8119-7_7

Miyazaki, Y., Mahankali, A., Matsuda, M., Mahankali, S., Hardies, J., Cusi, K., Mandarino, L.J., DeFronzo, R.A., 2002. Effect of Pioglitazone on Abdominal Fat Distribution and Insulin Sensitivity in Type 2 Diabetic Patients. The Journal of Clinical Endocrinology & Metabolism 87, 2784–2791. https://doi.org/10.1210/jcem.87.6.8567

Miyazaki, Y., Mahankali, A., Wajcberg, E., Bajaj, M., Mandarino, L.J., DeFronzo, R.A., 2004. Effect of Pioglitazone on Circulating Adipocytokine Levels and Insulin Sensitivity in Type 2 Diabetic Patients. The Journal of Clinical Endocrinology & Metabolism 89, 4312–4319. https://doi.org/10.1210/jc.2004-0190

Modak, M.A., Parab, P.B., Ghaskadbi, S.S., 2009. Pancreatic Islets Are Very Poor in Rectifying Oxidative DNA Damage: Pancreas 38, 23–29. https://doi.org/10.1097/MPA.0b013e318181da4e

Monsees, T.K., Opuwari, C.S., 2017. Effect of rooibos (Aspalathus linearis) on the female rat reproductive tract and liver and kidney functions in vivo. South African Journal of Botany 110, 208–215. https://doi.org/10.1016/j.sajb.2016.11.013

Monteiro, R., Azevedo, I., 2010. Chronic Inflammation in Obesity and the Metabolic Syndrome. Mediators of Inflammation 2010, 1–10. https://doi.org/10.1155/2010/289645

Moore, C.X., Cooper, G.J.S., 1991. Co-secretion of amylin and insulin from cultured islet β-cells: Modulation by nutrient secretagogues, islet hormones and hypoglycemic agents. Biochemical and Biophysical Research Communications 179, 1–9. https://doi.org/10.1016/0006-291X(91)91325-7

Morioka, T., Asilmaz, E., Hu, J., Dishinger, J.F., Kurpad, A.J., Elias, C.F., Li, H., Elmquist, J.K., Kennedy, R.T., Kulkarni, R.N., 2007. Disruption of leptin receptor expression in the pancreas directly affects β cell growth and function in mice. Journal of Clinical Investigation 117, 2860–2868. https://doi.org/10.1172/JCI30910

Mueller, M., Hobiger, S., Jungbauer, A., 2010. Anti-inflammatory activity of extracts from fruits, herbs and spices. Food Chemistry 122, 987–996. https://doi.org/10.1016/j.foodchem.2010.03.041

Muller, C.J.F., Joubert, E., de Beer, D., Sanderson, M., Malherbe, C.J., Fey, S.J., Louw, J., 2012a. Acute assessment of an aspalathin-enriched green rooibos (Aspalathus linearis) extract with hypoglycemic potential. Phytomedicine 20, 32–39. https://doi.org/10.1016/j.phymed.2012.09.010

Muller, D.C., Elahi, D., Tobin, J.D., Andres, R., 1996. Insulin response during the oral glucose tolerance test: The role of age, sex, body fat and the pattern of fat distribution. Aging Clinical and Experimental Research 8, 13–21. https://doi.org/10.1007/BF03340110

Muoio, D.M., Newgard, C.B., 2008. Molecular and metabolic mechanisms of insulin resistance and β-cell failure in type 2 diabetes. Nature Reviews Molecular Cell Biology 9, 193–205. https://doi.org/10.1038/nrm2327

Nojilana, B., Bradshaw, D., Wyk, V.P., Msemburi, W., Somdyala, N., Joubert, J.D., Groenewald, P., Laubscher, R., Dorrington, R.E., 2016. Persistent burden from non-communicable diseases in South Africa needs strong action [WWW Document]. SAMJ South African Medical Journal. URL https://link.galegroup.com/apps/doc/A451310183/AONE?sid=lms (accessed 11.27.19).

Nolan, C.J., Leahy, J.L., Delghingaro-Augusto, V., Moibi, J., Soni, K., Peyot, M.-L., Fortier, M., Guay, C., Lamontagne, J., Barbeau, A., Przybytkowski, E., Joly, E., Masiello, P., Wang, S., Mitchell, G.A., Prentki, M., 2006a. Beta cell compensation for insulin

resistance in Zucker fatty rats: increased lipolysis and fatty acid signalling. Diabetologia 49, 2120–2130. https://doi.org/10.1007/s00125-006-0305-5

Noriega-Cisneros, R., Ortiz-Ávila, O., Esquivel-Gutiérrez, E., Clemente-Guerrero, M., Manzo-Avalos, S., Salgado-Garciglia, R., Cortés-Rojo, C., Boldogh, I., Saavedra-Molina, A., 2012. Hypolipidemic Activity of *Eryngium carlinae* on Streptozotocin-Induced Diabetic Rats. Biochemistry Research International 2012, 1–5. https://doi.org/10.1155/2012/603501

Novials, A., Montane, J., Cadavez-Trigo, L., 2014. Stress and the inflammatory process: a major cause of pancreatic cell death in type 2 diabetes. Diabetes, Metabolic Syndrome and Obesity: Targets and Therapy 25. https://doi.org/10.2147/DMSO.S37649

Nwose, O.M., Jones, M.R., 2013. Atypical Mechanism of Glucose Modulation by Colesevelam in Patients with Type 2 Diabetes. Clinical Medicine Insights: Endocrinology and Diabetes 6, CMED.S12590. https://doi.org/10.4137/CMED.S12590

Odeleye, O.E., de Courten, M., Pettitt, D.J., Ravussin, E., 1997. Fasting Hyperinsulinemia Is a Predictor of Increased Body Weight Gain and Obesity in Pima Indian Children. Diabetes 46, 1341–1345. https://doi.org/10.2337/diab.46.8.1341

Ohsawa, H., Kanatsuka, A., Yamaguchi, T., Makino, H., Yoshida, S., 1989. Islet amyloid polypeptide inhibits glucose-stimulated insulin secretion from isolated rat pancreatic islets. Biochemical and Biophysical Research Communications 160, 961–967. https://doi.org/10.1016/0006-291X(89)92529-1

Okereke, O., Hankinson, S.E., Hu, F.B., Grodstein, F., 2005. Plasma C Peptide Level and Cognitive Function Among Older Women Without Diabetes Mellitus. Archives of Internal Medicine 165, 1651. https://doi.org/10.1001/archinte.165.14.1651

Opie, E.L., 1901. The relation of diabetes mellitus to lesions of the pancreas. hyaline degeneration of the islands of langerhans. Journal of Experimental Medicine 5, 527–540. https://doi.org/10.1084/jem.5.5.527

Oslowski, C.M., Urano, F., 2010. The binary switch between life and death of endoplasmic reticulum-stressed β cells: Current Opinion in Endocrinology, Diabetes and Obesity 17, 107–112. https://doi.org/10.1097/MED.0b013e3283372843

Ottosson-Laakso, E., Krus, U., Storm, P., Prasad, R.B., Oskolkov, N., Ahlqvist, E., Fadista, J., Hansson, O., Groop, L., Vikman, P., 2017. Glucose-Induced Changes in Gene Expression in Human Pancreatic Islets: Causes or Consequences of Chronic Hyperglycemia. Diabetes 66, 3013–3028. https://doi.org/10.2337/db17-0311

Pan, Y., Chen, X.-Y., Zhang, Q.-Y., Kong, L.-D., 2014. Microglial NLRP3 inflammasome activation mediates IL-1β-related inflammation in prefrontal cortex of depressive rats. Brain, Behavior, and Immunity 41, 90–100. https://doi.org/10.1016/j.bbi.2014.04.007

Paolisso, G., Scheen, A., Lefèbvre, P., 1995. Glucose Handling, Diabetes and Ageing. Hormone Research 43, 52–57. https://doi.org/10.1159/000184237

Papadopoulos, S., Jürgens, K.D., Gros, G., 2000. Protein Diffusion in Living Skeletal Muscle Fibers: Dependence on Protein Size, Fiber Type, and Contraction. Biophysical Journal 79, 2084–2094. https://doi.org/10.1016/S0006-3495(00)76456-3

Park, H.K., Ahima, R.S., 2014. Leptin signaling. F1000Prime Reports 6. https://doi.org/10.12703/P6-73

Park, Y.J., Lee, S., Kieffer, T.J., Warnock, G.L., Safikhan, N., Speck, M., Hao, Z., Woo, M., Marzban, L., 2012. Deletion of Fas protects islet beta cells from cytotoxic effects of human islet amyloid polypeptide. Diabetologia 55, 1035–1047. https://doi.org/10.1007/s00125-012-2451-2

Pascal, S.M.A., Veiga-da-Cunha, M., Gilon, P., Van Schaftingen, E., Jonas, J.C., 2010. Effects of fructosamine-3-kinase deficiency on function and survival of mouse pancreatic islets after prolonged culture in high glucose or ribose concentrations. American Journal of Physiology-Endocrinology and Metabolism 298, E586–E596. https://doi.org/10.1152/ajpendo.00503.2009

Patton, J., DeGolier, T., 2010. Modeling leptin receptor insensitivity by comparing how leptin or leptin receptor mutations in mice affect body weight, basal metabolism, body temperature and feeding behaviors. BIOS 81, 76–83.

Paulsson, J.F., Ludvigsson, J., Carlsson, A., Casas, R., Forsander, G., Ivarsson, S.A., Kockum, I., Lernmark, Å., Marcus, C., Lindblad, B., Westermark, G.T., 2014. High Plasma Levels of Islet Amyloid Polypeptide in Young with New-Onset of Type 1 Diabetes Mellitus. PLoS ONE 9, e93053. https://doi.org/10.1371/journal.pone.0093053

Pavo, I., Jermendy, G., Varkonyi, T.T., Kerenyi, Z., Gyimesi, A., Shoustov, S., Shestakova, M., Herz, M., Johns, D., Schluchter, B.J., Festa, A., Tan, M.H., 2003. Effect of Pioglitazone Compared with Metformin on Glycemic Control and Indicators of Insulin Sensitivity in Recently Diagnosed Patients with Type 2 Diabetes. The Journal of Clinical Endocrinology & Metabolism 88, 1637–1645. https://doi.org/10.1210/jc.2002-021786

Peña-Altamira, E., Petralla, S., Massenzio, F., Virgili, M., Bolognesi, M.L., Monti, B., 2017. Nutritional and Pharmacological Strategies to Regulate Microglial Polarization in Cognitive Aging and Alzheimer's Disease. Frontiers in Aging Neuroscience 9, 175. https://doi.org/10.3389/fnagi.2017.00175

Perini, F., Morra, M., Alecci, M., Galloni, E., Marchi, M., Toso, V., 2001. Temporal profile of serum anti-inflammatory and pro-inflammatory interleukins in acute ischemic stroke patients. Neurological Sciences 22, 289–296. https://doi.org/10.1007/s10072-001-8170-y

Pessin, J.E., Saltiel, A.R., 2000. Signaling pathways in insulin action: molecular targets of insulin resistance. Journal of Clinical Investigation 106, 165–169. https://doi.org/10.1172/JCI10582

Pi, J., Bai, Y., Zhang, Q., Wong, V., Floering, L.M., Daniel, K., Reece, J.M., Deeney, J.T., Andersen, M.E., Corkey, B.E., Collins, S., 2007. Reactive Oxygen Species as a Signal in Glucose-Stimulated Insulin Secretion. Diabetes 56, 1783–1791. https://doi.org/10.2337/db06-1601

Poitout, V., Robertson, R.P., 2002. Minireview: Secondary β-Cell Failure in Type 2 Diabetes—A Convergence of Glucotoxicity and Lipotoxicity. Endocrinology 143, 339–342. https://doi.org/10.1210/endo.143.2.8623

Potter, K.J., Abedini, A., Marek, P., Klimek, A.M., Butterworth, S., Driscoll, M., Baker, R., Nilsson, M.R., Warnock, G.L., Oberholzer, J., Bertera, S., Trucco, M., Korbutt, G.S., Fraser, P.E., Raleigh, D.P., Verchere, C.B., 2010. Islet amyloid deposition limits the viability of human islet grafts but not porcine islet grafts. Proceedings of the National Academy of Sciences 107, 4305–4310. https://doi.org/10.1073/pnas.0909024107

Potter, K.J., Werner, I., Denroche, H.C., Montane, J., Plesner, A., Chen, Y., Lei, D., Soukhatcheva, G., Warnock, G.L., Oberholzer, J., Fraser, P.E., Verchere, C.B., 2015. Amyloid Formation in Human Islets Is Enhanced by Heparin and Inhibited by Heparinase: Heparin Stimulates Islet Amyloid Formation. American Journal of Transplantation 15, 1519–1530. https://doi.org/10.1111/ajt.13134

Powers, M.J., Domansky, K., Kaazempur-Mofrad, M.R., Kalezi, A., Capitano, A., Upadhyaya, A., Kurzawski, P., Wack, K.E., Stolz, D.B., Kamm, R., Griffith, L.G., 2002. A microfabricated array bioreactor for perfused 3D liver culture. Biotechnology and Bioengineering 78, 257–269. https://doi.org/10.1002/bit.10143

Pradhan, A.D., 2001. C-Reactive Protein, Interleukin 6, and Risk of Developing Type 2 Diabetes Mellitus. JAMA 286, 327. https://doi.org/10.1001/jama.286.3.327

Pratley, R.E., Salsali, A., 2007. Inhibition of DPP-4: a new therapeutic approach for the treatment of type 2 diabetes. Current Medical Research and Opinion 23, 919–931. https://doi.org/10.1185/030079906X162746

Prentki, M., 2006a. Islet cell failure in type 2 diabetes. Journal of Clinical Investigation 116, 1802–1812. https://doi.org/10.1172/JCI29103

Qiu, N.C., Zhang, Q., Song, X., Liu, M.-E., Li, X.K., Shan, C.-X., Qiu, M., 2014. Impact of the hepatic branch of the vagus and Roux-en-Y gastric bypass on the hypoglycemic effect and glucagon-like peptide-1 in rats with type 2 diabetes mellitus. Journal of Surgical Research 191, 123–129. https://doi.org/10.1016/j.jss.2014.03.062

Quinn, L.P., Crook, B., Hows, M.E., Vidgeon-Hart, M., Chapman, H., Upton, N., Medhurst, A.D., Virley, D.J., 2008. The PPARγ agonist pioglitazone is effective in the MPTP mouse model of Parkinson's disease through inhibition of monoamine oxidase B. British Journal of Pharmacology 154, 226–233. https://doi.org/10.1038/bjp.2008.78

Rafacho, A., Gonçalves-Neto, L.M., Santos-Silva, J.C., Alonso-Magdalena, P., Merino, B., Taboga, S.R., Carneiro, E.M., Boschero, A.C., Nadal, A., Quesada, I., 2014. Pancreatic Alpha-Cell Dysfunction Contributes to the Disruption of Glucose Homeostasis and Compensatory Insulin Hypersecretion in Glucocorticoid-Treated Rats. PLoS ONE 9, e93531. https://doi.org/10.1371/journal.pone.0093531

Rasheedy, D., Adly, N.N., Ahmed, R.M., Amer, M.S., 2019. Salivary amyloid β42 levels in mild cognitive impairment among aged diabetics. European Geriatric Medicine 10, 631–638. https://doi.org/10.1007/s41999-019-00190-4

Ravi, M., Paramesh, V., Kaviya, S.R., Anuradha, E., Solomon, F.D.P., 2015. 3D Cell Culture Systems: Advantages and Applications: 3D CELL CULTURE SYSTEMS. Journal of Cellular Physiology 230, 16–26. https://doi.org/10.1002/jcp.24683

Reagan-Shaw, S., Nihal, M., Ahmad, N., 2008. Dose translation from animal to human studies revisited. The FASEB Journal 22, 659–661. https://doi.org/10.1096/fj.07-9574LSF

Rebelato, E., Santos, L.R., Carpinelli, A.R., Rorsman, P., Abdulkader, F., 2018. Short-term high glucose culture potentiates pancreatic beta cell function. Scientific Reports 8, 13061. https://doi.org/10.1038/s41598-018-31325-5

Renehan, A.G., Bach, S.P., Potten, C.S., 2001. The Relevance of Apoptosis for Cellular Homeostasis and Tumorogenesis in the Intestine. Canadian Journal of Gastroenterology 15, 166–176. https://doi.org/10.1155/2001/164727

Ritchie, R., Julius, T., Buxton, K., Xu, Q., Kiriazis, H., McMullen, J., Forbes, J., Du, X., Kaye, D., Tesch, G., 2008. Type 2 Diabetic Cardiomyopathy in db/db Mice is Associated with Progressive Cardiac Fibrosis, Cardiomyocyte Hypertrophy and Oxidative Stress. Heart, Lung and Circulation 17, S231. https://doi.org/10.1016/j.hlc.2008.05.577

Ritz, P., Berrut, G., 2005. Mitochondrial function, energy expenditure, aging and insulin resistance. Diabetes & Metabolism 31, 5S67-5S73. https://doi.org/10.1016/S1262-3636(05)73654-5

Robertson, R.P., Harmon, J., Tran, P.O., Tanaka, Y., Takahashi, H., 2003. Glucose Toxicity in -Cells: Type 2 Diabetes, Good Radicals Gone Bad, and the Glutathione Connection. Diabetes 52, 581–587. https://doi.org/10.2337/diabetes.52.3.581

Robertson, R.P., Harmon, J., Tran, P.O.T., Poitout, V., 2004. -Cell Glucose Toxicity, Lipotoxicity, and Chronic Oxidative Stress in Type 2 Diabetes. Diabetes 53, S119–S124. https://doi.org/10.2337/diabetes.53.2007.S119

Robertson, R.P., Zhou, H., Zhang, T., Harmon, J.S., 2007. Chronic oxidative stress as a mechanism for glucose toxicity of the beta cell in Type 2 diabetes. Cell Biochemistry and Biophysics 48, 139–146. https://doi.org/10.1007/s12013-007-0026-5

Saadeh, M., Ferrante, T.C., Kane, A., Shirihai, O., Corkey, B.E., Deeney, J.T., 2012. Reactive Oxygen Species Stimulate Insulin Secretion in Rat Pancreatic Islets: Studies Using Mono-Oleoyl-Glycerol. PLoS ONE 7, e30200. https://doi.org/10.1371/journal.pone.0030200

Sabra, G., Vermette, P., 2013. A 3D cell culture system: Separation distance between INS-1 cell and endothelial cell monolayers co-cultured in fibrin influences INS-1 cells insulin secretion. Biotechnology and Bioengineering 110, 619–627. https://doi.org/10.1002/bit.24716

Saini, V., 2010. Molecular mechanisms of insulin resistance in type 2 diabetes mellitus. World Journal of Diabetes 1, 68. https://doi.org/10.4239/wjd.v1.i3.68

Sako, Y., Grill, V.E., 1990. Coupling of -Cell Desensitization by Hyperglycemia to Excessive Stimulation and Circulating Insulin in Glucose-Infused Rats. Diabetes 39, 1580–1583. https://doi.org/10.2337/diab.39.12.1580

Salameh, T.S., Rhea, E.M., Banks, W.A., Hanson, A.J., 2016. Insulin resistance, dyslipidemia, and apolipoprotein E interactions as mechanisms in cognitive impairment and Alzheimer's disease. Experimental Biology and Medicine 241, 1676–1683. https://doi.org/10.1177/1535370216660770

Saltiel, A.R., 2012. Insulin Resistance in the Defense against Obesity. Cell Metabolism 15, 798–804. https://doi.org/10.1016/j.cmet.2012.03.001

Saltiel, A.R., Kahn, C.R., 2001. Insulin signalling and the regulation of glucose and lipid metabolism. Nature 414, 799–806. https://doi.org/10.1038/414799a

Salvadó, L., Palomer, X., Barroso, E., Vázquez-Carrera, M., 2015. Targeting endoplasmic reticulum stress in insulin resistance. Trends in Endocrinology & Metabolism 26, 438–448. https://doi.org/10.1016/j.tem.2015.05.007

Samuels, I.S., Bell, B.A., Pereira, A., Saxon, J., Peachey, N.S., 2015. Early retinal pigment epithelium dysfunction is concomitant with hyperglycemia in mouse models of type 1 and type 2 diabetes. Journal of Neurophysiology 113, 1085–1099. https://doi.org/10.1152/jn.00761.2014

Sanderson, M., Mazibuko, S.E., Joubert, E., de Beer, D., Johnson, R., Pheiffer, C., Louw, J., Muller, C.J.F., 2014. Effects of fermented rooibos (Aspalathus linearis) on adipocyte differentiation. Phytomedicine 21, 109–117. https://doi.org/10.1016/j.phymed.2013.08.011

Sandovici, I., Hammerle, C.M., Cooper, W.N., Smith, N.H., Tarry-Adkins, J.L., Dunmore, B.J., Bauer, J., Andrews, S.R., Yeo, G.S.H., Ozanne, S.E., Constância, M., 2016. Ageing is associated with molecular signatures of inflammation and type 2 diabetes in rat pancreatic islets. Diabetologia 59, 502–511. https://doi.org/10.1007/s00125-015-3837-8

Sastre, M., Walter, J., Gentleman, S.M., 2008. Interactions between APP secretases and inflammatory mediators. Journal of Neuroinflammation 5, 25. https://doi.org/10.1186/1742-2094-5-25

Sataranatarajan, K., Ikeno, Y., Bokov, A., Feliers, D., Yalamanchili, H., Lee, H.J., Mariappan, M.M., Tabatabai-Mir, H., Diaz, V., Prasad, S., Javors, M.A., Ghosh Choudhury, G., Hubbard, G.B., Barnes, J.L., Richardson, A., Kasinath, B.S., 2016. Rapamycin Increases Mortality in *db/db* Mice, a Mouse Model of Type 2 Diabetes. The Journals of Gerontology Series A: Biological Sciences and Medical Sciences 71, 850–857. https://doi.org/10.1093/gerona/glv170

Sato, T., Herman, L., Fitzgerald, P.J., 1966. The comparative ultrastructure of the pancreatic islet of Langerhans. General and Comparative Endocrinology 7, 132–157. https://doi.org/10.1016/0016-6480(66)90094-3

Savage, D.B., Petersen, K.F., Shulman, G.I., 2005. Mechanisms of Insulin Resistance in Humans and Possible Links with Inflammation. Hypertension 45, 828–833. https://doi.org/10.1161/01.HYP.0000163475.04421.e4

Scheen, A.J., 2003. Pathophysiology of type 2 diabetes. Acta Clinica Belgica 58, 335–341. https://doi.org/10.1179/acb.2003.58.6.001

Scheuner, D., Kaufman, R.J., 2008. The Unfolded Protein Response: A Pathway That Links Insulin Demand with β-Cell Failure and Diabetes. Endocrine Reviews 29, 317–333. https://doi.org/10.1210/er.2007-0039

Schultze, S.M., Hemmings, B.A., Niessen, M., Tschopp, O., 2012. PI3K/AKT, MAPK and AMPK signalling: protein kinases in glucose homeostasis. Expert Reviews in Molecular Medicine 14, e1. https://doi.org/10.1017/S1462399411002109

Schulz, H., Joubert, E., Schütze, W., 2003. Quantification of quality parameters for reliable evaluation of green rooibos (Aspalathus linearis). European Food Research and Technology 216, 539–543. https://doi.org/10.1007/s00217-003-0696-1

Seino, S., Shibasaki, T., Minami, K., 2011. Dynamics of insulin secretion and the clinical implications for obesity and diabetes. Journal of Clinical Investigation 121, 2118–2125. https://doi.org/10.1172/JCI45680

Seufert, J., Kieffer, T.J., Leech, C.A., Holz, G.G., Moritz, W., Ricordi, C., Habener, J.F., 1999. Leptin Suppression of Insulin Secretion and Gene Expression in Human Pancreatic Islets: Implications for the Development of Adipogenic Diabetes Mellitus [1]. The Journal of Clinical Endocrinology & Metabolism 84, 670–676. https://doi.org/10.1210/jcem.84.2.5460

Shahjalal, H.Md., Abdal Dayem, A., Lim, K.M., Jeon, T., Cho, S.-G., 2018. Generation of pancreatic β cells for treatment of diabetes: advances and challenges. Stem Cell Research & Therapy 9, 355. https://doi.org/10.1186/s13287-018-1099-3

Shanik, M.H., Xu, Y., Skrha, J., Dankner, R., Zick, Y., Roth, J., 2008. Insulin Resistance and Hyperinsulinemia: Is hyperinsulinemia the cart or the horse? Diabetes Care 31, S262–S268. https://doi.org/10.2337/dc08-s264

Shaw, J.E., Sicree, R.A., Zimmet, P.Z., 2010. Global estimates of the prevalence of diabetes for 2010 and 2030. Diabetes Research and Clinical Practice 87, 4–14. https://doi.org/10.1016/j.diabres.2009.10.007

Shay, J.W., Wright, W.E., 2000. Hayflick, his limit, and cellular ageing. Nature Reviews Molecular Cell Biology 1, 72–76. https://doi.org/10.1038/35036093

Shi, C., Zhu, Lijun, Chen, X., Gu, N., Chen, L., Zhu, Lu, Yang, L., Pang, L., Guo, X., Ji, C., Zhang, C., 2014. IL-6 and TNF-α Induced Obesity-Related Inflammatory Response Through Transcriptional Regulation of miR-146b. Journal of Interferon & Cytokine Research 34, 342–348. https://doi.org/10.1089/jir.2013.0078

Shi, X., Ren, Y., Wu, J., 2011. Intermittent High Glucose Enhances Apoptosis in INS-1 Cells. Experimental Diabetes Research 2011, 1–7. https://doi.org/10.1155/2011/754673

Shimmyo, Y., Kihara, T., Akaike, A., Niidome, T., Sugimoto, H., 2008. Flavonols and flavones as BACE-1 inhibitors: Structure–activity relationship in cell-free, cell-based and in silico studies reveal novel pharmacophore features. Biochimica et Biophysica Acta (BBA) - General Subjects 1780, 819–825. https://doi.org/10.1016/j.bbagen.2008.01.017

Sinha, S., Anderson, J.P., Barbour, R., Basi, G.S., Caccavello, R., Davis, D., Doan, M., Dovey, H.F., Frigon, N., Hong, J., Jacobson-Croak, K., Jewett, N., Keim, P., Knops, J., Lieberburg, I., Power, M., Tan, H., Tatsuno, G., Tung, J., Schenk, D., Seubert, P., Suomensaari, S.M., Wang, S., Walker, D., Zhao, J., McConlogue, L., John, V., 1999. Purification and cloning of amyloid precursor protein β-secretase from human brain. Nature 402, 537–540. https://doi.org/10.1038/990114

Skelin, M., 2010. Pancreatic beta cell lines and their applications in diabetes mellitus research. ALTEX 105–113. https://doi.org/10.14573/altex.2010.2.105

Smith, C., Swart, A.C., 2016. Rooibos (Aspalathus linearis) facilitates an anti-inflammatory state, modulating IL-6 and IL-10 while not inhibiting the acute glucocorticoid response to a mild novel stressor in vivo. Journal of Functional Foods 27, 42–54. https://doi.org/10.1016/j.jff.2016.08.055

Snel, M., Jonker, J.T., Schoones, J., Lamb, H., de Roos, A., Pijl, H., Smit, J.W.A., Meinders, A.E., Jazet, I.M., 2012. Ectopic Fat and Insulin Resistance: Pathophysiology and Effect of Diet and Lifestyle Interventions. International Journal of Endocrinology 2012, 1–18. https://doi.org/10.1155/2012/983814

Sodek, K.L., Ringuette, M.J., Brown, T.J., 2009. Compact spheroid formation by ovarian cancer cells is associated with contractile behavior and an invasive phenotype. International Journal of Cancer 124, 2060–2070. https://doi.org/10.1002/ijc.24188

Sone, H., Kagawa, Y., 2005. Pancreatic beta cell senescence contributes to the pathogenesis of type 2 diabetes in high-fat diet-induced diabetic mice. Diabetologia 48, 58–67. https://doi.org/10.1007/s00125-004-1605-2

Srodulski, S., Sharma, S., Bachstetter, A.B., Brelsfoard, J.M., Pascual, C., Xie, X., Saatman, K.E., Van Eldik, L.J., Despa, F., 2014. Neuroinflammation and neurologic deficits in diabetes linked to brain accumulation of amylin. Molecular Neurodegeneration 9, 30. https://doi.org/10.1186/1750-1326-9-30

Starkie, R., Ostrowski, S.R., Jauffred, S., Febbraio, M., Pedersen, B.K., 2003. Exercise and IL-6 infusion inhibit endotoxin-induced TNF-α production in humans. The FASEB Journal 17, 884–886. https://doi.org/10.1096/fj.02-0670fje

Steensberg, A., Fischer, C.P., Keller, C., Møller, K., Pedersen, B.K., 2003. IL-6 enhances plasma IL-1ra, IL-10, and cortisol in humans. American Journal of Physiology-Endocrinology and Metabolism 285, E433–E437. https://doi.org/10.1152/ajpendo.00074.2003

Stefan, Y., Orci, L., Malaisse-Lagae, F., Perrelet, A., Patel, Y., Unger, R.H., 1982. Quantitation of Endocrine Cell Content in the Pancreas of Nondiabetic and Diabetic Humans. Diabetes 31, 694–700. https://doi.org/10.2337/diab.31.8.694

Stridsberg, M., Sandler, S., Wilander, E., 1993. Cosecretion of islet amylid polypeptide (IAPP) and insulin from isolated rat pancreatic islets following stimulation or inhibition of β-cell function. Regulatory Peptides 45, 363–370. https://doi.org/10.1016/0167-0115(93)90362-C

Sun, L., Zhang, W., Wang, X., Song, J., Li, M., 2012. Inhibition of protein kinase C signal reduces ET receptor expression and basilar vasospasm after subarachnoid hemorrhage in rats. Journal of Integrative Neuroscience 11, 439–451. https://doi.org/10.1142/S0219635212500288

Talchai, C., Xuan, S., Lin, H.V., Sussel, L., Accili, D., 2012. Pancreatic β Cell Dedifferentiation as a Mechanism of Diabetic β Cell Failure. Cell 150, 1223–1234. https://doi.org/10.1016/j.cell.2012.07.029

Tonooka, N., Oseid, E., Zhou, H., Harmon, J.S., Robertson, R.P., 2007. Glutathione peroxidase protein expression and activity in human islets isolated for transplantation.

Clinical Transplantation 0, 070618134134003-??? https://doi.org/10.1111/j.1399-0012.2007.00736.x

Tripathy, D., Merovci, A., Basu, R., Abdul-Ghani, M., DeFronzo, R.A., 2019. Mild Physiologic Hyperglycemia Induces Hepatic Insulin Resistance in Healthy Normal Glucose-Tolerant Participants. The Journal of Clinical Endocrinology & Metabolism 104, 2842–2850. https://doi.org/10.1210/jc.2018-02304

Tuomilehto, J., Lindström, J., Eriksson, J.G., Valle, T.T., Hämäläinen, H., Ilanne-Parikka, P., Keinänen-Kiukaanniemi, S., Laakso, M., Louheranta, A., Rastas, M., Salminen, V., Aunola, S., Cepaitis, Z., Moltchanov, V., Hakumäki, M., Mannelin, M., Martikkala, V., Sundvall, J., Uusitupa, M., 2001. Prevention of Type 2 Diabetes Mellitus by Changes in Lifestyle among Subjects with Impaired Glucose Tolerance. New England Journal of Medicine 344, 1343–1350. https://doi.org/10.1056/NEJM200105033441801

Unger, R., Orci, L., 1975. THE ESSENTIAL ROLE OF GLUCAGON IN THE PATHOGENESIS OF DIABETES MELLITUS. The Lancet 305, 14–16. https://doi.org/10.1016/S0140-6736(75)92375-2

Valko, M., Leibfritz, D., Moncol, J., Cronin, M.T.D., Mazur, M., Telser, J., 2007. Free radicals and antioxidants in normal physiological functions and human disease. The International Journal of Biochemistry & Cell Biology 39, 44–84. https://doi.org/10.1016/j.biocel.2006.07.001

Van Antwerp, D.J., Martin, S.J., Kafri, T., Green, D.R., Verma, I.M., 1996a. Suppression of TNF-alpha -Induced Apoptosis by NF-kappa B. Science 274, 787–789. https://doi.org/10.1126/science.274.5288.787

Van Antwerp, D.J., Martin, S.J., Kafri, T., Green, D.R., Verma, I.M., 1996b. Suppression of TNF-alpha -Induced Apoptosis by NF-kappa B. Science 274, 787–789. https://doi.org/10.1126/science.274.5288.787

Vassar, R., 2004. BACE1: The β-Secretase Enzyme in Alzheimer's Disease. Journal of Molecular Neuroscience 23, 105–114. https://doi.org/10.1385/JMN:23:1-2:105

Vassar, R., 1999. Beta-Secretase Cleavage of Alzheimer's Amyloid Precursor Protein by the Transmembrane Aspartic Protease BACE. Science 286, 735–741. https://doi.org/10.1126/science.286.5440.735

Veniant, M., LeBel, C., 2003. Leptin: From Animals to Humans. Current Pharmaceutical Design 9, 811–818. https://doi.org/10.2174/1381612033455369

Viollet, B., Guigas, B., Garcia, N.S., Leclerc, J., Foretz, M., Andreelli, F., 2012. Cellular and molecular mechanisms of metformin: an overview. Clinical Science 122, 253–270. https://doi.org/10.1042/CS20110386

Visa, M., Alcarraz-Vizán, G., Montane, J., Cadavez, L., Castaño, C., Villanueva-Peñacarrillo, M.L., Servitja, J.-M., Novials, A., 2015. Islet amyloid polypeptide exerts a novel autocrine action in β-cell signaling and proliferation. The FASEB Journal 29, 2970–2979. https://doi.org/10.1096/fj.15-270553

Vozarova, B., Weyer, C., Lindsay, R.S., Pratley, R.E., Bogardus, C., Tataranni, P.A., 2002. High White Blood Cell Count Is Associated With a Worsening of Insulin Sensitivity and Predicts the Development of Type 2 Diabetes. Diabetes 51, 455–461. https://doi.org/10.2337/diabetes.51.2.455

Waisundara, V.Y., Hoon, L.Y., 2015. Free radical scavenging ability of Aspalathus linearis in two in vitro models of diabetes and cancer. Journal of Traditional and Complementary Medicine 5, 174–178. https://doi.org/10.1016/j.jtcme.2014.11.009

Wali, J.A., Rondas, D., McKenzie, M.D., Zhao, Y., Elkerbout, L., Fynch, S., Gurzov, E.N., Akira, S., Mathieu, C., Kay, T.W.H., Overbergh, L., Strasser, A., Thomas, H.E., 2014. The proapoptotic BH3-only proteins Bim and Puma are downstream of endoplasmic reticulum and mitochondrial oxidative stress in pancreatic islets in response to glucotoxicity. Cell Death & Disease 5, e1124–e1124. https://doi.org/10.1038/cddis.2014.88

Wang, C., Yang, S., Zhang, N., Mu, Y., Ren, H., Wang, Y., Li, K., 2014. Long-Term Supranutritional Supplementation with Selenate Decreases Hyperglycemia and Promotes Fatty Liver Degeneration by Inducing Hyperinsulinemia in Diabetic db/db Mice. PLoS ONE 9, e101315. https://doi.org/10.1371/journal.pone.0101315

Wang, H., Li, J., Gai, Z., Kullak-Ublick, G.A., Liu, Z., 2017. TNF-α Deficiency Prevents Renal Inflammation and Oxidative Stress in Obese Mice. Kidney and Blood Pressure Research 42, 416–427. https://doi.org/10.1159/000478869

Weindruch, R., Sohal, R.S., 1997. Caloric Intake and Aging. New England Journal of Medicine 337, 986–994. https://doi.org/10.1056/NEJM199710023371407

Weir, G.C., Bonner-Weir, S., 2013. Islet β cell mass in diabetes and how it relates to function, birth, and death: Islet β cell mass in diabetes. Annals of the New York Academy of Sciences 1281, 92–105. https://doi.org/10.1111/nyas.12031

Weir, G.C., Bonner-Weir, S., 2007. A dominant role for glucose in β cell compensation of insulin resistance. Journal of Clinical Investigation 117, 81–83. https://doi.org/10.1172/JCI30862

Weir, G.C., Bonner-Weir, S., 2004. Five Stages of Evolving Beta-Cell Dysfunction During Progression to Diabetes. Diabetes 53, S16–S21. https://doi.org/10.2337/diabetes.53.suppl_3.S16

Weir, G.C., Laybutt, D.R., Kaneto, H., Bonner-Weir, S., Sharma, A., 2001. Beta-cell adaptation and decompensation during the progression of diabetes. Diabetes 50, S154–S159. https://doi.org/10.2337/diabetes.50.2007.S154

Weir, G.C., Marselli, L., Marchetti, P., Katsuta, H., Jung, M.H., Bonner-Weir, S., 2009. Towards better understanding of the contributions of overwork and glucotoxicity to the β-cell inadequacy of type 2 diabetes. Diabetes, Obesity and Metabolism 11, 82–90. https://doi.org/10.1111/j.1463-1326.2009.01113.x

Weiss, M.A., 2009. Chapter 2 The Structure and Function of Insulin, in: Vitamins & Hormones. Elsevier, pp. 33–49. https://doi.org/10.1016/S0083-6729(08)00602-X

Wellen, K.E., Hotamisligil, G.S., 2005. Inflammation, stress, and diabetes. Journal of Clinical Investigation 115, 1111–1119. https://doi.org/10.1172/JCI25102

Westermark, P., Andersson, A., Westermark, G.T., 2011. Islet Amyloid Polypeptide, Islet Amyloid, and Diabetes Mellitus. Physiological Reviews 91, 795–826. https://doi.org/10.1152/physrev.00042.2009

Westermark, P., Wernstedt, C., Wilander, E., Hayden, D.W., O'Brien, T.D., Johnson, K.H., 1987. Amyloid fibrils in human insulinoma and islets of Langerhans of the diabetic cat are derived from a neuropeptide-like protein also present in normal islet cells. Proceedings of the National Academy of Sciences 84, 3881–3885. https://doi.org/10.1073/pnas.84.11.3881

Westermark, P., Wernstedt, C., Wilander, E., Sletten, K., 1986. A novel peptide in the calcitonin gene related peptide family as an amyloid fibril protein in the endocrine pancreas. Biochemical and Biophysical Research Communications 140, 827–831. https://doi.org/10.1016/0006-291X(86)90708-4

Westwell-Roper, C.Y., Ehses, J.A., Verchere, C.B., 2014. Resident Macrophages Mediate Islet Amyloid Polypeptide–Induced Islet IL-1β Production and β-Cell Dysfunction. Diabetes 63, 1698–1711. https://doi.org/10.2337/db13-0863

White, M.F., 2006. Regulating insulin signaling and β-cell function through IRS proteinsThis paper is one of a selection of papers published in this Special Issue, entitled Second Messengers and Phosphoproteins—12th International Conference. Canadian Journal of Physiology and Pharmacology 84, 725–737. https://doi.org/10.1139/y06-008

Wiederkehr, A., Wollheim, C., 2008. Impact of mitochondrial calcium on the coupling of metabolism to insulin secretion in the pancreatic β-cell. Cell Calcium 44, 64–76. https://doi.org/10.1016/j.ceca.2007.11.004

Willem, M., Tahirovic, S., Busche, M.A., Ovsepian, S.V., Chafai, M., Kootar, S., Hornburg, D., Evans, L.D.B., Moore, S., Daria, A., Hampel, H., Müller, V., Giudici, C., Nuscher, B., Wenninger-Weinzierl, A., Kremmer, E., Heneka, M.T., Thal, D.R., Giedraitis, V., Lannfelt, L., Müller, U., Livesey, F.J., Meissner, F., Herms, J., Konnerth, A., Marie, H., Haass, C., 2015. η-Secretase processing of APP inhibits neuronal activity in the hippocampus. Nature 526, 443–447. https://doi.org/10.1038/nature14864

Woo, S.-L., Xu, H., Li, H., Zhao, Y., Hu, X., Zhao, J., Guo, X., Guo, T., Botchlett, R., Qi, T., Pei, Y., Zheng, J., Xu, Y., An, X., Chen, Lulu, Chen, Lili, Li, Q., Xiao, X., Huo, Y., Wu, C., 2014. Metformin Ameliorates Hepatic Steatosis and Inflammation without Altering Adipose Phenotype in Diet-Induced Obesity. PLoS ONE 9, e91111. https://doi.org/10.1371/journal.pone.0091111

Wrzesinski, K., Fey, S., 2015. From 2D to 3D - a New Dimension for Modelling the Effect of Natural Products on Human Tissue. Current Pharmaceutical Design 21, 5605–5616. https://doi.org/10.2174/1381612821666151002114227

Wrzesinski, K., Fey, S.J., 2013. After trypsinisation, 3D spheroids of C3A hepatocytes need 18 days to re-establish similar levels of key physiological functions to those seen in the liver. Toxicology Research 2, 123–135. https://doi.org/10.1039/C2TX20060K

Wu, D., Yang, M., Chen, Y., Jia, Y., Ma, Z.A., Boden, G., Li, L., Yang, G., 2014. Hypothalamic Nesfatin-1/NUCB2 Knockdown Augments Hepatic Gluconeogenesis That Is Correlated With Inhibition of mTOR-STAT3 Signaling Pathway in Rats. Diabetes 63, 1234–1247. https://doi.org/10.2337/db13-0899

Xing, Z., Gauldie, J., Cox, G., Baumann, H., Jordana, M., Lei, X.F., Achong, M.K., 1998a. IL-6 is an antiinflammatory cytokine required for controlling local or systemic acute inflammatory responses. Journal of Clinical Investigation 101, 311–320. https://doi.org/10.1172/JCI1368

Xing, Z., Gauldie, J., Cox, G., Baumann, H., Jordana, M., Lei, X.F., Achong, M.K., 1998b. IL-6 is an antiinflammatory cytokine required for controlling local or systemic acute inflammatory responses. Journal of Clinical Investigation 101, 311–320. https://doi.org/10.1172/JCI1368

Yoon, K.H., Ko, S.H., Cho, J.H., Lee, J.M., Ahn, Y.B., Song, K.H., Yoo, S.J., Kang, M.I., Cha, B.Y., Lee, K.W., Son, H.Y., Kang, S.K., Kim, H.S., Lee, I.K., Bonner-Weir, S., 2003. Selective β-Cell Loss and α-Cell Expansion in Patients with Type 2 Diabetes Mellitus in Korea. The Journal of Clinical Endocrinology & Metabolism 88, 2300–2308. https://doi.org/10.1210/jc.2002-020735

Young, A., 2005. Inhibition of Gastric Emptying, in: Advances in Pharmacology. Elsevier, pp. 99–121. https://doi.org/10.1016/S1054-3589(05)52006-4

Yu, B.P., Chung, H.Y., 2006. Adaptive mechanisms to oxidative stress during aging. Mechanisms of Ageing and Development 127, 436–443. https://doi.org/10.1016/j.mad.2006.01.023

Zanoni, M., Piccinini, F., Arienti, C., Zamagni, A., Santi, S., Polico, R., Bevilacqua, A., Tesei, A., 2016. 3D tumor spheroid models for in vitro therapeutic screening: a systematic approach to enhance the biological relevance of data obtained. Scientific Reports 6, 19103. https://doi.org/10.1038/srep19103

Zhang, K., Kaufman, R.J., 2008. From endoplasmic-reticulum stress to the inflammatory response. Nature 454, 455–462. https://doi.org/10.1038/nature07203

Zhang, X.-X., Pan, Y.-H., Huang, Y.-M., Zhao, H.-L., 2016a. Neuroendocrine hormone amylin in diabetes. World Journal of Diabetes 7, 189. https://doi.org/10.4239/wjd.v7.i9.189

Zhang, X.-X., Pan, Y.-H., Huang, Y.-M., Zhao, H.-L., 2016b. Neuroendocrine hormone amylin in diabetes. World Journal of Diabetes 7, 189. https://doi.org/10.4239/wjd.v7.i9.189

Zheng, A., Li, Hao, Xu, J., Cao, K., Li, Hua, Pu, W., Yang, Z., Peng, Y., Long, J., Liu, J., Feng, Z., 2015. Hydroxytyrosol improves mitochondrial function and reduces oxidative stress in the brain of *db/db* mice: role of AMP-activated protein kinase activation. British Journal of Nutrition 113, 1667–1676. https://doi.org/10.1017/S0007114515000884

Zibolka, J., Bazwinsky-Wutschke, I., Mühlbauer, E., Peschke, E., 2018. Distribution and density of melatonin receptors in human main pancreatic islet cell types. Journal of Pineal Research 65, e12480. https://doi.org/10.1111/jpi.12480

Zierath, J.R., Krook, A., Wallberg-Henriksson, H., 2000. Insulin action and insulin resistance in human skeletal muscle. Diabetologia 43, 821–835. https://doi.org/10.1007/s001250051457

Zini, E., Osto, M., Franchini, M., Guscetti, F., Donath, M.Y., Perren, A., Heller, R.S., Linscheid, P., Bouwman, M., Ackermann, M., Lutz, T.A., Reusch, C.E., 2009. Hyperglycaemia but not hyperlipidaemia causes beta cell dysfunction and beta cell loss in the domestic cat. Diabetologia 52, 336–346. https://doi.org/10.1007/s00125-008-1201-y

APPENDIX

Appendix A: Cell culture reagents

Table 13: Cell culture reagents and preparation of stock solutions

Reagents / stock solution	Weight / volume
Krebs's-Ringer bicarbonate HEPES buffer	
• NaCl	3.36 g
• 115 NaHCO3	1.008 g
• 24 KCl	0.186 g
• 5 MgCl2	0.048 g
• 1 CaCl2	0.139 g
• 2.5 2% BSA	0.5 g 5 mL
• 10 mM HEPES Buffer	720.64 g Make up to the mark using a volumetric flask (500 ml)
Glucose	
• Glucose Stock: 500 mM	180.16 MW into 10 mL of KRHB
• Basal: 2.8 mM	252 µL into 45 mL of KRHB
• Stimulated: 16.7 mM	1.503 mL into 45 mL of KRHB
Roswell Park Memorial Institute (RPMI) 1640 Medium	
• 5 MgCl2	
• 1 CaCl2	
• 2.5 2% BSA	
• 10 mM HEPES Buffer	(500 mL)
Complete RPMI-1640 Media	
• FBS	50 mL
• RPMI-1640 medium	500 mL
Ethanol-acid Solution	
• EtOH	37.5 mL
• concentrated HCl	644 µL
• cell culture tested H2O	11.85 mL
• ddH2O	1 L

Appendix B: Western blot reagents

Table 14**: Stock solutions and buffer preparation used for Western blot analysis**

Solutions	**Weight / Volume**
Transfer buffer (1L)	
25 mM Tris (MW=121)	3.03 g
192 mM glycine (MW=75.07)	14.41 g
ddH2O	800 mL
100 % Methanol	200 mL
10 X Tris buffered saline (TBS) (pH=7.6)	
200 mM Tris (Mw)	24.22 g
1.37 M NaCl (Mw)	80.06 g
Dissolve in 1 L ddH2O	
Tris buffered saline with TWEEN 20 (TBST)	
10X TBS	100 mL
ddH2O	900 mL
Tween-20	1 mL
1X running buffer (1L)	
Dilute of 10X tris/glycine/SDS	100 mL
ddH2O	900 mL
5 % blocking solution	
Instant skimmed milk powder	5 g
1X TBST	100 mL
2.5 % blocking solution	
Instant skimmed milk powder	2.5 g
1X TBST	100 mL
Sample buffer (4X)	
900 µL of Laemli sample buffer	
100 µL of β-mercaptoethanol	950 µl
	50 µl

Appendix C: Equipment's

Table 15**: Equipment used in the study**

Description	**Manufacturer**
Absorbance microplate reader (ELX800)	Bio-Tek Instruments; Friedrichshall, Germany
Benchtop centrifuge (SL 16R)	Thermo Fisher Scientific
Benchtop microfuge (5415 R)	Eppendorf; Hamburg, Germany
Benchtop microfuge (5810 R)	Eppendorf
Biohazard safety cabinet, class II	Airvolution; Johannesburg, South Africa
Bunsen burner	INTEGRA Biosciences AG; Landquart, Switzerland
ChemiDoc	Bio-Rad
Fine Balance scale	United Scientific
Haemocytometer Bright-Line™	Hausser Scientific Company; Horsham, PA, USA
Heating block	Labnet International Inc.; NJ, US
Homogenising Beads	Qiagen; Hilden, Germany
Incubator (Galaxy R)	RS Biotech; West Lothian, United Kingdom
Inverted microscope (CKX 41)	Olympus; NY, USA
Mini Protean Tetra Cell	Bio-Rad
Multichannel Pipette	Eppendorf
Nikon Inverted fluorescence microscope	Nikon; NY, USA
Orbital shaker	Stoval life Science
pH meter	Lasec
Pipette boy	Labnet International; Edison, NJ, USA
Pipettes (10 ,20, 100, 200, 300, 1000 µl)	Eppendorf
PowerPac HC	Bio-Rad
Scale	United Scientific
SpectraMax i3	Molecular Devices, California, United States
Tissue Lyser	Qiagen
Trans-Blot® TurboTM	Bio-Rad
Waterbath	Memmert; Heilbronn, German

Embedding station	Leica EG 116 Embedder (SMM instruments. Johannesburg
Incubator	Model IH-150; Gallenkamp
Nikon Eclipse Ti Automated scanning microscope	Nikon Instruments Inc. Walt Whitman Road Melville. New York
Nikon Microscope camera	Nikon Digital Sight DS-Fic. Nikon corporation. Japan
Tissue processor	Shandon Elliot Duplex Processor OptoLaboratory. Cape Town

Appendix D: Software

Table 16**: Software**

Description	**Manufacturer**
ChemiDoc™ Touch Imaging System	BioRad; California, USA
Gen5 software (version 1.05)	Bio-Tek Instruments
GraphPad Prism 7	GraphPad Software; CA, USA
ImageLab	BioRad; California, USA
Leica Qwin Software	Leica Microsystems; Nussloch, German
Microsoft: Excel / Word / PowerPoint	Microsoft Corporation; WA, USA
NIS-Elements - Microscope Imaging Software	Nikon; NY, USA
SoftMax® Pro	Molecular Devices; CA, USA
Nikon NIS Imaging Software v4.40	Nikon Instruments Inc. Copyright 1991-2015
ImageJ	National institute of Health

Appendix E: All reagents

Table 17: All reagents catalogue and manufacturers details

Description	Catalogue Number	Manufacturer
10X Tris Buffer	161-0772	Bio-Rad
4X Laemmli sample buffer	161-0747	Bio-Rad
Anti-Amylin	115766	Abcam
Anti-BACE2	Ab5670	Abcam
Anti-Mouse IgG	sc-2318	Santa Cruz Biotechnology
Anti-Rabbit IgG	sc-2357	Santa Cruz Biotechnology
Anti-TMEM27	200664	Abcam
Anti-LC3A/B	4108	Cell signaling
Anti-p38	8690	Cell signaling
Anti-pdx-1	5679	Cell signalling
Anti-ERK	4370	Cell signalling
Anti-Glut 2	D3J3A	Cell signalling
Anti-phospho-AKT	4691	Cell signalling
Anti-Insulin receptor	3024S	Cell signalling
Anti-Ki67	ab15580	Abcam
Anti-LC3A/B	4108S	Cell signalling
BACE Inhibition Assay	CS0010	Sigma-Aldrich
BACE Inhibitor	2299-5, 25	BioVision
Bovine serum albumin (BSA)	A4919 03117332001	Roche
CaCl2	C5670	Sigma-Aldrich
Carbon dioxide (Co_2)	N/A	Air Products; Centurion, Cape Town, SA
CellTiter-Glo® Luminescent Assay	G7571	Promega
Clarity™ Western ECL Substrate	170-5061	Bio-Rad

DC Protein Assay Reagent A	500-0113	Bio-Rad
DC Protein Assay Reagent B	500-0114	Bio-Rad
DC Protein Assay Reagent S	500-0115	Bio-Rad
Dulbecco's phosphate buffered saline (DPBS)	BE17-513F	Lonza
Ethanol	32221	Sigma-Aldrich
Hepes	Hepes	Hepes
INS-1 rat insulinoma cells	-	Gift from Vrije Universiteit, Brussels, Belgium
Interleukin-1 beta (IL-1β)	I2393	Sigma-Aldrich
KCl	P5405	Sigma-Aldrich
Liquid Nitrogen	N/A	Air Products; Centurion, Cape Town, SA
Methanol	67-56-1	Sigma-Aldrich
MgCl2	M4880	Sigma-Aldrich
Mini-Protean® TGX Stain-Free™ Gels	456-8044	Bio-Rad
Molecular graded EtOH	34870	Sigma-Aldrich
PageRuler™ Prestained Protein Ladder	26619	Thermo Fisher Scientific
PMSF	78830	Sigma-Aldrich
Ponceau S Stain	P23295	Sigma-Aldrich
Precision plus protein™, WesternC™	1610399	Bio-Rad
Precision Protein™ StrepTactin-HRP Conjugate	1610381	Bio-Rad

Quick Start™ Bradford Protein Assay Kit	500-0203	Bio-Rad
Restore™ PLUS Western Blot Stripping Buffer	46430	Thermo Fisher Scientific

Appendix F: Assay kits

Table 18: Assay kits used in the study

Description	Catalogue Number	Manufacturer
CellTiter-Glo® Luminescent Cell Viability Assay	G7571	Promega
Rat IAPP ELISA Kit	E-EL-R2448	Elabscience
Ultra-Sensitive Mouse Insulin ELISA Kit	90080	Crystal Chem
Mouse C-peptide ELISA kit	90050	Crystal Chem
Mouse IL-6 Quantikine ELISA Kit	S6050	R&D systems
Mouse IL-10 Quantikine ELISA Kit	S1000B	R&D systems
Mouse TNF-alpha DuoSet ELISA	DY410-05	R&D systems

Appendix G: Supplementary results

Table 19: The relationship between insulin to amylin secretion following glucose stimulation in the spheroids. Data analysed with Pearson r correlation coefficient

Basal				Stimulation			
Group	r	P value	P value summary	Group	r	P value	P value summary
NG	0.8567	0.0032	**	NG	-0.1505	0.6991	ns
HG	0.3439	0.6480	ns	HG	0.0171	0.9651	ns
HG-GRT™	058862	0.0972	ns	HG-GRT™	0.7289	0.0259	*
HG-BACE	0.3931	0.2952	ns	HG-BACE	0.1317	0.7356	ns

Appendix H: Animal ethical approval

UNIVERSITY OF ZULULAND
RESEARCH ETHICS COMMITTEE
(Reg No: UZREC 171110-030)

RESEARCH & INNOVATION
Website: http://www.unizulu.ac.za
Private Bag X1001
KwaDlangezwa 3886
Tel: 035 902 6731
Fax: 035 902 6222
Email: DhanisA@unizulu.ac.za

ETHICAL CLEARANCE CERTIFICATE

Certificate Number	UZREC 171110-030 PGD 2017/207							
Project Title	BACE INHIBITION IN AGING PANCREATIC BETA CELLS: A POSSIBLE ROIBOOS							
Principal Researcher/ Investigator	Y Ntamo							
Supervisor and Co-supervisor	Dr N Chellan Prof AP Kappo		Prof C Muller					
Department	Biochemistry							
Faculty	Science and Agriculture							
Type of Risk	Med risk-Desktop, field work or laboratory							
Nature of Project	Honours/4th Year		Master's		Doctoral	x	Departmental	

The University of Zululand's Research Ethics Committee (UZREC) hereby gives ethical approval in respect of the undertakings contained in the above-mentioned project. The Researcher may therefore commence with data collection as from the date of this Certificate, using the certificate number indicated above.

Special conditions:

(1) This certificate is valid for 2 years from the date of issue.
(2) Principal researcher must provide an annual report to the UZREC in the prescribed format [due date-01 July 2018]
(3) Principal researcher must submit a report at the end of project in respect of ethical compliance.
(4) The UZREC must be informed immediately of any material change in the conditions or undertakings mentioned in the documents that were presented to the meeting.

The UZREC wishes the researcher well in conducting research.

Professor Gideon De Wet
Chairperson: University Research Ethics Committee
Deputy Vice-Chancellor: Research & Innovation
08 March 2018

CHAIRPERSON
UNIVERSITY OF ZULULAND RESEARCH ETHICS COMMITTEE (UZREC)
REG NO: UZREC 171110-30
09-03-2018
RESEARCH & INNOVATION OFFICE

ETHICS COMMITTEE FOR RESEARCH ON ANIMALS (ECRA)

29 March 2017

Miss Y Ntamo
BRIP
MEDICAL RESEARCH COUNCIL

Dear Miss Ntamo,

CERTIFICATE OF FINAL APPROVAL – REF. 05/17 "Amelioration of the longer term effects of diabetes on pancreatic beta cells and hepatotoxicity by *Aspalathus linearis* (Rooibos) in db/db mice"

The ECRA Committee reviewed your corrected Application and it was final approved.

Attached herewith please find your Certificate of Approval for the period 30 March 2017 – 31 July 2-18. Should this study period not be long enough, please write a letter to the ECRA Committee requested an extension on the study.

Should you encounter any difficulties duties your study or sudden death of the animals, please do not hesitate to inform the ECRA thereof as well as the reason for the death. You will need to submit every 6 months an interim report on the study to the ECRA Committee. The secretariat will inform you thereof in time.

Kind regards.

PROF D DU TOIT
Chairperson : ECRA Committee

Animal Ethics Approval Certificate

Decision of the Animal Ethics Committee for the use of living vertebrates for research, diagnostic procedures and product development

APPROVAL PERIOD: 30 March 2017 – 31 July 2018

PROJECT NUMBER:	05/17			
PROJECT TITLE:	**"Amelioration of the longer term effects of diabetes on pancreatic beta cells and hepatotoxicity by *Asapalthus linearis* (Rooibos) in db/db mice"**			
PROJECT LEADER:	Miss Yonela Ntamo			
DIVISION:	Biomedical Research and Innovation Platform (BRIP)			
CATEGORY:	Diabetes			
SPECIES OF ANIMAL:	Mouse BKS.Cg-Dock7 (m)	+/+ Lepr (db)/J	6 week old males 30gr	
NUMBER OF ANIMALS:	200			
NOT APPROVED:	n/a			
APPROVED:	29 March 2017			

PLEASE NOTE: Should the number or species of animal(s) required, or the experimental procedure(s) change, please submit a revised animal ethics clearance form to the animal ethics committee for approval before commencing with the experiment

PROF D DU TOIT **DATE** **29 March 2017**

CHAIRPERSON ANIMAL ETHICS COMMITTEE

Appendix I: Aspalathin structure

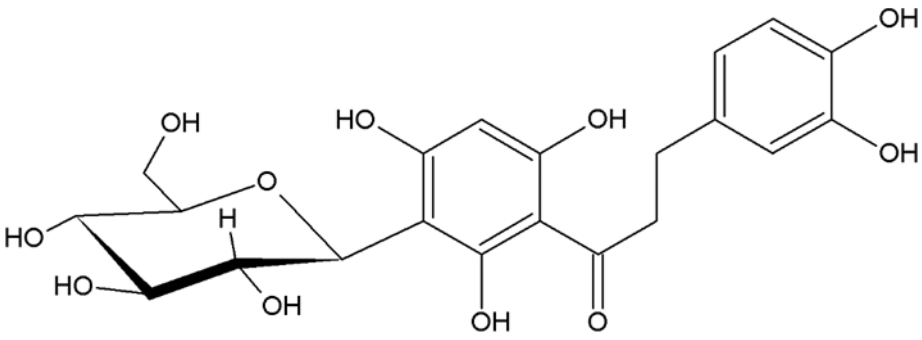

Figure 44: Chemical structure of aspalathin, a dihydrochalcone C-glucoside novel to Rooibos (Chemsketch).